EVALUATION OF VIDEOKERATOSCOPY

TRUSIT DAVE

Doctor of Philosophy

THE UNIVERSITY OF ASTON IN BIRMINGHAM

July 1995

The University of Aston in Birmingham

Evaluation of Videokeratoscopy

Trusit Dave
Doctor of Philosophy
1995

Summary

The present thesis evaluates various aspects of videokeratoscopes, which are now becoming increasingly popular in the investigation of corneal topography. The accuracy and repeatability of these instruments has been assessed mainly using spherical surfaces, however, few studies have assessed the performance of videokeratoscopes in measuring convex aspheric surfaces. Using two videokeratoscopes, the accuracy and repeatability of measurements using twelve aspheric surfaces is determined. Overall, the accuracy and repeatability of both instruments were acceptable, however, progressively flatter surfaces introduced greater errors in measurement, the possible reasons for these errors is discussed.

The corneal surface is a biological structure lubricated by the precorneal tear film. The effects of variations in the tear film on the repeatability of videokeratoscopes has not been determined in terms of peripheral corneal measurements. The repeatability of two commercially available videokeratoscopes is assessed. The repeatability is found to be dependent on the point of measurement on the corneal surface. Typically, superior and nasal meridians exhibit poorest repeatability. It is suggested that interference of the ocular adnexa is responsible for the reduced repeatability. This localised reduction in repeatability will occur for all videokeratoscopes. Further, comparisons with the keratometers and videokeratoscopes used show that measurements between these instruments are not interchangeable.

The final stage of this thesis evaluates the performance of new algorithms. The characteristics of a new videokeratoscope are described. This videokeratoscope is used to test the accuracy of the new algorithms for twelve aspheric surfaces. The new algorithms are accurate in determining the shape of aspheric surfaces, more so than those algorithms proposed at present.

Keywords: videokeratoscopy; keratometry; asphericity; cornea.

This thesis is dedicated to my parents, for a lifetime of love and support.

Acknowledgements

I am deeply grateful to Dr Colin Fowler who has provided excellent supervision. He has always shown a keen interest in the work and has provided me with invaluable advice.

Mr Derek Barnes has enabled me work in the department as a clinical demonstrator, were it not for the funding that this position eventually provided, the work presented here would undoubtedly have taken significantly longer to accomplish. Thank you.

Many thanks also to Nigel Burnett Hodd and David Ruston, the study involving the assessment of the EyeSys Corneal Analysis System would have not been possible without your co-operation.

Many people will undoubtedly be omitted in this acknowledgement, your help and interest has been appreciated. Particularly, Amit and Rohit, thanks for being so patient and of course Guruji, your precious words are more than encouraging.

Finally, thanks go to Sarah for proof reading, she has constantly helped me through the highs and lows, her motivation and kindness will not be forgotten. Don't forget Sarah, I'll be there to proof read your thesis too !

Contents

List of Figures

List of Tables

List of Appendices

Appendix

Chapter One

Descriptors of the Normal Cornea

1.1 Introduction

Eyecare practitioners have developed numerous methods of correcting refractive error. The numerous papers regarding the structure of the cornea makes it a considerable task to keep up-to-date with the latest developments in this field. A brief discussion of the anatomy of the cornea is relevant to the present text.

1.2 General Anatomy

Functionally, the cornea represents the 'window to the eye'. The cornea has the principle function of refracting light to form an image of the outside world and to protect the contents of the globe. In order to fulfill this function, the cornea must be transparent and avascular. In terms of its gross anatomy, it has an average diameter of approxiamtely 12mm and is generally 1mm longer horizontally than vertically. Its thickness is approximately 550μm centrally and 700μm peripherally (Waring 1984). The cornea represents the most powerful refracting surface of the eye. It must therefore possess a high quality surface structure. The precorneal tears create a smooth surface and also prevent the dessication of epithelial cells. It is the tear-air interface that produces the most powerful refracting surface of the eye.

The cornea is generally thought to be a rather delicate structure. However, it plays an important role in protecting the internal contents of the globe. The corneoscleral connective tissue has been shown to be able to withstand significant blunt force ($5kg/cm^2$) (Maurice, 1988) before rupturing. Most of the strength of the cornea is provided by the connective tissue within the stromal layer.

For an optical surface to successfully transmit light, it must be transparent. The cornea is composed of five layers. The fact that each structure is visible on unstained microscopic slides indicates that the refractive index is not idententical from one layer to the next. Numerous explanations have been postulated regarding the maintenance of corneal transparency (Cogan et al, 1942; Maurice, 1957). The least extravagant and most logical explanation was proposed by Maurice (1957). Maurice (1957) suggested that stromal fibrils are arranged such that they act as a series of diffraction gratings arranged in a hexagonal plane. Diffraction gratings effectively eliminate scattered light by destructive interference, thus, for the cornea, normally incident light would be transmitted through the stroma undeviated. A loss in transparency can also be explained using this theory. For example, when the cornea is oedematous, transparency is reduced. Using this lattice theory, the loss in transparency can be explained as a result of excessive liquid disturbing the spacing between stromal fibrils and thus reducing the efficacy of the diffraction grating. However, even with the results and conclusions of such extensive research, the high transparency of other layers of the cornea cannot be explained (Ruskell, 1989).

The maintanance of corneal transparency is clearly not only dependent on its anatomical nature. The cornea is a permanent resident in a liquid environment and maintains a solid to liquid ratio of approximately 1:4 (Ruskell, 1989). In certain conditions the cornea may become oedematous, for the cornea to return to its normal solid to liquid ratio certain physiological processes are involved. These physiological factors are beyond the scope of the present chapter and have been described in several other texts (Ruskell, 1989). The microscopic anatomy of the cornea will now be considered.

1.3 Microscopic Anatomy of the Cornea

The structure of the cornea is similar to other tissues in the body; both the epithelium and the endothelium lie on basement membranes (the epithelial basement membrane and Descemet's membrane, respectively). In addition, both basement membranes lie

adjacent to a connective tissue layer (the stroma). The cornea is composed of five layers:

- epithelium
- Bowman's layer
- stroma
- Descemet's membrane
- endothelium

Each layer will now be described in detail (also shown diagrammatically in figure

Figure 1.01: A section of the human cornea. Source: an atlas of clinical ophthalmology, 2nd edition, by Spalton, Hitchings and Hunter.

1.3.1 The Corneal Epithelium

The corneal epithelium is composed of a five to seven layer structure of stratified squamous epithelium and is between 30 to 50μm thick (Thoft et al, 1979). The

epithelium has an important role in the prevention of infection from microorganisms and also represents a barrier for protection against foreign bodies. It also has a role in the maintanence of corneal hydration as it acts as a barrier to the diffusion of water and solutes (Thoft et al, 1979).

There are three types of cells within the corneal epithelium. From anterior to posterior they are the superficial flat squamous cells (approximately three layers), the wing shaped polygonal cells (two layers) and the regular, single layered columnar cells (Gipson et al, 1987). The layers of cells are shown in figure 1.02. However, other cells are also present within the corneal epithelium such as melanocytes, neurons, leucocytes and Langerhans' cells. Langerhans' cells are essentially modified macrophages that are thought to have a role in the first steps of processing antigens (Rodrigues et al, 1981). Corneal epithelial cells contain apparatus (such as the endoplasmic reticulum and Golgi apparatus) that have a function in synthesis of protein. High protein synthesis is required because of the high turnover rate of the epithelium. The number of mitochondria are relatively few for such an active structure, this would suggest that energy requiring processes are less important compared to the production of structural molecules.

Figure 1.02: Diagram showing the various layers of the corneal epithelium. Source: an atlas of clinical ophthalmology, 2nd edition, by Spalton, Hitchings and Hunter.

A. Squamous Epithelium

The squamous epithelium layer is in direct contact with the tear film. The surface of the squamous cell layer is not smooth, instead there are numerous microvilli and microplicae. These fingerlike projections create a surface that helps to stabilise the tear film. Another function of the projections is in the absorption of metabolites, this is facilitated by the large surface area to volume ratio of the microvilli. However, the squamous cells also prevent the passage of fluid and other metabolites between the cells by having intercellular attachments known as demosomes and tight junctions. Oxygen may however diffuse across the barrier. Therefore, the majority of nutrients required by the cornea must be obtained from the posterior corneal surface. So far, only the passive nature of the barrier has been discussed, however, there is also an active barrier known as the chloride pump which has a small but useful role in the maintenance of corneal hydration. As mentioned earlier, it is not the aim of the present text to discuss any physiological concepts, but rather provide a basic overview of the anatomy of the cornea.

B. Polygonal Wing Cells

As their name implies, polygonal wing cells are irregularly shaped, multisided epithelial cells which interdigitate with each other. A combination of the interdigitation and the large number of desmosome attachments prevents the epithelium from splitting (Rodrigues et al, 1982). Polygonal wing cells constitute the second layer of the corneal epithelium.

C. Basal Epithelial Cells

The basal epithelial cells are columnar shaped cells arranged in a regular fashion along the basement membrane. These cells undergo mitosis and then differentiate into squamous and polygonal cells. Basal cells have the function of producing the basement membrane and the intercellular attachment complexes. The basal cells

(primarily because of their shape) interdigitate less. They also have fewer desmosome attachments compared to the polygonal wing cells (Waring, 1992).

D. The Epithelial Basement Membrane

The corneal epithelial cells rest upon the basement membrane. The epithelial cells remain attached to the basement membrane through complex attachments. The nature of these attachments is beyond the scope of this text, however, a detailed discussion of some of these attachments has been published by Gipson et al (1987) and Mosher (1984). Abnormalities in the attachments of the epithelium to the basement membrane may lead to recurrent corneal erosions.

1.3.2 Bowman's Layer

Bowman's layer lies adjacent to the basement membrane and is composed of a compact network of randomly orientated collagen fibrils. Bowman's layer is acellular and approximately 12μm thick. With respect to the physical properties of this layer, the thickness and composition helps to maintain corneal shape, Bowman's layer also exhibits little elasticity. However, exact knowledge of the biomechanical properties of this layer are not known at present. Owing to the acellular nature of Bowman's layer, it is not capable of regenerating. The implications of removing Bowman's layer in photorefractive keratectomy have yet to be investigated.

1.3.3 The Stroma

The corneal stroma is predominantly composed of collagen fibrils. The fibrils are of uniform diameter and are stacked in sheets of approximately two hundred lamellae. The significance of the arrangement of collagen fibrils was discussed earlier (Waring 1992). The regular array of the collagen fibrils is maintained by proteoglycans molecules. As well as collagen fibils, the stroma contains cells called keratocytes which synthesise the extracellular matrix of the stroma. Other cells that are found in

the stroma include phagocytic histocytes, plasma cells, lymphocytes and polymorphonuclear leukocytes. These cells are present in the normal stroma but become concentrated in areas of wound healing. Neurones also pass through the stroma at the limbus and eventually terminate as free nerve endings in the corneal epithelium (Ruskell, 1989).

1.3.4 Descemet's Membrane

Descemet's membrane is the basement membrane of the corneal endothelium. Endothelial cells are attached to the basement membrane, however, no attachment complexes are visible, thus the mechanism of attachment is unknown (Waring, 1982). Descemet's membrane thickens throughout life and serves as a barrier to prevent leukocytes and blood vessels from entering the stroma.

1.3.5 The Corneal Endothelium

The corneal endothelium is the most posterior layer of the cornea. The cells are arranged in a single layer between 4μm to 6μm thick. The cells are uniformly arranged in the form of a 'honey comb' mosaic (Sturrock et al, 1978). Cell divsion has been demonstrated in the corneal endothelium, however, the rate of regeneration is slow (Waring, 1982). As a result, when endothelial cells are damaged, neighbouring cells enlarge and reorganise themselves to maintain coverage of the cornea and also maintain the monolayer structure (Waring, 1982). Endothelial cells contain numerous mitichondria, their presence being explained by the energy requirements of the pump mechanism responsible for corneal hydration. Intercellular endothelial attachments are present but they do not prevent the passage aqueous into the stroma. Gap junctions between endothelial cells allow intercellular communication.

The corneal endothelium is responsible for maintaining corneal hydration and thus corneal transparency. The semi permeable, mechanical barrier provided by the intercellular endothelial attachments prevents most of the aqueous from entering the

cornea. One should note that some degree of permeability is required as certain corneal nutrients are derived from the aqueous humour. Another mechanism also exists to maintain corneal hydration. This mechanism relies on the active removal of water from the corneal stroma. The pump mechanism is known as the sodium-potassium, adenosine triphosphate-bicarbonate pump. Dysfunction of the pump leads to oedema and loss of transparency (Maurice, 1957; Ruskell, 1989).

1.4 Classification of Corneal Topography

Numerous terms are used to describe corneal topography, defining the terminology would provide greater understanding and clarity.

1.4.1 Surface Zones on the Corneal Surface

Since the early investigations by Javal and Helmholtz, a basic model of corneal topography was established (Miller et al, 1980). This classical model of the corneal contour was of a surface comprising of two distinct zones, a central spherical area (known as the corneal cap) measuring 4-5mm in diameter, and a peripheral zone that flattens progressively towards the limbus. The central zone is responsible for forming the foveal image and also corresponds to the entrance pupil. More recently, the cornea has described more specifically in terms of four anatomical zones (Waring, 1989). These zones are the central, paracentral, peripheral and limbal zones (see figure 1.03).

The centre of the cornea shown in figure 1.04 is known as the geometric centre. Once again, the significance of the geometric centre is only for localisation. The geometric centre should not be confused with the corneal apex which represents the point of maximum curvature on the cornea. The position of the corneal apex is independent of the geometric centre of the cornea and has been shown to lie, on average, approximately 0.5mm temporally (Edmund, 1987; Mandell et al, 1965b). In reality, classification of the cornea in terms of anatomical zones is inappropriate as the cornea is a smooth surface whose curvature changes in a continuous manner. Waring (1989)

suggested that classification of the cornea into anatomical zones is of use when designating locations on the cornea.

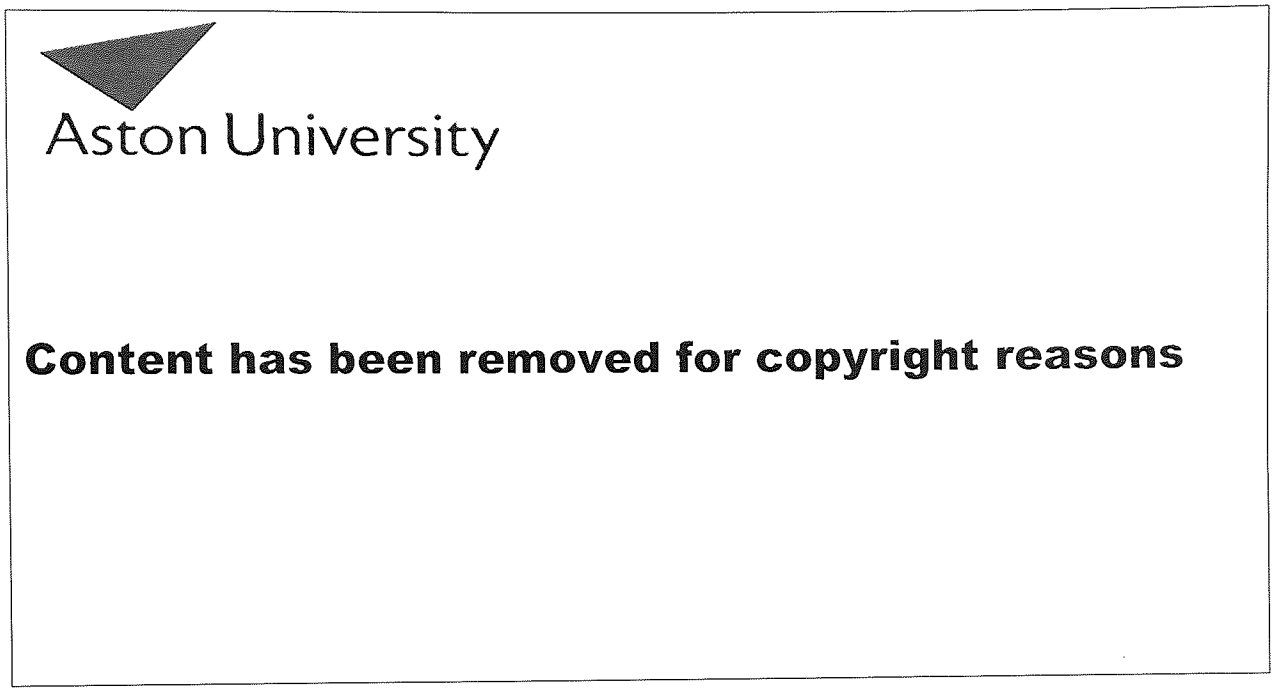

Figure 1.03: The anatomical zones on the corneal surface as described by Waring (1989).

1.4.2 The Central Cornea

The central corneal zone measures approximately 3-4mm (Waring, 1989), this area of the cornea is the most important region for image formation. There are two reasons for this, firstly, it is this portion of the cornea that overlies the entrance pupil. Secondly, the Stiles-Crawford effect states that when light of equal intensity passes through various points of the pupil, it is not perceived as being equally bright. Enoch (1958) showed that the more peripheral the ray of light entering the eye, the less the perceived brightness. Therefore, owing to the anatomical location of the central corneal zone and the Stiles-Crawford effect, the central corneal zone has the most significance in the determination of visual acuity.

The central cornea has sometimes been referred to as the apical zone and it represents that area in which the central refraction varies by less than 0.25D (Mandell et al, 1971). The terms apical zone should be reserved strictly to describe the location of the corneal apex. There is a wide variation in central corneal curvature within the general population, however, a mean keratometric value of 7.80mm ±0.25mm within the Caucasian population was found by Clark (1973a,b) and later confirmed by Ruben (1975). Guillon et al (1986) presented values in terms of the two principal meridians. The mean keratometric values were 7.856 ±0.254 (range 7.24-8.49) for the flattest meridian, and 7.692 ±0.256 (range 7.02-8.31).

1.4.3 The Paracentral Cornea

The paracentral zone is an annulus of approximately 4-7mm and extends 7-8mm across the diameter of the cornea (Waring, 1989) (see figure 1.03). It may also be known as the mid periphery of the cornea and represents a relatively spherical zone which is generally flatter in radius than the central portion of the cornea (Waring, 1989).

1.4.4 The Peripheral Cornea

In the majority of normal corneas, the peripheral radius of curvature flattens (Guillon et al, 1986). The peripheral zone is roughly a 7-11mm annulus (see figure 1.03). Townsley (1970), for the first time, reported the shape of human corneas from a sample of 350 patients. Peripheral corneal shape was modelled on an ellipse and described numerically using a term known as the eccentricity (defined in section 1.6.1). This term describes the rate of change in peripheral radius (a more detailed decription is provided in section 1.6.1). A mean eccentricity of 0.5 (a flattening ellipse) was found by Townsley (1970). Unfortunately, only 91 of the 350 patients could be said to be representative of the normal population. At present, the largest study is that conducted by Bibby (1976). With 2100 patients, Bibby (1976) found the peripheral cornea to resemble a flattening ellipse of mean eccentricity 0.387.

Guillon et al (1986) found a mean p-value of 0.83 ±0.13 (or an eccentricity of 0.41) with a range of 0.21 - 1.2 for flat meridians and 0.81 ±0.16 (or an eccentricity of 0.44) with a range of 0.11 - 1.16 for steep meridians. The term p-value has been shown to be uniquely related to the eccentricity as $p=1-e^2$ (Bennett, 1968). It is worth noting that a shape factor greater than 1 was found, indicating a steepening ellipse and also a large variation within the normal population. The peripheral zone therefore exhibits the most drammatic change in shape where the corneal profile deviates from a relatively spherical profile to an elliptical curve.

1.4.5 The Limbal Zone

The limbal zone marks the junction between the cornea and the sclera, otherwise known as the corneoscleral junction. The limbal annulus measures approximately 0.5mm. With respect to measuring corneal topography, this zone is of least significance as most of its topography will be masked due to disturbances in the tear film.

1.4.6 Defining points on the corneal surface

It is important to be able to locate and describe a point on the corneal surface and therefore some form of arbitrary notation is required. Having described some important landmarks such as the geometrical centre, a numerical system to locate a specific point on the cornea is required. Viewing the cornea from the front, it may be radially dissected through its geometrical centre into 180 meridians. An unknown point may then be located by its meridian (e.g. 90° superior or 180° left) and its distance along that meridian from the geometrical centre (see figure 1.04).

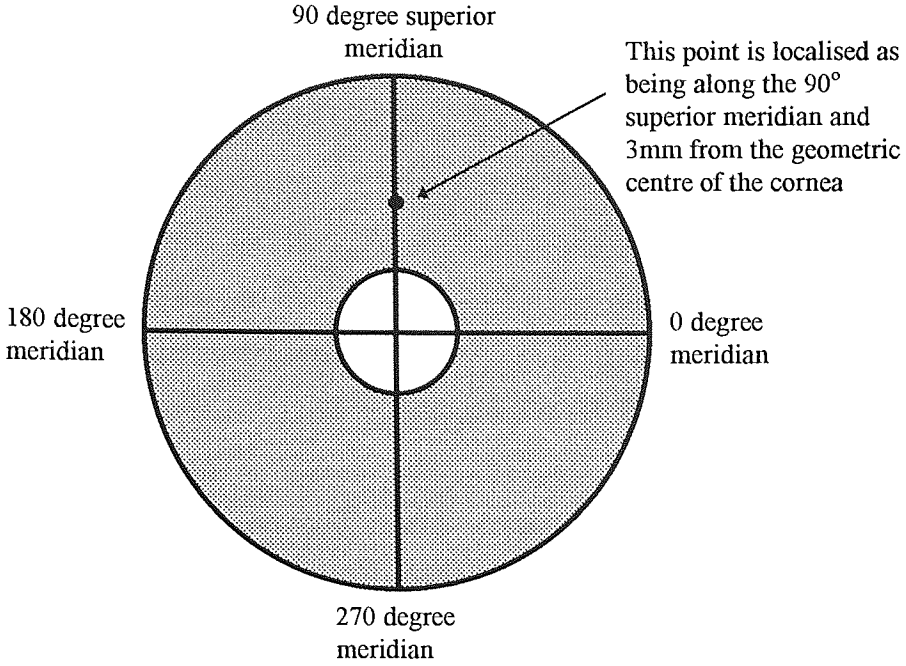

Figure 1.04: Notation used when localising a point on the corneal surface.

1.5 Qualitative descriptors of corneal topography

Once the three dimensional structure of the cornea has been derived, methods must be devised where the numerous data points may be presented in a clear and concise manner. The earliest qualitative descriptor of corneal topography was the Placido disc, where the image of a ring shaped target provided the user with information regarding the degree of corneal toricity, corneal apex position and peripheral corneal shape. More recently, with the development of computerised videokeratoscopes, investigators have been able to create more sophisticated qualitative descriptors. Some of these descriptors are described below.

1.5.1 Classification Of Topography With Contour Maps

Maguire et al (1987a) and Gormley et al (1988) have described the use of coloured isoptor contour maps in order to schematically present data obtained from topographical systems. A variety of colours are used to denote the sagittal power distribution across the entire cornea. Klein (1993) showed that the algorithms used in the calculation of corneal power are incorrect for areas outside the paraxial zone

because the formulae do not account for spherical aberration. Therefore, these maps are more useful qualitatively rather than quantitatively. Numerous patterns may be observed that may be used to describe certain forms of corneal topography. Bogan et al (1990) further simplified these by describing them as round, oval, symmetrical bowtie, asymmetric bowtie and irregular. In their classification scheme, Bogan et al (1990) used the shapes formed by colour coded contour maps in the paracentral and central corneal zones to define specific patterns (see figures 1.05 and 1.06). The paracentral and central areas of the cornea were used because they are the most important optically and also because these are the areas measured most accurately by the Corneal Modelling System (Hannush et al, 1989).

After observing the patterns from 216 eyes, Bogan et al (1990) defined these 'shapes' as follows:

- **Round:** When the ratio of the shortest to the longest diameter at the colour zone chosen for the pattern reading is two-thirds or more. This would represent an approximately spherical cornea as the change in power in the zone would not be significant.

- **Oval:** When the ratio of the shortest to longest diameter at the colour zone is less than two-thirds. This would represent an approximately spherical cornea; there is no detectable difference between oval and round patterns in terms of refraction and keratometry. One possible reason for this could be that keratometry only measures the central 3 - 4 mm of the cornea and this may not be a large enough area to detect any differences in astigmatism for the two patterns. Round and oval patterns accounted for 43.4 % of the patterns observed by Bogan et al (1990).

- **Symmetric Bowtie:** This pattern represents regular astigmatism. For a pattern to be classified as a symmetric bowtie there must be a central constriction in the outline of the colour zone from the colour coded contour maps. Also, the ratio X_0/X_1 or X_0/X_2 must be one-third or less and the ratios X_1/X_2 and Y_1/Y_2 must be

two-thirds or more (where Y represents the radius of the long axis of the bowtie and X represents the diameter of each half of the bowtie perpendicular to the long axis). Bogan et al (1990) found a statistically significant difference in the level of astigmatism between symmetric bowtie patterns and the round or oval patterns.

Figure 1.05: shows the five patterns observed in colour-coded topographic maps of normal eyes as described by Bogan et al (1990).

- **Asymmetric Bowties:** These patterns are very similar to symmetric bowtie patterns in that there is an area of constriction in the bowtie and the ratio of X_0/X_1 or X_0/X_2 is one-third or less. However, the difference in classification is that the ratio of X_1/X_2 and/or Y_1/Y_2 is less than two-thirds. Statistically significant differences between symmetric and asymmetric pattern astigmatism have been found and are attributed to factors such as eccentric fixation, corneal apex position, contact lens wear and radial asymmetry in the rate of change of peripheral curvature. Bowtie patterns accounted for 49.6 % of patterns observed by Bogan et al (1990).

- **Irregular:** No clear pattern can be identified according to the above criteria. Bogan et al (1990) found 7.1 % of subjects with this type of pattern, however, no sign of corneal disease in these people was observed. It is possible that tear film disturbances could cause this type of irregularity.

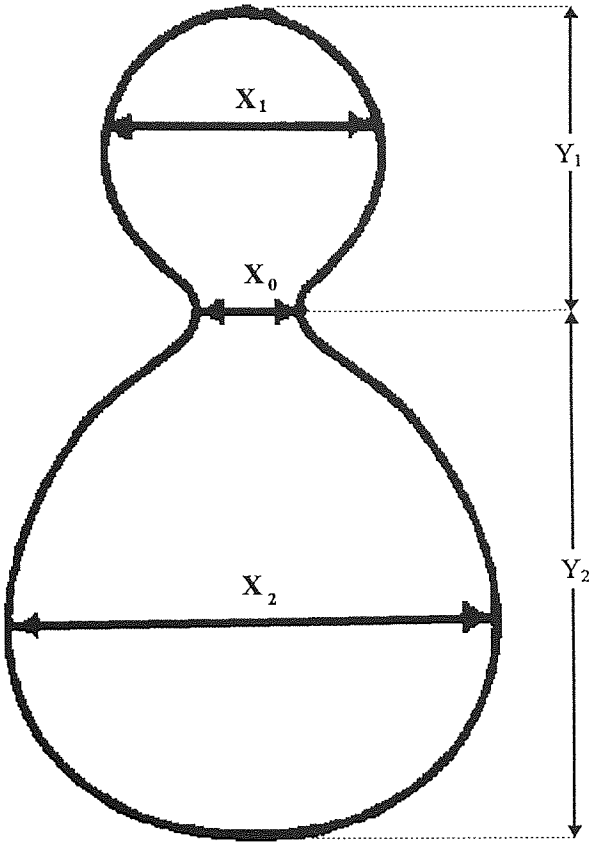

Figure 1.06: Shows classification of bowtie patterns as symmetrical and asymmetrical, based on specific ratios.

1.5.2 The Photogrammetric Index Method (PIM)

Cohen et al (1984) calculated several numerical indices that describe the pattern of keratoscopic ring shapes as they depart from circularity and also the pattern of several ring shapes from an individual cornea. Contrary to describing corneal power and radius, the numerical indices differentiate between symmetrical, regularly astigmatic and keratoconic corneas. Numerous indices are calculated, each ring index will now be described. The eccentricity (E) is simply calculated as the minor chord length divided by the major chord length (see figure 1.07). Angularity (A) assesses the angle between the major and minor chords, the measured angle is scaled such that 90° would be 1 and acute angles would be close to zero. Another indice of a particular keratoscope ring is the major symmetry index (SM_o). The index is the shorter length divided by the longer length of the major chord segments created by intersection of the

minor chord. The minor symmetry index (SM_a) is comparable to SM_o except that it relates to the minor chord.

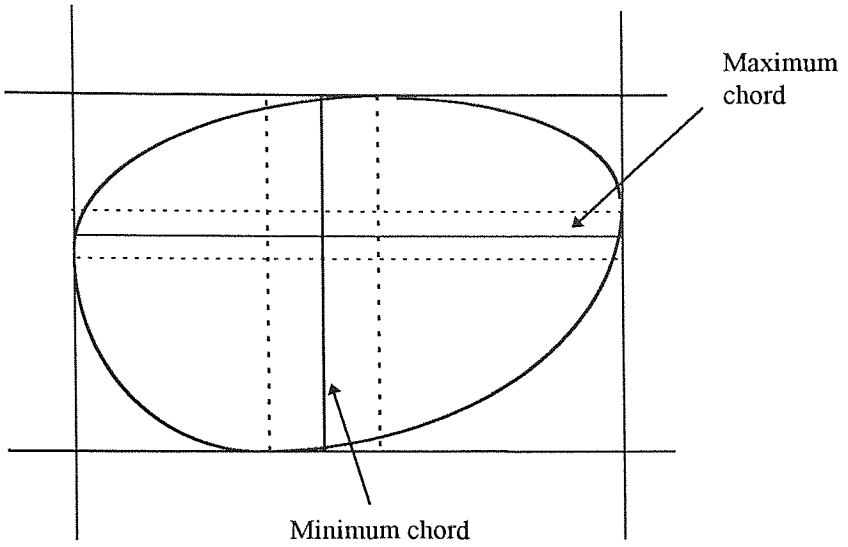

Figure 1.07: Major and minor chords, the looped profile represents a single keratoscope ring image.

Another three indices were also developed that combine the chords of all the rings of the keratograph. The angle cluster and distance cluster (C_A and C_D) are a measure of consistency. Angle cluster is the standard deviation of the angle between each chord and a reference line, it represents the consistency of chord directions. The distance cluster describes the trend of each chord to pass through a common point. The final whole eye index is the trend index (T). The trend index is the correlation (Spearman Rank) of each ring for each individual ring index (i.e. eccentricity, angularity etc.).

In order to validate these indices, Cohen et al (1984) assessed the indices on 30 eyes from a group of twenty subjects. The thirty eyes were then grouped into three astigmatic groups:- symmetrical (S), comprising six right and four left eyes in which the keratometer readings for the principle meridians were equal; regular (R), comprising five right and five left eyes with regular astigmatism > 0.5D. The final group (a keratoconic group, K) comprised of five right and five left eyes diagnosed according to defined clinical criteria. The eccentricity index successfully differentiated between the three groups. The symmetry indices were also able to distinguish between the keratoconic and other groups. However, angular indices for the regular

astigmatism and keratoconic groups showed no difference between the angular separation of the major and minor chords. Thus, the angular index was not capable of distinguishing between keratoconics and regular astigmatism. Angular cluster correctly distinguished between the symmetrical and regular astigmatic groups for the minor chord (showing greater variability for the symmetrical group). Distance cluster variability for the minor chord showed greater variability for the keratoconic group than the symmetrical and regular astigmatic groups. The results therefore showed that the combined use of all the proposed indices is a useful way of differentiating between different corneal forms. However, a study involving a larger sample should be performed in order to calculate 'normal' values for each group.

There are unfortunately two drawbacks of the PIM method of quantitative corneal topographic classification. Firstly, the number of indicies makes it difficult for the clinician to obtain a clear picture of the corneal shape: particularly as within their study some of the indices rendered conflicting results. Ideally, the PIM method should provide the clinician with a single index that carefully weights the values of all the indices calculated. Secondly, only twenty patients were used and yet thirty eyes were measured, it is therefore possible that statistically the results were biased because of any similarities in corneal shape between the two eyes in the same patient.

1.5.3 The surface regularity index and surface asymmetry index

Computer algorithms may be derived in order to calculate indices which complement the data from contour maps. Two such indices, the surface regularity index and the surface asymmetry index have been derived and assessed in a clinical study by Dingeldein et al (1989) and Wilson et al (1991a).

The surface regularity index (SRI) determines the central corneal optical quality, it is a measure of localized surface regularity. The lower the value of this index the smoother the surface. Thus, for a perfectly smooth surface a theoretical value of zero would be found. However, in practice this is not possible due to instrument errors. Wilson et al

(1991a) found a high correlation between the SRI and best corrected spectacle acuity ($r=0.8$, $p<0.001$) in 31 eyes which met their criteria for inclusion. Clinically, the SRI may be used to differentiate between reduced visual acuity due to factors other than corneal topography.

The surface asymmetry index (SAI) determines the asymmetry of the central corneal surface power. The value represents the centrally weighted summation of differences in corneal power 180 degrees apart over 128 equally spaced meridians. For a perfectly regular surface, such as a sphere, a theoretical value of zero would be found. Again, due to instrument errors, this is not the case. Dingeldein et al (1989) found a reasonable correlation between SAI and best spectacle corrected visual acuity ($r=0.76$, $p<0.001$) in 39 eyes with keratoconus, compound myopic astigmatism, epikeratophakia and 2 corneas from patients with 20/20 vision. The differences in values of SAI for normals and those with keratoconus with best corrected spectacle acuity of 20/20 were statistically significant ($p<0.001$). In a more recent study by Wilson et al (1991a), a relatively low correlation was found between this index and best corrected spectacle acuity ($r=0.62$, $p<0.005$). This discrepancy may be due to the relatively small sample sizes. Clinically, the SAI may be used as a quantitative indicator for monitoring changes in corneal topography. The derivation of these indices is described in the article by Wilson et al (1991a). They suggest that the incorporation of these indices would be a useful tool when combined with colour coded maps for the assessment of corneal topography.

1.6 Quantitative descriptors of corneal topography

For purposes such as contact lens fitting and surgical modification of the corneal surface, accurate knowledge of the corneal surface parameters is essential. Qualitative assessment is of use only to summarise the enormous amount of data derived from corneal topographic systems. However, quantitative descriptors in the form of mathematical functions may also be used to describe the corneal surface whilst allowing the practitioner to retain the concrete information provided from

videokeratoscopy. Details of some of these mathematical descriptors are provided below.

1.6.1 Corneal Radius and Shape

The radius of curvature of the anterior corneal surface and its refractive index determine the power of that surface. The smaller the radius the greater the refracting power of that surface. The apical radius of the cornea defines the size of the corneal profile. Guillon et al (1986) showed a wide variety of corneal shapes within the normal population. Therefore, mathematical descriptors that show a continuous change in curvature would more accurately model the shape of the cornea. It appears that descriptions have taken two separate forms; certain researchers have provided precise descriptions using complex polynomial formulae (Howland et al, 1992), whereas others have approximated corneal contour to conic sections (Townsley, 1970; Townsley, 1974; Bibby, 1976; Guillon et al, 1986). Generally the results of these studies have shown that modelling the corneal surface in terms of second order polynomials is acceptable. The family of second order polymonials curves that are used as desriptors of the cornea are known as conics. Mathematically, they are defined as follows:

$$\frac{x^2}{a^2}+\frac{y^2}{b^2}=1 \qquad \textit{Equation 1.01}$$

where a and b are the semi major and semi minor axes respectively. x is the sagittal depth at a chord length of y.

The family of surfaces and curves that may be derived from a cone (a solid surface produced by the revolution of either of two straight lines meeting at a point about the other) are defined below:

- **Conicoids**: On rotating conic sections about an axis symmetry, one produces surfaces known as conicoids.

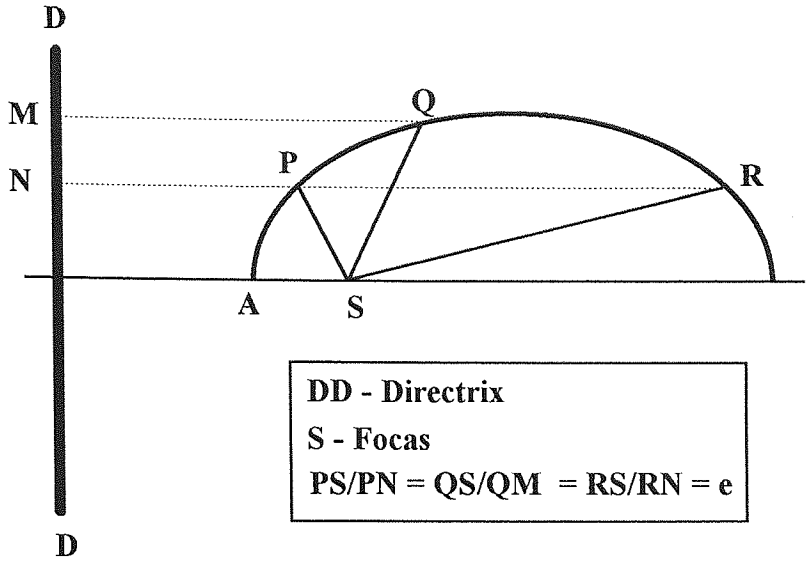

Figure 1.08: Defines a conic section. Bennett (1968) has defined a conic section as follows: conic section is considered as the locus of a point which moves such that its distance from a fixed point S, bears a constant ratio from a fixed straight line, the directrix (DD).

- **Conic Sections**: Bennett (1968) has geometrically defined a conic section as 'the locus of a point which moves such that its distance from a given fixed point, the focus, bears a constant ratio from a fixed straight line, the directrix (see figure 1.08). This ratio is termed the eccentricity (e) and may have any numerical value.

In addition, Baker (1943) also derived an equation to describe a conic section :-

$$y^2 = 2r_0x - px^2 \qquad \textit{Equation 1.02}$$

where x and y are the Cartesian co-ordinates (the origin is conveniently placed at the corneal apex), r_o is the radius of curvature at the apex, p is an index of peripheral flattening and indicates the level of asphericity. For example, $p < 0$, hyperbola; $p = 0$, parabola; $0 < p < 1$, prolate (flattening) ellipse; $p = 1$, sphere; $p > 1$, oblate (steepening) ellipse. As well as detailing the derivation of equation 1.02, Bennett (1968) also showed a direct relationship between p and e where,

$$p = 1 - e^2 \qquad \textit{Equation 1.03}$$

The advantage of Baker's and Bennett's notation is that the formula is simplified and it is capable of describing all conic sections. Furthermore, by changing the values of r_o and p, all conicoids are described. A simple mathematical relationship can be shown to link equations 1.01 and 1.02:

$$r_o = \frac{b^2}{a} \text{ and } p = \frac{b^2}{a^2} \qquad \textit{Equation 1.04}$$

In summary, the cornea can be described in mathematical terms using conic sections, the formulae derived by Baker (1943) and Bennett (1968) permit the cornea to described simply and effectively.

1.6.2 High Order Polynomial Descriptors

The corneal surface is a complex shape, in order to describe it mathematically high order polynomial expressions may also be used to describe its shape. A study by Howland et al (1992) attempted to describe corneal shape in precisely this manner. Using the Corneal Topographic Modelling System (TMS) (Computed Anatomy Inc., New York), 4th order polynomial expressions from the Taylor series were fitted to corneal surface coordinates. From these expressions the mean corneal curvature (MCC) at any point on the surface was computed and compared with the measured curvature derived from the TMS.

Howland et al (1992) concluded that polynomials captured gross features of curvature but did not resolve fine details. However, from their study they suggested that the use of polynomial fitting could form a classification scheme for describing corneal topography.

1.7 Summary

The human cornea is a tranparent, avascular five layered structure. Its shape has been shown to be highly variable within the normal population (Guillon et al, 1986).

Descriptions of corneal topography have taken two forms. Qualitative descriptors such as colour coded maps (where the sagittal power distribution of the cornea is denoted by a colour), and numerical indices, such as the PIM, SAI and SRI indices, have been used to summarise the enormous amount of data from topography systems. Quantitative descriptors of the cornea have applied mathematical functions to fit topographic coordinates. The use of conic sections has been the most commonly used mathematical function in corneal profile curve fitting.

Chapter 2 describes the various instruments used in deriving corneal topography.

Chapter Two

Past and Present Techniques Used In the Assessment of Corneal Topography

2.1 Introduction

The cornea is the most powerful refractive surface of the eye accounting for almost two-thirds of its total dioptric power. The importance of accurate measurement of the corneal contour has been appreciated for many years in the fields of contact lens design, computerised ray-tracing and ophthalmic surgery. More recently, with the development of modern day computer systems, researchers have been able to the process large amounts of information that has enabled the reconstruction of the cornea using detailed models. The present chapter has therefore been written to provide a review of the current principles and techniques used in resolving the topographical structure of the corneal surface.

Numerous methods have been proposed in order to calculate the topography of the cornea. However, the success of these methods ultimately depends on their accuracy, repeatability and ease of use. The accuracy of an instrument may be defined according to the tolerance that is expected when the instrument is to be used for a clinical function. For purposes such as contact lens fitting, Stone (1962) has stated that the radius of curvature should be measured within ± 0.02mm. Table 2.01 shows how the expected accuracy of radius of curvature was derived by Stone (1962).

Repeatability, on the other hand, may defined as the ability of an instrument to reproduce the same measurement on two independent occasions when no change in the structure to be measured has taken place.

Table 2.01: Expected accuracy of radius of curvature as derived by Stone (1962).

2.2 Keratometry

In optometric practice, the keratometer is the most frequently used instrument to measure the central radius of curvature of the anterior corneal surface. The principle utilises the reflecting properties of the cornea so that when the size of the reflected image (of a mire object) is measured, the central radius the cornea is determined. The cornea thus acts as a convex mirror producing a virtual image behind the corneal surface. The optical principles are shown in figure 2.01.

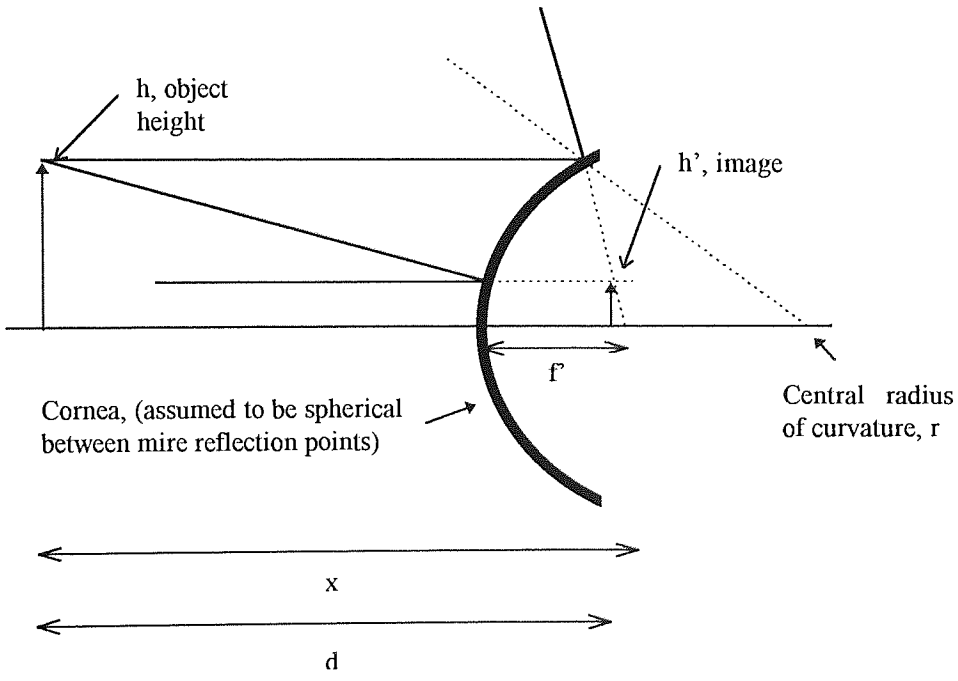

Figure 2.01: shows the optical principle of the keratometer. f' is the focal distance of the surface. d represents the object to image separation and x the distance from the object to the focus of the surface. The cornea is assumed to be spherical between the reflection points at the cornea.

From similar triangles the following equation can be derived:

$$\frac{h'}{h} = \frac{f'}{x} - \frac{r}{2x} \qquad \textit{Equation 2.01}$$

Thus, as linear magnification (m) is ratio of the image to object heights,

$$r = -2mx \qquad \textit{Equation 2.02}$$

In practice, d is large and may be approximated to x. Equation 2.02 may therefore be rewritten as

$$r = -2md \qquad \textit{Equation 2.03}$$

Owing to involuntary eye movements, the value of h' is difficult to determine, therefore, a doubling prism was introduced such the operator would simply have to measure the separation of the reflected object mires to determine the size of the reflected image. In this manner, the effect of errors due to poor fixation were reduced.

Figure 2.01 also shows that the central corneal radius is being measured between two points. Thus, the assumption is made that the central radius of curvature of the corneal surface between these two points is spherical. Although the magnitude of this error is small for measurements close to and on either side of the optical axis, it still exists and will invariably depend on how much the shape of the cornea deviates from that of a spherical surface. Measurements of peripheral corneal radius cannot be accurate using the keratometer due to the aspheric nature of the corneal surface (Stone, 1962).

Further errors in determining the central radius of curvature were discussed by Littman (1951), who suggested that the primary cause of any inaccuracies were due to incorrect focusing of the eyepiece of the instrument. When an eyepiece is incorrectly focused, the whole instrument has to be repositioned in order to view the reflected image of the mire clearly. As a result two errors occur. Firstly, a change in working distance inevitably alters the size of the reflected mires, thus the operator must adjust the mire separation. Secondly, in instruments where the doubling prism is placed between the eyepiece and the objective lenses of the keratometer, the amount of

doubling alters with the distance of the objective lens to the image. To eliminate the first error, the mires are collimated as this prevents any change in image size. The second error is eliminated by placing the doubling prism at the focal point of the objective, this is known as the telecentric principle.

Modern day electronics have led to some manufacturers developing automated keratometers. The use of electronic systems has enabled manufacturers to overcome some of the optical problems encountered in the design of keratometers. Two examples of automated keratometers will be discussed -the Canon Autokeratometer (Cannon USA Inc.) and the Humphrey Auto Keratometer (Allergan Humphrey).

The Canon Autokeratometer K-1 uses a ring target that is reflected from the cornea and focused by an objective lens (Goss et al, 1991). As opposed to an eyepiece system, a television monitor is used to view the reflected image; the use of a monitor eliminates the errors introduced from inaccurate focusing of the eyepiece.. The ring image is split into five images in the optical system and photodetectors are used to detect the separations of the rings in all five meridians. From the separations of the rings, the radius of curvature is calculated in each meridian and the principal meridian located. The instrument can measure up to 7D of astigmatism. Peripheral measurements can also be made by asking the patient to view peripheral fixation targets.

The Humphrey Auto Keratometer measures corneal radius in 3 locations by projecting 3 beams of light from an infra-red light emitting diode onto the cornea in a triangular pattern (Goss et al, 1991). The light from the L.E.Ds passes through a condensing lens system and a rotating chopping disc. The purpose of the disc is to modulate the illuminating sources. Light then passes through a series of apertures and a lens system, finally, an image is formed behind the corneal surface. Directional photodetector amplifiers are used to detect light which is at a specific angle from the optical axis of the instrument. The signals from the photodetector amplifiers are converted into digital values from which the radius of curvature is calculated.

The Humphrey Auto Keratometer can be used to measure peripheral radius of curvature by asking the patient to view peripheral fixation targets. The instrument uses the central and peripheral radii measurements to calculate the position of the corneal apex, the shape factor (Wesley-Jessen shape factor, e^2, see section 1.6.1 for a definition of e), the corneal vault height (which is the sagittal depth of the cornea at the apex) and the refractive power of the cornea at the line of sight (defined in section 2.6.1) and the corneal apex.

In a clinical trial by Tate et al (1987), two autokeratometers (the Canon and Humphrey autokeratometers) and a manual keratometer (the Javal Schiotz by Haag-Streit), were assessed in terms of their accuracy and reproducibility for spherical surfaces and 24 eyes. All three instruments showed a high level of accuracy and reproducibility.

2.3 Eye Impressions

Producing an impression of the eye would appear to be the most obvious method of determining the contour of the whole cornea. Unfortunately, there are limitations to this technique as the inevitable result of introducing impression material into the conjunctival sac is corneal deformation. Lid pressure also has an effect on corneal topography and therefore the final mould. Furthermore, corneal insult is likely and measurement of the cast is difficult (another error is introduced due to shrinkage of the cast material). Therefore, in view of these drawbacks, the technique of eye impressions is no longer considered a suitable technique in determining corneal topography.

2.4 Keratoscopy

Keratoscopy has for decades been used to determine the contour of the anterior corneal surface by observing the reflected image of an object. Various forms of keratoscopes have been developed since the first keratoscopic disc by Placido in 1880. The Placido disc is a simple hand held instrument used for observation rather than

actual measurement of corneal contour (see figure 2.02). The following valuable information may be found:-

- Whether the central portion of the cornea has marked toricity.
- The approximate location of the principal meridians of a toric cornea.
- Whether the cornea flattens in the periphery or steepens, and the approximate degree to which this occurs.
- Whether the changes in peripheral curvature are symmetrical in all meridians.
- Whether there are any localised surface irregularities.
- The approximate position of the corneal apex with respect to the line of sight.

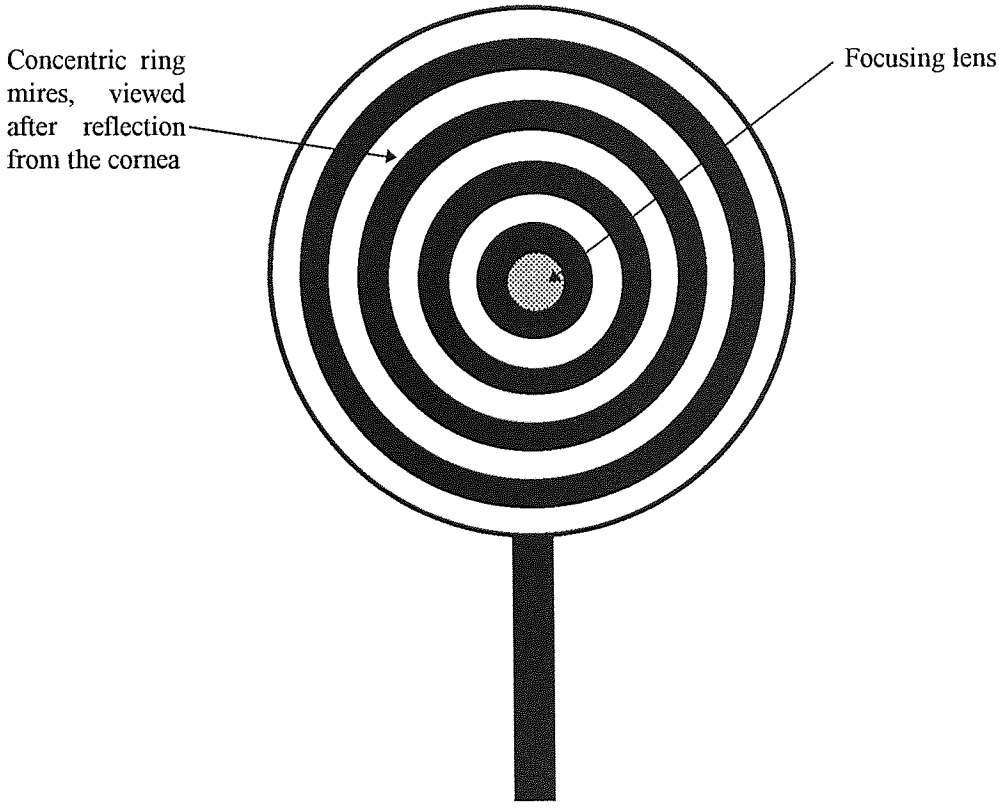

Figure 2.02: Concentric ring target used in the Placido disc.

Information of this nature would be of great use in clinical practice, particularly if a hard copy could be made such as a photographic recording. Gullstrand (1966) was one of the first investigators to introduce the photokeratoscope. Many new designs have since emerged all of which have attempted to measure a larger area of the cornea

by utilising various shaped targets. Gullstrand (1966) used a plane object surface, which prevented larger areas of corneal surface from being measured. Nevertheless, he found that the normal individual had a smooth corneal surface that flattened away from the corneal apex. Later, using a flat object of tangential design, measurements of up to 7mm in diameter were obtained (Fincham, 1953). Knoll et al (1957) used a hemispherical or cylindrical object surface that enabled an area of 10mm of corneal surface to be measured. The advantage of using an object of hemispherical design was that the size of the target was much reduced, thus making the instrument less bulky (see figure 2.03).

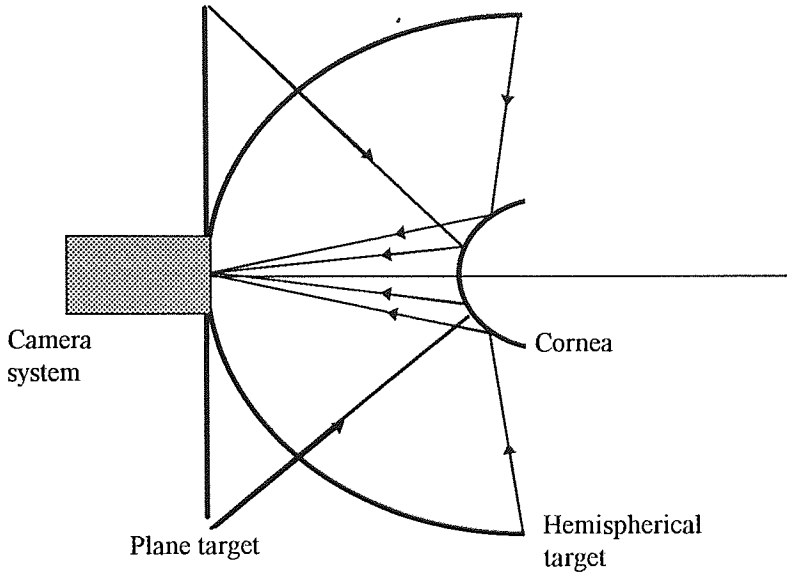

Figure 2.03: the difference in area of corneal surface measured for a plane target and a hemispherical target.

Ludlam et al (1966) considered the limitations of the photokeratoscopes at that time. Three suggestions were made from their study:-

- The image plane (located behind the cornea) should be flat. This point is particularly important with respect to the design of a target for the following reason: if the image lies on a curved image plane then there will be one point of focus on the flat plane of the photographic film. Ludlam et al (1966) found that for an ellipsoidal target surface, the image from a spherical reflecting surface lay on a

flat plane. The seven target rings of the Wesley-Jessen photoelectric keratoscope are arranged in the manner described by Ludlam et al (1966).

- The analysis of the data should be detailed and accurate. Numerous methods have been adopted to calculate the parameters describing the corneal profile, the various techniques are discussed in chapter 3.

- There should be accurate and reproducible alignment of the patient's line of sight with that of the instrument. Accurate alignment is necessary in order to position the vertex normal of the cornea (that point on the corneal surface that is perpendicular to the keratoscope axis when the subject is viewing the fixation target) relative to the line of sight. Alignments systems are discussed in section 2.6.1.

More recently, computers have been used to analyse the data supplied from the photographic image of the corneal surface. Known as computer-assisted photokeratoscopy, it has been used for clinical applications such as contact lens fitting. Bibby (1976) has described a system (Wesley Jessen PEK Mark IIIA) of this type for the use of contact lens design.

Bibby (1976) stated the technical requirements for reliable photokeratoscopy as:

- the units to describe corneal topography must be independent of the shape being measured.
- The instrument should measure the total area of interest.
- All information should be acquired simultaneously.
- The technique should have high accuracy and reproducibility.

If one accepts the above technical requirements then it is possible to assess the suitability of other techniques. Thus, applying the first requirement, instruments such as the keratometer that only measure central radius of curvature make the assumption

that the surface being measured is spherical. This is not true for the cornea which has been shown to be best approximated to a conic section (Bibby, 1976; Guillon et al, 1986). Further, keratometry does not fulfill the second requirement because only the central three millimetres of the corneal surface is measured. In order to measure larger areas of the surface, the keratometer requires the use of an accessory device (the topogometer) which involves repeated measurement and the additional inaccuracy of asking the patient to alter fixation to another point (see third requirement).

The Wesley Jessen photoelectric keratoscope consists of seven concentric rings on an ellipsoidal surface, this permits the analysis of the central 9mm of the cornea from which an enlargement (X50.8) of the reflected image is made (Bibby, 1976). The computer then begins its analysis in order to determine the shape of the cornea. A device, similar to a densitometer head, is moved over the projected image to locate position of the reflected rings on the photograph. Bibby (1976) stated that the positional accuracy of the densitometer in locating the reflected rings is 1/360mm. Data from a number of points is then taken along a specific meridian, from this the central radius of curvature and the 'shape factor' are calculated.

The term 'shape factor' describes the degree of peripheral flattening. Bennett (1968) described this term mathematically as $1\text{-}e^2$ where e is the eccentricity (defined in section 1.6.1). The shape factor referred to by Bibby (1976), the Wesley-Jessen shape factor, is e^2. The Wesley-Jessen system occasionally produces a negative value for shape factor which is not mathematically possible for the square of a real number.

A variety of corneal topographic systems are available, a description of the past and present systems based on the principles of keratoscopy are now presented.

2.5 The Autocollimating Photokeratoscope

As its name implies, the autocollimating photokeratoscope (Wesley-Jessen IIIA PEK) was a keratoscopic device that captured the image of reflected ring targets on a

photographic film. The primary advantage of this instrument over its predecessors was that it was capable of accurate alignment. Basically, light from a neon fluorescent source (see Figure 2.04) was reflected through a series of mirrors and fine apertures such that when light was incident normal to the corneal surface, it would be reflected back along its original path a process known as autocollimation. Under this condition the observer would see a dark centre spot with a bright surround. By reducing the depth of field, errors were further reduced. Thus, measurements were only performed when the line of sight was coaxial with the optic axis of the instrument and light was normal to the cornea.

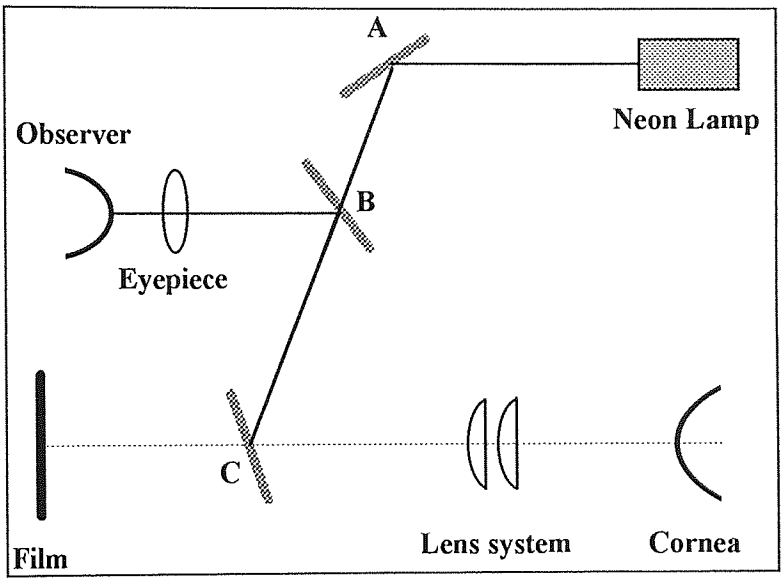

Figure 2.04: Shows a simplified version of the mirror and aperture system used to increase accuracy and reproducibility during the alignment procedure. Light from the neon source reflects off mirror A to B, this mirror also has a small pinhole through which the light travels to mirror C where light is reflected to the cornea. If at this point the light incident on the corneal surface is normal to it, then it will be reflected back along its own path (there is however some divergence) and some of the light travels to the photographic film and some back to mirror B which reflects it to the observer.

The accuracy of the system, according to instrument manufacturers, was within 0.015mm for radius of curvature of 3 known spherical steel balls (Bibby, 1976). Clark (1974) performed extensive validation tests on the autocollimating photoelectric keratoscope with actual aspheric and displaced spherical surfaces. Errors in

asphericity 'at the edge of the observed field of approximately 4 micro-metres' were found. Unfortunately, Clark's definition of asphericity was not in accordance with the standard terms used by Bennett (1968), Bibby (1976) and Guillon et al (1986). Clark (1974) defined asphericity as the departure of the actual surface normally from the reference spherical surface. In clinical terms this value is difficult to interpret. Townsley (1974) compared the accuracy of the photokeratoscope on non-spherical and spherical surfaces. After the values were compared with those obtained from mechanical measurements, he found that the mean sagittal depth reading fell within 0.002mm of the mechanical reading out to a semi-chord of 4.5mm for spherical and non-spherical surfaces. Again, the units used do not provide a clear indication of the accuracy of the instrument in clinical terms.

2.6 Computer-Assisted Videokeratography

Computer-assisted videokeratography combines the principle of keratoscopy with computerised image analysis and data processing using personal computers (Gormley et al, 1988). Examples of commercially available systems are the TMS-1 (Computed Anatomy), EyeSys Corneal Analysis System (EyeSys Laboratories), MasterVue Smart Topography (Optical Radiation Corporation, California, U.S.A) and C-Scan Colour-Ellipsoid-Topometer (Technomed Technology, Baesweiler, Germany).

With the development of computer hardware in terms of both processing speed and storage capacity, the number of points analysed on the corneal surface has increased dramatically. The number of rings and points of analysis are chosen in order to provide adequate resolution of the corneal surface (the TMS-1 has 22 rings, 256 points are digitised along each mire; the CAS has 8 rings, 360 points are digitised at the centre and periphery of each ring, the MasterVue has 20 rings with 360 degree semi meridian analysis and the C-scan has alternating coloured rings with a maximum of 11520 point analysis). Images obtained from the videokeratoscopes are digitised and topographic data points are extracted in polar coordinates. Various forms of

presentation of this data are available such as colour coded dioptric maps, photokeratoscopic images, wire mesh models and solid models.

A significant amount of research has taken place regarding the accuracy of modern computer-assisted keratoscopic devices on test surfaces (Hannush et al, 1989; Koch et al, 1989; Hannush et al, 1990; Koch et al, 1992). The results show an acceptable level of accuracy and reproducibility. Hannush et al (1989) found measurements to be within 0.5D in 76% of the readings on human corneas for rings 2 through to 13 for the TMS. In a study by Koch et al (1992), the mean absolute differences between the keratometer and the EyeSys in terms of power were 0.19D and 0.21D for the steep and flat meridians, respectively. Tsilimbaris et al (1991) found a clinically significant difference between the EyeSys and Javal keratometer when measuring astigmatic eyes with a cylinder greater than 1.50D. A mean difference of 0.84D was found but only 18 eyes were measured. Tsilimbaris et al (1991) suggested that a possible explanation could be poor focusing on one of the two astigmatic meridians.

Antalis et al (1993) compared the EyeSys (CAS) and the TMS-1 in terms of central corneal curvature in 18 eyes with a variety of corneal conditions. The average differences for the two instruments were -0.2 ± 0.7D for the flat central meridian and -0.7 ± 0.9D for the steep central meridian. Correlations for the two instruments were 0.9901 and 0.9937 for the flat and steep meridians, respectively. Both instruments were also found to correlate relatively well with the keratometer (correlation coefficient, r, 0.9617 and 0.9844). The use of correlation coefficients to compare the agreement of instruments is not an appropriate statistical test. Bland et al (1986) suggested that a plot of the difference of the two readings versus their respective means is a more accurate method.

Unfortunately, there are limitations of the keratoscopic approach in the analysis of corneal shape. Firstly, as already stated by Ludlam et al (1966), the image of the target mires should lie on a flat plane. Even with the modification of the target plane, it is not possible to achieve this for all corneas because of the large variety of normal corneal shapes. Thus there could be errors induced from poor focus of different rings.

Secondly, it has been shown that slight decentration of the alignment and focus results in large errors in actual measurement (Nieves et al, 1992).

Various modifications in the design of instruments have a role in reducing errors due to poor focus and misalignment, these will now be discussed.

2.6.1 Design Factors

A. Working Distance

Working distance, mire size and the size and position of the reflected mire image are all intimately related. For example, as working distance decreases the influence of instrument alignment error will increase (Nieves et al, 1992; Antalis et al, 1993), however, the influence of facial anatomical factors is reduced. Using a micron positioner (a device used to accurately position a test surface with respect to the videokeratoscope axis), Nieves et al (1992) determined the effect of working distance on the accuracy of measurements found with the TMS and EyeSys videokeratoscopes for two acrylic spheres (r=7.1153mm and r=7.9497mm). The results showed that the EyeSys (which has a larger working distance) consistently measured the sphere to a higher degree of accuracy than the TMS for both frontal plane (x and y-axis) and axial (z-axis) misalignment (see figure 4.02 for definition of axes, section 4.3.1). Applegate (1992) pointed out that the working distance chosen by the manufacturers of the EyeSys and TMS probably represents two extremes of realistic values.

B. Defining a Reference Point for Corneal Modelling

Irrespective of manufacturer design, all videokeratoscopes at present use the same alignment principle (Mandell, 1992). The subject views a luminous fixation point, the image of which is viewed by the practitioner on the monitor. At this point, the subject's line of sight is coaxial with the instrument axis. Finally, the practitioner must then centre the reflected image of the luminous markers with respect to a reference

marker on the monitor. The final stage of alignment fulfills one of the assumptions and criteria for videokeratoscopy (stated in chapter 3):- that the instrument axis should be perpendicular to the cornea. The consequence of the alignment procedure is that the instrument axis may be perpendicular to any point on the cornea. Figure 2.05 shows the point of alignment with the cornea when the conventional procedure of alignment is performed. Definitions of the terms used are given below.

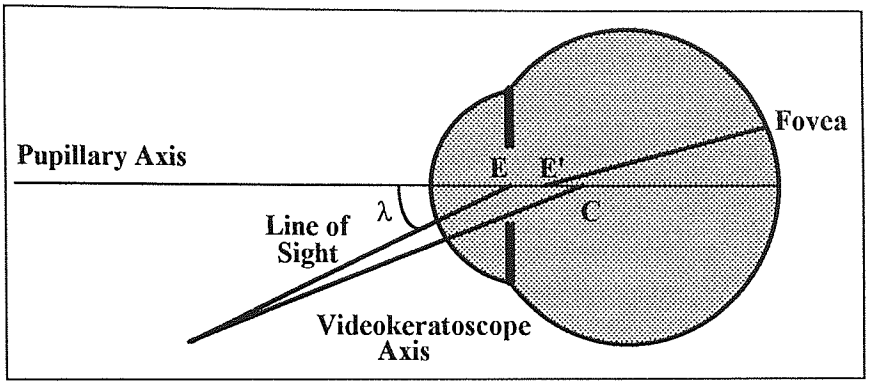

Figure 2.05: Shows the position of the various reference points and axes after alignment has been performed. E and E' are entrance and exit pupils respectively, C is the centre of curvature of the cornea. The videokeratoscope axis is aligned with an unknown point on the cornea.

- The entrance pupil is the image of the real pupil as formed by the optics in front of it. When light is directed towards the entrance pupil it will emerge through the exit pupil.
- The exit pupil is the image of the real pupil as formed by the optical components of the eye of behind the iris.
- The line of sight: is the straight line from fixation to the centre of the entrance pupil. A light ray passing along the line sight passes through the exit pupil to the fovea because the subject is actually fixating on the object. Hence, the line of sight specifies the beginning and end of a light pathway. The use of the entrance pupil has the additional advantage that it may be easily determined in a non-laboratory environment. The commonly used reference line known as the visual axis should not be used in videokeratoscopy (Mandell, 1992; Mandell et al, 1993). The visual axis is defined as the line from fixation that passes undeviated through the nodal

points to the fovea. As the nodal points cannot be determined in a clinical environment, the visual axis should not be used.

- The pupillary axis: is the line from the centre of the entrance pupil that is perpendicular to the corneal surface. The principal feature of the pupillary axis is that as it is perpendicular to the corneal surface, it must therefore pass through an instantaneous centre of curvature of the cornea.
- Angle lambda: is the angle formed at the intersection of the pupillary axis and line of sight. Angle lambda is present in most eyes and is due to the fact that the fovea is decentred slightly temporally with respect to the eye's axis of symmetry. As the fovea is decentred horizontally, angle lambda is greatest on the horizontal meridian.

Although after alignment, the optic axis of the instrument is perpendicular at a point on the cornea and is therefore directed towards the instantaneous radius of curvature, measurements are performed from an eccentric and unknown point. The point on the cornea from where measurements are performed with present videokeratoscopes is unique, however, as the measurements are centred about an unknown eccentric point, another method of alignment is required that would enable alignment with a suitable reference point.

Earlier investigators attempted to align the instrument axis with the corneal apex. Alignment with the apex was been performed using luminous cross targets (Ludlam et al, 1967), Moire targets (Mandell et al, 1971) and a small mire keratometer (Mandell et al, 1971). With the latter technique a keratometer was used to locate the corneal apex and the optic axis of the photokeratoscope was aligned perpendicular to this point. Unfortunately, this technique was time consuming and cumbersome. Alignment with the corneal apex is not suitable as its anatomical position does not necessarily relate to the line of sight.

From a clinical and functional view point, the ideal reference point would be the intersection of the line of sight with the corneal surface. Manufacturers of videokeratoscopic systems have recently updated instruments to locate the entrance

pupil on dioptric maps. Mandell (1992) described a simple modification to conventional videokeratoscope alignment where measurements are centred about a unique point on the corneal surface where the line of sight and the instrument axis intersect. This point is not as peripheral on the cornea as with conventional alignment procedures. Figure 2.06 summarises the modification as described by Mandell (1992).

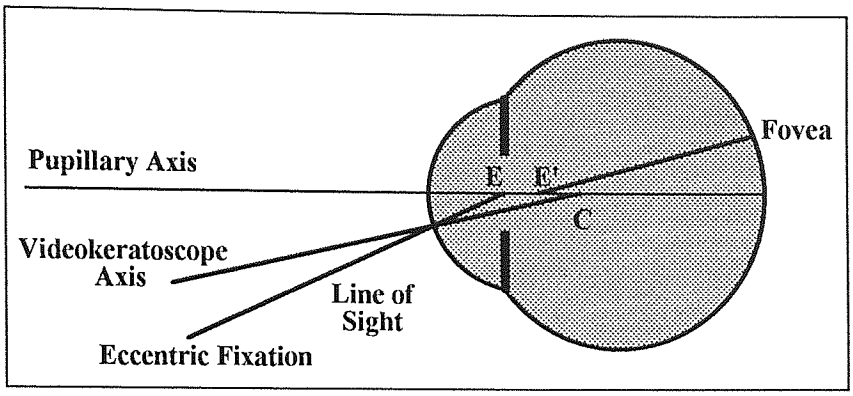

Figure 2.06: Alignment proposed by Mandell (1992) in order to align the videokeratoscope axis with the line of sight at the corneal surface.

Observation of figure 2.05 shows that from the videokeratoscope view, the monitor reference pattern will be displaced away from the centre of the entrance pupil. The reason for this is that the instrument requires the optic axis of the instrument to be perpendicular to the corneal surface. In figure 2.06, the subject is asked to view an eccentric target so that the monitor reference pattern of the videokeratoscope is placed in the centre of the entrance pupil as viewed in the monitor. Once this has been accomplished, the luminous fixation marker is then aligned with the monitor reference pattern. Observation of figure 2.06 shows that after alignment in this manner, the line of sight and the optic axis of the videokeratoscope intersect at a unique point on the cornea and measurements are centred about a point where the line of sight intersects the cornea.

More recently, Hubbe (1994) evaluated the effect of alignment of the EyeSys CAS in five corneas and three aspheric test surfaces of varying radius with the line of sight directed at 2.5 °, 5 ° and 10° below the videokeratoscope axis (the instrument axis was still perpendicular to the surface under test). Hubbe et al (1994) found that a 5 ° deviation from the fixation source, a significant difference between opposing semi-

meridians in the aspheric surfaces and patient corneas ($p<0.05$) occurred. Furthermore, the colour coded maps mimiced the appearance of keratoconus. Hubbe (1994) concluded that accurate alignment with the line of sight is important as it can induce errors in the subsequent calculations to determine corneal topography.

C. Focusing Systems

User errors can only be attributed to alignment inaccuracy. The importance of accurate z-axis (i.e. along the instrument axis) alignment has been shown to be critical in the accurate measurement of corneal topography (Mandell, 1992; Nieves et al, 1992). Mandell (1992) found that the impact of z-axis alignment error on corneal radius derivation was greater with instruments that operated at shorter working distances. Using the EyeSys and the TMS videokeratoscopes (the EyeSys has a longer working distance than the TMS), Mandell (1992) found that the effect of z-axis defocus was greater with the TMS than the EyeSys. The graph below (figure 2.07) shows the results of radius of curvature measurements obtained with the TMS using a 42.5D spherical surface for z-axis defocus. It can be seen that errors in measurement of up to ± 1.00 D in the periphery of the cornea occurred due to small errors in defocus. Nieves et al (1992), confirmed these results in a similar study using the same instruments.

Figure 2.07: the effect of z-axis defocus on a 42.5D spherical surface using the TMS, according to the results by Mandell (1992).

More recently, manufacturers have attempted to redesign instruments in order to minimise errors due z-axis misalignment. The MasterVue Smart Topography system incorporates a dual camera system that enables the operator to view a magnified image of the centrally reflected rings as well as the overall cornea. Theoretically, z-axis errors should be reduced because smaller depth of focus is obtained using the second high magnification camera. Figure 2.08 shows how the dual camera system operates (reproduced from MasterVue literature).

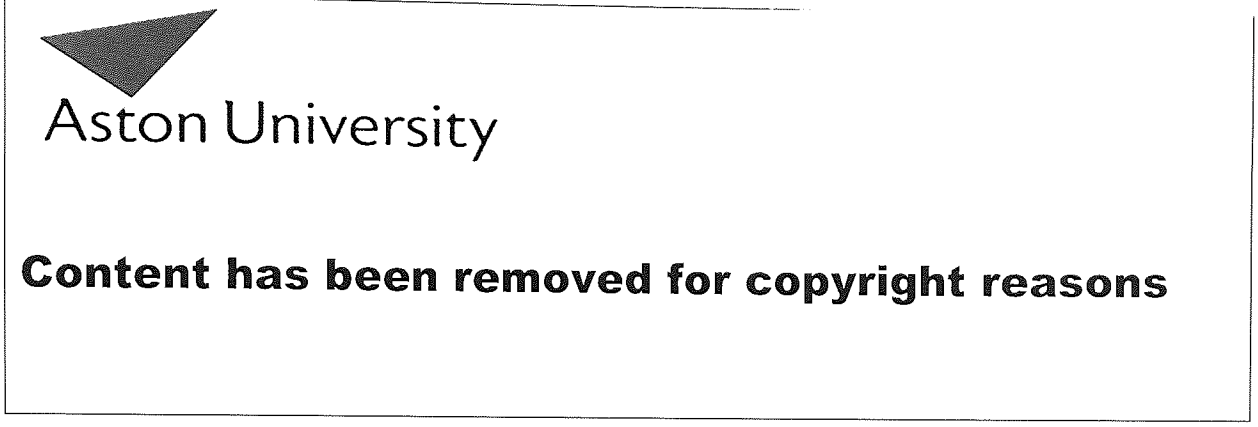

Figure 2.08: The MasterVue dual camera system used to obtain accurate z-axis alignment (reproduced from MasterVue literature).

D. Analysis of Distorted Images

Videokeratoscopic systems have a major role in analysing irregular corneas for purposes such as therapeutic contact lens fitting, refractive surgery or post-operative cataract management. If irregular corneas cannot be analysed, then there is a major drawback associated with videokeratoscopy. Modern day videokeratoscope can analyse most distorted corneas due to advances in the digitisation of the image and improvements in computer software. However, a recently developed system (the C-Scan Colour Ellipsoid Topometer) uses coloured ring mires to enable accurate localisation of the rings on the corneal surface (Ocular surgery news, 1994). Unfortunately, no papers have been published regarding the superiority of this system over the current videokeratoscopes.

2.7 Rasterstereography

Rasterstereography was initially used for the measurement of corneal topography by Bonnet et al (1962). It has been used successfully in other fields of medicine, for example, in the assessment of spinal curvature (Koepfler, 1983). The principle involves projecting a grid of light onto the corneal surface. As the cornea is transparent, the technique involves rendering the cornea opaque. Originally, talcum powder (with the use of a suitable anaesthetic) was used to form a real image of the target. The use of talcum powder to make the cornea opaque was the major drawback of this technique.

More recently, this method has attracted more popularity as the use of talcum powder has been replaced with sodium fluorescein. The mechanics have been concisely described by Arffa et al (1989), where a projected grid of light is used to illuminate the cornea and then viewed at a specific angle from the projection source (see figure 2.09). The whole system is incorporated on a Zeiss stereo photo slit lamp. Image aquisition involves focusing the slit lamp on the corneal surface, when in focus, a flash is triggered which provides the required intensity for image analysis. The flash light passes through the cobalt blue excitation filter causing the projected grid pattern to fluoresce. The image is then viewed by the video camera through a yellow barrier filter so that the residual blue light is absorbed. The resulting image is then digitised and analysed using suitable computer software.

The shape of the corneal surface can then be determined by the distortion and separation of the projected grid. The computer calculates the elevation of the corneal surface by comparing the displacement of the projected grid lines on the cornea to the position of the grid lines when projected on a flat plane. A two dimensional matrix of approximately 3000 elevation points is created for each image. From this, a three dimensional display of the corneal surface is produced.

Figure 2.09: The design of the apparatus used by Arffa et al (1989).

The accuracy of elevation measurements is dependent on the magnification used on the slit lamp. At X16 the whole of the cornea can be visualised and elevation has an accuracy of approximately 10μm. At higher magnifications even more accuracy is possible. Furthermore, the accuracy is also dependent on the length of the profile examined. Arffa et al (1989) found that for a length of 8mm of the corneal profile, the accuracy was 0.11D, but for only 5mm the accuracy was reduced to 0.5D. This was determined in a laboratory using matt finished steel balls, no aspheric test surfaces were used in their analysis.

With respect to alignment, any section of the projected grid may be analysed and used as a reference point. Generally, the apex of the cornea is chosen as the reference point. A commercially available device has been developed (the PAR technology Corneal Topography System). Recent studies (Belin et al, 1992; Belin et al, 1993) indicate that the instrument is both highly accurate and reproducible in determining the topography of spheres. An 8mm test area was used on non-calibrated steel balls of 20mm, 18mm and 12mm diameter, from which standard deviations of 0.03, 0.02 and 0.01D, respectively were found. Contrary to the study by Arffa et al (1989), smaller test areas did not result in significant reductions in the accuracy of elevation measurements. No tests were performed on mechanically measured aspheric test pieces.

Belin et al (1993) assessed the accuracy of the PAR system using decentred spheres, whole cadaver eyes before and after epithelial removal, lamellar keratectomy and laser photoablation. Four spheres were used (37.49, 42.21, 48.05 and 55.76D), the effect of decentration (0.5mm in the X, Y and Z axes) and the size of the optical zone (5,6 and 8mm) were assessed and the best fitting sphere determined. The principle of rasterstereogrammetry calculates elevation points and thus, in theory, there is no need for accurate alignment with the apex of a surface as it will be the point with the greatest elevation with the smallest radius of curvature. Belin et al (1993) found an average error of 0.04D when decentring by 0.5mm, the maximum error was 0.1D for the 37.49D sphere with a 5.0mm optical zone. They concluded that the effect of misalignment and optical zone diameter had little effect on the results obtained.

Rasterstereography is a very accurate technique for measuring corneal curvature. It utilises a real image as opposed to a virtual image as used in reflective methods such that used in keratometry and keratoscopy. The analysis of a reflected image on highly distorted corneas can cause significant distortion of the image such that analysis is almost impossible. On the other hand, a projected target is effected considerably less (Belin et al (1993) successfully obtained images from de-epithelialized, keratectomized and photoablated corneas). Unfortunately, there are very few publications that have assessed the accuracy of the technique of rasterstereography using aspheric surfaces. Assessment of the accuracy of an instrument in determining the topography of spherical surface is not suitable when we are performing measurements on corneas which most resemble aspheric surfaces.

2.8 Summary

Eye-care practitioners have always been aware of the need to understand the topographical nature of the corneal surface. Within the last decade, researchers in this field have made a number of improvements to older systems. Data is now stored as digitised images on computer disks to enable easy access and to eliminate errors such as shrinkage and distortion that occurred with photographic storage media. Accurate

localisation of the target rings (using techniques which allow the reflected Placido rings to be located accurately) from digitised images has also aided the increase in accuracy compared to instruments where ring images were located manually. The improvement of target design (by having a greater number of rings and by modifying the spatial arrangement of the rings) has also permitted more detailed analysis of the cornea. Representation of the data has now evolved into detailed mathematical descriptors and schematic colour coded topographical maps (see chapter 1).

Commercially available systems have mainly adopted the principle of computerised videokeratography. However, a system is available that is based on rasterstereogrammetry (PAR technology corneal topography system) where preliminary research has shown promising results (Belin et al, 1992; Belin et al, 1993). There are numerous applications for use of topographical systems in areas such as contact lens fitting (Hodd et al, 1993; McCarey et al, 1993), diagnosis and monitoring of keratoconus (Maguire et al, 1989; Maguire et al, 1991; Wilson et al, 1991b), monitoring of corneal shape after refractive surgery (Maguire et al, 1987b; McDonnell et al, 1989), corneal grafting and post-operative management of cataract patients.

The final stage of determining corneal topography requires processing the data derived from image digitisation. In order to calculate the parameters of an unknown surface, numerous algorithms have been proposed, these are discussed in the next chapter.

Chapter Three

Calculation of the Corneal Profile in Videokeratoscopy

3.1 Introduction

The first method of quantitatively measuring corneal contour was introduced by Gullstrand (1896). Using a four ring target, Gullstrand (1896) attempted to calculate the angular subtense (see figure 3.01) of the normal at a point on the corneal surface with the optic axis of the instrument. The small size of the target effectively meant that the corneal diameter measured was small. Gullstrand increased the length of corneal profile measurement by asking the subject to view a peripheral point within the same semi-meridian.

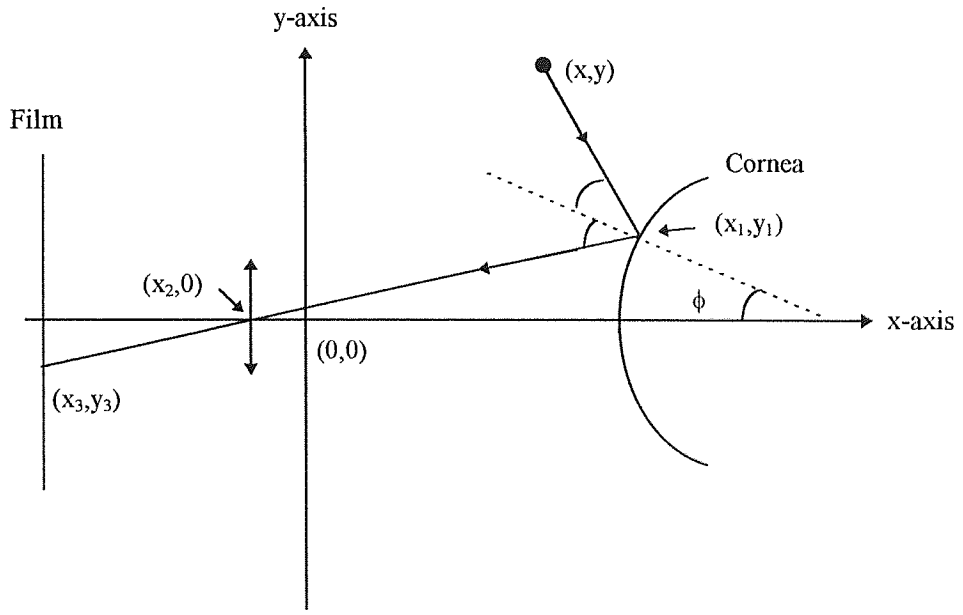

Figure 3.01: Outlines the problem described by Gullstrand (1896). Given (x,y), (x_2,0) and (x_3,y_3), the aim is to find x_1 as a function of y_1. The angle ϕ is the angle between the x-axis and the normal to the surface at (x_1,y_1).

Gullstrand (1896) derived the formula (equation 3.01 and figure 3.02) to calculate the radius of curvature, r.

$$y_{n+1} - y_n = r_n(Sin(\beta_{n+1}) - Sin(\beta_n)) \qquad \textit{Equation 3.01}$$

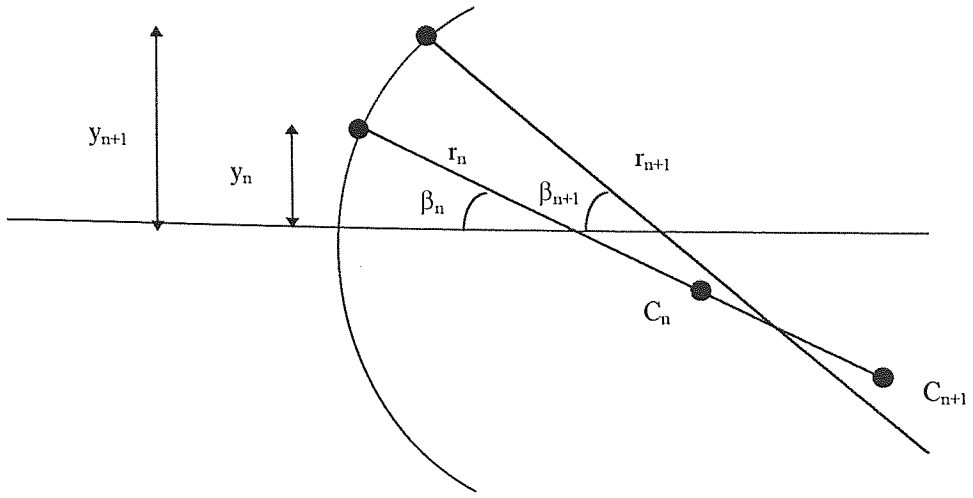

Figure 3.02: Calculation of the tangential radius of curvature r, where y_n and y_{n+1} are the heights at which reflection at the cornea occurs at points n and n+1. β is the angular subtense of the normal to the optic axis.

Numerous discrepancies in equation 3.01 exist. Firstly, in order for the equation to be valid, the centre of curvature C_n and C_{n+1} must coincide: in a normal cornea they would not. Secondly, Gullstrand (1896) calculated angle β using the following formula:

$$Tan(2\beta_n) = \frac{\text{actual ring height from axis}}{\text{horizontal distance of ring from cornea}} \qquad \textit{Equation 3.02}$$

For equation 3.02 to be valid, the reflected light from the cornea must be parallel to the keratoscope axis. For this to occur, a stop must be placed at the principal focus of the camera lens. There was no mention of this in Gullstrand's paper. Finally, during measurements of the photographed rings (after accounting for the system magnification), Gullstand (1896) assumed that the values measured were equivalent to y_n and y_{n+1}. The basic aim of Gullstrand's method was correct - to determine the angular subtense of the normal for points on the corneal surface, however, the design and algorithms were not appropriate to accurately derive the corneal coordinates.

With the improvement in contact lens design and the advent of refractive surgical procedures, there has been a renewed interest in the measurement of corneal contour. For the last decade the only instruments used to measure the corneal surface have been the keratometer and the photokeratoscope. Although the use of the keratometer has

been firmly established in routine clinical practice, it has limitations in the screening for keratoconus, contact lenses fitting and refractive surgery. The photokeratoscope, on the other hand, has been more useful to practitioners as its reflected mires cover a larger proportion of the corneal surface. However, a system that provides accurate quantitative results has long since been required. Since the work of Gullstrand (1896), numerous other investigators have constructed new keratoscopes and evaluated the performance of their algorithms. Most of the earlier work is accurately described in a critical review by Clark (1973c). The present chapter will therefore concentrate on the more recent proposed methods of calculating corneal topography.

3.2 Difficulties of Deriving Corneal Topography from a Reflected Target Image

To appreciate the basic problems involved in corneal shape measurement, it is worth considering what actually occurs when capturing the reflected image of a known target source (see figure 3.03).

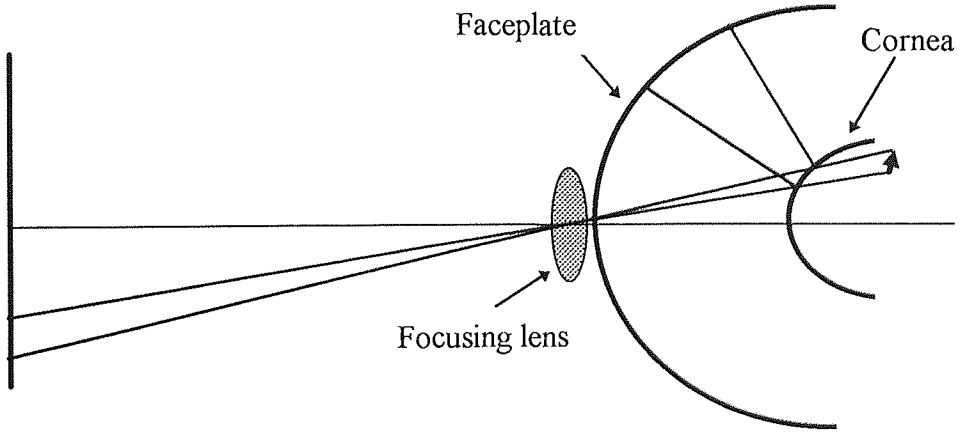

Figure 3.03: The principles of videokeratoscopy.

Essentially, a target source of known dimensions and shape (housed in a faceplate) illuminates the cornea. Owing to the reflective properties of the cornea, light is reflected towards the focusing lens so producing a virtual image of the target source behind the cornea. As the shape of the reflecting surface dictates the appearance of the reflected image, reverse ray-tracing from the image plane to the target source would

enable calculation of the reflecting surface parameters. Unfortunately, the problem is not as simple as it may initially appear.

A. Reconstruction of a 3D Surface from a 2D Photograph

In order to define the corneal profile, three parameters are required, the value of x, y, and z coordinates of the corneal surface. The image captured in videokeratoscopy is two dimensional. In order to determine the corneal profile, the two dimensional image must be converted into a three dimensional surface. Unfortunately, the two dimensional image in videokeratoscopy has insufficient information to enable a point by point localisation of the reflected mires in three dimensional space.

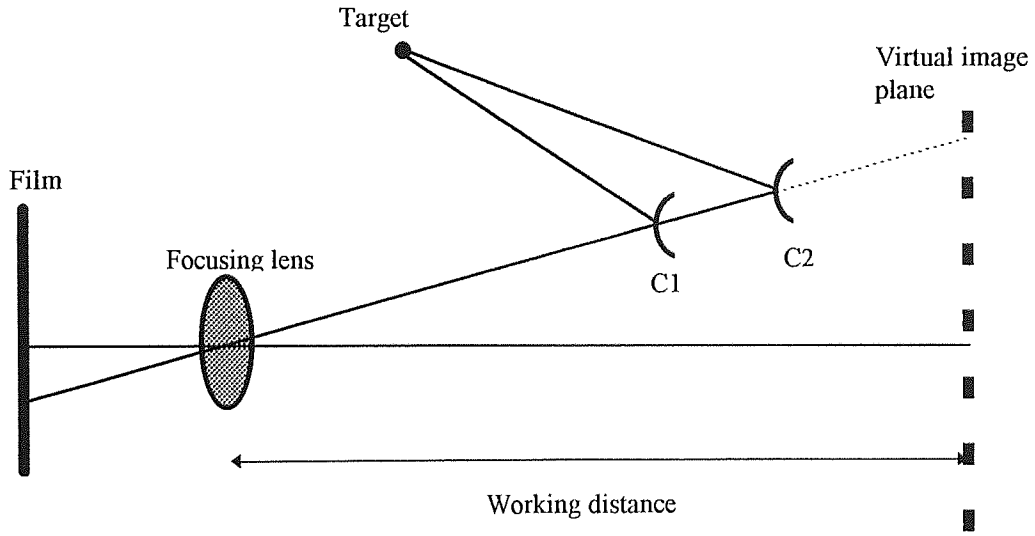

Figure 3.04: shows how two corneal surfaces of different radii of curvature (C1 and C2) can result in the reflected mire image lying at the same point on the photographic film. When the system is in focus, the working distance is always constant and spans from the focusing lens to the virtual image behind the cornea. Therefore, the two surfaces cannot be differentiated at the film plane. After Wang et al (1989).

Wang et al (1989) concisely illustrated this problem (see figure 3.04). It can be seen from figure 3.04 that the difficulty arises because two corneal surfaces with different radii of curvature and at different distances from the film plane can produce a reflection of the target rings at the same point on the film. Thus, the instantaneous radius of curvature at a point on the corneal surface cannot be uniquely determined from

measurements of the film plane unless assumptions are made. All that can be stated is that there is a reflecting surface that intercepts the reflected ray path and that the distance from the focusing lens to the virtual image (and therefore the focal plane) is constant. A unique relationship for corneal curvature can only be determined if the object and image distances are known. However, assumptions need to be made as the object distance is not known (i.e. the distance from the target to the cornea).

B. The Effect of Continuous Targets and Meridional Skew

A common assumption made in some videokeratoscopes using concentric ring targets (e.g. Wesley-Jessen PEK IIIA) is that light commencing at one meridian from the object plane lies in the same meridian at the film plane. This does not apply to targets which consist of point sources as each point can be easily located in the image plane (as with the L.E.D. targets used in chapter 6), therefore any 'skewing' of the image can be easily detected as the target is not continuous like a ring. Assuming that there is no meridional skew could to lead errors in the reconstruction of the corneal surface. The magnitude of this error has yet to be evaluated. In conditions such as keratoconus, the magnitude of this error will increase significantly.

C. Instrument Misalignment with the Corneal Surface

The dimensions of the reflected rings can be easily found by simply measuring their horizontal and vertical positions. In order to reconstruct the cornea three dimensionally, the sagittal depth of the reflected target points at the surface must be determined (i.e. the value of z, defined in figure 3.05). However, it is necessary to adopt a suitable reference point from which numerical data such as peripheral radius of curvature may be identified. The various reference points and the most suitable point to use in videokeratoscopy has been discussed in section 2.6.1.

At present, the reference point used in corneal videokeratoscopic systems is the geometric centre of the central mire (once alignment has been performed). It is worth

considering the consequence when the videokeratoscope axis is not perpendicular with the cornea. Figure 3.06 shows that the net result is that of induced corneal asymmetry. It has been widely accepted that the cornea is asymmetric (Mandell, 1965a; Dingledein et al, 1989; Wilson et al,1991a), however, if the instrument induces asymmetry (due to improper alignment) then it is difficult to differentiate between actual asymmetry and artifactual (or instrument induced) asymmetry. All videokeratoscopic instruments now have the facility to enable correct alignment with the videokeratoscope axis and the cornea.

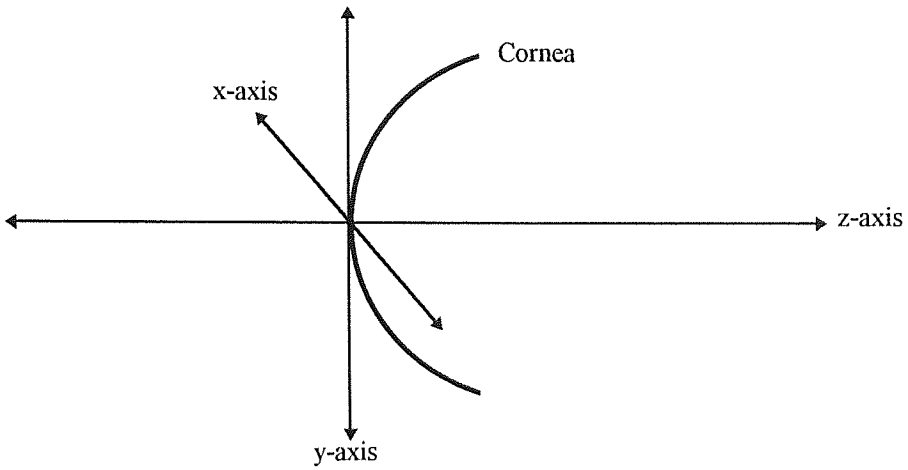

Figure 3.05: Defines the directions of the axes in relation to the corneal surface.

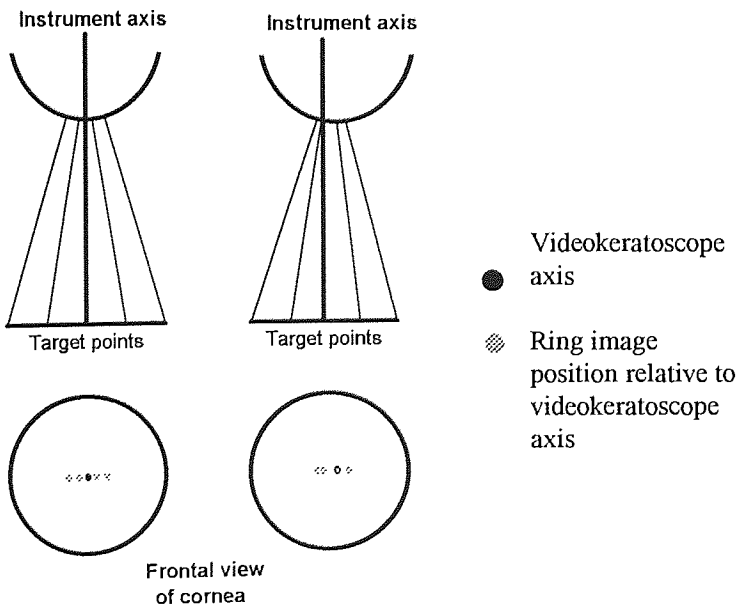

Figure 3.06: Shows the effect of the misalignment (when the videokeratoscope axis is not perpendicular to the corneal surface) on the position of the reflected image of the targets relative to the videokeratoscope axis.

D. Data Resolution in Videokeratoscopy

Before any assumptions are made in the actual reconstruction of the corneal profile, measurement of the reflected rings is performed. The x and y measurements are used in all subsequent calculations to find the third geometric co-ordinate, z, shown in figure 3.05. The accuracy of the reconstruction will therefore ultimately depend on the resolution of the digitisation procedure.

Maguire et al (1987a) calculated the effect of frame resolution on corneal position accuracy and the subsequent error that could occur for a 40D surface (see table 3.01). The EyeSys corneal analysis system measures ring separation to sub-pixel resolution (Hodd et al, 1993). Andersen et al (1993b) have described a similar procedure, where the distribution of light intensity is measured and plotted as a function of pixel distance. The location of the ring was given by the peak of the intensity distribution.

Table 3.01: the influence of frame resolution on the localisation accuracy of the cornea and measurement error for a 40D surface (after Maguire et al, 1987a).

Frame resolution (lines per frame)	Localisation accuracy at the cornea (μm)	Measurement error with 40D surface (D)
500	30	1.2
1000	15	0.6
2000	7.5	0.3

3.3 Algorithms used in the Reconstruction of the Corneal Profile

Having captured and digitised the reflected mire image, the corneal profile must be reconstructed. As described earlier, there are numerous difficulties in reconstructing a three dimensional surface from a two dimensional image but by making certain assumptions these difficulties may be overcome. In general, the following assumptions are made for the various reconstruction techniques:

- the working distance from the target to the image is constant.
- The instrument axis is perpendicular to the corneal surface.

- The light from one meridian of the target is reflected in the same meridian in the film plane. The assumption here is that there is no circumferential tilt of the corneal surface. For point targets, this assumption is not required.
- The position of the image at the film plane is unique for a particular surface.
- The image plane lies on a flat plane.

The various methods of reconstruction of the corneal surface have generally taken three forms, these will now be described.

3.3.1 Calibration Method

The classical method of calibration involves taking photographs of reflected target rings from steel balls of known radii. The separation of adjacent ring images are measured and a set of calibration graphs are constructed that plot ring image separation for various spherical surfaces against the radius or power of that surface (Mandell, 1967; Mandell et al, 1968; Townsley, 1970). Then, for actual subjects, ring separations are measured again and radius values are obtained from the calibration graphs. The calibration method assumes that the cornea is spherical between adjacent rings. Errors result in this technique because it is assumed that the instantaneous centre of curvature for the various reflected rings lie on the optic axis of the instrument, although this applies to a spherical surface, its does not apply to an aspheric cornea where the instantaneous radius of curvatures lie on an evolute (Bennett, 1968).

Mandell et al (1969) used decentred spherical steel balls so that the error of the calibration method in measuring corneal radius of curvature could be assessed. Figure 3.07 shows an aspheric surface, the point (x, y) has an instantaneous radius of curvature of r_t. The instantaneous radius of curvature of the point (x, y) would be the same for a spherical surface with its centre at (x', y') and a radius of curvature of r_t. Mandell et al (1969) thus simulated aspheric surfaces by decentring spheres by a distance y' from the optical axis of the instrument (the value of y' was calculated for an

ellipse of predefined central radius of curvature with an eccentricity of e=0.48). The accuracy of the technique was assessed by comparing the difference in size of the separation of adjacent reflected ring images. From their calibration graphs, although little variation was found for the central ring, differences in ring separation increased for the 2nd and 3rd rings and also the 9th to 10th and 10th to 11th rings. Unfortunately, Mandell et al (1969) did not qualify this difference in ring separation in terms of an error of radius of curvature for the various surfaces measured, therefore, any differences in adjacent ring size were of no significance as they were specific to the instrument used in their study.

Knoll (1961) found an error in radius of curvature of ± 0.2mm using spherical surfaces for the calibration method. Stone (1962), also found a comparable error of ± 0.25mm, again, with spherical surfaces. Calculating peripheral radius of curvature of non-spherical surfaces such as the cornea using a calibration method based on spherical surfaces unnecessarily introduces and biases the derived radius to that of a spherical surface.

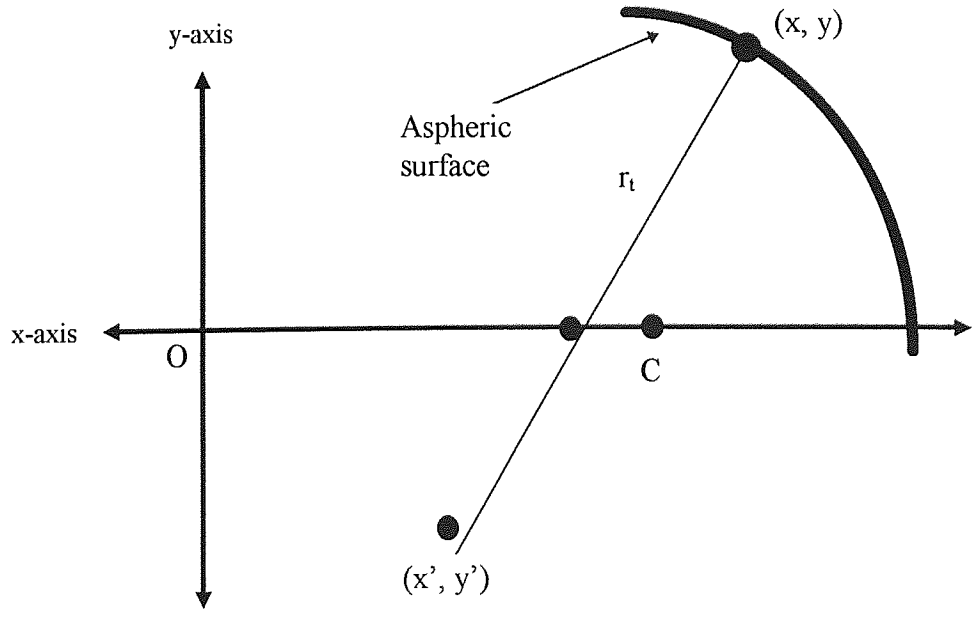

Figure 3.07: shows an aspheric surface. The instantaneous radius of curvature at point (x, y) in any one meridian is given by r_t.

3.3.2 One Step Curve Fitting

Originally proposed by El-Hage (1969), this method attempts to fit a polynomial curve of the form,

$$x = A_0 + A_1 y + A_2 y^2 .....$$

to the cornea with the origin (0,0) at the corneal apex. Differential equations were used to derive the polynomial equation matching the corneal surface. The order of the polynomial used was dependent on the number of rings in the keratoscope target. Furthermore, the keratoscope used was unusual in design in that a stop was placed at the principal focus of the camera lens to ensure that reflected light would return parallel to the instrument axis. Designing the keratoscope in this manner enabled El-Hage (1969) to simplify the differential equation used to calculate the polynomial function describing corneal shape. Using spheres and conic surfaces, El-Hage (1972) found an error of 0.02mm in terms of sagittal depth measurements at the periphery of the curve.

More recently, Edmund et al (1985) derived a method where the size of reflected rings from hypothetical conic sections were found by calculation and compared with the size of reflected rings from a photograph of a surface. The corneal profile is fitted to a conic curve by comparing the reflected ring size by the use of least squares.

The disadvantage of one step curve fitting is that the cornea is modelled on a specific mathematical function, as a result of such approximations it is likely that the derived profile will be relatively insensitive to local corneal variation.

3.3.3 The Multiple Arc Technique

Originally devised by Townsley (1967), Doss et al (1981) ascribed the name to this method of calculating the corneal profile. The model considers that a meridional section of the cornea can be composed of several multiple arcs between corneal

reflection points. A smooth curve would be guaranteed by the fact that each adjacent arc would share a common tangent where they meet (see figure 3.08).

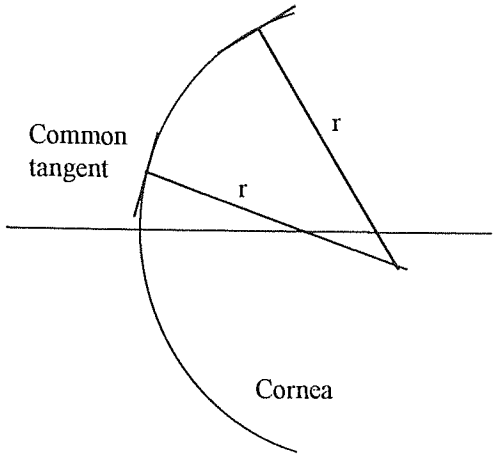

Figure 3.08: The multiple arc technique. r is the radius of curvature of the arc.

A detailed analysis of how the corneal contour is reconstructed using this method will now be described.

A. Calculation of the Central Corneal Radius

The first value that must be calculated after image digitisation is the central corneal radius. It is the value of the central corneal radius that will determine the 'size' of the cornea when modelling ellipses to the profile. Doss et al (1981) preset the value of the central radius of curvature to 7.80mm. It is well known that the range of central radius varies significantly within the normal population (Guillon et al, 1986). Therefore, biasing the central corneal radius introduces an unnecessary error into the calculation of corneal profile. Klyce (1984) derived a method where the value of the central corneal radius need not be preset. Figure 3.09 shows a diagrammatic representation of a videokeratoscope where l is the distance between the camera and the target ring and wd is the working distance of the videokeratoscope (i.e. the distance from the videokeratoscope and the cornea).

The average value of y_1, the distance from the innermost or first ring, to the geometrical centre of the innermost ring, may be written as:

$$\bar{y}_1 = \frac{\sum_{i=1}^{n} y_{1.i}}{n} \qquad \textit{Equation 3.03}$$

In addition, through simple geometry, further geometric statements may be made from figure 3.09.

$$\tan\alpha = \frac{\bar{y}_1}{wd} \qquad \textit{Equation 3.04}$$

$$\tan(2\phi - \alpha) = \frac{(l_1 - \bar{y}_1)}{wd} \qquad \textit{Equation 3.05}$$

$$\phi = \theta + \alpha \qquad \textit{Equation 3.06}$$

$$2\phi - \alpha = 2\theta + \alpha \qquad \textit{Equation 3.07}$$

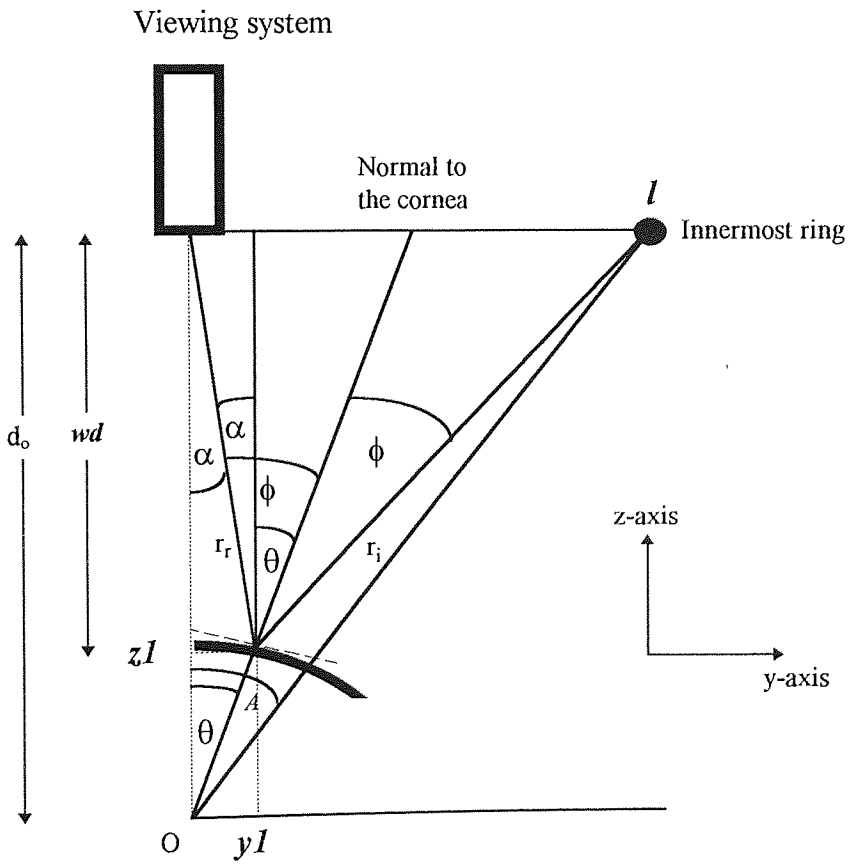

Figure 3.09: Note that r_i and r_r represent the incident and reflected rays respectively. Definitions of the labels are shown below:

α is the angle subtended by the reflected ray at the videokeratoscope axis.
ϕ is the angle between the reflected and incident rays to the normal.
θ is the angle between the normal and the vertical axis.
A is the angle between the ring target and the videokeratoscope axis.
d_o is the distance from the videokeratoscope and the origin (O).
z_1 is the position of the first corneal reflection point along the z-axis.
y_1 is the position of the first corneal reflection point along the y-axis.

Ultimately, the value of z_1 is required. Figure 3.10 (below) shows the relationship of the normal to the cornea and the videokeratoscope axis.

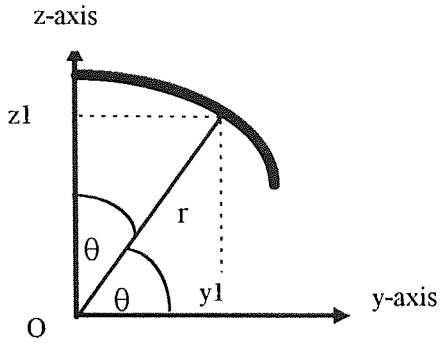

Figure 3.10: The sagittal depth (z1) of the first ring reflection point at the cornea. The origin is the intersection of the normal to the first ring reflection point and the videokeratoscope axis.

From figure 3.10 it can be seen that

$$Tan(\theta) = \frac{\bar{y}_1}{z_1} \qquad \textit{Equation 3.08}$$

Solving equations 3.03 to 3.08 in terms of z an estimate of the mean elevation of the corneal surface at the central target point can be derived:

$$z_1 = \frac{\bar{y}_1}{Tan\{0.5\tan^{-1}[(l_1 - \bar{y}_1)/wd] - 0.5\tan^{-1}(y^1/wd)\}} \qquad \textit{Equation 3.09}$$

Note that the assumption here is that the central ring is reflected from a point on the cornea that is close to the videokeratoscope axis. Klyce (1984) suggested that measurement error may be reduced by careful focusing of the central mire on the cornea. The central elevation calculated by Klyce (1984) was different to that in equation 3.09. It would appear that there was a typographical error.

At this point it is essential to note that both Doss et al (1981) and Klyce (1984) assumed that the reflected image heights (b, in figure 3.11) were at the same as the reflected heights at the cornea (a, in figure 3.11). The image, however, lies behind the cornea at the tangential plane. Wittenburg (1966) demonstrated that the finite distance between the camera and the eye introduced a difference between image height and the height at the corneal reflection point.

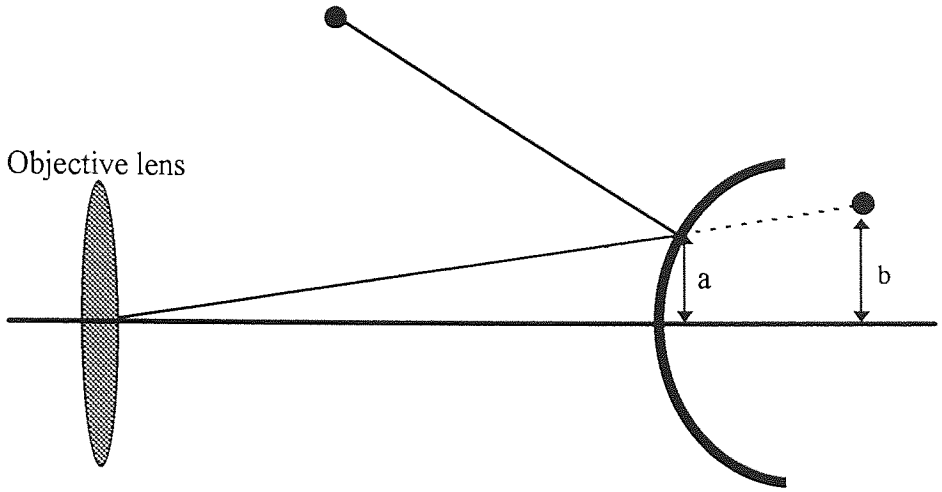

Figure 3.11: Shows the different 'image' sizes measured. The multiple arc technique assumes that **b** and **a** are equal. Such an assumption leads to errors in the calculation of corneal topography.

B. Calculation of z, the Elevation of Peripheral Reflected Target Points

After calculating the central corneal elevation, the elevation of other target points at the cornea must be found. Each point of elevation is related to the origin. Figure 3.12 illustrates the basis on which these elevations are calculated. The angle t represents the angle between the tangent to the cornea and the y-axis. For a point corresponding to rings i-1 and i an expression for the angles t_{i-1} and t_i may be written as

$$\sin t_{i-1} = \frac{(\bar{y}_{i-1} - A)}{r} \qquad \textit{Equation 3.10}$$

and

$$\sin t_i = \frac{(\bar{y}_i - A)}{r} \qquad \textit{Equation 3.11}$$

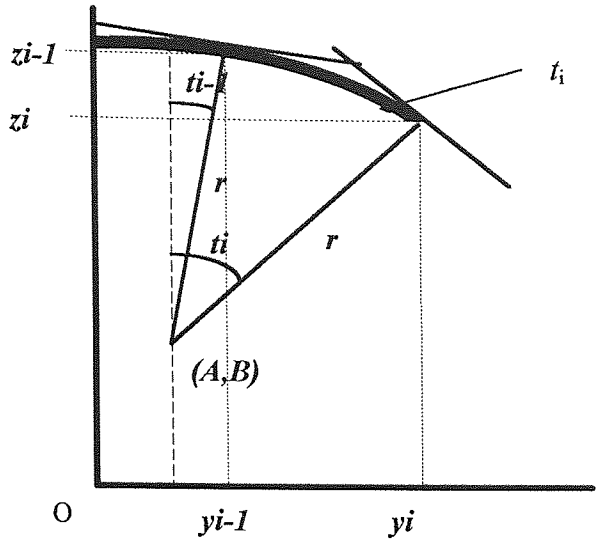

Figure 3.12: shows the relationship between the corneal reflection points and the corneal elevation from a point (A,B). The angles t_{i-1} and t_i represent the angle between the tangent to the cornea and the horizontal.

Equating 3.10 and 3.11 in terms of A,

$$y_{i-1} - r\sin t_{i-1} = y_i - r\sin t_i \qquad \textit{Equation 3.12}$$

also,

$$\cos t_{i-1} = \frac{(z_{i-1} - B)}{r} \qquad \textit{Equation 3.13}$$

and

$$\cos t_i = \frac{(z_i - B)}{r} \qquad \textit{Equation 3.14}$$

Equating 3.13 and 3.14 for B,

$$z_i - r\cos t_i = z_{i-1} - r\cos t_{i-1} \qquad \textit{Equation 3.15}$$

Substituting equation 3.12 into 3.15 for r, an **initial estimate** of the corneal elevation can be found.

$$z_i = z_{i-1} + \frac{(y_{i-1} - y_i)(\cos t_i - \cos t_{i-1})}{(\sin t_{i-1} - \sin t_i)} \qquad \textit{Equation 3.16}$$

From simple geometry, an approximate estimate of t_i is $A/2$ (see figure 3.13).

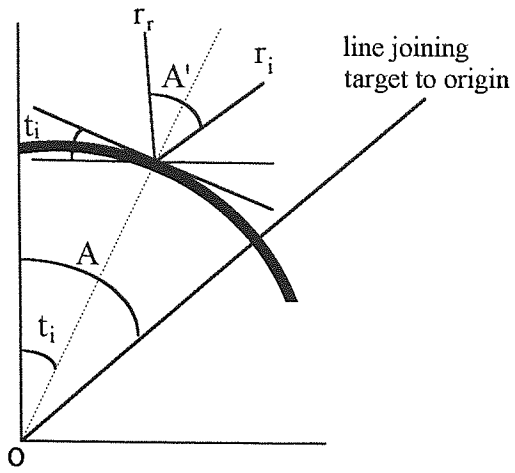

Figure 3.13: shows how an initial estimate of t_i is found from the angular subtense of the first ring target at the origin. r_i and r_r represent the incident and reflected rays respectively.

The initial estimate of t_i ($A/2$) may therefore be calculated as

$$t_i = 0.5 \times \tan^{-1}\left(\frac{l_i}{d_o}\right)$$

Where the distance of the viewing system from the origin may be written as

$$d_0 = wd + \bar{z}_1 \qquad \textit{Equation 3.17}$$

If equation 3.16 is used to calculate the corneal elevation, errors will be introduced due to the initial estimate of t_i. Therefore, the value of t_i must be refined and then repeatedly iterated in equation 3.16. From figure 3.09, a set of equations may be derived that enable refinement of the angle t_i.

From the Pythagoras theorem,

$$r_i^2 = (l_i - y_i)^2 + (d_0 - z_i)^2 \qquad \textit{Equation 3.18}$$
$$r_r^2 = (d_0 - z_i)^2 + y_i^2 \qquad \textit{Equation 3.19}$$

using the Cosine rule,

$$A' = \cos^{-1}\frac{(l_i^2 - r_r^2 - r_i^2)}{(-2r_r^2 r_i^2)} \qquad \textit{Equation 3.20}$$

$$t_i = \frac{\pi}{2} - \frac{A'}{2} - \tan^{-1}\frac{(d_o - z_i)}{(l_i - y_i)} \qquad \textit{Equation 3.21}$$

The initial value of z_i is then substituted into equations 3.17 to 3.21 in order to calculate a new value of t_i. t_i is then re-substituted into equation 3.16. The process of re-substitution is continued to improve the accuracy of t_i and eventually, z_i. Klyce (1984) suggested that this process should be performed until successive changes in the value of z_i are less than 0.00001%. Thus, for an entire profile, the values of the x, y and z co-ordinates of all the target reflections points are found.

C. Corneal Radius Calculation from the Corneal Profile

Once the x, y and z locations of the reflected targets have been calculated, the actual radius of curvature of the surface at the reflection points may be found. As stated earlier, the multiple arc technique assumes the cornea to be composed of multiple spherical arcs which together form a non spherical smooth surface (see figure 3.08).

Using the Pythagoras theorem, three equations may be derived from figure 3.14.

$$r^2 = (y_1 - a)^2 + (z_1 - b)^2 \qquad \textit{Equation 3.22}$$

$$r^2 = (y_2 - a)^2 + (z_2 - b)^2 \qquad \textit{Equation 3.23}$$

$$r^2 = (y_3 - a)^2 + (z_3 - b)^2 \qquad \textit{Equation 3.24}$$

Equations 3.22-3.24 can be solved for r, a and b (3 equations and 3 unknowns):

$$a = \frac{[(y_3 - y_1)(y_1 - y_2)(y_2 - y_3) + (z_1^2 - z_2^2)(y_2 - y_3) + (z_3^2 - z_2^2)(y_1 - y_2)]}{\{2[(z_1 - z_2)(y_2 - y_3) + (z_3 - z_2)(y_1 - y_2)]\}}$$

Equation 3.25

$$b = \frac{(y_1 + y_2)}{2} - \frac{(z_1 + z_2 - 2a)(z_1 - z_2)}{2(y_1 - y_2)} \qquad \textit{Equation 3.26}$$

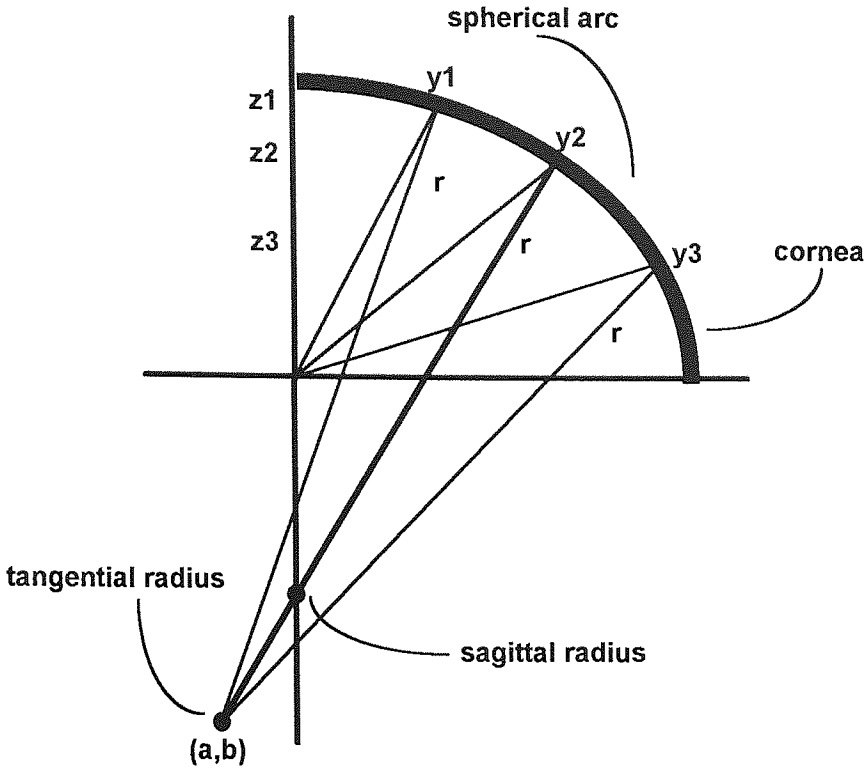

Figure 3.14: shows a small portion of the cornea which, because of its small size, may be regarded as spherical. The point (a,b) may be defined as the centre of curvature of the spherical arc between y_1 and y_3. The points y_1, y_2 and y_3 represent the horizontal displacement of the targets at the cornea. Conversely, z_1, z_2 and z_3 represent the elevation of the target points at the cornea. The spherical arc enclosed by y_1 and y_3 has a radius of curvature r.

Having located the co-ordinates of the centre of curvature of the spherical arc, substitution of these values back into either equation 3.22, 3.23 or 3.24, the value of ***r*** can be found.

$$r = \left|\sqrt{(y_1 - a)^2 + (z_1 - b)^2}\right| \qquad \textit{Equation 3.27}$$

The multiple arc technique, in its present form, is not a suitable method to resolve the topographic details of a non spherical surface (Wang et al, 1989). The fact that the image height is assumed to be equal to the height at which reflection from the corneal surface occurs is a significant source of error (Wang et al, 1989). Wang et al (1989) corrected this source of error by calculating the value of the angle α, using an angle avoided making the above assumption. Further, they compared the accuracy of the old and new methods for a spherical and aspheric surface (r_o=7.33, e=0.5). They found

that the new method significantly improved the accuracy of the algorithms for an aspheric surface. There was very little difference in the accuracy in calculating the radius of curvature for a spherical surface.

D. What Radius is Measured ?

When light from an off-axis, oblique point is reflected from a curved surface, two focal points arise. These are generally referred to as the tangential and sagittal points of focus. They arise due to the aberration effects of oblique astigmatism. The calculated value of ***r*** in equation 3.27 is of the tangential radius. Tangential radius is the value which is of most interest as it represents the radius of curvature of the corneal surface that contains the target row of light emitting diodes (L.E.Ds). The sagittal radius would represent the radius of the corneal surface perpendicular to the targets. Figures 3.15 and 3.16 clarify the difference between the tangential and sagittal radius.

Figure 3.15: measurement of tangential radius.

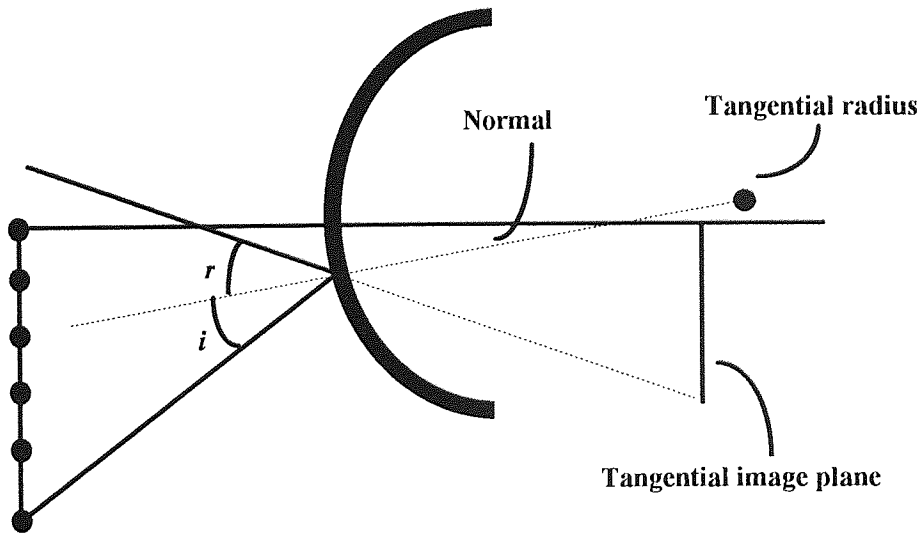

Figure 3.16: measurement of sagittal radius.

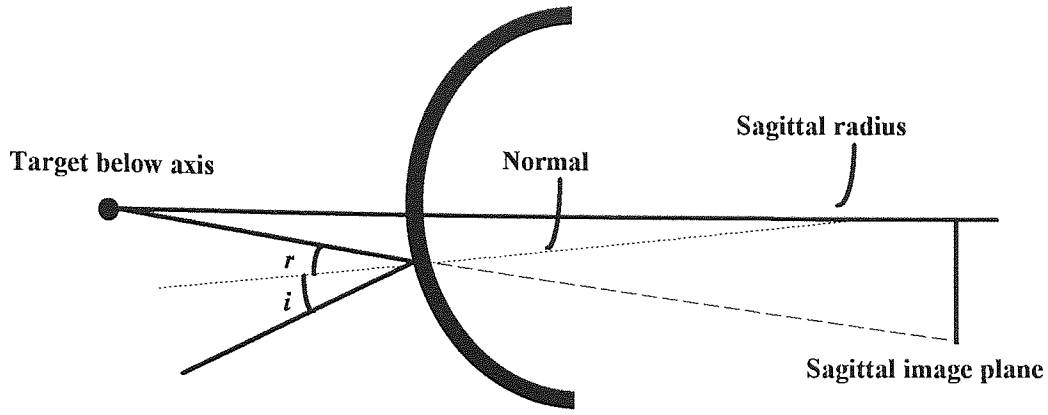

Klyce (1984) suggested that once the local radius of curvature was calculated, the local power could be calculated,

$$\mathbf{F} = \frac{(n-1)}{r} \qquad \textit{Equation 3.28}$$

where n is the refractive index of the cornea and r the local radius of the spherical arc. This formula only holds for paraxial rays. Klein (1993) suggested that the use of this method was incorrect as it was being applied to non paraxial zones of the cornea.

A distinction must be made between anterior corneal power and total corneal power. For clinical purposes, such as post cataract surgery etc., total corneal power is required. In order to calculate total corneal power, the effects of the steeper posterior corneal surface must be considered. As the posterior corneal surface cannot be measured using videokeratoscopy, the refractive index of the cornea must be adjusted. In addition to adjusting the refractive index of the cornea, the calculation of total corneal power is complicated by the fact that the cornea has a variable refractive index. Therefore, one must reassess the average value of the refractive index of the cornea. Dunne et al (1992) calculated the refractive index of the total cornea as 1.3283.

3.4 Summary

Chapter 3 has described the difficulties encountered during videokeratoscopy. The key problems area are in reconstructing a three dimensional surface from a two dimensional image. Wang et al (1989) have shown how two surfaces of differing radius reflect target rings at identical points on a film. The solution to this problem involves locating the apical point of the surface being measured. Once a video image of the surface has been obtained, the effects of image skew must also be accounted for. The use of point source targets would detect skew and thus the user would be informed of the possibility of error being introduced.

The present chapter has also described algorithms used in deriving the corneal profile. The calibration method is the most inaccurate as it biases results to a spherical surface. The multiple arc technique originally proposed by Townsley (1967) and later modified by Klyce (1984) attempts to derive the corneal profile by considering the cornea as multiple spherical sections of changing radius. Wang et al (1989) have shown that the algorithms used in the multiple arc technique are not suitable for measurement of aspherical surfaces. The principle reason for this is that an incorrect assumption is made - that the height of the reflected image is the same as the point of reflection at the cornea.

Chapter Four

A Clinical Trial of the SUN SK-2000 Computer Assisted Videokeratoscope - its Accuracy and Repeatability

4.1 Introduction

Over the last decade investigators have tried to develop instruments that accurately measured corneal topography. Most concentrated on the development of keratoscopic devices (Knoll et al, 1957; Ludlam et al, 1966; Townsley, 1967; El-Hage, 1971; Klyce, 1984; Wang et al ,1989; Andersen et al 1993a). The SUN SK-2000 (Version 3.1, Sun Contact Lens Company Ltd., Kyoto, Japan) was a computer assisted videokeratoscopic device, it was based on the principle of keratoscopy where a target (usually a Placido disc type) was reflected from the cornea and the resulting image analysed. By measuring the consecutive target separations and then using algorithms, the corneal profile could then be reconstructed (Mandell and York, 1969; El-Hage, 1972; Doss et al, 1981; Klyce, 1984; Edmund et al, 1985; Wang et al, 1989; Andersen et al, 1993b). Depending on the algorithms used, various assumptions would be made in the calculations (see Chapter 3).

4.2 Aims

There were four principle aims in the study:

- to assess the accuracy of the instrument in determining an 8mm calibration sphere.
- Assess the level of agreement with the Javal Schiotz keratometer.
- Assess the repeatability or precision of the SUN SK-2000 videokeratoscope for the central cornea and eight peripheral meridians at a point which was approximately 4mm in the periphery of the cornea (according to manufacturers). This value

would vary from one surface to another. Unfortunately, manufacturers did not state for what surface the instrument performed measurements.

- Evaluate the alignment system used in the SUN SK-2000 videokeratoscope.

4.3 Instrumentation

4.3.1 The SUN SK-2000

The faceplate of the SUN SK-2000 housed 15 rings arranged on an ellipsoidal surface, which enabled a large area of the cornea to be measured (approximately 8mm according to manufacturers) and also reduced the peripheral blurring of targets due to curvature of the image plane (Knoll, 1961; Stone, 1962; Mandell and St. Helen, 1968; Mandell and York, 1968). The alignment system comprised of two luminous fixation targets which after reflection off the cornea were viewed on the monitor by the operator. The monitor had two square reference alignment markers (see figure 4.01) that were used to align the reflected luminous targets. Alignment was accomplished by adjusting the joystick so that the reflected fixation targets were centred and focused within the reference squares. The purpose of the alignment procedure was to align the videokeratoscope axis such that it was perpendicular to the corneal surface.

The importance of accurate z-axis alignment was clearly noted by Nieves et al (1992) who showed that for the TMS (Topographical Modelling System, by Computed Anatomy) an error of 0.9D occurred for 0.33mm misalignment in the z-axis (see figure 4.02 for illustration of misalignment axes). The focusing mechanism in the SUN SK-2000 was automated. Presumably, an automated approach to focusing was adopted by the manufacturers in order to reduce errors due to z-axis misalignment.

Once alignment was accomplished, the image of the reflected Placido rings was captured by pressing the joystick button. Digitisation of reflected rings was shown by a small cross being superimposed at each ring along the eight semi-meridians. The

SUN SK-2000 had the facility for the user to manually adjust the position of the crosses in case an error in digitisation occurred.

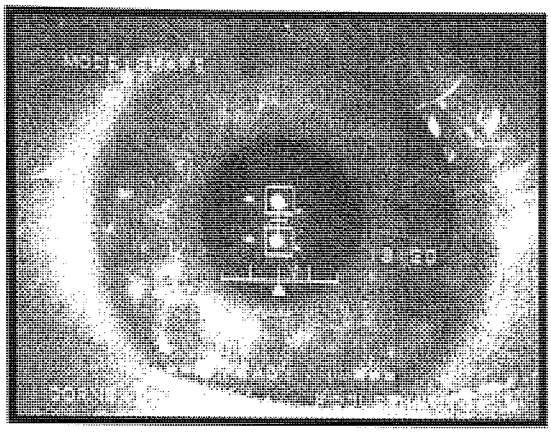

Figure 4.01: The alignment system in the SUN SK-2000 videokeratoscope.

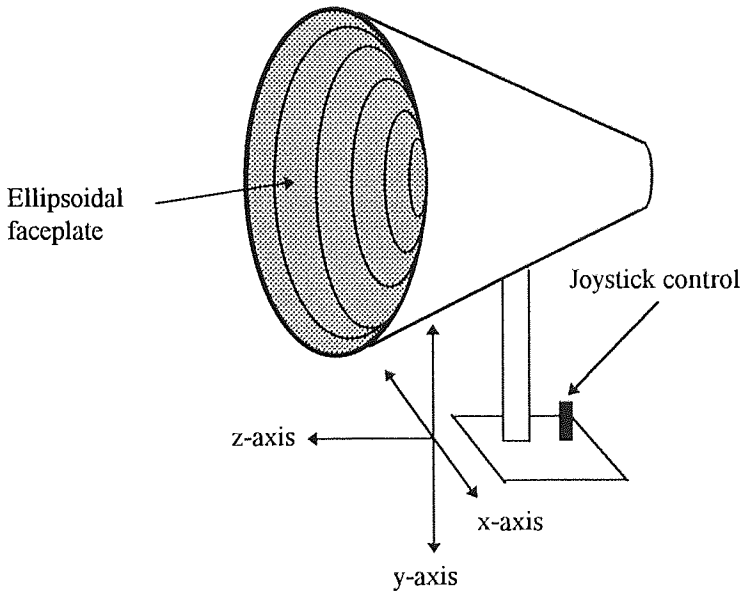

Figure 4.02: Shows the classification of axes of alignment and the videokeratoscope faceplate.

As previously stated in section 4.2, peripheral measurements were taken at a point on the cornea 4mm from the vertex normal. This value was only approximate and would change from one corneal shape to another. The manufacturer's instructions, however, provided no information regarding the point on the corneal surface from where the

results of central radius of curvature measurements were performed using the SUN SK-2000 device.

Similar to other videokeratoscopes, the SUN SK-2000 displayed data in various forms such as colour coded maps, wire mesh models and simple Placido ring displays with superimposed radius measurements. Unfortunately, radius measurements of only eight peripheral meridians at approximately four millimeters from the reference point were available.

Calibration was performed by taking 4 readings of an 8mm calibration surface (provided by manufacturers). The results were transferred directly into the internal computer of the SUN SK-2000. During calibration it was essential that the surface was aligned correctly otherwise asymmetries occurred in the measurement of the surface. Calibration was performed prior to the usage of the SUN SK-2000.

4.3.2 Keratometer

A Javal Schiotz keratometer was used. The principle of the keratometer was described in chapter 2. Basically, the keratometer calculates central radius of curvature by measuring the size of the reflected image and comparing it to the size of the object (of known size and position). The central radius of curvature is measured between two points, thus the assumption is made that the corneal surface between these two points is spherical. Although errors resulting from this assumption are small for measurements on either side of the optical axis, it still exists. Furthermore, the magnitude of the error depends on how much the shape factor of the cornea deviates from a spherical surface. Comparisons were made with the keratometer because at the present time it is the most widely used instrument for the measurement of central corneal curvature. The Javal Schiotz keratometer was used to compare central radius of curvature measurements with the SUN SK-2000 videokeratoscope. The Javal Schiotz keratometer was calibrated prior to its use.

4.4 Method

The SUN SK-2000 computer assisted keratoscope was used to derive central and peripheral corneal radii. Peripheral measurements were displayed even though ring images were not necessarily in that particular area of the cornea. In these cases one assumes that the SUN SK-2000 extrapolated the profile to compute the radius at the required point. There were unfortunately some limitations in that only eight peripheral points could be measured and no other points along a semi-meridian could be assessed.

The calibration procedure was performed prior to conducting each trial, measurements were performed by a single operator. Only one 8mm spherical calibration surface was provided by the manufacturers. No aspheric surfaces or other spherical surfaces were available. During the trial, calibration was checked before each experimental period on the keratometer and the SUN SK-2000. The influence of centration of the first Purkinje images with respect to the alignment system was noted.

The accuracy and repeatability of the system was assessed by observing the mean and standard deviation of five measurements using the calibration sphere. The level of agreement between SUN SK-2000 and the keratometer was also assessed. The importance of this comparison was that as the keratometer is the currently used standard for measuring central corneal curvature, the interchangeability of the two instruments must be examined. An instrument may be said to be in agreement with another when both can be used interchangeably and when any difference that may occur from one instrument to another will be so small as to have no clinical significance. The mean of three measurements of keratometry and videokeratoscopy compared (the method of statistical comparison for both agreement and repeatability is described in the results section).

In order to demonstrate any agreement between keratometry and the SUN SK-2000 videokeratoscope, central radii were converted to the Mean Refractive Error (MRE) of the cornea (a mathematical description of MRE is shown below). The term MRE is misleading when used in the present context. MRE was originally used to represent

the mean corneal power (particularly for an astigmatic eye) when assessing a patient's refractive error (or correction). In order to avoid any confusion, MRE will be referred to as Mean Corneal Power (MCP). The MCP was used to account for differences in the directions (or axis) of the flattest meridians found on both instruments so that direct comparisons of the results could be made. The process of astigmatic decomposition (converting radius of curvature into MCP) as described by Bennett and Rabbetts(1989) is shown below:

$$MCP = S + \frac{C}{2} \qquad \textit{Equation 4.01}$$

where S is the spherical component and C the cylindrical component of corneal power. A cylindrical component can be resolved into two plano cylinders at an axis of 0^0 and 45^0. These two components may be written as follows:

$$C_0 = C.\cos 2\theta$$
$$C_{45} = C.\sin 2\theta$$

where θ is the true axis of the cylinder C.

Thus, for example the keratometer may measure corneal power as +43.00/-2.00x50, and a videokeratoscope +43.50/-1.00x40, the power measured could be compared directly due to the difference in axis. However, converting the measurements into MCP permits direct comparison.

$\therefore$ **MCP** for the keratometer = +42.00D

MCP for the videokeratoscope = +43.00D

For the cylinder with keratometry C_o = -2.00 x Cos (100)

For the cylinder with videokeratoscopy C_o = -1.00 x Cos (80)

Repeatability of the instrument in measuring central and peripheral radius of curvature within subjects was evaluated by comparing the differences between two repeated sets of measurements. The mean of three readings was taken on each occasion and

compared. For an instrument to be repeatable, it must be capable of consistently reproducing the same result when no change in the topography of that surface has taken place.

Previous studies investigated agreement and repeatability by analysing data in terms of correlation coefficients, standard deviations and significant tests (Hannush et al, 1989; Tsilimbaris et al, 1991; Koch, 1992; Antalis et al, 1993). In the present study, the level of agreement and repeatability were assessed by analysis of the variance of the difference between either the keratometer and the SUN SK-2000 (in the case of agreement analysis) or measurements from one occasion to another (in the case of repeatability). Although observation of the variance would be correct, it would not present a clear picture of agreement or repeatability (particularly graphically).

A population of 20 male optometry students was chosen for this study. From these, three measurements of auto refraction, keratometry and videokeratoscopy were made in the right eye. A list of these 20 subjects , their age and refractive error is shown in table 4.01.

Table 4.01: List of subjects' age, race, mean ocular spherical and cylindrical refraction (using an autorefractor).

Subjects	Age	Race	Mean Sph RE	Mean Cyl RE
AK	18	C	-2.35	-0.25
BM	20	A	-0.05	-0.05
BW	18	C	-3.00	-0.50
CW	19	C	+4.25	-1.75
CS	20	C	+0.50	-0.65
DS	39	C	-4.10	-0.25
GH	18	C	-5.25	-0.60
JD	20	A	-3.00	-1.65
KD	18	C	-1.55	-0.20
LS	35	C	-1.55	-1.20
MH	19	C	+0.50	-0.35
MM	20	A	-2.45	-1.20
NC	19	C	-6.00	-0.50
NP	18	C	-0.25	-0.65
NS	19	A	-0.20	-0.35
PS	18	A	-0.30	-0.30
RS	19	A	-0.90	-0.5
RSB	18	C	+0.90	-0.10
SB	19	A	-7.90	-1.15
VK	19	A	-0.45	-1.15

* **C** -Caucasian **A**-Asian

4.5 Results

4.5.1 Accuracy and repeatability in determining the 8mm calibration surface

Evaluation of the accuracy of the SUN SK-2000 for five measurements of the 8.00mm sphere showed no significant difference between the mean spherical equivalent radius of curvature (this value was the mean of the central flattest and steepest radii of curvature) and the actual value of the calibration sphere (p=0.776). The standard deviation (± 0.013mm) of the mean of central and peripheral radius of curvature for

five measurements showed that the instrument was repeatable for spherical surfaces. The central mean spherical equivalent radius was found to be 8.001mm and the mean peripheral radius 7.999mm. Unfortunately, no measurements such as micrometry or interferometry were performed on the 8mm sphere. Thus, unless one accepted the manufacturer's measurements, there was no way of knowing whether the surface was actually 8mm. No other surfaces were provided by the manufacturers and therefore the range over which this accuracy holds was unknown.

4.5.2 The level of agreement between the SUN SK-2000 and the keratometer

A plot of MCP against keratometry was made (see figure 4.03). However, it has been shown that representation of results in such a manner is largely incorrect. The weakness of this method was described by Bland et al (1986) and Shaw et al (1994). A plot of SUN SK-2000 MCP against keratometer MCP was a useful initial step, however, unless there was very little agreement, the points would be clustered near a straight line and between method differences would be difficult to assess. The correlation coefficient is a measure of association not necessarily agreement; it depends directly on the variation within individuals (or measurement error). Also, the correlation coefficient would be predictably high for repeat measurements because the same variable was being measured on each occasion.

Altman et al (1986) and later and Shaw et al (1994) suggested that a plot of the difference between the variables against their mean would be more useful and informative. Both methods were used so that the results could be compared with other studies that used either form of presentation. Observation of table 4.02 and figure 4.03 shows that a high level of correlation was found in terms of MCP between the SUN SK-2000 and the keratometer, however the 95% limits of agreement (table 4.02 and figure 4.04) showed that there was very little agreement between the two instruments. The 95% limits of agreement (or confidence limits) were calculated as follows:

95% Limits of agreement = Bias $\pm$ 1.96 x Standard deviation *Equation 4.02*

The bias represents the mean of the differences. It must be stressed that the 95% limits of agreement were only estimates and only applied to this trial. However, one would not expect significantly different results in another trial providing the sample was normally distributed. The bias (the mean of the differences) showed that on average the SUN SK-2000 over estimated central corneal power by 0.33D compared to keratometry.

Table 4.02: Summary of the results obtained, where bias represents mean of the difference between keratometry and SUN SK-2000 videokeratoscopy; **S.D** represents the standard deviation, and **r** the correlation coefficient.

	Bias (D)	**S.D (D)**	**r**	**paired t-test**	**95% limits of agreement (D)**
MCP	+0.33	± 0.52	0.97	0.011	+1.32 to -0.69
C_0	-0.52	± 1.32	0.31	0.093	+2.07 to -3.11
C_{45}	+0.09	± 0.67	0.00	0.555	+1.40 to -1.22

Figure 4.03: Comparison of MCP (or MRE) obtained using the SUN SK-2000 and the Keratometer in the R.E of 20 males. r=0.97.

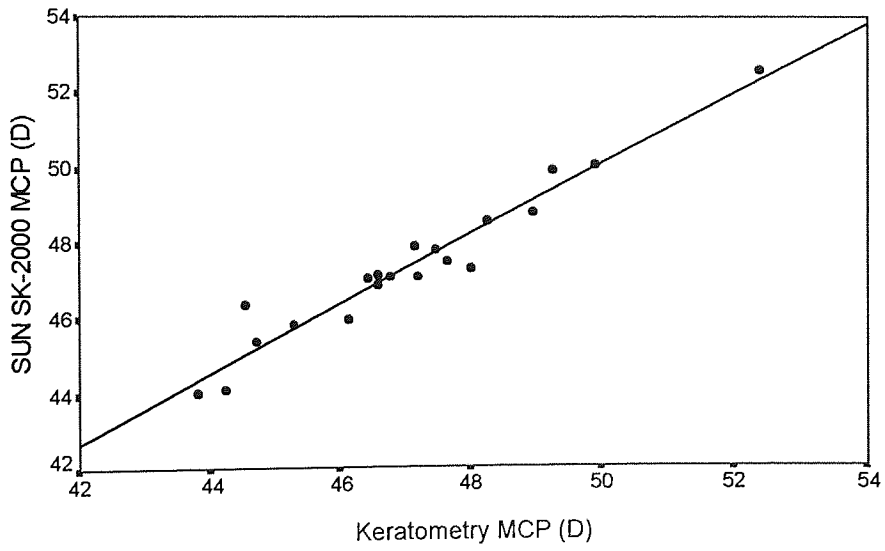

Figure 4.04: Agreement between the Javal Schiotz keratometer and the SUN SK-2000 in terms of MCP (or MRE).

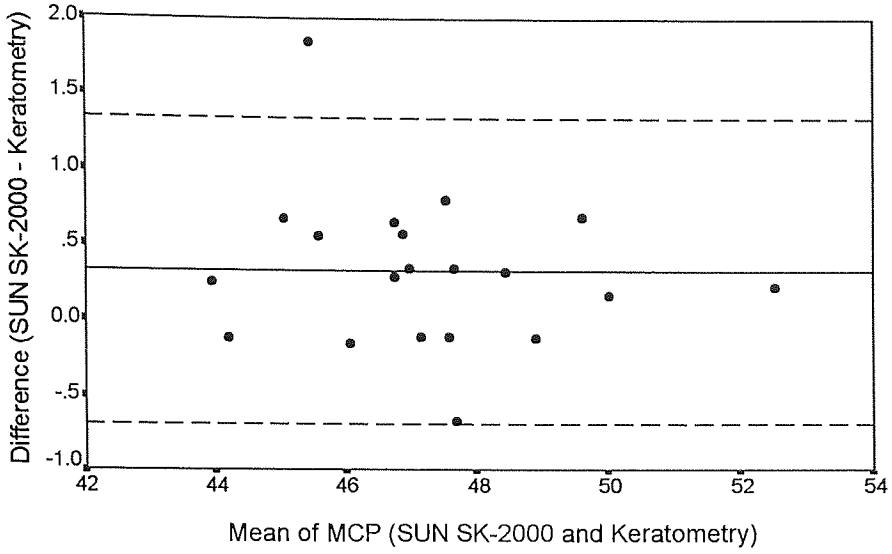

A paired t-test was also performed on the two samples. There was a significant difference between the central MCP of the SUN SK-2000 and central MCP of the keratometer (p=0.011). With regards to the $\mathbf{C_0}$ and the $\mathbf{C_{45}}$ components of corneal astigmatism, the paired t-test showed that the mean values were not significantly different (p=0.093 and p=0.555, respectively). However, the correlation coefficient showed a lack of association between the keratometer and the SUN SK-2000 with respect to the $\mathbf{C_0}$ and $\mathbf{C_{45}}$ components of corneal astigmatism.

4.5.3 The repeatability of the SUN SK-2000 videokeratoscope

The central flattest and eight peripheral meridians were compared on two separate occasions using the SUN SK-2000. Topographic analysis of the subjects' corneas was repeated three times on each occasion and the mean of the three readings from each occasion were compared in order to assess the repeatability. The abbreviations used to represent the central and peripheral curves are shown in figure 4.05.

Figure 4.05: Shows the abbreviations used in the assessment of repeatability.

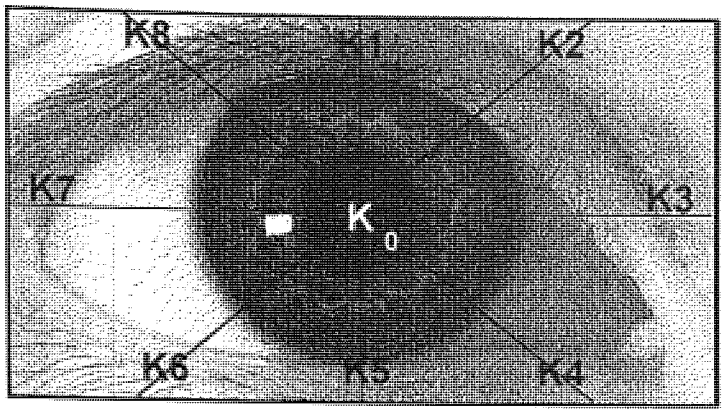

Table 4.03 shows the bias, standard deviation and the 95% limits of agreement of the central flattest meridian and eight peripheral meridians. Figures 4.06 to 4.14 show the repeatability results for each meridian.

Table 4.03 and figure 4.06 show that repeatability of the central flattest radius was reasonable (95% limits of agreement of +0.079mm to -0.013mm). As far as the peripheral radii were concerned, there seemed to be a trend such that the superior peripheral radius of curvature measurements were far less repeatable than those in the horizontal meridian.

Table 4.03: repeatability results of the R.E. The bias, standard deviations and 95% limits for the peripheral meridians (K1 to K8) are shown.

Meridian	Bias (mm)	Standard deviation (mm)	95% limits (mm)
K0	0.003	± 0.023	+0.079 to -0.013
K1	0.165	± 0.276	+0.705 to -0.376
K2	0.179	± 0.403	+0.969 to -0.610
K3	0.056	± 0.045	+0.144 to -0.033
K4	0.072	± 0.038	+0.145 to -0.002
K5	0.043	± 0.032	+0.106 to -0.021
K6	0.061	± 0.083	+0.233 to -0.102
K7	0.095	± 0.232	+0.549 to -0.36
K8	0.115	± 0.239	+0.583 to -0.354

Figure 4.06: Repeatability of the central flattest radius of curvature (K_o).

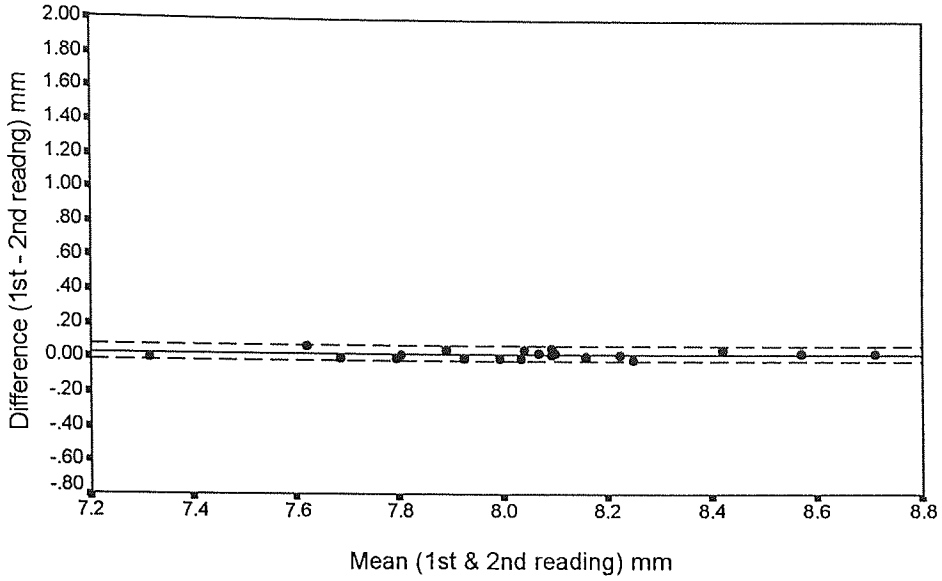

Figure 4.07: Repeatability of the superior meridian (K_1).

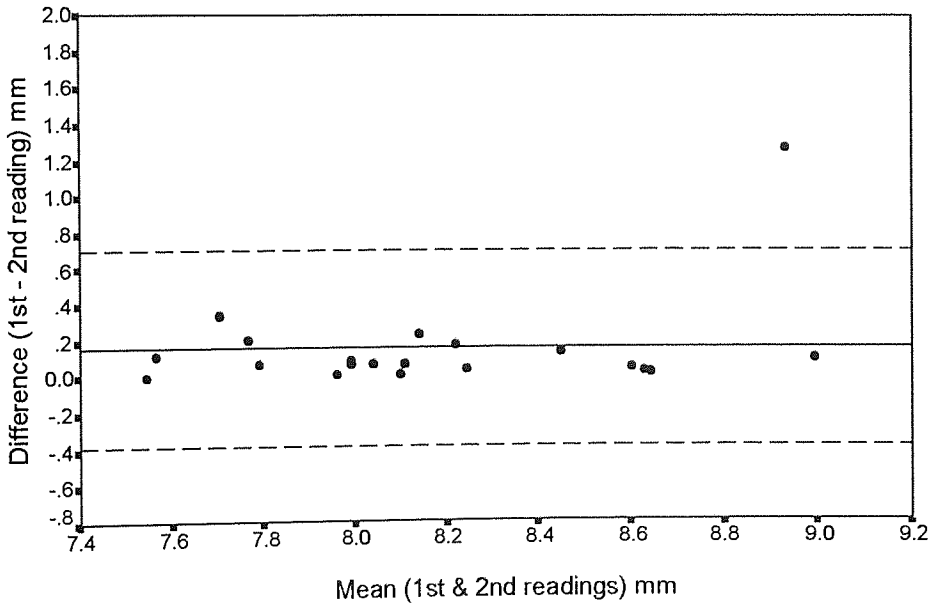

Figure 4.08: Repeatability of the superior nasal meridian (K_2).

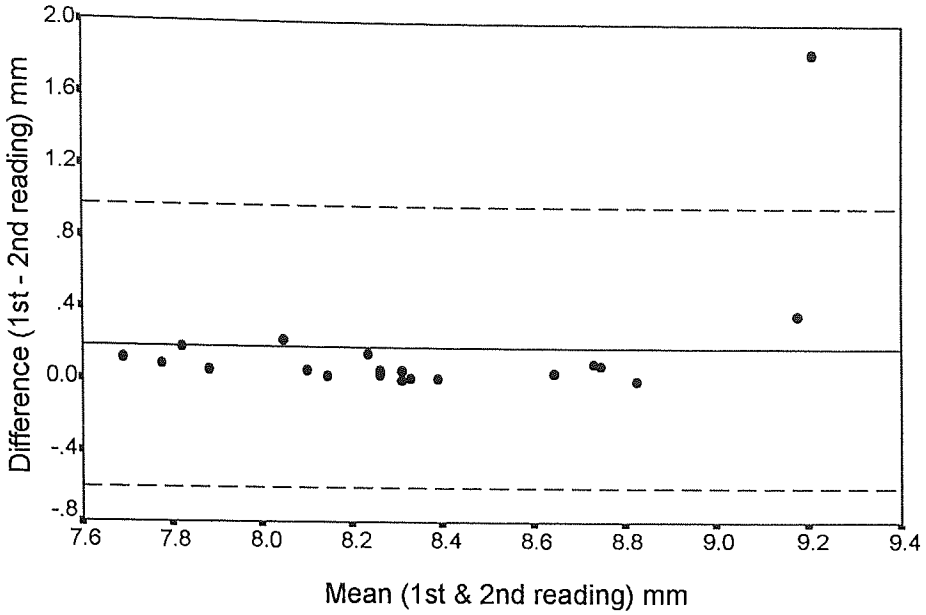

Figure 4.09: Repeatability of the nasal meridian (K_3).

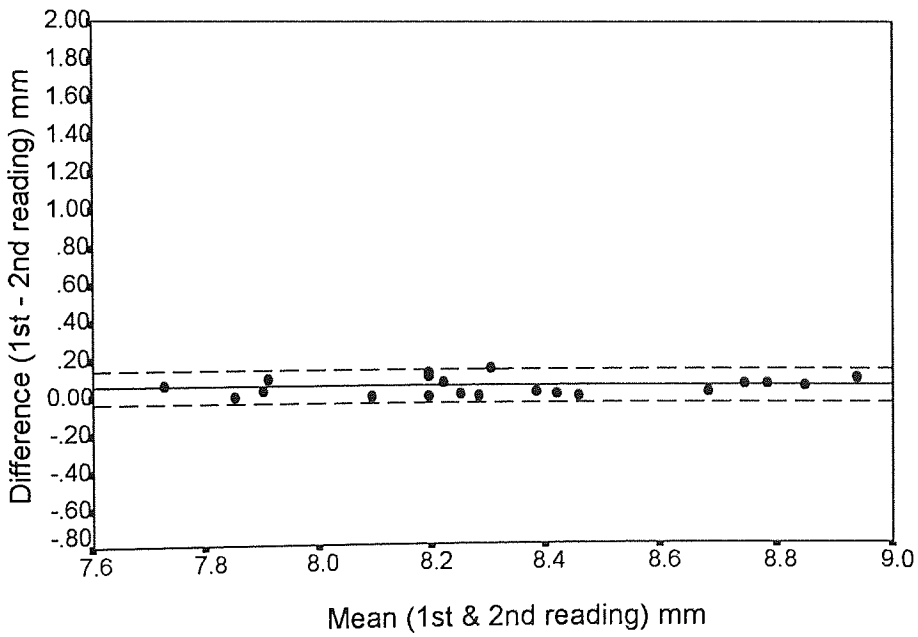

Figure 4.10: Repeatability of the inferior nasal meridian (K_4).

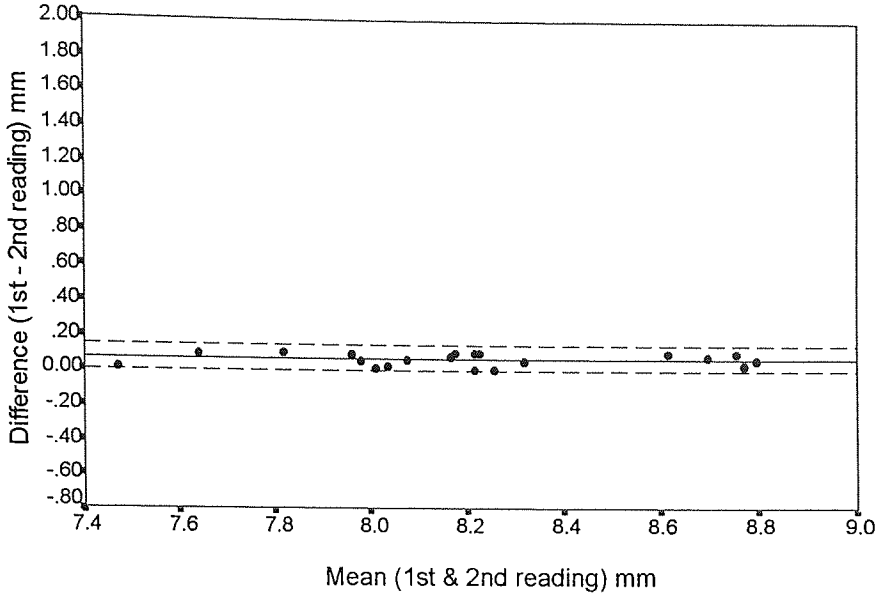

Figure 4.11: Repeatability of the inferior meridian (K_5).

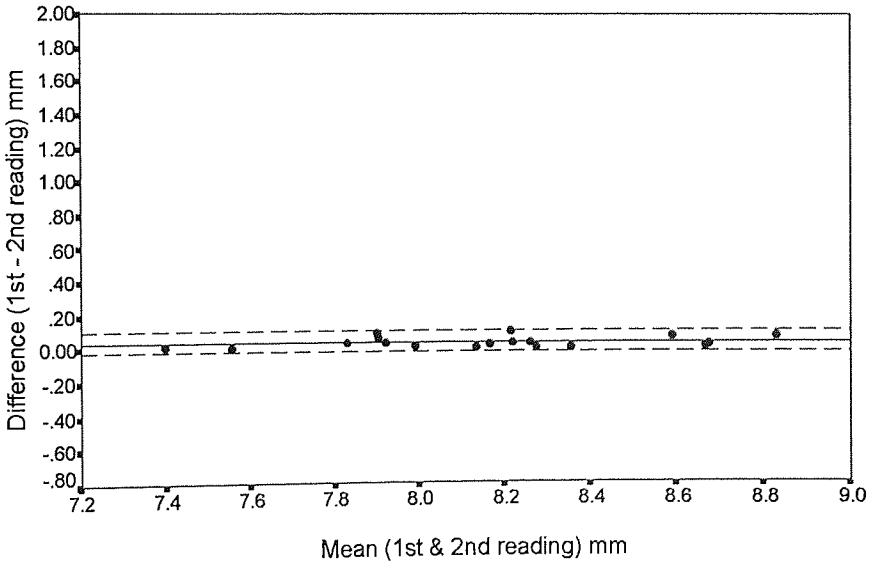

Figure 4.12: Repeatability of the inferior temporal meridian (K_6).

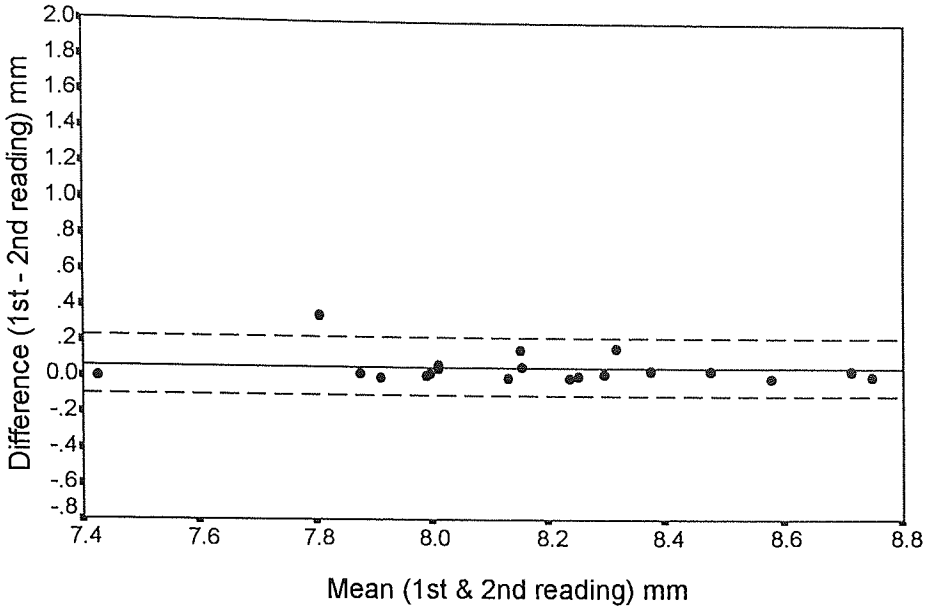

Figure 4.13: Repeatability of the temporal meridian (K_7).

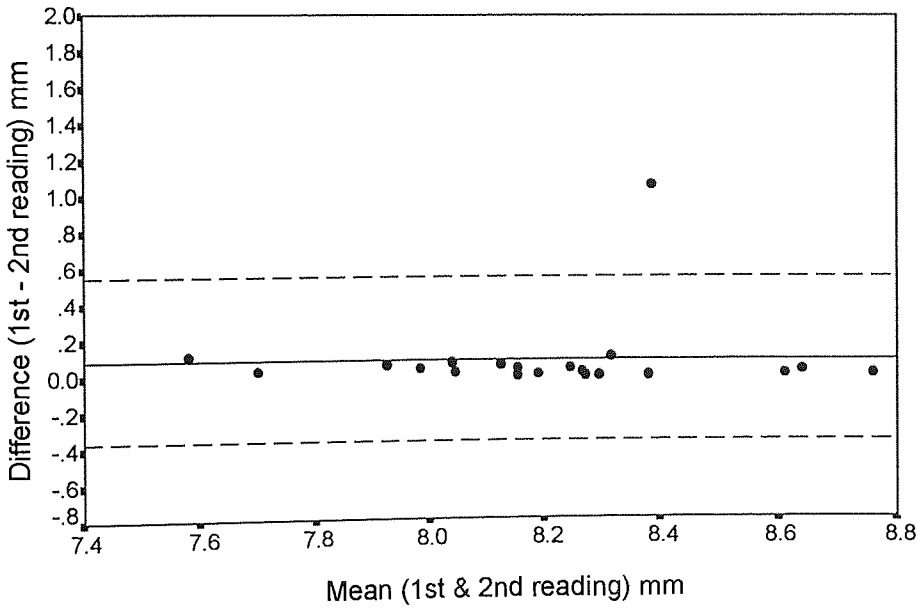

Figure 4.14: Repeatability of the superior temporal meridian (K_8).

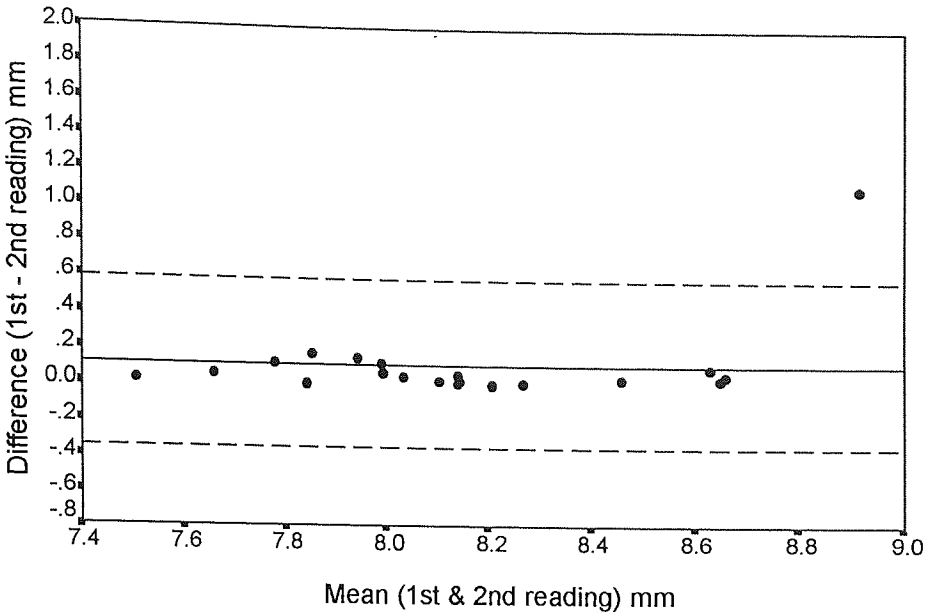

4.5.4 Evaluate the alignment system used in the SUN SK-2000 videokeratoscope

The SUN SK-2000 was also used to measure the 8mm spherical surface with normal alignment and then at a point that was superior temporal to the apex. Figures 4.15 and 4.16 show the effect of misalignment on induced asymmetry. Misalignment caused significant asymmetry in the peripheral readings. Unfortunately, at the time of performing the experiment, there was no method of accurately locating the position of the sphere relative to the videokeratoscope axis. However, it was not the purpose of the study to investigate the effect of degree of misalignment on induced asymmetry.

Figure 4.15
Peripheral radius with correct alignment.

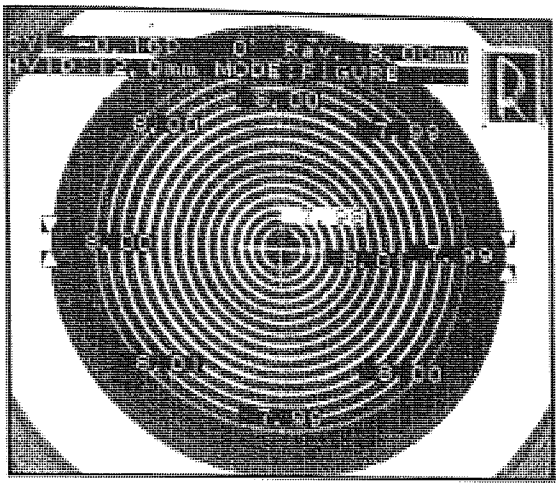

Figure 4.16
Peripheral radius misaligned superior and temporally

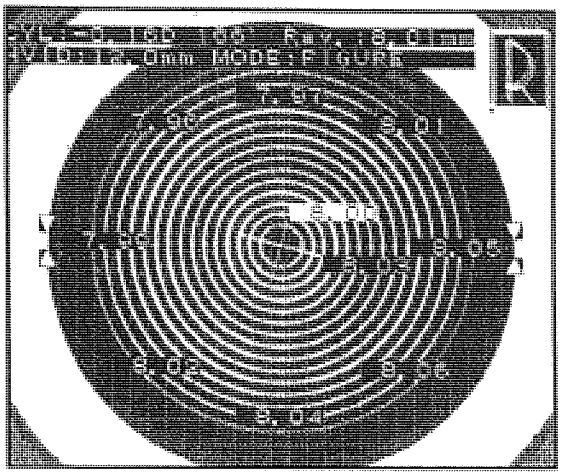

4.6 Discussion

4.6.1 Accuracy in Determining the 8mm Calibration Surface

Assuming that the manufacturer's value for the radius of curvature of the 8mm calibration sphere was correct, then the SUN SK-2000 videokeratoscope measured this to a high degree of accuracy (mean spherical equivalent radius of 8.001mm and mean peripheral radius of 7.999mm). No significant difference between the actual and measured radius of curvature was found (p=0.776) and the SUN SK-2000 exhibited a high level of reproducibility (standard deviation=$\pm$0.013mm). However, the accuracy of the system could not be judged by the accuracy of the SUN SK-2000 in measuring a single calibration sphere. Multiple spherical and aspheric surfaces would have to be used (see chapter 5 for the use of spherical and aspheric surfaces with the EyeSys CAS, EyeSys Laboratories, Houston, TX, USA). Unfortunately, at the time of the study, no such surfaces were available.

In a comprehensive study by Hannush et al (1989) the accuracy of a keratometer (Bausch and Lomb, Rochester, New York), Kera Corneascope (Kera Corp., Santa Clara, California) and the Corneal Modelling System (Computed Anatomy Inc, New York) was compared using four steel spherical balls (43.00D, 42.52D, 50.14D and

38.66D). Each instrument was compared with the Bausch and Lomb keratometer by calculating the simulated keratometer values of the Kera Corneascope and the Corneal Modelling System. Their results showed that the Corneal Modelling System was the most accurate (mean deviation, or bias, of 0.10D; standard deviation of the difference between the actual and measured value=$\pm$0.07). There was no significant difference between the keratometer and the Corneal Modelling System in terms of accuracy (p=0.19) or precision (p>0.05). However, both the Keratometer and the Corneal Modelling System were more accurate and precise than the Kera Corneascope (P<0.01)

Centration of the Purkinje images (figure 4.01) with the alignment squares was essential for accurate measurement, although no physical measurements of decentration were made, on deliberate decentration along the x and y axes (see figure 4.02) asymmetries occurred with the calibration sphere. This observation was in agreement with the results of McCarey et al (1992) who actually controlled x and z axis decentration using a micrometer and then measured the radius of a 47D sphere using the EyeSys CAS. McCarey et al (1992) found that a lateral decentration of approximately 1mm led to significant differences in radius/power measurements from the true value of the sphere; they also noticed the EyeSys measured the sphere to be more toroidal on decentration. For z-axis misalignment, the accuracy of the EyeSys deteriorated after 1mm decentration towards the sphere and up to 2mm away from the test sphere.

4.6.2 The level of agreement between the SUN SK-2000 and the keratometer

In clinical practice most eye-care practitioners only have access to the keratometer, nevertheless, it has been successfully used to measure central corneal radius for many years. Based on results of the present study, the level of agreement between the keratometer and the SUN SK-2000 was not acceptable in terms of MCP (95% limits from +1.32D to -0.69D and p=0.011) on the grounds that in a clinical environment

measurements need to be performed to the nearest 0.02mm or 0.1D for applications such as contact lens fitting (Stone, 1962).

Zadnik et al (1992) assessed the agreement Bausch and Lomb keratometer (Bausch and Lomb, Rochester, New York) and a nine ring Kera Corneascope (Kera Corp. Santa Clara, CA) using the same method of statistical analysis as the present study in forty subjects. Their results also showed a lack of agreement between the two methods of central corneal curvature analysis (95% limits of agreement: +0.59D to -1.72D). However, the bias (or the mean difference between the two instruments) of -0.57D was different to that found in the present study. The bias found in the study by Zadnik et al (1992), indicates that on average, measurements of central corneal power using the Kera Corneascope were less than the keratometer (Bausch and Lomb) by -0.57D. Discrepancies between the two types of instruments may be attributed to the method of central corneal alignment (see section 4.6.4), the algorithms used in the subsequent reconstruction of a three dimensional corneal surface and the ring zones used in the videokeratoscopes to simulate keratometer readings.

In another study by Tsilimbaris et al (1991) comparisons of the Javal Ophthalmometer and the EyeSys Corneal Analysis System were made in ninety-two normal eyes. A mean difference (bias) of +0.03D was found indicating that the EyeSys only slightly over-estimated central corneal power compared to the Javal Ophthalmometer. Although no limits of agreement were stated, a standard deviation of ±0.46 was found. From this it was possible to calculate the 95% limits of agreement (see table 4.04).

Table 4.04: Summarises the results of comparative studies of keratometers and videokeratoscopes. VK is an abbreviation for videokeratoscope.

Study	VK	Keratometer	Bias (D)	SD (D)	95% Limits (D)
Present study	SUN SK-2000	Javal	+0.33	± 0.52	+1.34 to -0.69
Zadnik et al (1992)	Kera Corneascope	B+L	-0.57	± 0.59	+0.59 to -1.72
Tsilimbaris et al (1991)	EyeSys	Javal	+0.03	± 0.46	+0.93 to -0.87

The limits of agreement found in the study by Tsilimbaris et al (1991) were not within the narrow band whereby videokeratoscopy would be interchangeable with keratometry. None of the studies showed that the two types of instruments were interchangeable. The low bias found by Tsilimbaris et al (1991) showed that on average the EyeSys resembled keratometer readings more than the Kera Corneascope and the SUN SK-2000. Nevertheless, Tsilimbaris et al (1991) stated that there was no significant difference between the Javal keratometer and the EyeSys CAS in terms of mean central corneal power (p=0.471). However, the statistical test performed was not an appropriate method of assessing agreement between two methods (Bland and Altman, 1986; Shaw et al, 1994), hence the incorrect conclusion drawn by Tsilimbaris et al (1991) that both instruments were in agreement. According to Bland and Altman (1986), tests of significance may show that two methods are related but to prove that the two methods are significantly different would be highly unusual.

It is worth considering the actual radius measurement performed by each instrument. Whenever rays from an oblique point are reflected from an optical surface (as in videokeratoscopy), oblique astigmatism is induced. The result is that two images are formed - the sagittal and the tangential images (see figure 4.17). Hence, two radii must be considered. Bennett et al (1991) showed that the keratometer is focused on the tangential image plane. However, measurements are made on the axis of the keratometer and therefore it is impossible for a standard keratometer to perform measurements of tangential radius. The eventual outcome of the numerous computations and proofs made by Bennett et al (1991) was that the radius measured during keratometry most closely approximated the sagittal radius of the surface. In addition, Bennett et al (1991) found that for central corneal measurement, the sagittal radius of curvature was a better determinant of the actual central radius of curvature than the tangential radius. Indeed, the radius of curvature found with keratometry (which is effectively $\mathbf{r_s \times constant}$) is a more accurate method of finding $\mathbf{r_0}$ (the apical radius of an aspheric surface).

The sagittal radius, for a flattening conic, is always less than the tangential radius and both are larger than the apical radius (r_o). The difference between the two measurements depends on the actual central radius of the surface and the degree of peripheral flattening (the p-value). Observation of the results show that the SUN SK-2000, on average overestimated MCP by 0.326D i.e. the radius obtained using the SUN SK-2000 was steeper. If the central corneal radius obtained using the SUN SK-2000 was tangential then the error of the instrument in determining central corneal radius was actually worse than has been shown by the results. Unfortunately, the manufacturer's literature did not state whether radius measurements were tangential or sagittal. In contrast, Zadnik *et al* found that the Kera Corneascope on average underestimated corneal power. The different types of radius measured may therefore have a role in the lack of agreement in their study.

From data values published in a paper by Bennett et al (1991), for a surface having an apical radius of 8.00mm, p-value of 0.8 at a chord length of 1.4381mm, the sagittal radius was found to be 8.026mm and the tangential radius 8.078mm (a difference of 0.052mm). Thus, the actual radius measurement performed has a significant influence on the radius obtained.

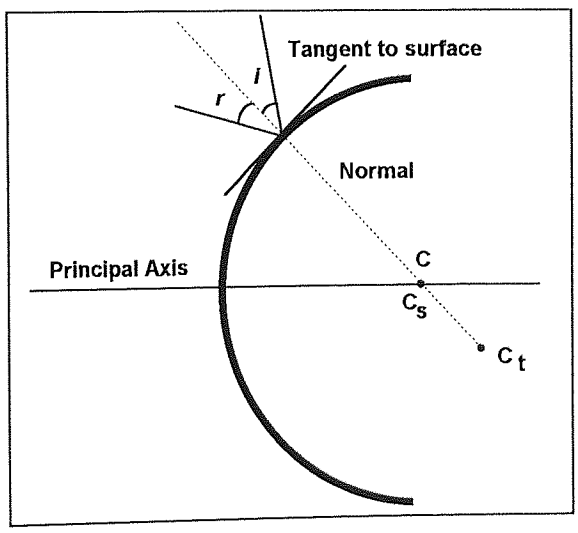

Figure 4.17: Shows the location of the sagittal C_s and tangential C_t radius of curvature (after Bennett et al, 1991). The tangential plane is in the plane of the diagram, containing the normal and the principal axis. The sagittal plane is perpendicular to the tangential plane and also perpendicular to the plane of the diagram, it also contains the normal.

The C_0 and C_{45} components of corneal astigmatism for the SUN SK-2000 showed poor correlation with the keratometer ($r = 0.31$ and 0.00, respectively). The low levels of association between the keratometer and the SUN SK-2000 were accounted for by the fact that the magnitude of the corneal cylinder values were comparable to the differences found between the two instruments. A two dioptre difference in MCP would not significantly alter the correlation coefficient as the values of MCP were often in the 40D range. However, as corneal astigmatism was small, differences as little as 0.5D would alter the correlation coefficient. The 95% limits of agreement showed that the keratometer and the SUN SK-2000 were not in agreement for measurements of MCP, C_0 and C_{45}.

4.6.3 The repeatability of the SUN SK-2000 videokeratoscope

For effective use of an instrument in clinical practice the instrument must be repeatable i.e. any changes in the results of the SUN SK-2000 on two separate occasions should not be due to the of instrument but due to an actual change in corneal topography.

The SUN SK-2000 exhibited greatest repeatability in measuring central radii. This was demonstrated by the low bias (mean difference=0.003mm) and also the 95% limits of agreement having the narrowest bands (+0.079mm and -0.013mm). The 95% limits of agreement showed that in 95% of cases a difference from one occasion to another of +0.079mm to -0.08mm could be attributed to the instrument and not to an actual change in corneal topography. The obvious assumption made was that from one occasion to another no change in corneal topography had taken place in subjects' corneas. Depending on practitioner criteria, such variance in the instrument measurement may or may not be acceptable.

Zadnik et al (1992) examined the repeatability the Kera Corneascope in the central region of the cornea. The 95% limits were presented in terms of dioptres. Their results may be converted to radius measurements so that a comparison can be made. Assuming that a difference of 0.50D from one measurement to another corresponds to

a 0.1mm difference in radius, the 95% limits in the Zadnik et al (1992) study in millimetres would be +0.118mm to -0.344mm. A considerable difference between the two studies was observed, indicating a very poor repeatability for the Kera Corneascope for the central area of the cornea.

Although experimental studies have been performed on reproducibility (Koch et al, 1989; Koch et al, 1992; Legeais et al, 1993), few studies have used the statistical methods suggested by Bland and Altman (1986). The SUN SK-2000 only displayed the peripheral radius at one point in a semi meridian and there was no option available to display the radii of other points. Therefore, as opposed to other studies, where the repeatability of individual rings was assessed (Koch et al, 1989; Hannush et al, 1990; Legeais, 1993), for the SUN SK-2000 the repeatability of peripheral readings was evaluated.

Peripheral radii showed variable repeatability depending on the meridian measured. Generally, the horizontal and inferior meridians were more repeatable than the superior meridians. One possible reason could be the influence of the ocular adnexa i.e. the lids and lashes. If this were the case, then repeatability would be poor in all videokeratoscopic devices of this nature. Another factor that could have accounted for the reduction in repeatability was incomplete target ring imaging (therefore there could be some extrapolation to calculate peripheral radii).

4.6.4 Evaluation of the alignment system used in the SUN SK-2000 videokeratoscope

The actual alignment system was useful in that the position of the entrance pupil with respect to the Placido rings could be seen. Hard copies also displayed the entrance pupil, Applegate (1992) suggested that from a functional and clinical viewpoint, the entrance pupil represents a good reference point from which other keratographs could be compared.

It was interesting to note the actual point from which measurements were being taken. The alignment system required the patient to view a fixation point in an attempt to align the line of sight with the optic axis of the instrument. According to Klyce (1984), for the algorithms to be valid, the instrument axis must be perpendicular to the cornea i.e. the instrument axis must be directed towards the centre of curvature of a point on the cornea. In the case to the SUN SK-2000 this was achieved when the first Purkinje images were aligned inside the reference squares (see figure 4.01). Unfortunately, when this condition was met the instrument axis was no longer coincident with the line of sight and measurements were being performed from some unknown point (Mandell, 1992; Mandell, 1994), see figure 4.18.

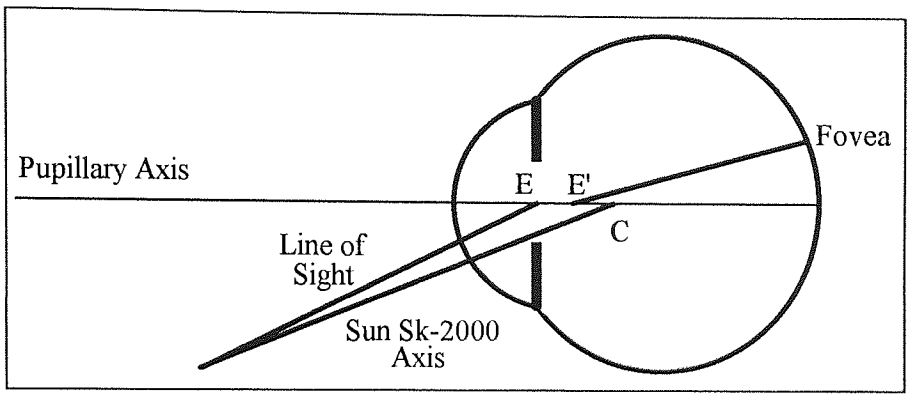

Figure 4.18: Current alignment system in the SUN SK-2000 videokeratoscope, alignment was made at a unknown point on the cornea. **E** and **E'** are the entrance and exit pupils, respectively and **C** the centre of curvature of the unknown peripheral point.

Therefore, with reference to the MCP found using the keratometer and the SUN SK-2000, the lack of agreement could be explained because measurements were not being taken from the same point on the cornea. A more suitable reference point on the cornea would be where the line of sight intersects with the cornea. Alignment with the line of sight could be made by asking the patient to view an eccentric fixation point and then centring the system at the centre of the entrance pupil. In this way, the videokeratoscope would be aligned at a point on the cornea through which the line of sight passes (see figure 4.19).

In chapter 3, the conditions or assumptions of videokeratoscopy were stated. One of the assumptions was that the centre of curvature of the surface being measured should be coincident with that of the videokeratoscope axis, this was to prevent artifactual asymmetry from occurring (see figure 3.03). The method of alignment suggested by Mandell (1994) enables the videokeratoscope axis to be perpendicular to the centre of the curvature of a point on the cornea, however, the fundamental difference is that alignment is being made at a point on the cornea that is closer to the apex and coincident with the line of sight. The alignment of videokeratoscopic systems should be performed with respect to the line of sight.

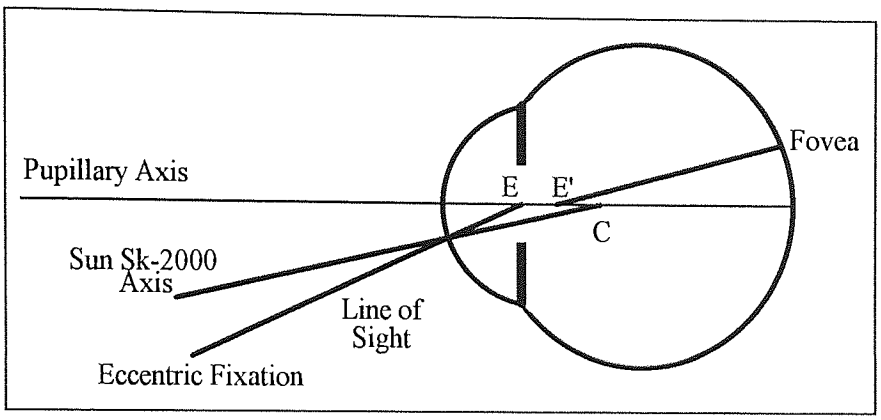

Figure 4.19: Modification of the alignment system (after Mandell, 1992; Mandell, 1994) so that alignment is at a unique point on the cornea where the line of sight and the videokeratoscope axis intersect. **E** and **E'** are the entrance and exit pupils, respectively and **C** the centre of curvature of a unique point on the cornea where the line of sight and the optic axis of the SUN SK-2000 coincide.

4.7 Summary

The SUN SK-2000 computer assisted videokeratoscope attempted to provide potentially useful information that if repeatable would be of invaluable use to eye-care practitioners. Colour coded maps, on screen rigid contact lens fitting and a feature that suggested the optimal commercial contact lens were useful features of this system. Unfortunately, little agreement was found between the keratometer and the SUN SK-2000. Furthermore, peripheral corneal measurements showed poor repeatability particularly in the superior corneal region. It was suggested that the ocular adnexa and

possibly extrapolation of data points could have a role in the poor repeatability in the superior meridian.

Manufacturer's should clearly state which radius videokeratoscopic systems are measuring. With the development of software both sagittal and tangential radii could be displayed. Other limitations were that only eight peripheral meridians could be analysed and that colour coded maps did not allow the user to assess corneal radius values with a cursor. Finally, method agreement and repeatability analysis should be performed using appropriate statistical methods (Bland and Altman, 1986; Shaw et al, 1994). Further investigations as to the accuracy of the system using spherical and aspheric test pieces should be conducted.

Chapter Five

A Clinical Trial of the EyeSys Model II Computerised Videokeratoscope

5.1 Introduction

The development of contact lenses has provided a major step forward in the correction of refractive error. However, since their development many problems have also arisen. For example, every practitioner involved in contact lens fitting will have noticed a case where a soft contact lens moves either excessively or not at all when fitted in the recommended manner. This shows how little bearing keratometer readings have on the final fit of a soft contact lens as more information on the shape of the periphery of the cornea is required. Similarly, with the development of numerous rigid lens designs manufacturer's claims of superior fitting design may only be said to apply to a specified proportion of the population because there is such a wide range of normal corneal shapes (Guillon et al, 1986). These problems, together with the difficulty encountered in surgically modifying the corneal surface, necessitate the use of an instrument that is capable of evaluating the corneal surface quantitatively and qualitatively.

Since the development of the Placido disc, many researchers have attempted to accurately measure the corneal surface (Knoll et al, 1957; Townsley, 1967; Koch et al, 1989; Klyce 1984; Wang et al 1989). The majority of investigations have concentrated on the development of devices based on the Placido disc method - namely keratoscopy. The technique and the subsequent derivation of the corneal profile has been described in chapter 3, however, essentially the consecutive ring separations of a reflected ring shaped target are measured and then algorithms are applied that enable the shape of corneal surface to be calculated. The algorithms have taken three forms, a brief summary is appropriate to the present study.

- **Calibration method** - this method was devised by Mandell (1967) where ring separations were compared and matched with those from a known reflecting sphere. This technique is no longer used as it assumes that the corneal surface is spherical and that the images of the rings are focused at a fixed distance from the videokeratoscope.

- **One step curve fitting method** - in this method the derived geometry of the corneal surface was fitted to a predetermined model of the cornea. Researchers have generally used conic sections as models to represent the corneal surface (Edmund et al, 1985, Edmund, 1986). El Hage (1972) derived a differential equation for a specific type of keratoscope (where a pinhole was inserted between at the focal point in the image plane). The Computerised Corneal Topographer (EH-270) utilises these principles.

  One step curve fitting to an entire section of the cornea placed a global constraint on the reconstructed surface and inevitably resulted in a reduction in the resolution of the system. It is important to appreciate that although the cornea can be modelled using conic sections, the asphericity of the cornea may not necessarily be constant in a single meridian. It would be more accurate to fit conic sections or polynomial curves to a semi-meridian (i.e. from some peripheral point to the point of alignment) after individual co-ordinate points of the reflecting surface have been calculated.

- **One step co-ordinate method** - originally described by Doss et al (1981), this novel method assumed that the reflecting surface could be reconstructed using multiple arcs of varying radius of curvature which shared the same normal. The multiple arc model was analogous to the continuous curve or 'offset' lens design (see figure 5.01). The principle disadvantage of the one fit method was that the various radii of curvature were all directed towards the origin of the co-ordinate system. Klyce (1984) improved the algorithm by adding a separate algorithm for the calculation of central corneal elevation (previously Doss et al (1981) pre-set the

central radius of curvature to 7.80mm and thereby biased the profile). Further, Klyce (1984) also made an allowance for the centres of curvature to lie on a point other than the optic axis of the instrument. One fundamental assumption made in the calculations was that the height of the point of reflection at the cornea was equal to that at the image plane. More recently, Wang et al (1989) modified this approach such that the latter assumption was not made. Andersen et al (1993a, 1993b) derived a similar technique based on locating the angular subtense of the targets at the image plane using a reference sphere and then using these values to derive the corneal co-ordinates using other algorithms (a detailed description is provided in chapter 7).

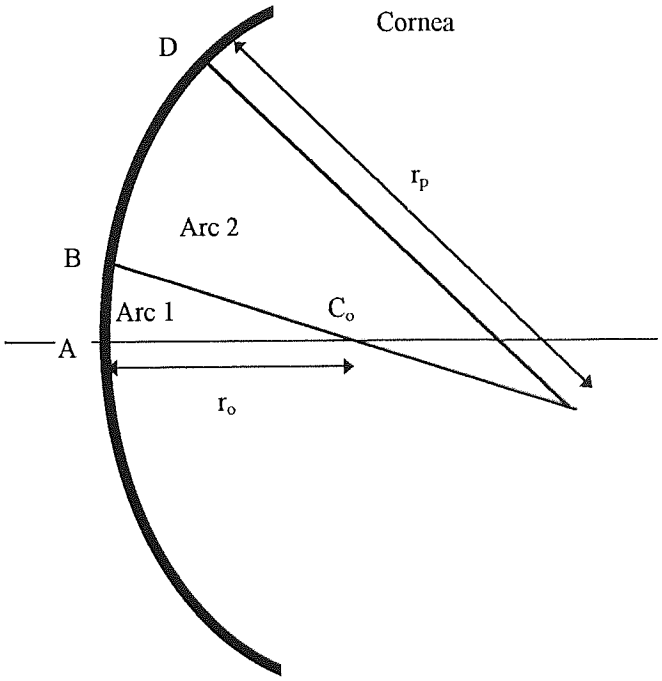

Figure 5.01: shows how the cornea may be composed of two spherical arcs that share a common normal BC_o. This allows continuity between adjacent sections. The arc containing the part of the cornea AB and BD is assumed to be spherical. r_o is the apical radius of the cornea, r_p is the radius of curvature of a peripheral point on the cornea at point D.

Many corneal topographic systems have now been developed each with their own proprietary software for corneal profile reconstruction. It is therefore essential that a clear evaluation of these systems is performed. Numerous studies have been published regarding the accuracy and repeatability of computerised videokeratoscopes (Hannush

et al, 1989; Koch et al, 1989; Hannush et al, 1990; Tsilimbaris et al, 1991; Koch et al, 1992; Zadnik et al, 1992; Dave et al, 1995). The statistical analysis has varied, comparisons of instruments have been performed with correlation coefficients and paired t-tests.

5.2 Aims

The repeatability of videokeratoscopic devices in various meridians and any relationship regarding the repeatability with respect to the distance from the vertex normal has not been well documented. Moreover, in the previous chapter, the repeatability of the SUN SK-2000 (SUN Contact Lens Company, Kyoto, Japan) was assessed in eight meridians, a poorer repeatability in the superior meridian of the cornea was found. It was suggested that the reduced repeatability was due to a combination of some form of extrapolation from curve fitting and the interaction of the ocular adnexa with the measurement process. Unfortunately, the SUN SK-2000 did not permit evaluation at specified points on the cornea. Furthermore, the analysis of the accuracy was limited due to the unavailability of aspheric and spherical surfaces. In present study, the EyeSys Corneal Analysis System (EyeSys Laboratories, Houston, Texas) was used to evaluate the following:

- the level of agreement of the EyeSys CAS with the Bausch and Lomb keratometer (Bausch and Lomb, Rochester, NY) in forty eyes.

- To assess the repeatability of the EyeSys CAS in four meridians (nasal, temporal, superior and inferior) in twenty-two eyes.
- To assess any relationship between repeatability and the distance from the vertex normal in 22 subjects. The vertex normal refers to the point on the cornea whose tangent is perpendicular to the videokeratoscope axis.
- To evaluate the accuracy of EyeSys CAS in measuring aspheric surfaces.
- To evaluate the repeatability of the EyeSys CAS in measuring aspheric surfaces.

5.3 Instrument Description

The EyeSys CAS is based on the familiar principles of keratoscopy. The target system comprised of an eight ring Placido disc (eight light and eight dark shown in figure 5.02) mounted on a conical surface (Hodd et al, 1993). The conical surface had the effect of optimising target size and reducing the curvature of the image plane (Bibby, 1976). The EyeSys version model I operates at a working distance of 92mm (Koch, 1992) this relatively moderate working distance has been shown by Nieves et al (1992) to reduce the error due to misalignment and defocus compared to the TMS (Computed Anatomy, Inc.). As a consequence of the working distance and the cone design, the EyeSys has been shown to measure a diameter of 9.2mm for a 42.5D cornea (Koch et al, 1993).

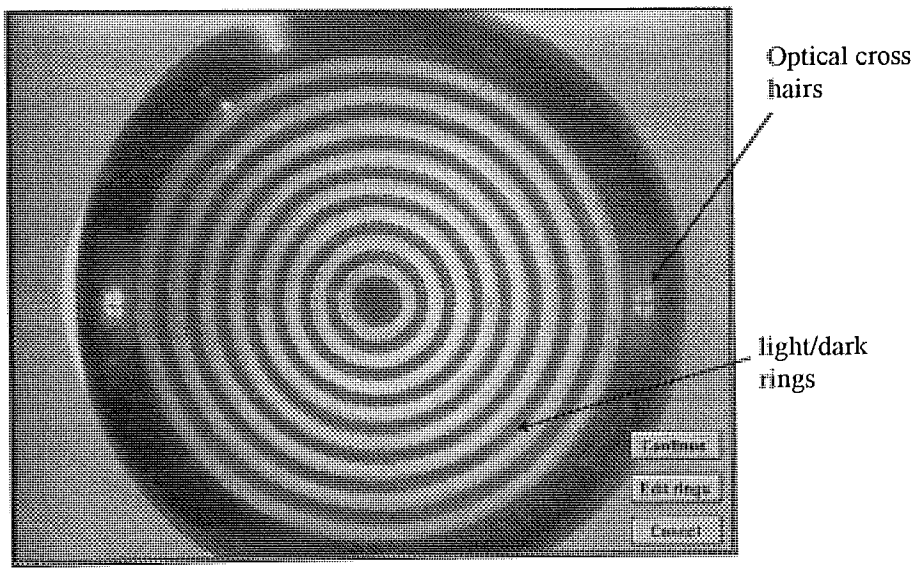

Figure 5.02: shows the eight rings of the EyeSys CAS.

Typically, the system hardware comprised of a high resolution (512x512) CCD (charge coupled device) camera for image capture, a 486 processing IBM compatible computer and an ink-jet colour printer. Fixation was achieved by the subject viewing a green fixation light. The instrument was then focused by alignment of the optical cross hairs (shown in figure 5.02). Once the image was captured, the EyeSys applied a sophisticated and proprietary 'sub-pixel' resolution program that located the ring

interfaces (see figure 5.03). The purpose of such a program would be to accurately locate the reflected ring images. The inner edge of the white rings were outlined by a yellow line and the outer edges with a red line. Having located and digitised the image, analysis of each of the sixteen white/black ring interfaces was commenced at one degree intervals over 360°. The result was a high resolution analysis brought about by the analysis of a total of 5760 points. Manual digitisation was also possible in cases where there was significant distortion of the reflected rings.

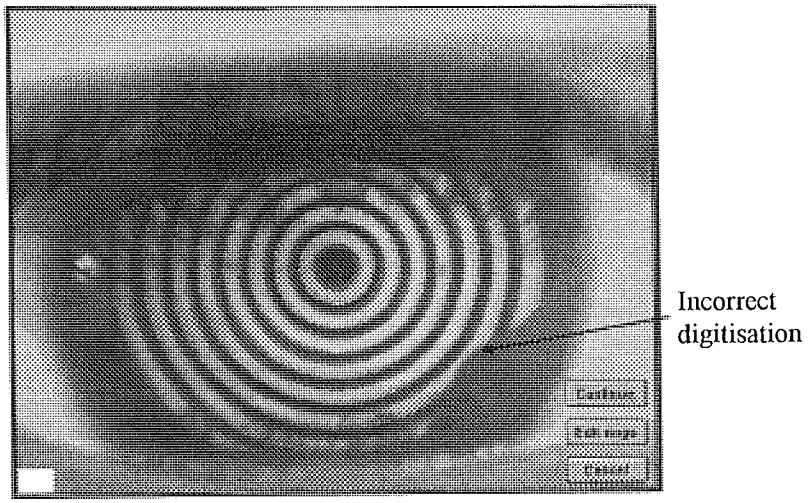

Figure 5.03: The EyeSys 'sub-pixel' digitisation for a human eye. Note how the left inferior rings were incorrectly digitised.

More recently, EyeSys manufacturer's devised a method for the location of the entrance pupil. For the purpose of measurement and alignment it has been suggested that the entrance pupil serves as the most suitable reference point (Applegate, 1992). Mandell (1992) suggested a modified method for alignment in which the entrance pupil was used in the actual alignment procedure to permit alignment with a unique point on the cornea where the line of sight intersected the instrument axis (see chapter 2, figure 2.05) .

It was suggested by Antalis et al (1993) that the radius and the sagittal depths of each point analysed are calculated using the method of one step corneal profile fitting as described by Doss et al (1981), Klyce (1984) and more recently by Wang et al (1989). However, the algorithms used by the EyeSys CAS were unique and proprietary.

Numerous data presentations were available such as keratometric displays, profile graphs, colour coded contour maps, data fusion displays and raw data tables. The present study obtained data from the keratometric plots and the raw data tables (see figure 5.04 and 5.05). These tables could be used to find the radius at any meridian for each ring imaged on the cornea. Only the radius of curvature of points where the rings were imaged was displayed.

5.4 Samples and Procedure

For the comparison of the EyeSys CAS and the Bausch and Lomb keratometer, forty eyes were compared. The Bausch and Lomb keratometer was also calibrated in the normal fashion and the eyepiece focused. The simulated keratometer readings at 3mm from the vertex normal (figure 5.04) were used in the comparison with the keratometer. Instrument accuracy was assessed by measuring twelve convex aspheric surfaces (CLS Ltd., Huntington, U.K.) and comparing the measured central and peripheral radius with the actual central and peripheral radius at the same points on the surfaces. The accuracy of the manufactures values were confirmed by Form Talysurf analysis (by Rank-Taylor-Hobson laboratories, Leicestershire, U.K.).

In order to assess the repeatability of the EyeSys CAS, a total of 22 eyes were measured twice. The measurements were repeated by the same operator by aligning the EyeSys with the subject's eye then withdrawing the patient and then realigning the instrument. Repeatability of only the instrument i.e. not including any variation from human subject variability was evaluated by performing repeated measurements in four meridians (superior, inferior, nasal and temporal) for each of the aspheric surfaces. The raw data tables (figure 5.05) were used analyse any relationship between peripheral radius and the distance from the vertex normal from where measurements were taken. The operator had used the EyeSys CAS many times as part of the patient examination procedure in a busy contact lens practice, the keratometer used was that resident in the operator's consulting room. Prior to the experimental procedure, the EyeSys CAS was calibrated in accordance with manufacturer's recommendations.

Figure 5.04: The simulated keratometric display in the EyeSys Corneal Analysis System. The astigmatic torque describes the change in directions of the principal meridians at two zones on the corneal surface.

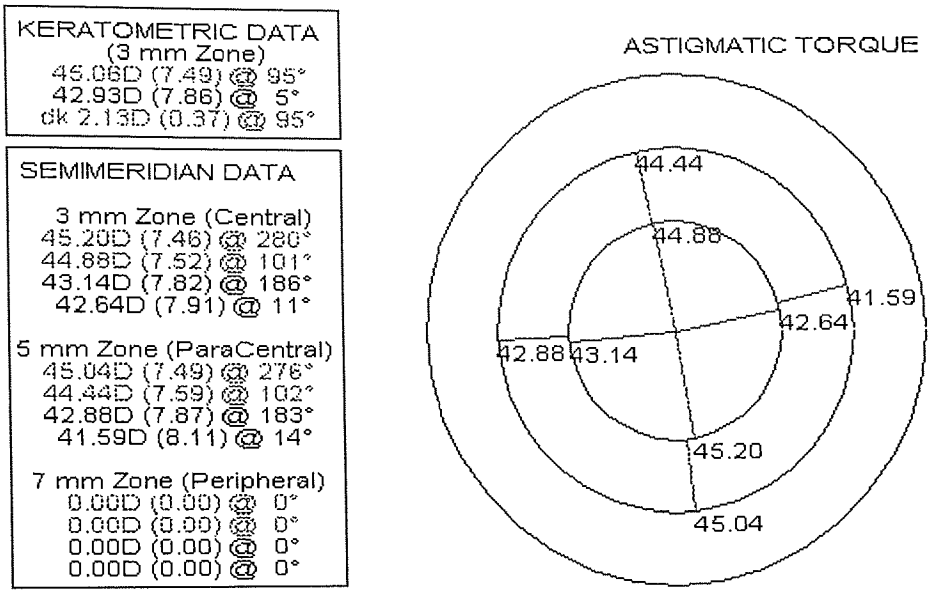

Figure 5.05: The EyeSys raw data table shows the distance along a meridian from which measurements were performed and also the actual sagittal radius at these points.

				Flattest Axis (at 4 degrees)			
NAS quad	Distance	Radius(mm)	Diopters	TMP quad	Distance	Radius(mm)	Diopters
# 01	0.47	7.84	43.05	# 01	0.47	7.83	43.10
# 02	0.75	7.84	43.05	# 02	0.75	7.82	43.16
# 03	0.99	7.85	42.99	# 03	0.99	7.81	43.21
# 04	1.27	7.87	42.88	# 04	1.28	7.81	43.21
# 05	1.54	7.90	42.72	# 05	1.52	7.82	43.16
# 06	1.84	7.93	42.56	# 06	1.80	7.83	43.10
# 07	2.10	7.98	42.29	# 07	2.05	7.84	43.05
# 08	2.42	8.03	42.03	# 08	2.35	7.85	42.99
# 09	2.70	8.09	41.72	# 09	2.61	7.87	42.88
# 10	3.05	8.16	41.36	# 10	2.91	7.89	42.78
# 11	3.36	8.22	41.06	# 11	3.18	7.92	42.61
# 12	3.77	8.26	40.86	# 12	3.48	7.95	42.45
# 13	0.00	0.00	00.00	# 13	3.78	8.00	42.19
# 14	0.00	0.00	00.00	# 14	4.11	8.05	41.93
# 15	0.00	0.00	00.00	# 15	4.45	8.09	41.72
# 16	0.00	0.00	00.00	# 16	4.80	8.11	41.62
				Steepest Axis (at 95 degrees)			
SUP quad	Distance	Radius(mm)	Diopters	INF quad	Distance	Radius(mm)	Diopters
# 01	0.44	7.45	45.30	# 01	0.44	7.44	45.36
# 02	0.70	7.47	45.18	# 02	0.69	7.45	45.30
# 03	0.92	7.49	45.06	# 03	0.92	7.46	45.24
# 04	1.21	7.51	44.94	# 04	1.19	7.47	45.18
# 05	1.42	7.53	44.82	# 05	1.42	7.47	45.18
# 06	1.71	7.54	44.76	# 06	1.69	7.47	45.18
# 07	1.95	7.55	44.70	# 07	1.91	7.48	45.12
# 08	2.21	7.58	44.53	# 08	2.16	7.48	45.12
# 09	2.46	7.60	44.41	# 09	2.41	7.49	45.06
# 10	2.76	7.63	44.23	# 10	2.67	7.51	44.94
# 11	3.07	7.64	44.18	# 11	2.92	7.55	44.70
# 12	0.00	0.00	00.00	# 12	3.20	7.60	44.41
# 13	0.00	0.00	00.00	# 13	3.48	7.66	44.06
# 14	0.00	0.00	00.00	# 14	3.81	7.71	43.77
# 15	0.00	0.00	00.00	# 15	4.23	7.75	43.55
# 16	0.00	0.00	00.00	# 16	0.00	0.00	00.00

5.5 Statistical Analysis

The results of previous studies that have evaluated the EyeSys CAS have shown that the instrument to be accurate and repeatable for spherical surfaces and human corneas (Koch et al, 1989; Tsilimbaris et al, 1991; Koch et al, 1992). When a sample of subjects are used to assess the repeatability of an instrument, the influence of human subjective variation is included. In a clinical environment the crucial element of human biological variability must be considered upon the effect of measurement error and therefore the measurement of repeatability using a subject sample is necessary. However, when the accuracy and repeatability of the instrument alone is required, test surfaces must be used. Most studies have only evaluated the accuracy and repeatability of instruments using spherical surfaces with respect to central radius of curvature (Koch et al, 1989; Hannush et al, 1989; Legeais et al, 1993); this is not appropriate as the normal cornea is not spherical. Furthermore, by only measuring one particular shaped surface the implication is that the accuracy of the instrument is constant for all shapes.

In order to assess measurement error all that is required is a repeated set of readings. One method is to observe the standard deviation of the differences and also the mean difference. The mean difference or bias suggests how much on average one instrument over estimates or under estimates the other (when comparing two different instruments) or the average difference of two readings (when assessing repeatability). The bias, for comparative studies i.e. when comparing the keratometer with the EyeSys, should be calculated as the mean of the actual difference (including the sign) and not the absolute difference. The absolute difference estimates the mean difference in readings between two measurements and results in an exaggerated value. For repeatability, on the other hand, it is not important for the sign of the difference to be taken into account. Hence, the bias for repeatability was the mean absolute difference.

Alternatively, if the measurement error follows a normal distribution, then measurement error may be described in terms of the 95% confidence limits. The

confidence limits show the probable range over which 95% of the measurement errors (the difference between the two measurements) are likely to lie. In addition, it is necessary to observe any relationship between measurement error and the actual value of measurement or another independent variable. This was accomplished by plotting a scatter graph of the difference (or measurement error) for each subject against its mean or another independent variable. Repeatability and agreement for the EyeSys and the keratometer were evaluated in this manner.

Part of the present study evaluated the agreement between the EyeSys CAS and the Bausch and Lomb keratometer. Two instruments may be said to be in agreement with each if they can be used interchangeably and when any difference between them is so small as to be clinically insignificant. In order to account for any differences in the location of the principle axes, dioptric measurements from the keratometer and the EyeSys were converted into a term called the Mean Corneal Power (MCP). Transforming measurements to MCP was achieved using a process known as astigmatic decomposition as described in chapter 4.

When evaluating the accuracy of the EyeSys in determining the aspheric test surfaces, comparisons of radius measurements were made in the central and peripheral areas of the surface. The radii measured by the EyeSys were clearly displayed in an output table (see figure 5.05). The table also displayed the distance from the vertex normal from where measurements were performed. This distance could then be used to calculate the actual sagittal radius of the known aspheric surface at the specified points. The equation used to derive peripheral sagittal radius was derived by Bennett (1968) and is shown below.

$$r_s = \sqrt{r_o^2 + (1-p).y^2} \qquad \textit{Equation 5.01}$$

The terms in equation 5.01 are as follows: r_s is the sagittal radius at a point on the surface y mm away from the vertex normal. p is the p-value of the aspheric surface and r_o is the apical radius.

5.6 Results

Evaluation of the EyeSys CAS was performed using two distinctly different samples: a subject sample and a aspheric test surface sample. The results from each of these samples is described separately.

5.6.1 Agreement between the EyeSys and the Bausch and Lomb keratometer

Any relationship between measurements obtained using the keratometer and the EyeSys was shown by figure 5.06. The correlation coefficient of 0.973 showed that the readings from both instruments had a relationship. The central dotted line showed the best fit line from linear regression analysis, the two other lines represent the 95% confidence intervals for the regression line. The confidence intervals showed that the accuracy of the regression line was relatively constant. However, the use of correlation coefficients did not show that both instruments were in agreement.

Figure 5.06: the correlation between the EyeSys CAS and the Bausch and Lomb keratometer in terms of mean corneal power for 40 eyes.

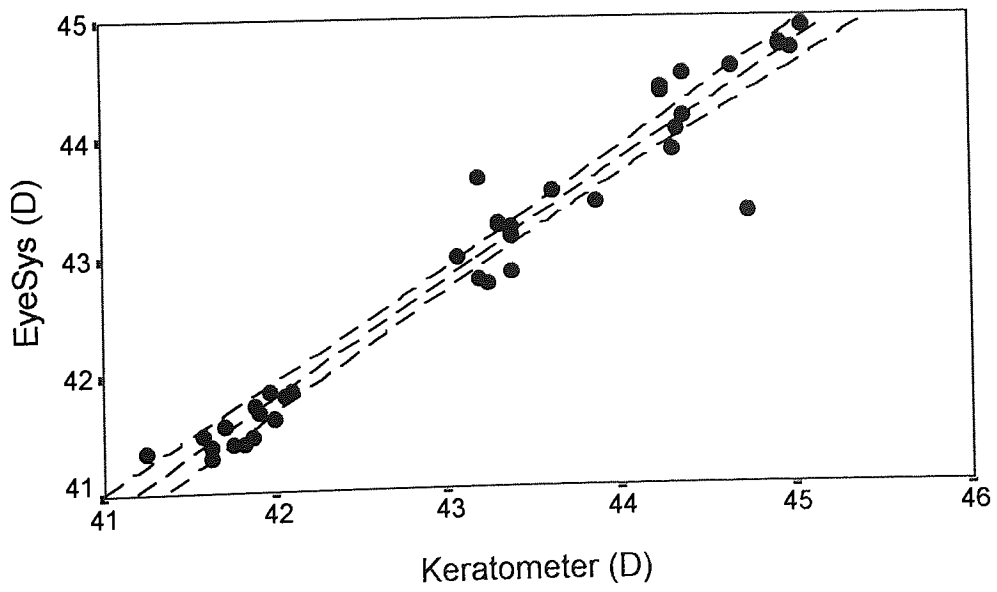

In order to assess the agreement between the two instruments, the deviation scores

(the difference in readings of both instruments) were plotted against the MCP for both instruments (see figure 5.07). The 95% confidence intervals ranged from +0.353D to -0.758D. Assuming a normal distribution, 95% of the differences would lie within this range, therefore, as the difference could be up to -0.758D, the two instruments were not in agreement as such a difference would be clinically significant. Further, the bias of -0.2D suggested that on average the EyeSys underestimated MCP compared to the Bausch and Lomb keratometer. A linear regression line (method of least squares) was also fitted to the scattered data in figure 5.07. No relationship was found (correlation coefficient, r, of 0.04) in terms of the difference between EyeSys/keratometer values and their mean.

As stated earlier, the 95% confidence limits were based on the assumption that the sample distribution was normal. Bland (1993) stated that by calculating the differences the resulting distribution was likely to be normal. The reason for this being that the difference solely represents the disparity in measurement between the two instruments.

Figure 5.07: the level of agreement between the EyeSys CAS and the Bausch and Lomb keratometer. The linear regression line showed little or no correlation (r=0.04) in terms of measurement error i.e. the difference in readings obtained from both instruments and the mean MCP.

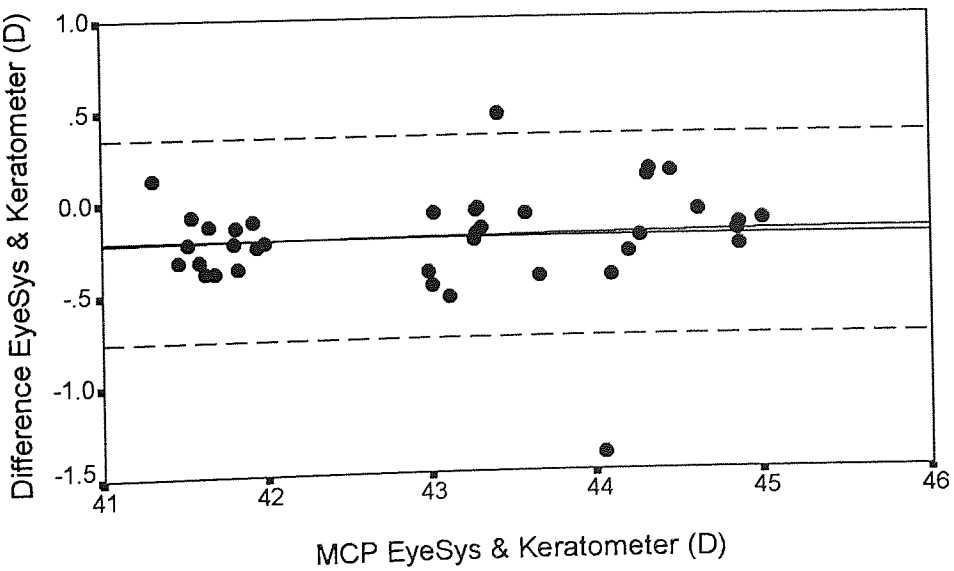

5.6.2 The repeatability of the EyeSys CAS and the Bausch and Lomb keratometer for MCP in the central corneal region

The repeatability of both instruments was determined in measuring the central MCP. Figures 5.08 and 5.09 show the repeatability of the keratometer and the EyeSys CAS respectively. The keratometer showed a marked improvement in repeatability compared to the EyeSys CAS for central MCP, this was shown by the narrow confidence limits for the keratometer (+0.295D to -0.069D) and the smaller standard deviation (±0.093D), see table 5.01 for complete results. The bias for both instruments was close to zero, it suggested that on average there was little difference between repeated measurements for central corneal curvature. The linear regression line (method of least squares) fitted to figures 5.08 and 5.09 showed that there was little correlation between the difference in repeated readings and their mean.

Figure 5.08: the repeatability of the Bausch and Lomb keratometer for central MCP in 20 subjects. r=0.046.

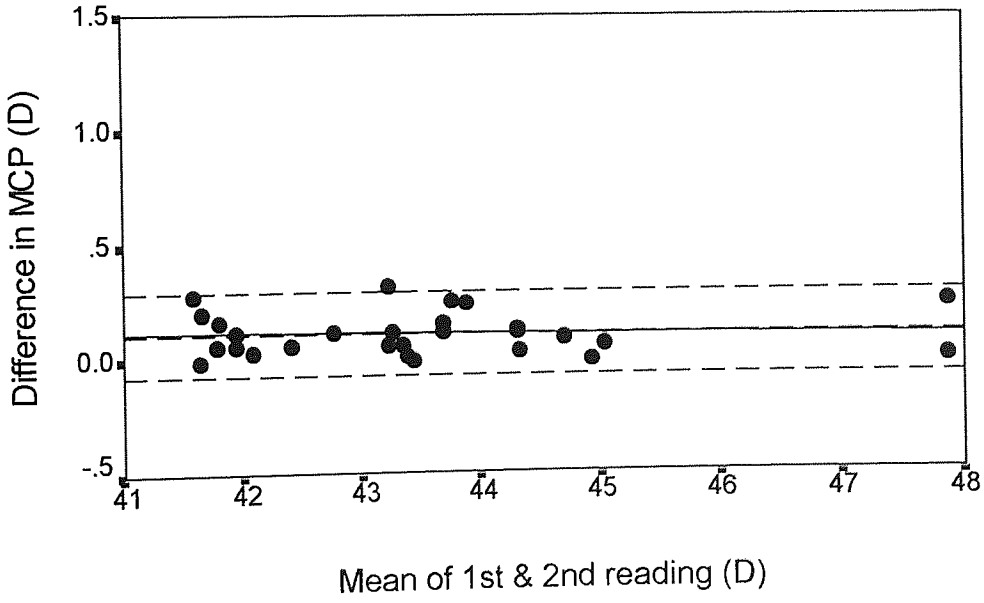

Figure 5.09: shows the repeatability of the EyeSys CAS for central MCP in 20 subjects. r=0.274.

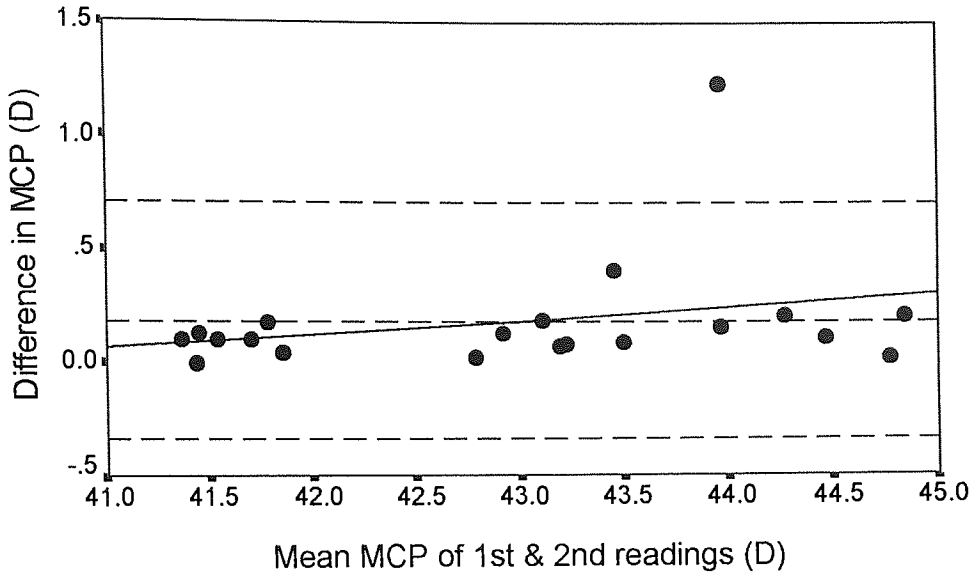

Table 5.01: the standard deviation, bias and confidence limits for repeatability analysis of MCP with the keratometer and the EyeSys CAS for central corneal curvature.

	Bias (D)	**95% confidence limits (D)**	**Standard deviation (D)**
B & L Keratometer	+0.113	+0.295 to -0.069	± 0.093
EyeSys CAS	+0.183	+0.700 to -0.335	± 0.264

5.6.3 Repeatability of EyeSys CAS for peripheral corneal measurements

The level of repeatability required for peripheral measurements in a clinical environment has not been well documented. Any reduction in repeatability using a subject sample would be induced from a combination of two factors: the variation due to instrument error (this includes errors from digitisation, alignment, operator error) and also the variation induced by subjective variability. In chapter 4, subjective variability was suggested to be caused by localised corneal variation due to factors such as blinking, lachrimation and possibly corneal deformation. The importance of assessing subjective variability was obvious: if an instrument had excellent in vitro repeatability, but the in vivo repeatability was poor, then practitioners must be aware of the magnitude of variability and also the areas on the corneal surface where this variability was greatest.

The criteria for accuracy and repeatability of peripheral measurements (i.e. after 1.5mm from vertex normal within a semi-meridian) was ±0.1mm. The reason for this was that the peripheral cornea has been shown to have reduced importance in the image forming properties of the eye (Enoch, 1958). The repeatability of the EyeSys CAS was assessed in four meridians (nasal, temporal, superior and inferior). The corresponding graphs are shown (figures 5.10-5.13).

The figures 5.10 to 5.13 show that from the two measurements there was greatest variation in the superior meridian closely followed by the nasal meridian. The inferior and temporal meridians showed considerably less variation. In addition, a significantly larger proportion of the corneal surface was analysed in the latter two meridians. For the superior and nasal meridians, a poorer repeatability occurred further into the periphery of the cornea. All the bias lines were close to zero, showing that on average there was little variation between repeated measurements over the corneal profile.

Figure 5.10: shows the repeatability of the inferior meridian with respect to the actual points of measurement on the corneal surface. r=0.108.

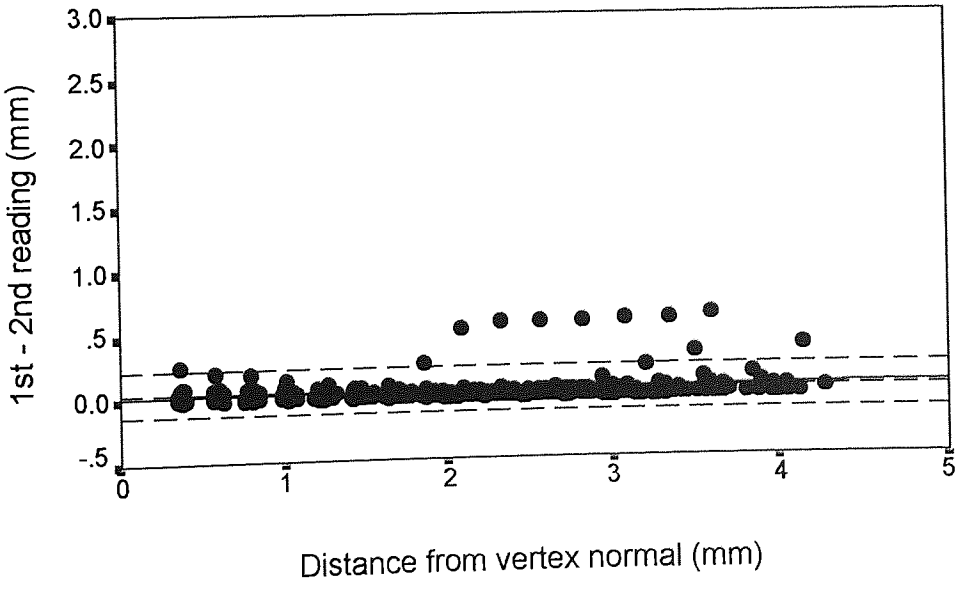

Figure 5.11: shows the repeatability of the superior meridian with respect to the actual points of measurement on the corneal surface. r=0.209.

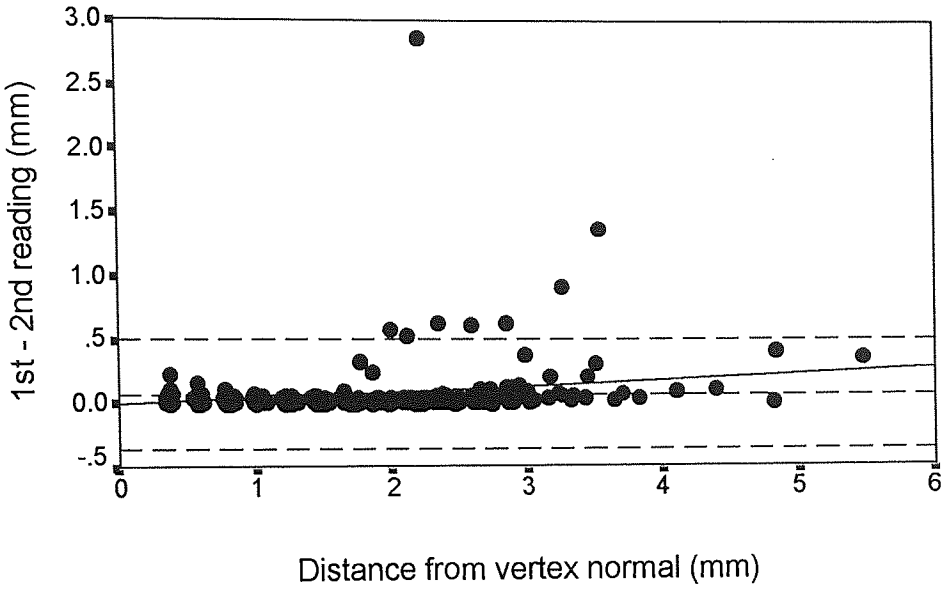

Figure 5.12: shows the repeatability of the nasal meridian with respect to the actual points of measurement on the corneal surface. r=0.284.

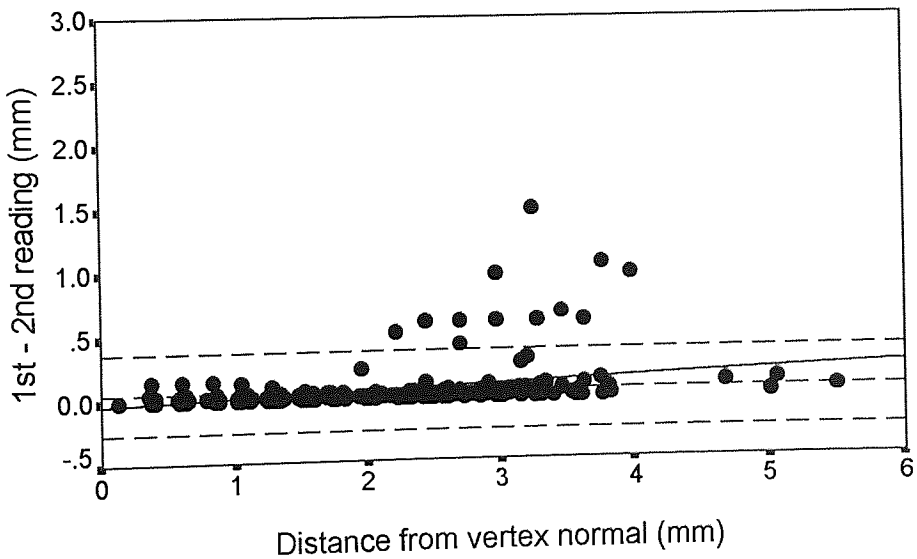

Figure 5.13: shows the repeatability of the temporal meridian with respect to the actual points of measurement on the corneal surface. r=0.092.

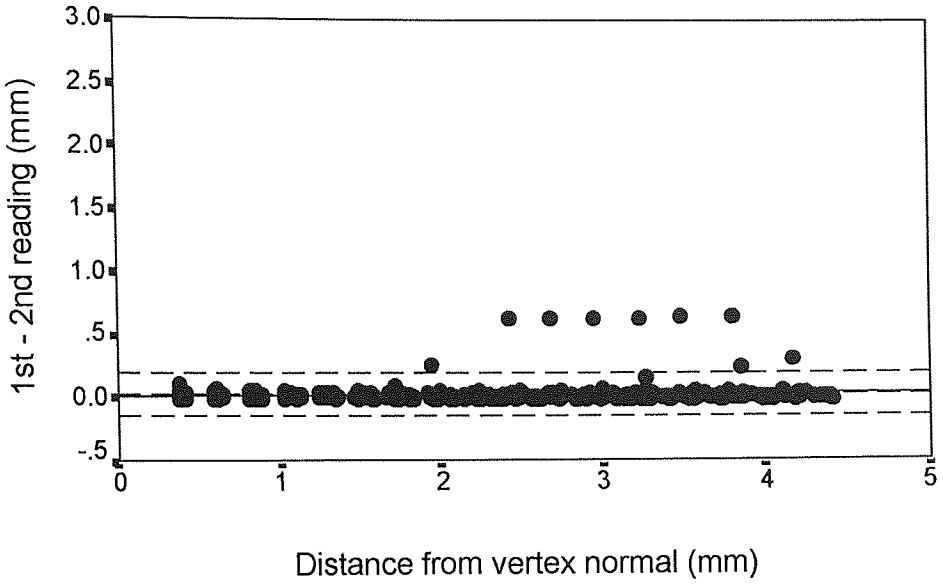

Table 5.02: shows the bias, standard deviations and 95% confidence limits for the repeatability of the EyeSys CAS in four meridians

	Bias (mm)	**Standard deviation (mm)**	**95% confidence limits (mm)**
Inferior	0.05	± 0.09	+0.2264 to -0.1264
Superior	0.07	± 0.22	+0.5012 to -0.3612
Nasal	0.06	± 0.16	+0.3736 to -0.2536
Temporal	0.03	± 0.09	+0.2064 to -0.1463

The standard deviations and confidence limits shown in table 5.02 were as a result of the variation within the whole corneal profile. Figures 5.10 to 5.13 showed a tendency for poorer repeatability in the periphery of the cornea, particularly for the nasal and superior meridians. Tables 5.03 to 5.06 show the standard deviation and bias for data points grouped with respect to four annular zones on the corneal surface (from 1mm to 4mm within a semi-meridian). From tables 5.03 to 5.06 it was observed that generally, the standard deviation and the bias were less for measurements taken up to the two millimetre zone, indicating that a greater repeatability was achieved in the central 4mm of the cornea. Thereafter, repeatability was significantly worse in the superior and nasal meridians. The temporal and inferior meridians showed only a minor deterioration in terms of repeatability further in the periphery of the cornea.

Table 5.03: Inferior corneal meridian repeatability at four corneal zones. For the inferior meridian, there was only a small deterioration in repeatability in the periphery of the cornea.

Corneal zone (mm)	Bias (mm)	Standard deviation (mm)
0mm to 1mm	+0.04	± 0.05
1mm to 2mm	+0.03	± 0.03
2mm to 3mm	+0.05	± 0.12
3mm to 4mm	+0.07	± 0.13

Table 5.04: Temporal corneal meridian repeatability in four zones. Very little variation in standard deviation occurred from the centre to the periphery of the corneal profile.

Corneal zone (mm)	Bias (mm)	Standard deviation (mm)
0mm to 1mm	+0.03	± 0.02
1mm to 2mm	+0.02	± 0.02
2mm to 3mm	+0.02	± 0.02
3mm to 4mm	+0.02	± 0.04

Table 5.05: Nasal corneal meridian repeatability at four zones. Although the repeatability for the central 2mm of the cornea was good, there was a marked reduction in the periphery.

Corneal zone (mm)	Bias (mm)	Standard deviation (mm)
0mm to 1mm	+0.03	± 0.03
1mm to 2mm	+0.03	± 0.03
2mm to 3mm	+0.07	± 0.16
3mm to 4mm	+0.18	± 0.33

Table 5.06: Superior corneal meridian repeatability at four zones. The repeatability showed the most marked reduction in the corneal periphery for the superior meridian.

Corneal zone (mm)	Bias (mm)	Standard deviation (mm)
0mm to 1mm	+0.04	± 0.04
1mm to 2mm	+0.04	± 0.07
2mm to 3mm	+0.11	± 0.35
3mm to 4mm	+0.21	± 0.37

5.6.4 Accuracy of central radius of curvature measurements using twelve aspheric surfaces

When the exact parameters of surface are known, assessing the accuracy of an instrument is a relatively easy task. The standard deviation and 95% confidence limits of the difference between measured and actual radius were used to describe the accuracy of the instrument. The central or apical radii of the test surfaces were taken to be the radius readings at ring 1 (see figure 5.05). The reason for this was because for an aspheric surface, changes in curvature would occur as soon as measurements were taken away from the apex. Figure 5.14 shows the correlation between measured and actual central radius for all twelve surfaces.

A high level of association was found between the actual values and measured values of central radius (r=0.996). However, the accuracy of the EyeSys CAS in determining the exact value was clearly illustrated in figure 5.15 where the difference of the EyeSys values from the true values were plotted against the actual central radius. The standard deviation was small (± 0.04mm) showing that only a slight deviation occurred in the EyeSys values. The 95% limits of agreement were also narrow (+0.121mm to -0.037mm), indicating that the EyeSys CAS accurately calculated central radius of curvature. The EyeSys CAS also has a tendency to overestimate the central radius of curvature (bias=+0.042mm).

Figure 5.14: The relationship between the actual and measured values of central radius of curvature for 12 aspheric surfaces using the EyeSys CAS.

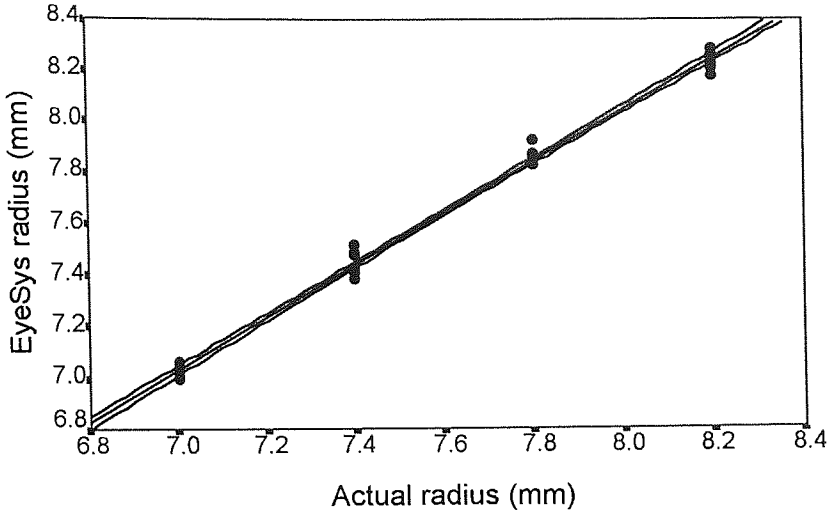

Figure 5.15: shows the limits of agreement of the EyeSys central radius curvature for all twelve aspheric surfaces.

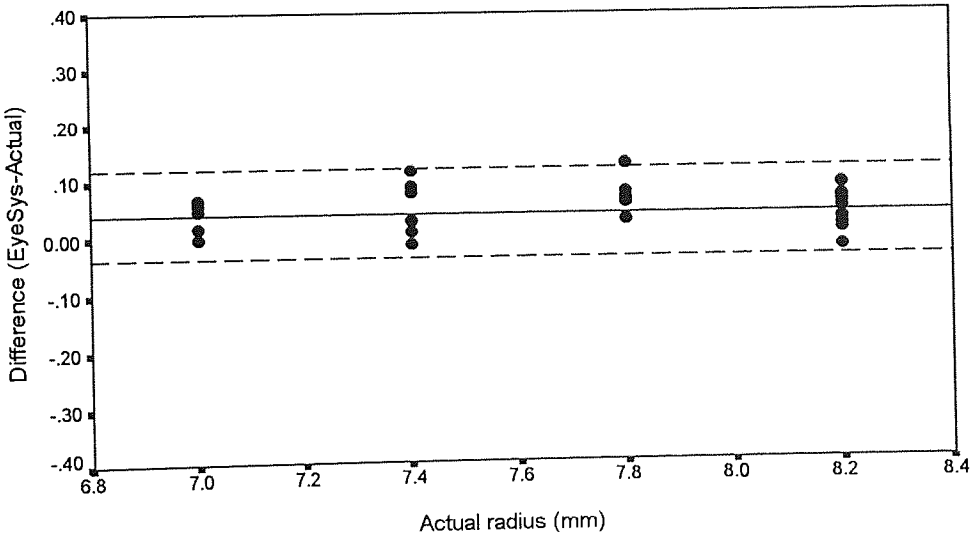

Grouping each of the differences in terms of the shape of the surface (the p-value) showed that greatest accuracy was obtained in measuring spherical surfaces. With progressively flattening surfaces greater error in the measurement of central radius of curvature occurred (see table 5.07).

Table 5.07: The accuracy of the EyeSys CAS in determining central radius of curvature for three p-values.

p-value	Bias (mm)	Standard deviation (mm)
0.5	+0.088	±0.02509
0.8	+0.031	±0.02500
1.0	+0.008	±0.01974

5.6.5 Accuracy of the EyeSys CAS in calculating peripheral radius for known aspheric surfaces

The disparity between calculated and actual sagittal radius of all twelve aspheric surfaces were plotted against the distance from the vertex normal from which the measurements were performed (see figure 5.16). Typically, within a semi-meridian, up to sixteen measurements were assessed. On average, the EyeSys overestimated peripheral sagittal radius (bias=+0.022mm). The error from the upper 95% confidence limits was found to be +0.105mm or 0.525D.

The measured and actual peripheral radii of all twelve aspheric surfaces were also grouped in terms of their respective p-value in order to evaluate any relationship between the disparity in measurements and the shape of the surface being measured. Figures 5.17 to 5.19 and table 5.08 show the accuracy of peripheral radius measurements for each group of aspheric surfaces.

Table 5.08: the accuracy of the EyeSys CAS in determining the peripheral radius of 12 known aspheric surfaces grouped in terms of their respective p-values.

p-value	Bias (mm)	Standard deviation (mm)	95% limits (mm)
Overall	+0.022	±0.0422	+0.105 to -0.061
1	+0.0003	±0.0134	+0.026 to -0.026
0.8	+0.0167	±0.028	+0.072 to -0.038
0.5	+0.049	±0.056	+0.159 to -0.061

Spherical surfaces (p-value=1), were measured to a high level of accuracy (standard deviation=±0.0134mm). However, a clear trend was observed through figures 5.17 to 5.19 such that with progressively flatter surfaces greater error occurred particularly in the extreme periphery.

Figure 5.16: The accuracy of peripheral measurements for all twelve surfaces.

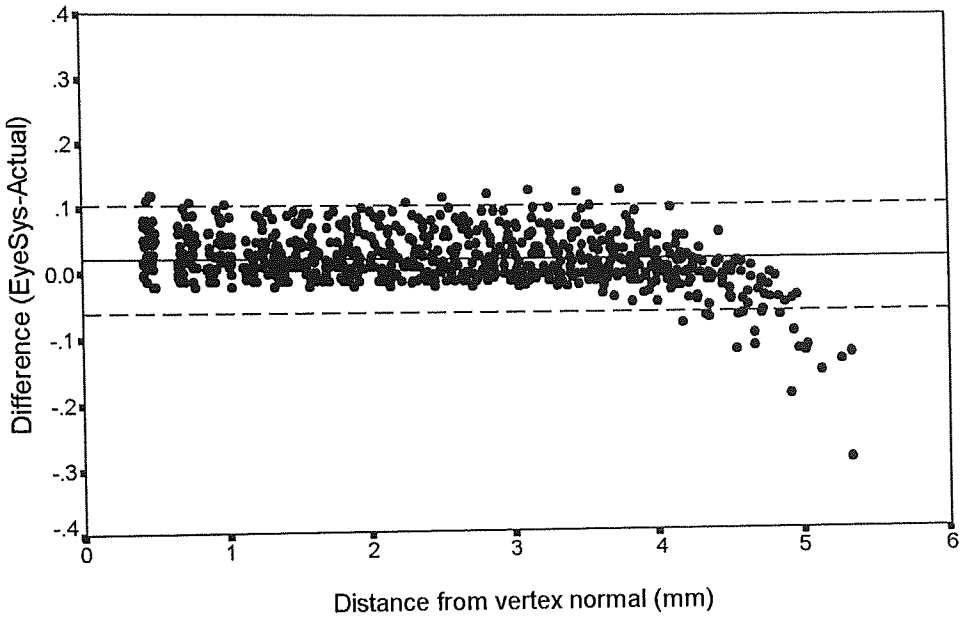

Figure 5.17: The accuracy of peripheral radius measurements for all surfaces with a p-value of 1.

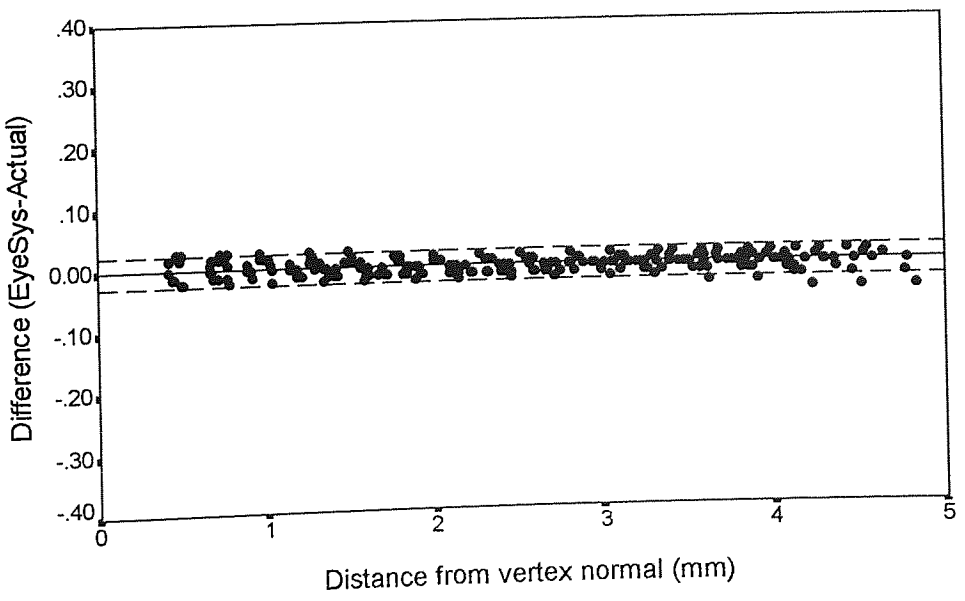

Figure 5.18: The accuracy of peripheral radius measurements for all surfaces with a p-value of 0.8.

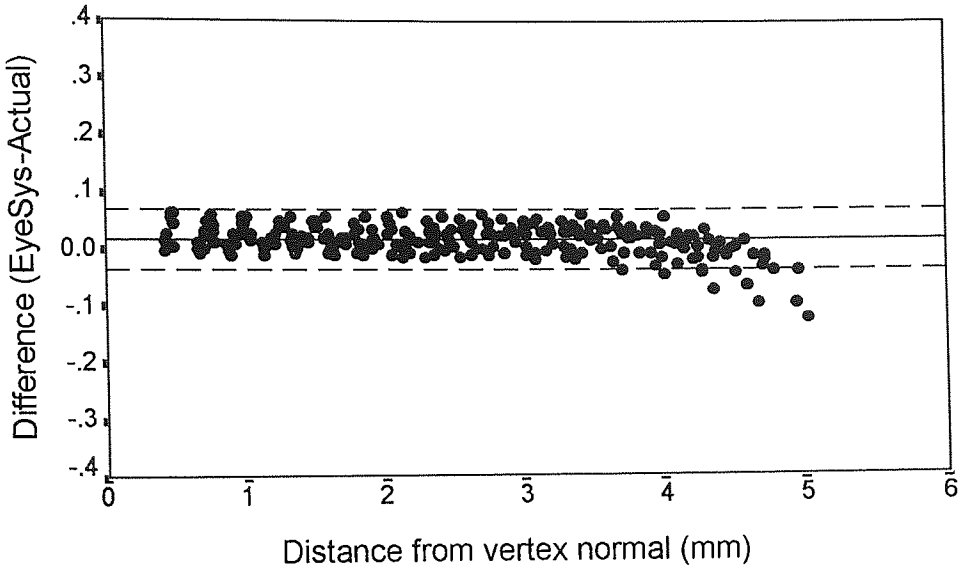

Figure 5.19: The accuracy of peripheral radius measurements for all surfaces with a p-value of 0.5.

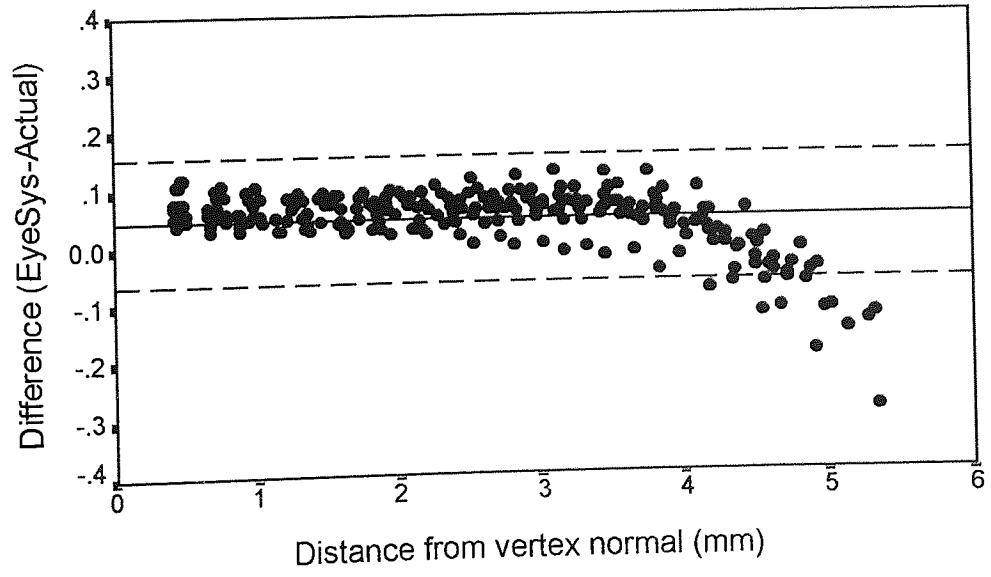

5.6.6 Repeatability of the EyeSys CAS for twelve aspheric surfaces

In order to assess instrument variability alone, each surface was measured twice and the disparity between each reading at comparable locations was observed for four meridians. No difference in bias and standard deviation was observed with respect to each meridian analysed. The bias (+0.01mm) showed that on average there was very little difference on repeated readings, furthermore, the narrow range of the 95% confidence limits (+0.0296mm to -0.0096mm) confirmed that EyeSys CAS had a high level of repeatability. Figures 5.20 to 5.23 show scatter graphs of the difference in repeated readings as a function of the mean distance from the vertex normal.

Table 5.09: Repeatability of the EyeSys CAS for measurements of twelve aspheric surfaces.

Meridian	Bias (mm)	Standard deviation (mm)	95% limits (mm)
Temporal	+0.01	±0.01	+0.0296 to -0.0096
Nasal	+0.01	±0.01	+0.0296 to -0.0096
Superior	+0.01	±0.01	+0.0296 to -0.0096
Inferior	+0.01	±0.01	+0.0296 to -0.0096

Figure 5.20: Repeatability of the temporal meridian.

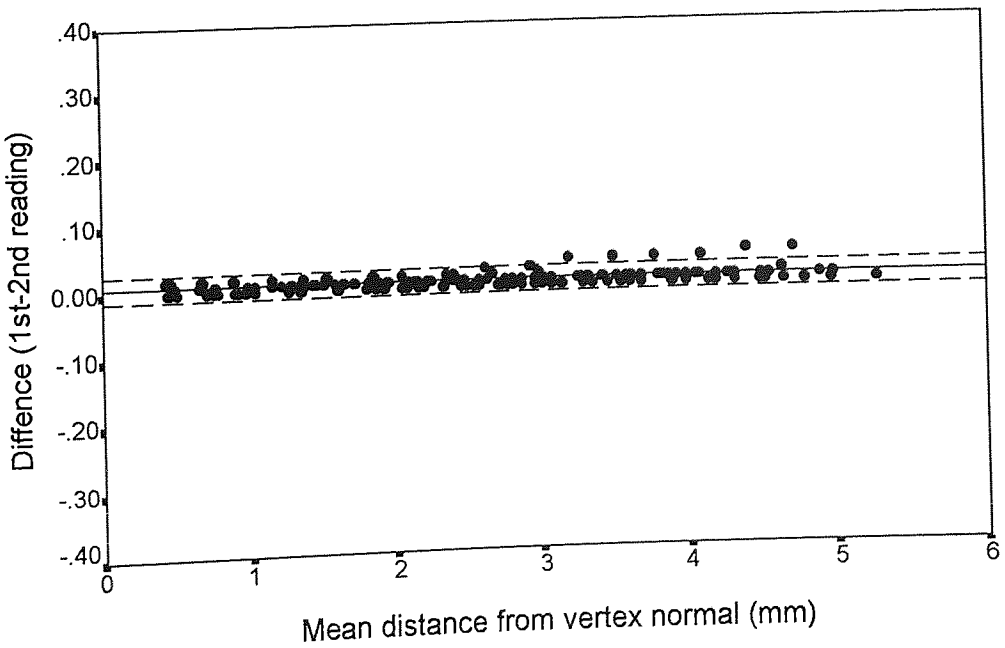

Figure 5.21: Repeatability of the nasal meridian.

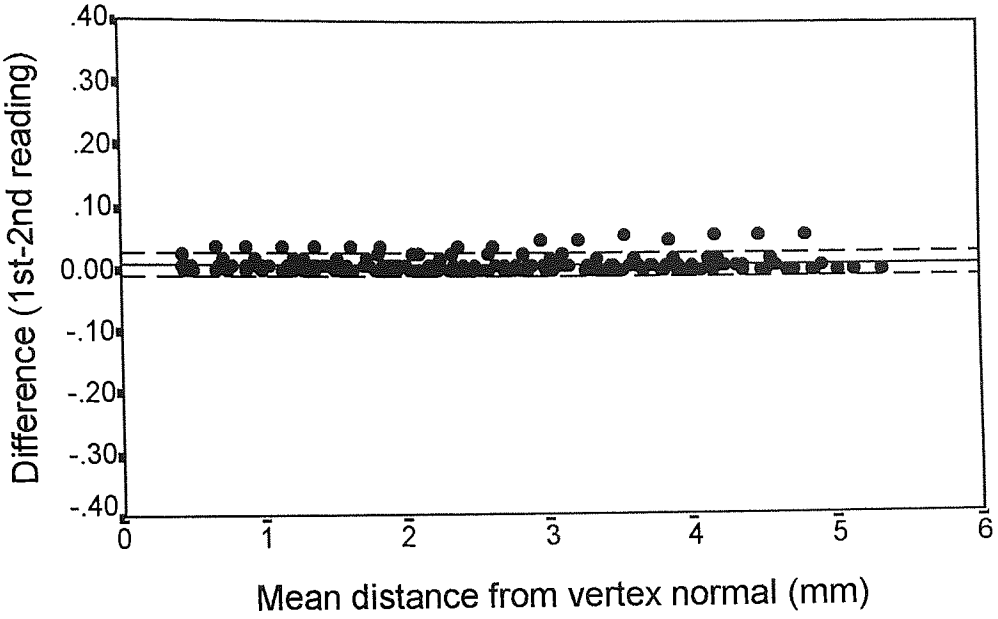

Figure 5.22: Repeatability of the superior meridian.

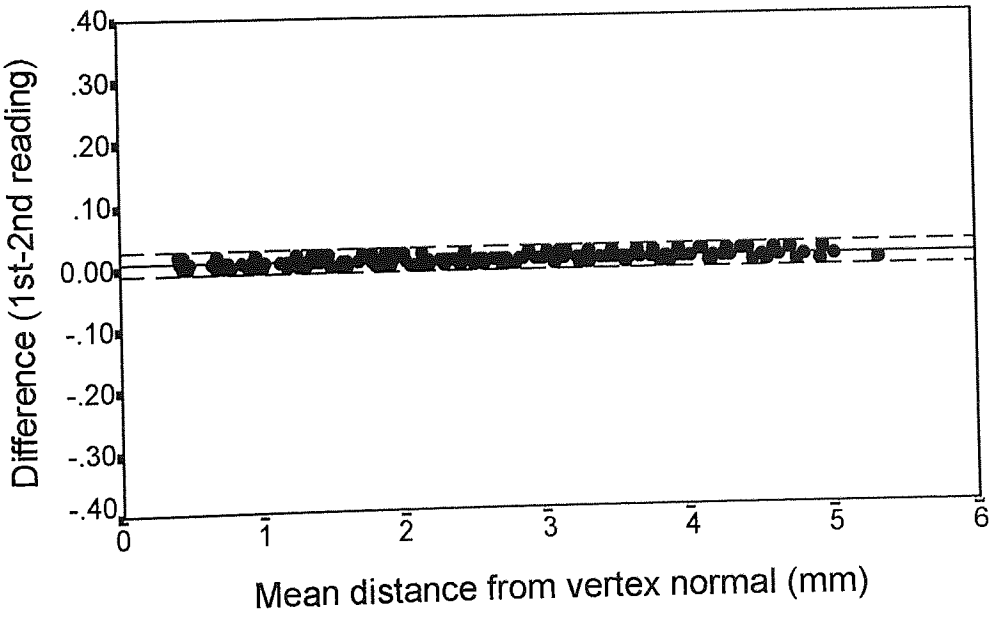

Figure 5.23: Repeatability of the inferior meridian.

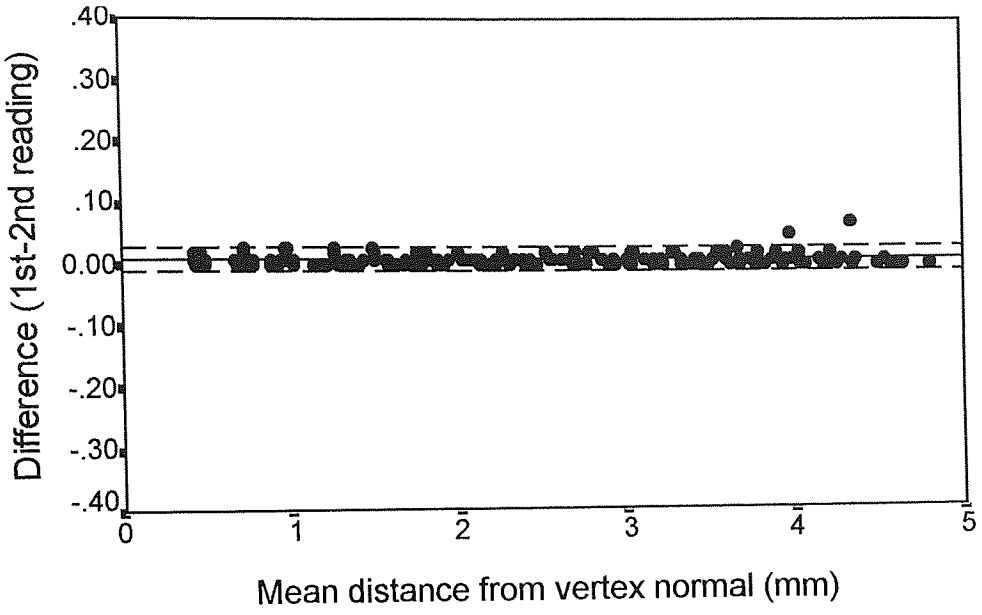

5.7 Discussion

5.7.1 Agreement between the EyeSys CAS and the Bausch and Lomb keratometer

The majority of practitioners utilise the keratometer to measure the central radius of curvature of the cornea. When a videokeratoscope is introduced into practice it is important to establish whether readings are in agreement and interchangeable with the keratometer. The present study showed that the measurements obtained using the keratometer and the EyeSys were not in agreement. Although figure 5.06 illustrated a strong relationship between keratometer readings and EyeSys simulated keratometer readings (r=0.973), the 95% confidence limits (figure 5.07) ranged from +0.353D to -0.758D. Clearly this range was not acceptable for two instruments to be used interchangeably.

The previous chapter investigated the agreement of the SUN SK-2000 (SUN Contact Lens Company, Kyoto, Japan) with the Javal keratometer. A poor level of agreement was established between these instruments (+1.32D to -0.69D). In a similar study by

Zadnik et al (1992) using the Bausch and Lomb keratometer and the Kera Corneascope (Kera Corp., Santa Clara, CA), the 95% confidence limits ranged from +0.59D to -1.72D. Again, this range showed that the two instruments were not in agreement. However, the EyeSys compared more favourably with the keratometer than the SUN SK-2000 and the Kera Corneascope as the confidence limits were considerably more narrow. Table 5.10 summarises the results from these studies.

Tsilimbaris et al (1991) compared the EyeSys CAS with the Javal keratometer and found a standard deviation of the differences between the EyeSys and keratometer of ± 0.46D. In spite of the fact that the standard deviation was higher than that calculated in the present study, Tsilimbaris et al (1991) stated that there was no significant difference between the EyeSys and the keratometer based on the results of a paired t-test ($p=0.471$). The confidence limits for the Tsilimbaris et al (1991) study (calculated in chapter 4) were too large to suggest that the two instruments were in agreement. Medical statisticians (Bland and Altman, 1986) state the following with respect to the use of tests of significance for evaluating agreement and repeatability:

'The test of significance may show that the two methods are related, but it would be amazing if the two methods designed to measure the same quantity were not related. The test of significance is irrelevant to the question of agreement.'

Thus, the conclusions drawn by Tsilimbaris et al (1991) were in fact incorrect due to method of statistical analysis of their data. Fortunately, as standard deviations were provided, the confidence limits could be calculated. Bland and Altman (1986) advocate the use of confidence limits and scatter plots as used in the present study.

Koch et al (1992) compared the EyeSys CAS with the Marco model I keratometer (Marco, Jacksonville, FL.) and showed that both instruments were in agreement (only 5% of measurements differed by more than 0.50D for the steeper meridian of the cornea). Their results differed from those in the current study, one possible explanation would be that both studies used different keratometers, it was therefore

possible that the EyeSys was in agreement with the Marco model I keratometer used by Koch et al (1992).

The bias (or the mean difference) varies from one study to another. The mean difference between two instruments ultimately depends on the instruments used. It would be interesting to compare the bias from comparative studies on identical instruments in order to determine exactly how much one instrument over or under estimates the other. The lack of agreement between the Bausch and Lomb keratometer and the EyeSys CAS in the present study could be attributed to the fact that measurements from both instruments were being taken at different points on the cornea.

Table 5.10: Comparison of the results from other studies. The standard deviation is denoted by S.D..

Study	Sample size	Instrument compared	Bias (D)	S.D. (D)	95% confidence limits (D)
Present study	40	EyeSys	-0.2	+/-0.28	+0.35 to -0.76
Chapter 4	20	SUN SK-2000	+0.33	+/-0.52	+1.34 to -0.69
Zadnik (1992)	40	Corneascope	-0.57	+/-0.59	+0.59 to -1.72
Tsilimbaris (1991)	92	EyeSys	+0.03	+/-0.46	+0.93 to -0.87

5.7.2 Repeatability of the Keratometer and the EyeSys CAS

In addition to analysing the agreement between the Bausch and Lomb keratometer and the EyeSys, the repeatability of both of these instruments was also evaluated. Figures 5.08 and 5.09 show that the keratometer was more repeatable than the EyeSys. From consideration of the confidence limits (see table 5.01) the obvious conclusion was that the keratometer had greater repeatability than the EyeSys CAS. However, more information regarding the central cornea was available with the EyeSys as more of the central cornea was resolved.

Other studies have also assessed the repeatability of the keratometer and other

videokeratoscopes. However, comparisons between studies are difficult due to the variety of statistical methods used. Hannush et al (1990) compared the Bausch and Lomb keratometer with the Corneal Modelling System (Computed Anatomy, Inc., New York). Using a criteria of a 0.5D difference from one reading to another, the percentage of repeated readings within this criteria were found for each instrument. The results obtained by Hannush et al (1990) agree with those found in the present study i.e. that the Bausch and Lomb keratometer was more repeatable than the videokeratoscope for measurements of central corneal curvature.

Zadnik et al (1992) determined the repeatability of the keratometer and Corneascope. The confidence limits were +0.84D to -1.03D for the Bausch and Lomb keratometer for the vertical meridian and +1.76D to -2.24D for the Corneascope. The limits suggest that photokeratoscopy had poorer repeatability compared to keratometry. One explanation could be that the keratometer, because of its doubling principle, was relatively insensitive to small involuntary ocular movements. Measurements performed using videokeratoscopy, on the other hand, were not independent of these small ocular movements and therefore the repeatability could be reduced.

5.7.3 Repeatability of the EyeSys CAS in the corneal periphery

The repeatability of the EyeSys CAS was determined by calculating the 95% confidence limits for the difference in sagittal radius of two readings at comparable locations on the corneal surface. Table 5.02 showed that the repeatability was dependent on the meridian in which measurements were performed. Temporal and inferior meridians showed the greatest repeatability with the superior meridian having the potential for the largest disparity in repeated readings. The graphs shown in figures 5.10 to 5.13 were plotted in order to ascertain whether there was any relationship between the position from the vertex normal where measurements were taken and the difference in sagittal radius from repeated measurements. For each graph a linear regression line (method of least squares) was fitted and the correlation coefficient calculated. The degree of correlation indicated the likelihood of any relationship

between the difference in repeated readings and the distance from the vertex normal from where measurements were performed. The graphs in figures 5.11 and 5.12 showed a positive correlation (r=+0.209 and +0.284 for superior and nasal meridians, respectively) indicating that for these meridians, a greater difference in repeated measurements occurred further into the periphery of the cornea. Conversely, figures 5.10 and 5.13 showed almost no relationship (r=0.108 and 0.092 for the inferior and temporal meridians, respectively). In order to quantify the observations from figures 5.10 to 5.13, the standard deviations of the differences for four, one millimetre corneal zones were calculated. For each meridian, differences in the sagittal radius of curvature increased in the corneal periphery.

In the previous chapter the repeatability of the SUN SK-2000 device also deteriorated in the corneal periphery. It was suggested that the ocular adnexa could have caused the reduction in repeatability. However, the SUN SK-2000 displayed peripheral radii even if the Placido rings were not imaged. Thus, extrapolation could also have reduced the repeatability. With the EyeSys CAS, only points on the cornea where the Placido rings were imaged were analysed, any errors due to extrapolation were therefore eliminated. Measurements beyond 2mm from the vertex normal in the superior and nasal meridians were subject to error from human biological variation due to the interaction of the ocular adnexa. Another error that could have influenced the poorer repeatability in the peripheral cornea was the accuracy of the digitisation process. On occasions, the red and yellow digitisation markers (see section 5.3) incorrectly located the ring intersections. Figure 5.03 showed that part of the ring in the nasal area of the cornea was missing. The digitisation process would therefore incorrectly locate the ring interface and the calculated sagittal radius at this point on the cornea would not be correct. Careful inspection of the Placido image should be performed, particularly in the periphery of the cornea prior to topographic evaluation.

Hannush et al (1990) determined the repeatability of the Corneal Modelling System in corneal periphery of 17 eyes. They analysed the mean dioptric power of each ring (1 to 27), only 54% of the rings repeated measurements within 0.5D. Hannush et al

(1990) suggested that the poorer repeatability of the peripheral rings was presumably due the algorithms not accounting for the aspheric nature of the corneal surface. However, their suggestion would not explain why different levels of repeatability were encountered in different meridians of the cornea. Furthermore, the algorithms would have a bearing on the accuracy of an instrument, not the repeatability. In addition, one should note Hannush et al (1990) did not localise measurements to a specific meridian on the corneal surface as they calculated the difference in mean power of each ring on repeated measurement. Hannush et al (1990) therefore assessed the repeatability of peripheral corneal power for a particular zone rather than specific points on the cornea. Comparing repeated measurements of the mean power of a ring is not an accurate method of assessing the repeatability of an instrument as the assumption is made that the repeatability is constant within a meridian.

5.7.4 Accuracy of central and peripheral measurements using the EyeSys CAS

A high level of association was found between the EyeSys values of central radius of curvature and the actual values for all twelve aspheric surfaces (r=0.996). Overall, the upper 95% confidence limit suggests that an error of +0.121mm or 0.61D would occur. Comparing this error to that obtained from other studies shows an apparent exaggerated error for the current study. Hannush et al (1989), using the Corneal Modelling System (Computed Anatomy), found that 96% of measurements of central radius of curvature were obtained within 0.25D for four spherical surfaces. Koch et al (1992) reported the EyeSys CAS to obtained measurements using a 42.5D sphere to within 0.25D. The primary difference between these studies and the present study was in the surfaces used to investigate the accuracy. Grouping surfaces in terms of their respective p-values showed much more comparable results for the accuracy of central radius of curvature (upper 95% confidence limit of 0.047mm).

Furthermore, grouping the radii in terms of the p-value of the surface also showed that errors in accuracy increased in surfaces with lower p-values (table 5.07). For example, with a 7.80mm spherical surface, the innermost ring was reflected from a point

0.46mm from the vertex normal, the corresponding radius of curvature was measured to be 7.83mm. For a surface with the same central radius but with a p-value of 0.5, the point of reflection was 0.48mm and the radius of curvature was found to be 7.93mm (see appendix 1). Thus, the primary factor causing the error in measurement of central radius of curvature would appear to be the level of central resolution (the central resolution of a videokeratoscope was the distance from the vertex normal to the point of reflection of the innermost ring at the surface). Since the present study was conducted, the manufacturers of the EyeSys have launched a new version of the EyeSys model II - the EyeSys system 2000 which has an additional two rings. The improved central resolution of the new EyeSys 2000 should help increase the accuracy in determining the apical radius of curvature. However, based on the 0.02mm accuracy suggested by Stone (1962), the EyeSys model II was not accurate in measuring aspheric surfaces (95% confidence limits of +0.121mm to -0.037mm).

Although studies have evaluated the accuracy of peripheral measurements performed by computerised videokeratoscopic devices for spherical surfaces, few have evaluated these systems using aspheric surfaces. Matilla et al (1994) determined the accuracy and precision of the TMS videokeratoscope using thirty conicoidal buttons. High levels of association for both p-value and central radius of curvature were found (r=0.9997 and 0.995, respectively). The 95% confidence intervals for p-value showed that the TMS overestimated the p-value from +0.028 to +0.077. The TMS also overestimated central radius of curvature by +0.063 to +0.092 (95% confidence interval). However, it must be noted that the confidence intervals are not the same as the confidence limits or the 95% limits of agreement used in the present study. The confidence intervals represent the range over which the bias is likely to lie in 95% of cases. Unfortunately, Matilla et al (1994) did not state the standard deviation of the differences between TMS measured and actual p-value or central radius of curvature, therefore, the confidence limits could not be calculated.

For the present study, the accuracy of peripheral measurements were evaluated in terms of the deviation of measured peripheral radius from the actual peripheral radius

of twelve aspheric surfaces. The actual values of sagittal radius of curvature were determined by substituting the values of the distance from the vertex normal in the raw data table (figure 5.05) into the variable y in equation 5.01. The error from the upper 95% limits was found to be 0.105mm or 0.525D. For clinical purposes, this level of accuracy was acceptable. The error in measurements were found to increase in the periphery (figure 5.16) with maximum errors occurring after 4mm from the vertex normal. Figures 5.17 to 5.19 showed that a distinct relationship existed between the nature of the surface i.e. the p-value and the error in measuring it. For flattening surfaces greater error was observed with the EyeSys CAS in the periphery of the surface. A reasonable explanation would be an error or inappropriate assumption made in the EyeSys algorithms. Other studies have assessed the accuracy of the EyeSys CAS in measuring spherical surfaces (Koch et al, 1989; Hannush et al, 1989) and concluded that it was an accurate instrument. With regards to the present study, the narrow confidence limits (+0.105mm to -0.061mm) and low standard deviation ($\pm$0.022mm) showed that the EyeSys CAS model II had an acceptable level of accuracy.

5.7.5 Repeatability of the EyeSys CAS for twelve aspheric surfaces

As opposed to investigating the repeatability of the EyeSys in measuring human corneas, using aspheric surfaces eliminated any biological variation in the cornea induced by the tear film, lids and lashes. Therefore, not surprisingly, the repeatability was equal for each meridian. Furthermore, the EyeSys CAS was found to be highly repeatable (bias=+0.01mm and standard deviation=$\pm$0.01mm). Figures 5.20 to 5.23 illustrated that there was no deterioration in the repeatability of peripheral measurements across the entire profile for aspheric surfaces. Thus, the maximum error induced by the characteristics of the instrument alone, such as focusing and alignment, resulted in an error in measurements of only 0.0396mm, or 0.198D (upper 95% confidence limit). As a result of the repeatability analysis using aspheric surfaces, it would appear that the EyeSys CAS was a highly repeatable instrument.

In a study conducted by Matilla et al (1994), repeatability was assessed by measuring

two surfaces ten times and then observing the standard deviation. A standard deviation of ±0.025mm and ±0.022mm was found for the two surfaces indicating that the TMS also had acceptable repeatability. Few studies have evaluated repeatability using aspheric test surfaces. Further, those that have do not state which aspheric surfaces were used in their analysis (Koch et al, 1989; Matilla et al, 1994).

5.8 Summary

The EyeSys CAS was compared with the Bausch and Lomb keratometer in order to assess the agreement between the two instruments. A poor level of agreement from the 95% confidence limits (+0.353D to -0.758D) was found in a sample of forty subjects. The results suggested that the measurements obtained using the EyeSys CAS and the keratometer were not interchangeable. Unfortunately, direct comparisons were not possible with other studies as a result of different statistical methods used to evaluate agreement (Tsilimbaris et al, 1991; Hannush et al, 1990). In order to assess agreement, observation of the variance in the difference between readings obtained by both instruments must be performed as described by Bland and Altman (1986).

The repeatability of the keratometer was also greater in measuring 20 normal corneas (standard deviation=±0.093D for the keratometer and ±0.264D for the EyeSys). One possible reason was that the doubling principle allowed the keratometer to be relatively independent of small involuntary ocular movements. With respect to the repeatability of the EyeSys in the periphery of the cornea, poorest repeatability was found in the superior and nasal meridians (figures 5.11 and 5.12). Repeatability decreased as a function of distance from the vertex normal and thus it was suggested that measurements beyond 2mm in these meridians should be viewed with some scepticism. The poor repeatability in these areas was attributed to the interference of the ocular adnexa on measurement and not to instrument error. Further confirmation that repeatability was reduced due to the variation induced by the adnexa was shown by the fact that no difference in repeatability was found with the twelve convex aspheric surfaces (figures 5.20 to 5.23).

The accuracy of the EyeSys CAS in measuring central and peripheral radius of curvature was shown to be dependent on the shape of the surface to be measured. For flatter surfaces a decrease in accuracy was found for both central and peripheral radius of curvature (figure 5.17 to 5.19). Overall, the EysSys CAS was an extremely powerful tool in the assessment of corneal topography. The present study showed that although it was relatively accurate in measuring aspheric surfaces, the biological variations in the human cornea restricted the instrument's performance. Practitioners using the EyeSys CAS and indeed any other videokeratoscopic system should be aware of these practical constraints inherent in the principles of videokeratoscopy.

Chapter Six

Description of a New Videokeratoscope

6.1 Introduction

At the present time, few commercially available videokeratoscopes are available. The instrument review has described these instruments. In addition, part of this thesis has evaluated the accuracy and repeatability of two of these instruments (chapters 4 and 5). Owing to the commercial availability of these videokeratoscopes, little is known regarding the algorithms used to calculate the corneal surface parameters by these instruments. The analysis of the reflected mires has so far resulted in assumptions being made with regard to the corneal surface (chapter 3). Furthermore, descriptions of the corneal surface have resulted in analysis of radius/power descriptions, colour coded dioptric maps, meridional curve fitting and various numerical indices (chapter 1).

The purpose of the remainder of this thesis is to describe the construction of a videokeratoscopic device and software capable of deriving the three dimensional nature of the corneal surface without prior assumptions of the nature of the surface under test. The basic principle involved in videokeratoscopy was considered in chapter 3 (figure 3.03).

Essentially, an array of light sources of known size and position illuminate the cornea. Owing to the reflective properties of the cornea, light is reflected towards the focusing lens so producing a corresponding virtual image of the array of light sources behind the cornea. As the shape of the reflecting surface dictates the size and position of each image (Purkinje image I), calculation of the shape of the cornea effectively involves tracing backwards from the image plane to the target source. Unfortunately, this problem is not as straight forward as it may initially appear. Firstly, the output image (usually a photograph or a video image) is a two dimensional image, the aim is to

derive a three dimensional image. Secondly, no knowledge regarding the location of the position of the vertex normal of the cornea is available (the term vertex normal defines the point on the corneal surface that is perpendicular to the videokeratoscope axis); this point was clearly illustrated by Wang et al (1989) (see chapter 3, figure 3.04). The net result of which is that surfaces of differing radii may produce images of equal size. The remainder of the present chapter describes the apparatus and software used to overcome these problems.

6.2 Apparatus description

A diagram of the apparatus is shown in figure 6.01. The target and camera system were mounted on a X, Y, Z axis moveable table that facilitated alignment and focusing of the mires. The target consisted of a series of light emitting diodes (L.E.D.s) arranged in a radial pattern (figure 6.02). A total of 8 semi-meridians were analysed each containing eight L.E.D.s, thus a total of sixty four points on the corneal surface could be evaluated. The L.E.D.s were mounted on a matt black plastic hemispherical bowl (the faceplate). The use of a hemispherical faceplate enabled a larger area of the cornea to be measured (see figure 2.03). Further, the hemispherical design reduced peripheral image blur due to curvature of the image plane (Knoll, 1961; Stone, 1962; Mandell and St. Helen, 1968; Mandell and York, 1968). Thus, for a 8.2mm spherical surface, the outermost L.E.D. was capable of performing measurements at a point 4.7mm from the centre of the sphere. The centre of the faceplate housed a telescopic lens system (aperture 10mm) that provided a magnified view of the reflected mires on the monitor.

The video camera used was a charge coupled device (Monochrome CCD, ZA35Q, Maplin electronics), this had the advantage of portability and reduced power consumption. CCD systems are based on an image unit that convert light focused by a lens into an electronic charge using the photoelectric principle. The monochrome CCD camera was used as a colour camera offered no advantages over monochrome when capturing the raw image. In fact, a colour camera would have had the

detrimental effect of increasing computation time due to the requirement for more computer memory when analysing colour images.

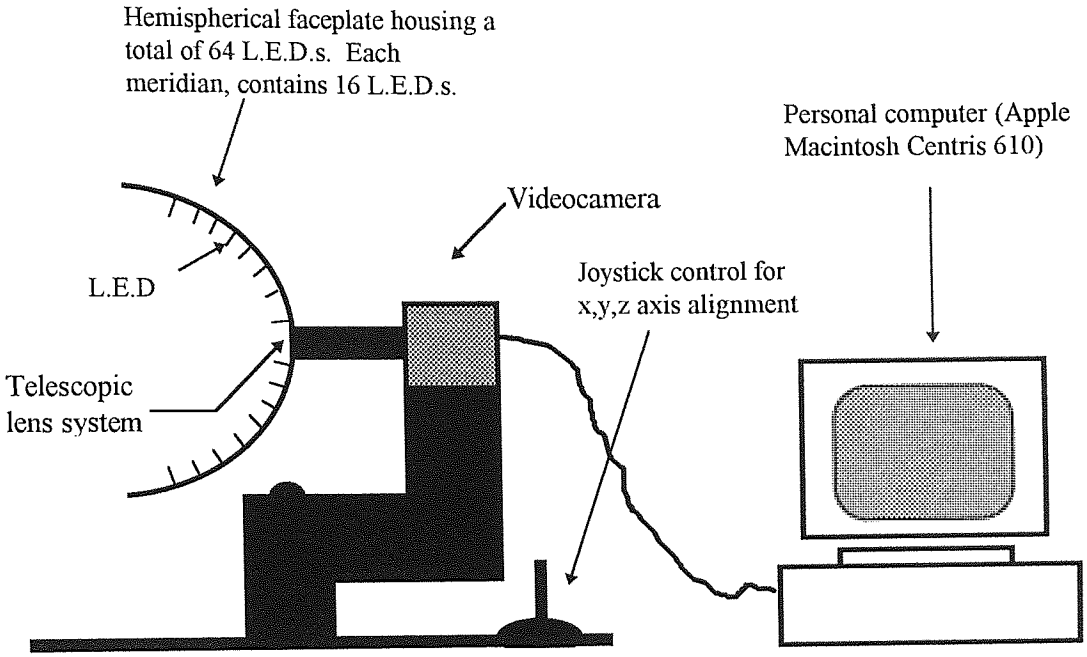

Figure 6.01: Apparatus used in the construction of the videokeratoscope. A magnification factor of approximately 32.4 pixels/mm was found using the above system for manual digitisation. The magnification factor was approximate because is it may be altered during each calibration procedure (which will be described in section 7.4.3.).

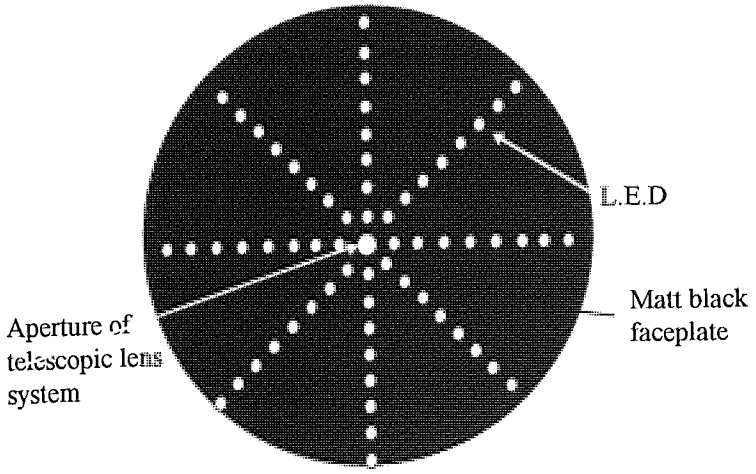

Figure 6.02: A frontal view of the faceplate, showing the radial arrangement of L.E.D.s (8 within each semi-meridian and a total of 64). The centre of the faceplate housed the telescopic lens system which enabled a magnified image of the reflected mires to be viewed.

Subjects were held steady with a chin and forehead rest. Alignment of the videokeratoscope axis with the cornea (viewed on the monitor) was achieved using the joystick control to align the central L.E.D.s with an on-screen reference marker (an overlay on the monitor) that was coaxial with the videokeratoscope axis (see figure 6.03).

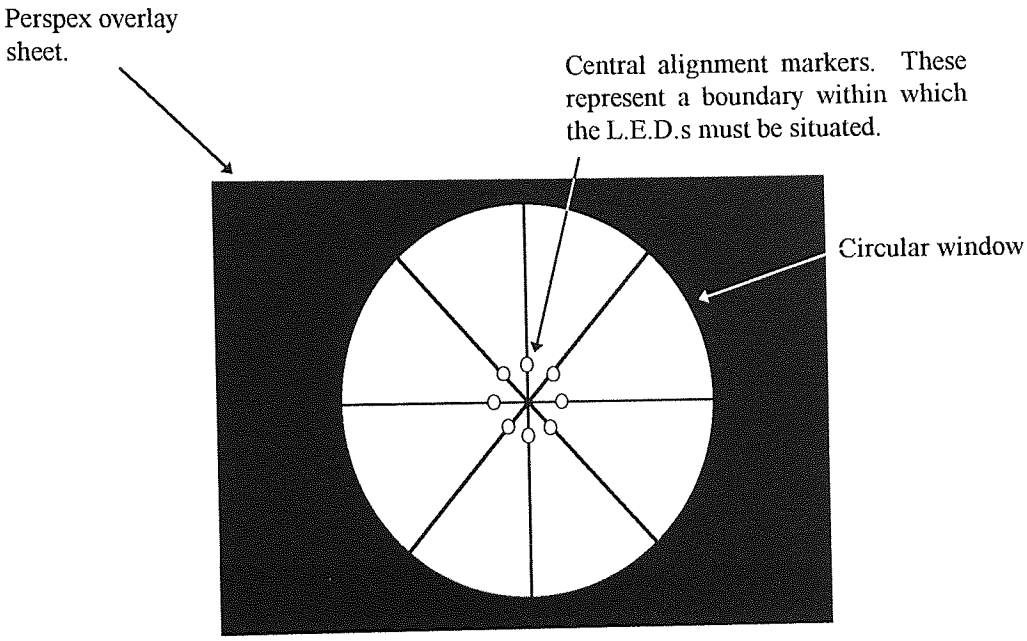

Figure 6.03: The alignment on-screen reference marker. The circular window matched the size of the output from the telescope. The references L.E.D. markers were positioned at the centre of the circular window.

A power supply was connected to the L.E.D.s (not shown in figure 6.01). The voltage of this power supply was adjusted to obtain an image of all the L.E.D.s - particularly the central ones. Earlier (Chapter 2), the relevance of alignment with respect to the cornea was described. The procedure used here was that described by Mandell (1993) where alignment was centred about the entrance pupil. This was achieved by guiding the subject's fixation to a series of eccentric targets. These targets comprised of markings on the faceplate that could only be observed by the patient.

The video image was captured using a image grabber (QUICKIMAGE 24, Ver 2.0, MASS Microsystems, Inc.) situated in the Apple Macintosh personal computer. Two image capture sizes were available; large (640 x 480 pixels) and small (320 x 240

pixels). The image grabber software was capable of displaying 1-bit, 8-bit gray-scale or 24-bit colour images. Images could be captured in sequential time intervals or as single images, however, only single images were captured. Each image could be saved on the computer hard disc in various formats. Ideally, 24-bit images would retain the maximum amount of detail. The computation time and the expense of the hardware required to be able to perform intricate image analysis using 24-bit images prohibited their use. Both 1-bit and 8-bit images were used depending on the type of image analysis program used. Two such image analysis program were devised, both are discussed in section 6.3.

Once the reflected image of the L.E.D.s was located in terms of their position and distance from the geometric centre of the innermost reflected L.E.D., the data was transferred to the topography analysis program. In general terms, this program calculated the exact L.E.D. reflection point at the cornea. After computation was complete, the resulting data could be used to derive the sagittal radius of curvature at each reflection point, or to calculate the subsequent p-value and apical radius of curvature (chapter 1). Figure 6.04 summarises the procedures involved in the calculation of corneal topography.

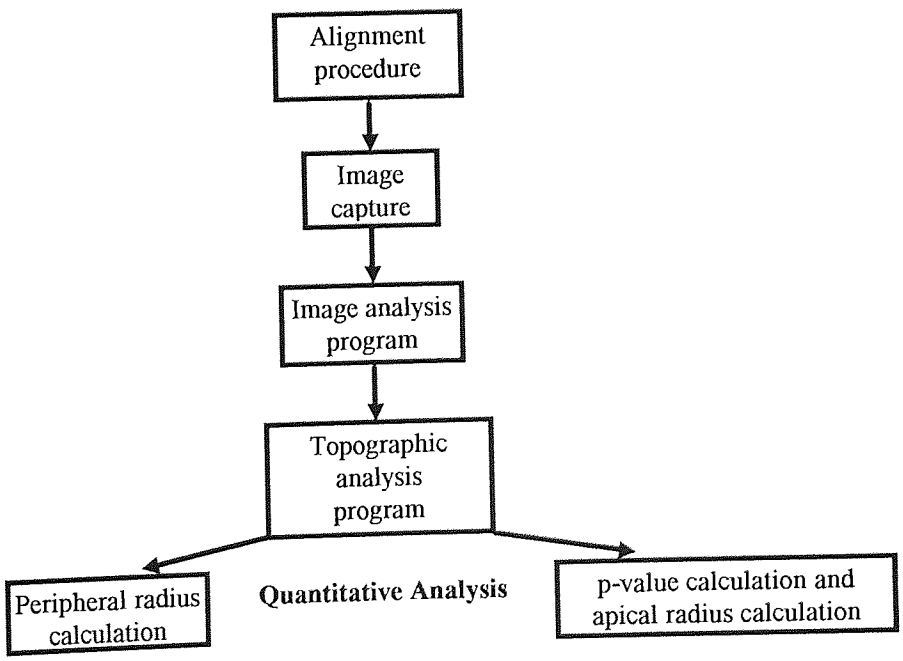

Figure 6.04: Procedures involved in videokeratoscopy.

6.3 Image analysis programs

Accurate location of the L.E.D. images was essential to ensure a high degree of accuracy of the instrument. Previous keratoscopes have used projectors to magnify keratographs to enhance measurement accuracy (Bibby, 1976). With the continual advances made in computing, the more modern videokeratoscopes use computer software to digitise and locate the reflected mires. As mentioned earlier, two image analysis programs were devised through the course of the study; the manual digitisation program and the automated digitisation program. Each method is now described.

6.3.1 Manual digitisation

Using the QUICKBASIC (Microsoft Corporation, version 1.0) application program for the Apple Macintosh, a program was written to allow an image to be imported and analysed. Whilst writing the program, the principal aim was to analyse the reflected mire images such that each L.E.D. could be located relative to a specific point (the geometric centre of the reflected central L.E.D. images). A description of the procedure involved in manual digitisation follows; however, for a full listing and documentation of the program see appendix 2.

The manual digitisation program requires the operator to locate the geometric centre of individual L.E.D.s displayed on the computer monitor. The program begins by importing a 1-bit image of the reflected L.E.D.s. Although the 1-bit image had the least amount of detail, it was the only type of image capable of being imported into the QUICKBASIC programming application. The disadvantage of using a 1-bit image was known prior to developing the program, however, the QUICKBASIC programming application was used only as a trial. The digitisation program imported the captured image and then magnified it by a factor of X3.75, this allowed only the central L.E.D.s to be viewed on the computer monitor.

In order to make the location of the geometric centre of each L.E.D. easier to find, the appearance of the mouse cursor was changed from an arrow to a cross-hair. All L.E.D. positions were found relative to a reference point, this reference point was the geometric centre of the innermost L.E.D.s (see figure 6.05). The geometric centre was found by drawing two lines perpendicular to one another from opposing L.E.D.s . The position of a central L.E.D. was then found by moving the cursor to the centre of the L.E.D. and pressing the mouse button. Whilst keeping the mouse button depressed, the cross-hair was moved to the reference point. The mouse button was then released and the distance of the central L.E.D. from the reference point calculated. For the central L.E.D.s, measurements were performed twice and the mean obtained. The manual digitisation program contained a sub-program called SUBR that calculated the distances of the L.E.D. images in pixels.

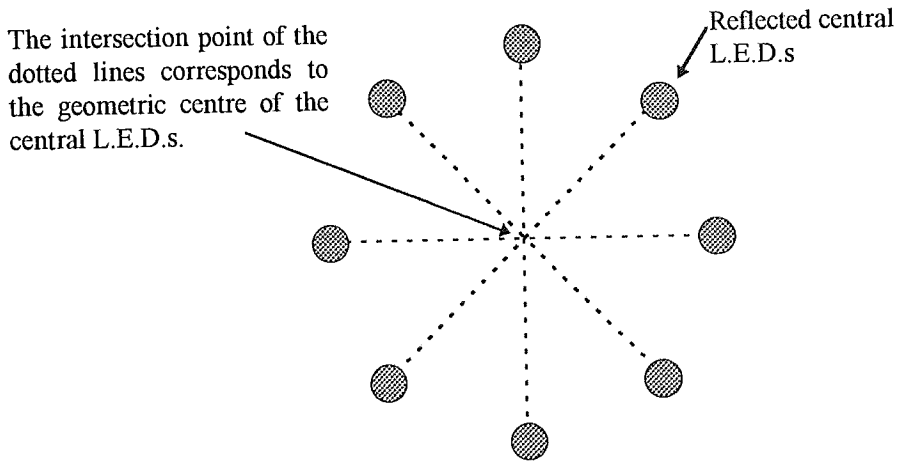

Figure 6.05: Illustrates how the geometric centre is derived from the central or innermost L.E.D.s.

In order to calculate the position and distance of the peripheral L.E.D. images, the program imported the image again, however, now all the L.E.D.s were available. Furthermore, the user had the ability to increase the magnification. Once again, the geometric centre was obtained using the same method as described earlier. L.E.D. positions were then found for each meridian in turn. Both the central and peripheral L.E.D. distances were then scaled according to their respective magnification factors. The pixel distances of the L.E.D.s measured were then displayed in an output that could then be printed or saved on the computer hard disc.

6.3.2 Semi-automated computerised digitisation

A software package called *NIH Image 1.52* (Public Domain software, version 1.55) was used to analyse the image captured from the QUICKIMAGE (Microsoft Corporation, version 1.0) software package. Before describing how *NIH Image 1.52* was used, it is useful to consider what a digital image actually is. A digital image is simply an array of numbers that are displayed on the monitor as image points (pixels), each with specific intensity and colour. When an image is processed, the array of numbers is altered. Like most image processors, *NIH Image* works with 8-bit numbers giving a maximum of 256 colours or grey-levels on the monitor at any one time.

Unlike the program written in QUICKBASIC (which could only analyse 1-bit images), *NIH Image 1.52* was capable of performing image analysis using 8-bit grey scale images, which has the obvious advantage of maintaining image quality (see figure 6.06). A useful and very powerful feature of *NIH Image 1.52* was the ability for the user to write a macro program. This program was written in a Pascal-like programming language and enables the user to automate a specific sequence of image operations. A macro program was written and used to calculate the pixel distances from the centroid of each L.E.D. to the reference geometric centre of the central L.E.D.s. (see appendix 3 for a complete listing and documentation).

A detailed description of the semi-automated digitisation program follows.

The semi-automated digitisation program started by displaying a set of instructions for the user (see appendix 3). The user was asked to open the image that was previously saved using the QUICKIMAGE application and then centre the cursor at a point that represented the geometric centre of the innermost L.E.D.s. Throughout the program, *NIH Image 1.52* displayed the coordinates of the position of the cursor. The co-ordinates at the reference point were noted by the operator.

Figure 6.06: Shows an 8-bit 256 grey-scale image of a subject's cornea.

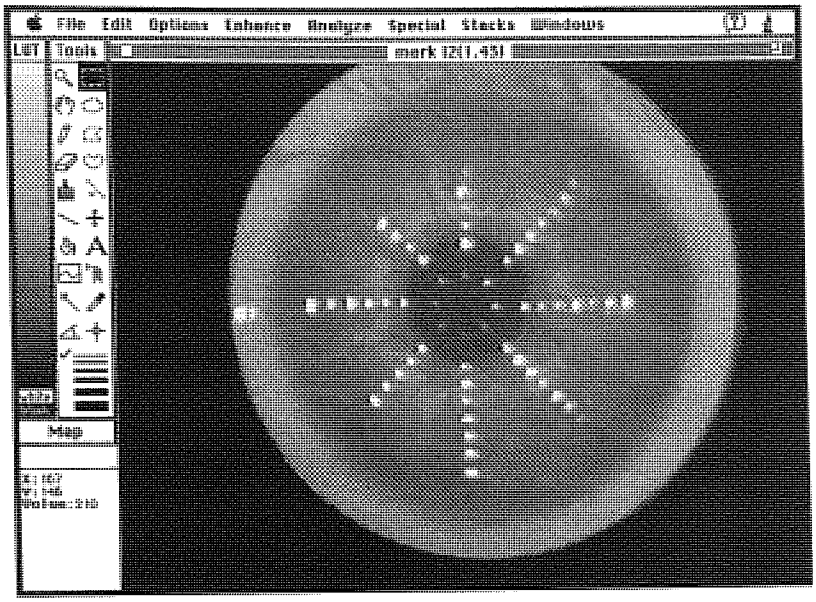

Image analysis for a complex image such as that shown in figure 6.06 requires that the background intensity (i.e. the intensity of light outside the reflected L.E.D. zone) is constant. If one considers a videokeratoscope image of a human eye then it is obvious that there are obvious differences in background intensity at the centre of the cornea compared to the peripheral cornea because of the influence of the iris. The changes in background intensity were removed by firstly inverting the image i.e. forming a negative and then subtracting a predefined level of light intensity from the digitised image. It was found, mainly through trial and error, that inverting the image led to more accurate detection of the L.E.D.s.. The background removal process effectively eliminated any variability in the light intensity of the background (figure 6.07). Once background intensity was constant, the user had the option to adjust the threshold level for the overall image. Thresholding altered the total image intensity and was used to refine the background normalisation procedure and displayed L.E.D.s as 'hot-spots' on the monitor (see figure 6.08). If any other 'hot-spots' were visible, they too were digitised. Once the digitisation procedure was complete the L.E.D. images were shown with numbers superimposed. These numbers showed the order in which each L.E.D. was digitised. Each numbered L.E.D. was therefore allocated a co-ordinate. The final part of the macro program therefore reorganised the digitised L.E.D.s into radial order in terms of the meridian analysed (figure 6.08).

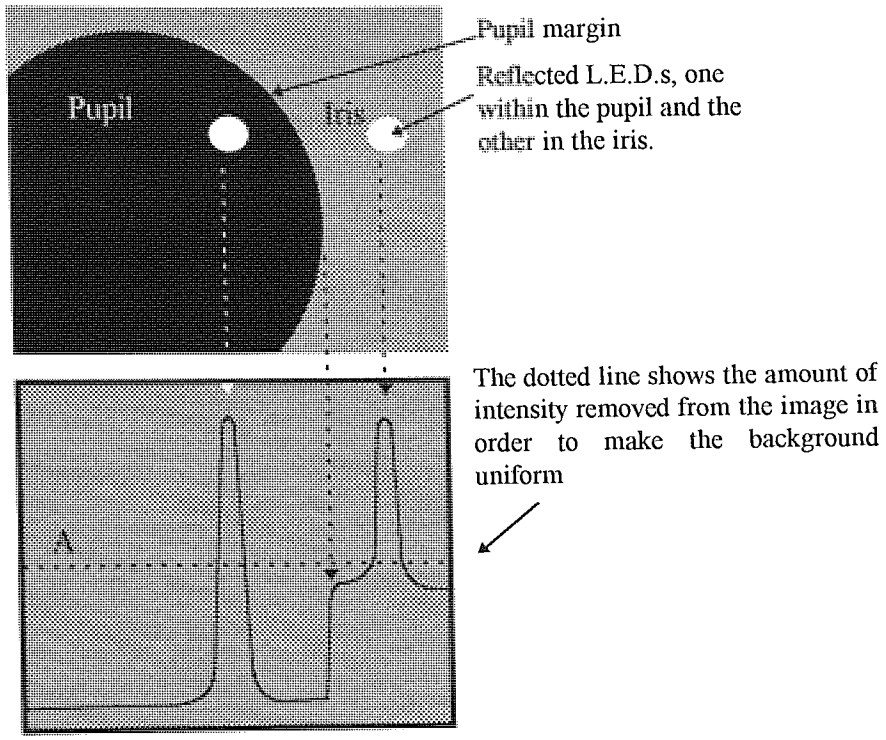

Figure 6.07: Illustrates how the background intensity was made constant. The line graph shows a profile of intensity across the image. The thresholding procedure simply moves the position of the dotted line (A) up or down, thereby revealing more or less of the image.

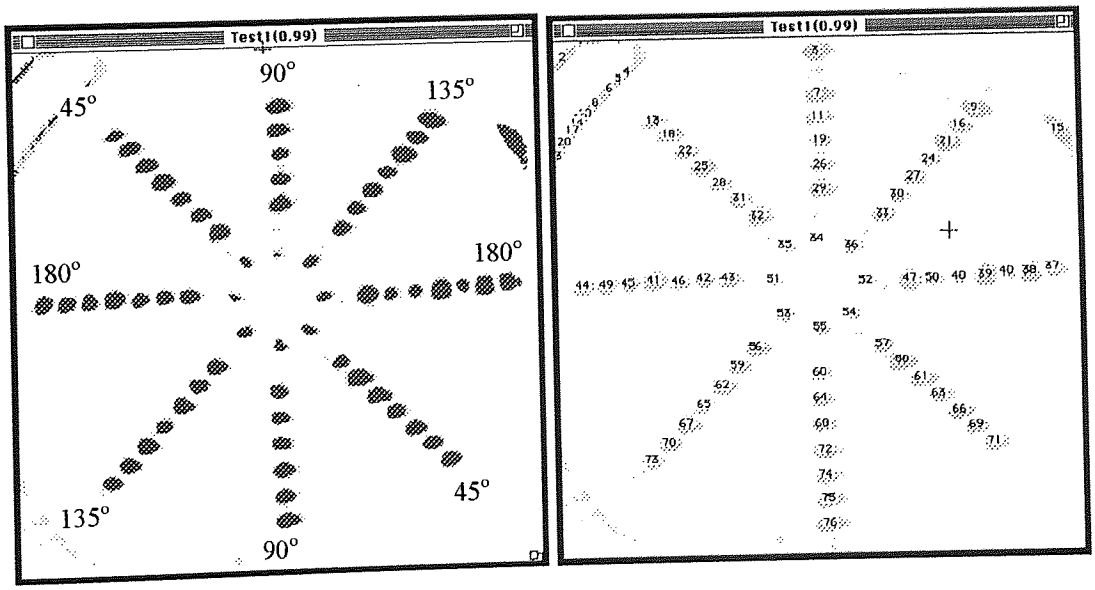

Figure 6.08: Right - shows the image at threshold with the background luminance constant. The radial lines of L.E.D.s were labelled according to the meridian in which they were located. Left - shows the L.E.D. images with superimposed numbers, showing the order in which the L.E.D.s were digitised.

Reorganisation of the L.E.D. positions was performed using basic geometry. The co-ordinates of the geometric centre were noted when the image was first imported into the semi-automated digitisation program. Although the L.E.D.s were not in any order, their co-ordinates were known. Thus, the final part of the program scanned through all the digitised particles (a particle is that point on the image that had a superimposed number, see figure 6.08) selecting those particles whose co-ordinates most closely matched the co-ordinates of the points on an imaginary straight line orientated along the four meridians (see figure 6.09). It was possible that not all of the L.E.D.s would share the same co-ordinates as the grouping line (the solid line in figure 6.09). Therefore, an error margin of 15 degrees was permitted between the inclination of the line at the geometric centre and the L.E.D.s. Whilst the program grouped all the L.E.D.s with respect to their radial arrangement, the distance of each L.E.D. was also calculated from the geometric centre.

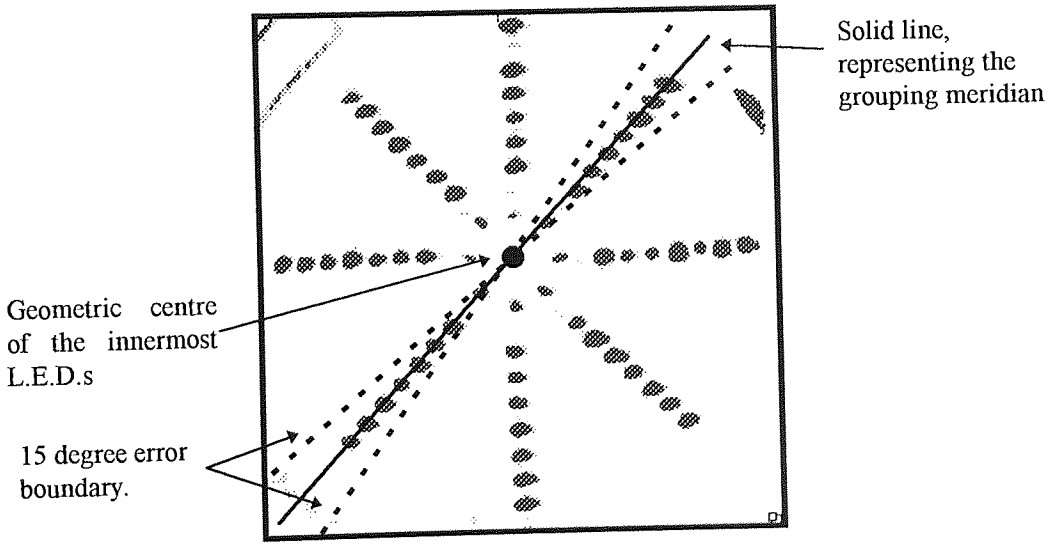

Figure 6.09: Reorganisation of each L.E.D. in terms of its meridian.

The L.E.D. distances from the reference point for the 180°, 45° , 135° and 90° meridians were then displayed in a results table (see figure 6.10). The table could then be saved as a Apple Macintosh text file and be input into the topography program (see appendix 4).

File Edit Options Enhance Analyze Special Stacks Windows

Results

	X	Y	Length	Angle	X-x0	Y-y0
1.	-28.94	-147.02	117.89	0.00	117.06	-13.97
2.	84.01	-132.90	88.24	0.00	87.45	-11.74
3.	-148.43	-129.63	151.62	0.00	-151.16	-11.74
4.	-29.53	-129.44	97.55	0.00	-96.70	-12.86
5.	73.11	-121.07	105.00	0.00	103.96	-14.76
6.	-138.20	-118.59	115.96	0.00	-115.32	-12.16
7.	-28.43	-112.12	133.90	0.00	-133.46	-10.91
8.	62.75	-109.26	69.61	0.00	68.62	-11.70
9.	-126.55	-106.35	186.86	0.00	-186.61	-9.62
10.	50.74	-97.16	169.98	0.00	-169.69	-9.94
11.	-113.99	-94.55	52.07	0.00	51.14	-9.80
12.	-28.53	-94.80	63.38	0.00	-62.50	-10.50
13.	39.39	-84.55	58.29	0.00	-56.57	14.04
14.	-101.34	-82.42	197.07	45.00	-148.43	-129.63
15.	-28.84	-76.93	182.11	45.00	-138.20	-118.59
16.	27.70	-72.10	165.31	45.00	-126.55	-106.35
17.	-88.36	-70.53	148.10	45.00	-113.99	-94.55
18.	-74.65	-58.39	130.63	45.00	-101.34	-82.42
19.	15.97	-58.68	113.06	45.00	-88.36	-70.53
20.	-32.43	-40.43	94.77	45.00	-74.65	-58.39
21.	-55.09	-36.24	51.83	45.00	-32.43	-40.43
22.	-8.02	-34.88	65.94	45.00	-55.09	-36.24
23.	117.06	-13.97	74.12	45.00	40.84	61.85
24.	87.45	-11.74	90.71	45.00	53.29	73.40
25.	-151.16	-11.74	108.98	45.00	67.63	85.45

Figure 6.10: Results table showing reorganised data from the digitisation program.

6.4 Apparatus characterisation

6.4.1 Focusing characteristics

Before evaluating the accuracy of the instrument, it was important to assess the performance of the videokeratoscope with respect to image capture. Focusing precision is an important factor in the absolute accuracy of any videokeratoscopic system (Applegate, 1992; Nieves et al, 1992). In order to assess the focusing precision of the videokeratoscope, a flat engineers ruler was placed in front of the videokeratoscope and focused ten times. The distance between the ruler and the videocamera was measured using an electronic micrometer capable of performing measurements to within ± 0.01mm.

In order to analyse the influence of defocus on linear measurements, images of the ruler were captured with the ruler situated at specific distances from the optimum point of focus (a distance of 128mm). The ruler was defocused by 1mm intervals up to ± 5mm from the best focus, this defocus will be referred to as z-axis defocus as the ruler was displaced along the z-axis. Accurate positioning of the object was achieved by displacing it using the electronic micrometer.

Eleven images were captured and the pixel distance between eleven millimeter markings on the ruler measured. Measurements were performed using the *NIH Image 1.52* software package which has the facility to display light intensity profiles. In addition, *NIH Image 1.52* also displayed the x and y co-ordinates (in pixels) of any point on the intensity profile specified using the mouse cursor. Thus, the exact location of the markings on the ruler could be found by positioning the mouse cursor at each minima of the light intensity profile (figure 6.11 shows a typical intensity profile).

In order to characterise the errors induced on linear measurements due to focusing errors, the videokeratoscope was focused on a the target ten times. The procedure involved focusing, defocusing and then re-focusing on the target. Electronic calipers (capable of measurement to ± 0.01mm) were used to measure the distance from the object to the optical centre of the lens system.

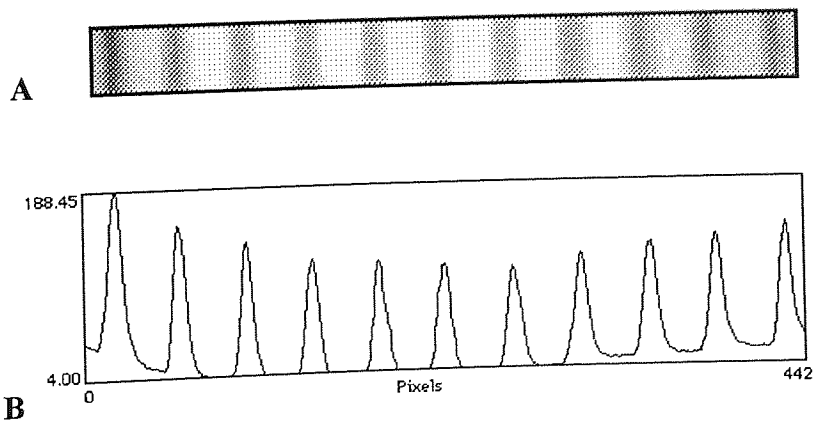

Figure 6.11: **A** - Shows the image of the target ruler used to assess the effects of linear defocus (in this case the target was defocused by 3mm). **B** - Shows the intensity profile plot of the same target.

6.4.2 Central corneal resolution

Observation of the point of reflection of the innermost L.E.D.s at the corneal surface indicates the resolution of the videokeratoscope in determining the topographical nature of the central corneal surface. The central resolution of a videokeratoscope is the distance from the vertex normal to the point of reflection of the innermost L.E.D. at the surface. Using an 8.20mm sphere, the semi-automated digitisation program was used to calculate the reflection points of the L.E.D.s. These values were obtained for the 135 degree inferior meridian (see figure 6.08 for classification) and were then input into the topographical analysis program in order to calculate the surface coordinates.

The further away measurements are performed from the vertex normal the less the resolution of the central cornea or surface under test. Central resolution is dependent on two factors - the spatial separation of the central L.E.D.s and the working distance of the instrument. Measurements with the videokeratoscope were compared to the data collected using the EyeSys CAS on same 8.2mm sphere (see appendix 1).

6.5 Results

Analysis of the accuracy of focusing showed that the mean position of focus was 0.336mm from the optimum focus. The precision of the working distance was calculated as ± 0.157mm (the standard deviation of the focusing distances found using the electronic micrometer).

Figure 6.12 demonstrates the linear relationship between the relative image size and the level of z-axis defocus. Linear regression showed that the equation of the best fit line (method of least squares) was

$$y = 100.17 + 0.69x \qquad \textit{Equation 6.01}$$

and the correlation coefficient, R, 0.998. The gradient ($\Delta y/\Delta x$) of the regression line was found to be 0.69 (% relative image size/mm). Therefore, a 1mm level of defocus resulted in 0.69% change in linear measurement of the image. Focusing precision was

calculated to be ±0.157mm, therefore, the corresponding error in relative image size for the instrument was found to be 0.11% (calculated by multiplying the precision of the instrument, ±0.157mm and the percentage change in image size per millimeter of defocus, 0.69%/mm). The true value of the central L.E.D. distance and the value of the L.E.D. distance when maximum error occurred in image size (i.e. in 95% of cases) was input into the topographic analysis program to determine the error in central radius of curvature due to focusing precision. The value of the L.E.D. distance when maximum error occurred was calculated as follows:

% Maximum error due to focusing in 95% of cases= 1.96 x 0.157mm

=0.3077mm

The change in relative image size induced by 0.3077mm defocus was then calculated by substituting this value into equation 6.01. The change in image size was found to be 0.382%. For a 7.80mm spherical surface, the central L.E.D. distance measured 36.297 pixels, the measured L.E.D. distance for the maximum defocus error (in 95% of cases) would be 36.436 pixels. Computing these values into topography program (see appendix 4) showed that the error in calculating the correct central radius of curvature would be 0.039mm or 0.195D. This error would be dependent on the size of the image, however, for the example used, the actual central radius of curvature was 7.80mm, therefore, the 0.195D error represents the maximum error that would be encountered from inaccurate focusing.

Table 6.01: Data values showing effect of linear defocus on relative image size.

Linear defocus (mm)	Image size (pixels)	Relative image size (%)
5	417	103.731
4	414	102.985
3	411	102.239
2	407.5	101.368
1	405	100.746
0	402	100
-1	400	99.502
-2	398	99.005
-3	395	98.2587
-4	391	97.264
-5	389	96.766

Figure 6.12: The effect of linear z axis defocus on image size.

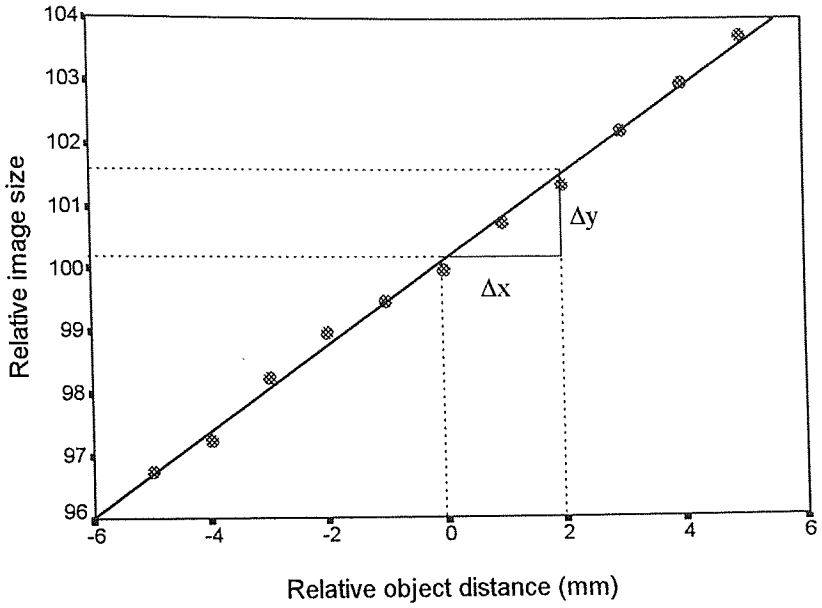

Computing the results obtained from image processing showed that for an 8.2mm sphere (135 degree inferior meridian), the central L.E.D. was reflected at a semi-diameter of 0.926mm (see table 6.02). For the same surface but using the EyeSys CAS, the central ring was reflected about a semi-diameter of 0.495mm (see appendix 1). In effect, the EyeSys CAS provided greater resolution of the central portion of the surface.

Table 6.02: The sagittal depth and distance from the vertex normal for reflection points of 8 L.E.D.s on the spherical surface.

Sagittal depth (mm)	Distance from vertex normal (mm)
000000	.000000
.051629	.926473
.201041	1.817931
.322430	2.290937
.473246	2.758418
.648932	3.207948
.864533	3.674382
1.099325	4.111281
1.372723	4.552123

6.6 Discussion

Accurate description of the anterior corneal surface plays a major role in our understanding of the image forming properties of the eye. Although principally correct in design, many videokeratoscopes have not succeeded in accurate measurement because of out dated methods of image processing and inappropriate algorithms that derive the corneal profile (Bibby, 1976; Mandell et al, 1969; Edmund et al, 1985; Zadnik et al, 1992, Dave et al, 1994).

The mean error in focusing was found to be of 0.336mm from the optimum focus and the focusing precision was found to be high (standard deviation ± 0.157mm). Figure 6.12 shows the linear relationship between level of defocus and relative image size. A 1mm level of defocus introduced an error in linear measurement of 0.69%. With respect to focusing precision of the videokeratoscope, the error in linear image size for the instrument was 0.11%. From a statistical point of view, 95% of measurements would be performed at a working distance of ± 0.307mm from the true value (1.96 x standard deviation). Substitution of the error in working distance into the regression line equation results in a change in image size of 0.382%. For a 7.8mm sphere, the central L.E.D. was situated at a distance of 36.297 pixels from the geometric centre. In 95% of measurements performed, the central L.E.D. distance from the geometric centre would range from 36.297 pixels to 36.437 pixels. Computing the later value into the topography and radius program resulted in an error in central radius of curvature of 0.039mm or 0.195D for 95% of cases. Therefore, the focusing characteristics of the videokeratoscope were found to be accurate and any errors introduced were clinically insignificant.

Andersen et al (1993a) also evaluated the accuracy of their photokeratoscope, they found that from the 95% confidence intervals, errors due to inaccurate focusing resulted in a 0.1D error. Comparing their results to those obtained with the present videokeratoscope, very little difference was observed. Nieves et al (1992) found that for 0.33mm decentration along the z-axis, the TMS (Computed Anatomy, Inc.)

produced an error of 0.9D using two spherical surfaces. However, Nieves et al (1993) did not evaluate the focusing accuracy or precision of the TMS and therefore the errors discussed do not relate to the absolute error induced from focusing accuracy.

Errors in z-axis alignment occur as a resulted of a combination of two factors, firstly from inaccurate determination of the point of focus and secondly, from the change in image size introduced from inaccurate positioning of the videokeratoscope. The latter only occurs as a result of the former. Short working distances enable a smaller depth of focus and therefore more accurate determination of the optimum point of focus (Nieves et al, 1992). However, when a small error in positioning occurs, the use of a shorter working distance introduces a larger degree of error in image size than a longer working distance. This explains why the present system obtained similar accuracy in focusing to the system used by Andersen et al (1993a).

The reason for the high accuracy of the videokeratoscope was attributed to the magnification system, which provided a small depth of focus, and the long working distance. These factors led to only small changes in linear magnification of the image when the system was defocused. Other corneal topography systems are capable of higher focusing accuracy (Andersen, 1993a), however, the design of such systems makes it difficult for them to be easily incorporated into a clinical environment. Nevertheless, it must be stated that the system designed by Andersen et al (1993a) is an experimental system and presumably not intended as a tool to be used in clinical practice.

With the present videokeratoscope, the instrument design enabled a large area of measurement by the use of a hemispherical bowl (table 6.02). In a study conducted by Nieves et al (1992), the effect of working distance on alignment error was evaluated. A large working distance was found to reduce errors in focusing. The EyeSys CAS (which has a larger working distance than the TMS-1) was found to be more accurate (Antalis et al, 1993). The EyeSys CAS operates at a working distance of 92mm. The videokeratoscope used in the present study operated at a working distance of 128mm,

this together with the spatial separation of the central L.E.D.s enabled a central resolution of 1.92mm for an 8.2mm sphere. For the same surface the EyeSys CAS central resolution was 0.99mm. The EyeSys CAS therefore, would provide greater resolution of the central cornea. Andersen et al (1993a), using their photokeratoscope, obtained central corneal resolution of 0.2mm. This significantly high level of resolution was attained by a combination of using a modified Haag-Streit perimeter as the faceplate and a large working distance (312mm). The only disadvantage of their system was in its design - namely that it was bulky; the trend in modern consulting room equipment is portability.

Compared to the keratometer, the videokeratoscope provided greater central resolution and therefore would be more likely to measure that portion of a cornea representing the true apical radius. Older keratoscopic systems have been shown to resolve only 2-3mm of the central cornea (Bibby, 1976; Rowsey, 1983). The central resolution of the present videokeratoscope may be improved by simply inserting another ring of L.E.D.s closer towards the optical system or increasing the working distance. The importance of having a high degree of central resolution must be put into perspective. Anomalies that occur in the central portion of the cornea are most detrimental to vision. The keratometer measures about a 4mm diameter of the cornea and hence has the greatest potential for overlooking irregularities in this area. However, with respect to the design of the current videokeratoscope, an introduction of another ring of L.E.D.s would introduce disturbances in the digitisation procedure i.e. the adjacent L.E.D.s would interfere with one another and hence introduce digitisation errors. Nevertheless, the videokeratoscope provided twice as much resolution of the central cornea than the keratometer.

6.7 Summary

Numerous computerised videokeratoscopes are currently available (see Chapter 2). Little detailed information has been published regarding the methods by which images are processed or the algorithms used to derive the topographical nature of the corneal

surface. In the present chapter a detailed description of a new computerised videokeratoscope was provided. The accuracy of the topographical system with respect to central corneal resolution showed that although the new videokeratoscope did not provide as much central resolution as the EyeSys CAS, it provided twice as much resolution as the keratometer. Furthermore, evaluation of the focusing system and its influence in radius and power measurements showed that the videokeratoscope exhibited a high level of focusing accuracy and that 95% of measurements would be performed to within 0.039mm radius of curvature. The characteristics of the videokeratoscope were suitable for corneal topographic analysis. However, further evaluation of the algorithms that derive the corneal topographic coordinates must be performed. Chapter seven will therefore describe the optical theory used to derive the topographic coordinates.

Chapter Seven

Accuracy and Repeatability of a Computerised Videokeratoscope using Convex Aspheric Surfaces

7.1 Introduction

An accurate and repeatable description of the corneal surface is essential for numerous ophthalmological and optometric procedures. In Chapter 6 the design and characteristics of the computerised videokeratoscope were described. This device was designed to provide a quantitative description of the central and peripheral cornea. Few studies have evaluated the accuracy and repeatability of corneal topographic systems using convex aspheric surfaces. The present chapter will therefore describe the algorithms used in the derivation of the corneal/test surface coordinates and evaluate the accuracy (i.e. how close the videokeratoscope results are to the actual dimensions of the convex aspheric surfaces) and precision (i.e. the variation in repeated observations).

Various quantitative methods of presenting topographic data have been published (Edmund et al, 1985; Edmund, 1986; Dingledein et al, 1989; Wilson et al, 1991a). For purposes such as contact lens fitting and for a gross overall description of corneal topography, a mathematical model applied to the corneal surface coordinates would, in theory, provide an adequate description of its topography. Researchers have already used mathematical models to describe the corneal surface (Bibby, 1976; Edmund et al, 1985; Edmund, 1986; Howland et al, 1992). Howland et al (1992) applied complex 4th order polynomials to corneal coordinates, although it has been shown that simpler conic sections may be sufficient to model the cornea (Townsley, 1970; Townsley, 1974; Bibby, 1976; Guillon et al, 1986). However, the normal cornea is asymmetric, thus, mathematical fitting of a conic section to the cornea is not appropriate. Nevertheless, the use of conic sections would provide a useful descriptor of peripheral corneal shape within semi-meridians. Conic sections utilise a term known as the p-

value (or conic constant) which determines the level of peripheral flattening; this term, together with apical radius (r_o) of the surface describe the whole family of ellipsoids. For the videokeratoscope developed in the present study, a quantitative method of data presentation was therefore adopted that fitted a conic section to corneal semi-meridians.

7.2 Aims

- Describe the quantitative method of analysis.
- Assess the accuracy and repeatability of the computerised videokeratoscope for 12 convex aspheric surfaces.
- Compare the accuracy and precision of the manual digitisation program (section 6.3.1) with the semi-automated program (section 6.3.2) for all 8 semi-meridians.

7.3 Convex Aspheric Test Surfaces

In order to assess the accuracy and precision of the videokeratoscope, twelve convex aspheric test surfaces were used. Each surface was aligned and captured as a video image (as described in section 6.2) and saved on the computer hard drive. The parameters of the twelve surfaces were as follows:

p=1 (sphere) with an apical radius (r_o) of 7.0mm, 7.4mm, 7.8mm, 8.2mm;
p=0.8 (oblate ellipse) with an apical radius (r_o) of 7.0mm, 7.4mm, 7.8mm, 8.2mm;
p=0.5 (oblate ellipse) with an apical radius (r_o) of 7.0mm, 7.4mm, 7.8mm, 8.2mm.

The 7.8mm radius sphere was used for calibration of the videokeratoscope.

The test surfaces were produced on a computer-controlled lathe capable of making convex aspheric buttons (CLS Ltd., Huntington, U.K.). The surface with an apical radius of 7.0mm and p-value of 0.5 was sent to a laboratory (Rank-Taylor-Hobson, Leicestershire, U.K.) for Form Talysurf analysis, this is an extremely accurate method

of measuring the surface parameters. From the laboratory printout, the apical radius and p-value were calculated, the results confirmed the manufacturer's values.

7.4 Methods

Analysis of the captured video images was performed in two ways; using manual digitisation and semi-automated digitisation.

7.4.1 Manual Digitisation

The entire program listing and documentation is provided in appendix 2. However, a brief description of procedure is relevant to the present section. In order to accurately locate the position of the central L.E.D.s, the captured 1-bit video image is enlarged so that it almost occupies the entire monitor. The mouse is then used to locate the geometric centre of the innermost L.E.D.s (see figure 6.05). The user then positions the mouse cursor at the geometric centre, depresses the mouse button and then moves the mouse cursor to the centre of the innermost L.E.D. whose distance is to be measured. This procedure is performed twice and the computer then averages these readings. Next, the entire image is displayed and the user is required to locate the centre of the L.E.D.s (from the innermost to the most peripheral) of each meridian. In the assessment of accuracy and repeatability of the videokeratoscope, all the eight meridians were measured. The procedure is time consuming; digitisation of all 64 L.E.D.s takes approximately 15 minutes. Manual digitisation was performed for all twelve surfaces..

7.4.2 Semi-automated Digitisation

Through the course of this study, it was appreciated that current topography systems were already capable of complete automated digitisation and that the videokeratoscope would greatly benefit from this form image processing. Towards the end of this study an image processing application (*NIH image 1.52*, Public Domain software, version

1.55) became available that allowed semi-automated digitisation thereby eliminating some of the subjective error from manual digitisation. This alternative technique was therefore included for direct comparison with manual digitisation in terms of the accuracy and precision of the videokeratoscope. The *NIH Image 1.52* image processing application and associated macro programs were described in chapter 6, section 6.3.2.. Briefly, the procedure involved importing an image (previously saved from the image capture program, Quickimage 24) and then removing the background light intensity variation so that accurate detection of the L.E.D.s was possible. A thresholding procedure was applied so that refinements to the total image intensity could be made to enable only the L.E.D.s to be viewed and not any other artifacts in the image. Digitisation of the L.E.D.s was then commenced that resulted in each L.E.D. being labelled with a number. As the computer sequentially detected each L.E.D. from the top left of the monitor to the bottom right, the L.E.D.s were in incorrect order. A reorganisation program then grouped each L.E.D. into a radial format with respect to its meridian (a detailed description of the semi-automated digitisation program is provided in section 6.3.2). Output of the results was displayed in terms of a results table that showed the x and y coordinates of each L.E.D. (the origin of the Cartesian coordinates was at the geometric centre of the innermost L.E.D.s.

7.4.3 Topography Calculation

The most recent method of calculating the corneal coordinates has been based on the multiple arc technique devised by Doss et al (1981) and later modified by Klyce (1984) (see section 3.3.3). Here, the cornea is considered to comprise of a non spherical surface that is composed of several small spherical arcs of varying radius of curvature. Each arc would extend over three rings (the rings were equivalent to the L.E.D.s used in the present videokeratoscope). Depending on the separation of each of the rings, such a model may not be wholly appropriate as a large separation would extend over a larger portion of the cornea and the assumption of sphericity between the rings would not be valid. In addition to this, the multiple arc technique assumes that the distance of

the L.E.D. or ring images from the videokeratoscope axis corresponds to the distance from the point of reflection at the corneal surface to the videokeratoscope axis. As the image of the reflected rings or L.E.D.s actually lies behind the corneal surface (see figure 7.01) the distance of the imaged L.E.D. from the videokeratoscope axis (labelled b in figure 7.01) will not equal the distance of the point of reflection from the cornea to the videokeratoscopic axis (labelled a in figure 7.01).

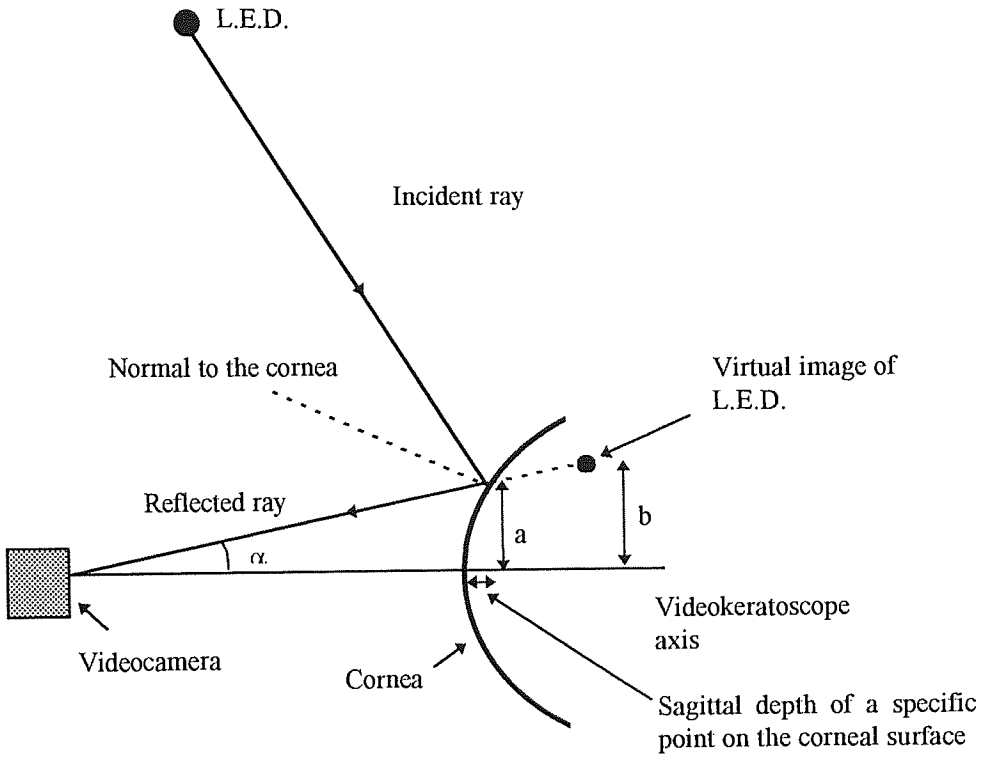

Figure 7.01: shows that the cornea acts as a convex mirror that forms a virtual image of the object L.E.D. behind the corneal surface. The multiple arc technique assumes the distances **a** and **b** are equal.

Wang et al (1989) described a method which assumes that only the central cornea is spherical. According to Wang et al (1989), the reflected ring images are assumed to originate from some point behind the cornea. The major difference between the method multiple arc technique described by Klyce (1984) and the algorithms used by Wang et al (1989) is that Klyce (1984) only calculated the sagittal depth of specific points on the corneal surface using ring image distances from the videokeratoscope axis. Conversely, Wang et al (1989) used the angular subtense (α) of the image to the

optical system to calculate the sagittal depth and height of the point of reflection from the videokeratoscope axis (a).

The method of deriving topographic coordinates for the videokeratoscope used in the present study was much the same as that described by Andersen et al (1993a,b) and will now be described. The procedure involved analysing the reflected mire image from a suitable reference sphere (a 7.8mm sphere was used in this case, Andersen et al used an 8.00mm sphere) in order to calculate the angular subtense (F) of the target mires at the optical axis of the videokeratoscope (see figure 7.02).

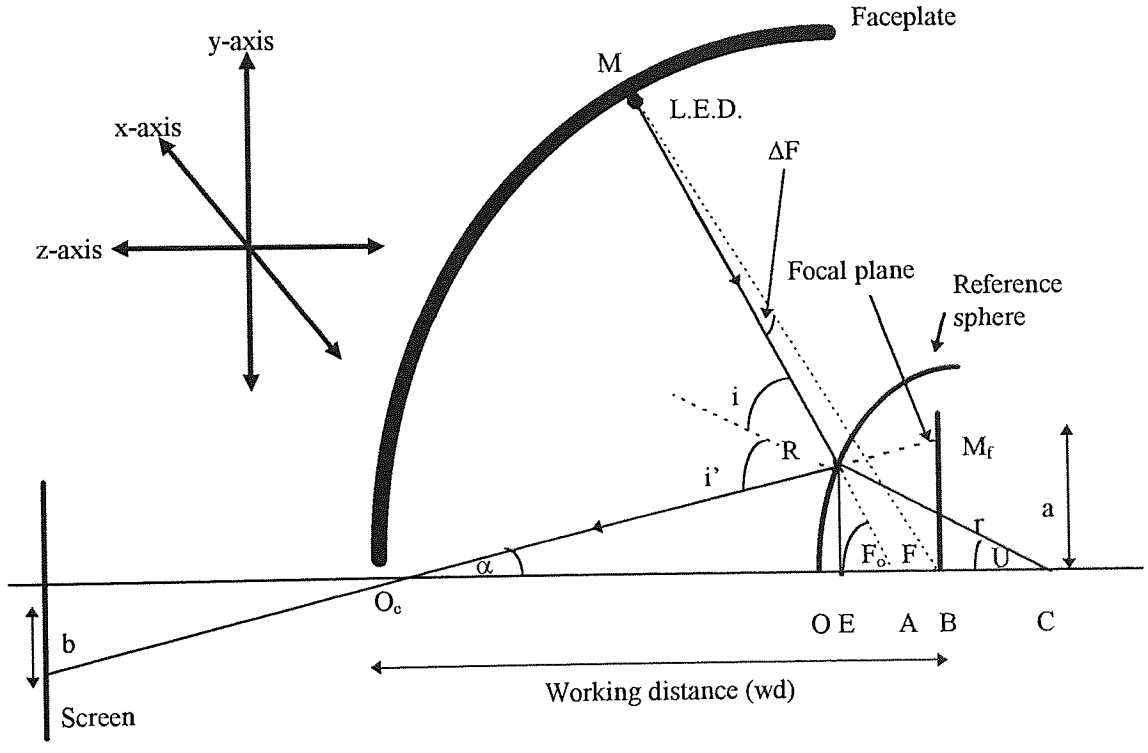

Figure 7.02: Shows the various notations used, after Andersen et al (1993a), for the calculation of F using the reference sphere.

i - is the angle of incidence,
i' - is the angle of reflection,
a - is the actual height of the reflected mire from the videokeratoscope axis,
b - is the height of the reflected mire at the screen or film plane,
B - is the distance along the z-axis (defined above) of the plane of focus,
C - is the central radius of curvature of the reference sphere,
α - is the angular subtense of the reflected ray at the videokeratoscope axis,
F_o - is the angular subtense of the incident ray at the videokeratoscope axis,
F - is the angular subtense of the L.E.D.s at the videokeratoscope axis,

ΔF - is the angular separation of A and B from point M,
U - is the angle between the normal at any point on the surface and the videokeratoscope axis,
x, y, z are the reference axes with origin at O (the vertex normal of the reference sphere),
R - is a point on a surface defined by (y, z, U),
E - is the distance along the z-axis for a point on the surface,
A - is the distance along the z-axis of the intersection of the incident ray,
O_c - is the optical centre of the objective lens,
O - is the origin of the Cartesian coordinates (placed at the vertex normal).

A. Calculation of the Angular Subtense of the each L.E.D. at the Image Plane

From the video image or photograph of the reflected L.E.D.s, b was measured for a reference spherical surface (r=7.80mm). b may be equated to a (the actual height of the virtual image) by simply dividing b by the magnification of the videokeratoscope system. The magnification was determined by focusing on an engineer's ruler over 10mm and then measuring the same distance in pixels in both the manual digitisation and semi-automated digitisation programs. The linear magnification of the entire system was then calculated as follows:

$$\text{Magnification factor (pixels / mm)} = \frac{\text{Image size (pixels)}}{\text{Object size (mm)}} \qquad \textit{Equation 7.01}$$

The magnification of the system and the L.E.D. distances for the 7.80mm reference sphere within semi-meridians were calculated as part of the calibration procedure (see section 7.4.3F.). The angular subtense of light entering the optical centre of the focusing lens may therefore be written as:

$$\alpha = \tan^{-1}\left(\frac{a}{wd}\right) \qquad \textit{Equation 7.02}$$

One assumption made was that as the object (the L.E.D.s) to image distance was large (by a factor of 16.4) for the spherical reference surface, the resulting image of the central mires would lie at half the central radius of curvature from the point O (i.e. at point B). Confirmation of this was obtained by simple substitution into the vergence formula:

$$\frac{1}{l'} = \frac{2}{r} - \frac{1}{l} \qquad \textit{Equation 7.03}$$

Substituting the values for r (in metres) and the object distance l (a negative value must be input as the incident ray is divergent), the image distance may be found. Thus,

$$\frac{1}{l'} = \frac{2000}{7.8} + \frac{1000}{128}$$

$$l' = 3.785\,\text{mm}$$

Comparing this value to the case if the incident light were actually from infinity, then only a difference of 0.11mm exists.

Using the sine rule in triangle CRO_c a relationship for angle U can be obtained in terms of wd, α and r.

$$\frac{Sin\alpha}{r} = \frac{Sin(180 - U - \alpha)}{(wd + 0.5.r)} \qquad \textit{Equation 7.04}$$

$Sin(180\text{-}U\text{-}\alpha)$ may be rewritten as $Sin(U+\alpha)$; transforming equation 7.04 in terms of U,

$$\frac{(wd + 0.5r).Sin\alpha}{r} = Sin(U + \alpha)$$

$$U = Sin^{-1}\left(\frac{(wd + 0.5.r).Sin(\alpha)}{r}\right) - \alpha \qquad \textit{Equation 7.05}$$

By the law of reflection, the line CR bisects the angle MRO_c,

therefore, $i = i' = U + \alpha$ *Equation 7.06*

also, $F_o = 2.U + \alpha$ *Equation 7.07*

The angle F_o denotes the angle at the axis from the L.E.D. (M) through the point of reflection at the reference surface. However, the aim is to calculate angle F (the angular subtense of the central mire at the focal plane).

Using the sine rule in triangle ABM provides a solution for angle AF.

$$\frac{Sin(\Delta F)}{BA} = \frac{Sin(180 - F_o)}{BM} \qquad \textit{Equation 7.08}$$

Equation 7.08 may be rewritten as

$$\Delta F = Sin^{-1}\left(\frac{BA.Sin(F_o)}{BM}\right) \qquad \textit{Equation 7.09}$$

The distance BM is derived using the Pythagoras' theorem knowing the horizontal and vertical location of each L.E.D. on the faceplate (these must be measured manually and are shown in table 7.01). Measurement was accomplished using a set of external calipers, the distance between opposing L.E.D.s within a meridian was measured, the distance of each L.E.D. was therefore determined by halving each distance. Each L.E.D. was located in terms of its numerical and meridional label, the convention is shown in figure 7.03.

Figure 7.03: sign convention used to describe the position of each L.E.D..

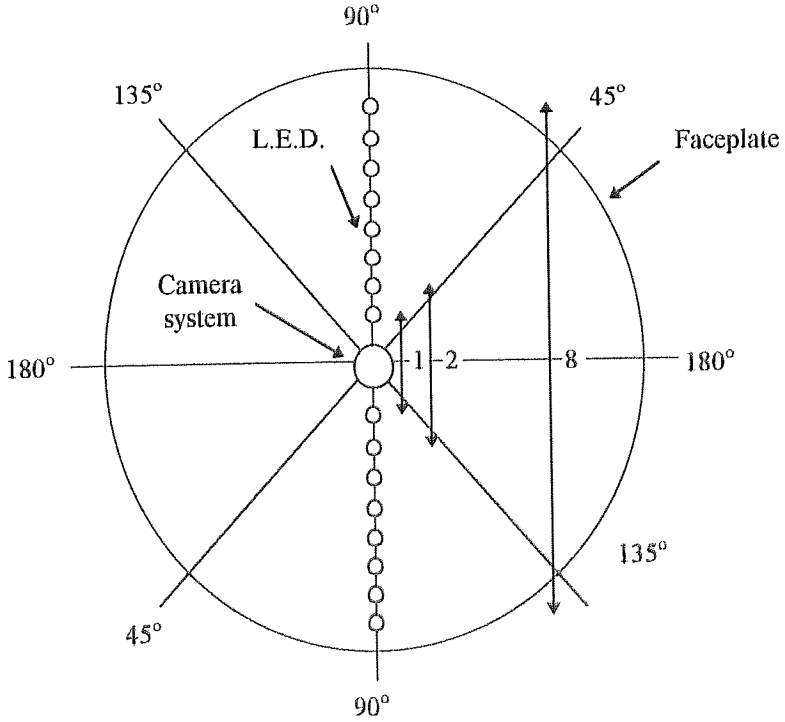

Table 7.01: the distances of opposing L.E.D.s on the faceplate was measured using external calipers. Individual L.E.D.s were located by halving the distances shown in the table. Measurement accuracy was within ±0.25mm, each distance was measured three times and the mean calculated. Each meridian was denoted by a number and meridian, the convention is shown in figure 7.03.

	1	2	3	4	5	6	7	8
90°	54	117.5	147.5	175.5	200	220.5	236.5	248
180°	55.75	117	147	175.5	200.25	220.5	236.5	247.5
45°	55.75	116.5	147	175.5	200	220	237	247.5
135°	55.75	118	148.5	176	200	220.5	237	248

However, the distance BA is not known and may be calculated as follows:

$$BA = CE - AE - CB \qquad \textit{Equation 7.10}$$

Andersen et al (1993b) calculated the distance AE as follows,

$$AE = \frac{Sin(U)}{t.wd.F_o}$$

the term t was not defined in their paper. The formula for calculation of AE is shown in the equation 7.11.

$$AE = \frac{r.Sin(U)}{Tan(F_o)} \qquad \textit{Equation 7.11}$$

Substitution of CE, AE and CB into equation 7.10 results in the following:

$$BA = r.Cos(U) - \frac{r.Sin(U)}{Tan(F_o)} - 0.5.r \qquad \textit{Equation 7.12}$$

From the triangle BMA, angle F is calculated as

$$F = F_o - \Delta F \qquad \textit{Equation 7.13}$$

Hence, through step-by-step computation of equations 7.02 to 7.12 the angular subtense of each L.E.D. at the optic axis can be found.

B. To find the position of the vertex normal (the origin, OB) and the central radius of curvature (r) for an unknown surface

In order to calculate the central radius of curvature for an unknown surface, the value of U_1 (the angular subtense of the normal to the cornea at the first reflected L.E.D. on the corneal surface and the videokeratoscopic axis) and α_1 (the angular subtense of the reflected ray for the central (first) L.E.D. and the videokeratoscopic axis) must be found. α_1 can be easily calculated from equation 7.02. From equation 7.07:

$$U = \frac{(F_o - \alpha)}{2} \qquad \textit{Equation 7.14}$$

Because the distance between A and B is small, we state that

$$U \approx \frac{(F - \alpha)}{2} \qquad \textit{Equation 7.15}$$

and therefore U_1 can be found for the surface under investigation.

With respect to the angle α_1,

$$Tan(\alpha_1) = \frac{a}{wd} = \frac{RE}{EO_c} \qquad \textit{Equation 7.16}$$

also,

$$RE = r.Sin(U) \qquad \textit{Equation 7.17}$$

$$EO_c = wd + 0.5.r - r.Cos(U) \qquad \textit{Equation 7.18}$$

Substitution of equations 7.17 and 7.18 into equation 7.16 gives:

$$\frac{a}{wd} = \frac{r.Sin(U)}{(wd + 0.5.r - r.Cos(U))} \qquad \textit{Equation 7.19}$$

Therefore, in terms of r (the central radius of curvature of the surface),

$$r = \frac{a.wd}{(wd.Sin(U) + a.Cos(U) - 0.5.a)} \qquad \textit{Equation 7.20}$$

Having found r the position of the intercept OB is given by $0.5.r$. Locating the position of OB is important as it defines the position of the vertex normal and also forms the origin of Cartesian coordinates.

C. Describing the corneal topography

The origin of the axes is defined by the point O (see figure 7.04) located at the intersection of the normal to the surface and the optical axis of the videokeratoscope. Individual points on the corneal surface may be defined according to the points *y*, *z* (which simply represent the reference coordinates), and U (the angle subtended by the tangent to the point on the corneal surface and the videokeratoscope axis).

Figure 7.04

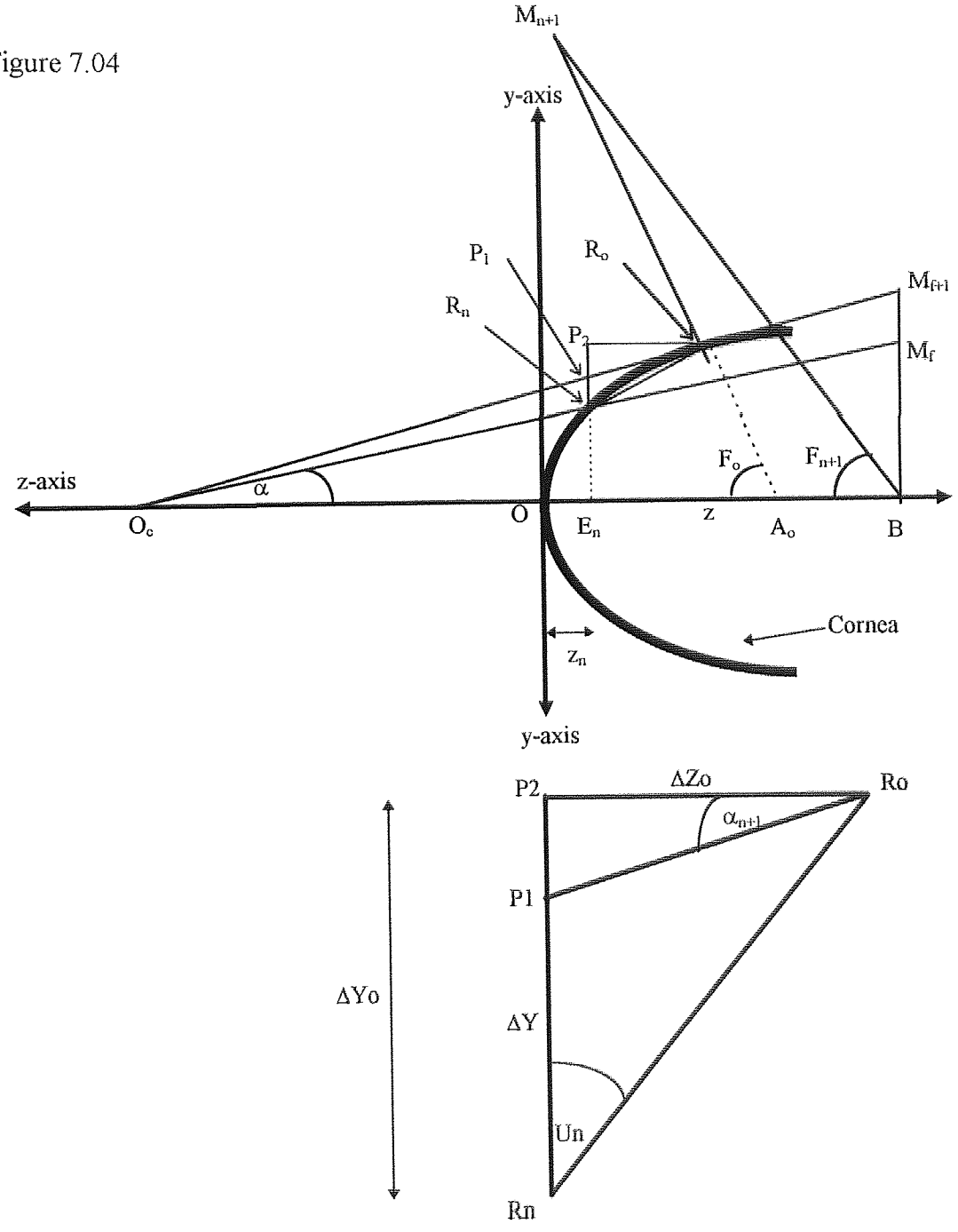

Figure 7.04: above, shows R_o, the approximate reflection point on the cornea corresponding to an L.E.D. M_{n+1}. R_o is derived from R_n (the exact location of the corneal point for the previous L.E.D. M_n). M_f and M_{f+1} represent the virtual images of L.E.D.s M_n and M_{n+1}. The second part of figure 7.04 is simply an enlargement of the triangle R_o P_2 R_n, where Δy_o the distance along the y-axis from point R_n to R_o and Δz_o the distance along the z-axis from point R_n to R_o. Δy is the y-axis intersept of the line $O_c M_f$.

At the corneal surface location, O (the vertex of the corneal surface) z=0, y=0, U=0. The next step is to calculate the reflection point of the first L.E.D. (R_1) at the corneal surface. As an initial approximation, the angle U_n is considered to be constant when moving from the point R_n to R_{n+1} (i.e. $U_n = U_{n+1}$). The reason for this is that at present no values relating to the point R_{n+1} are known, using an iterative procedure (which is described later in the calculations) the values of R_n may be used in order to calculate the geometric coordinates of R_{n+1}. Each approximated point on the corneal surface is denoted by R_o. From figure 7.04, triangles O_c E_n P_1 and O_c B M_{f+1} are similar.

Therefore,
$$\Delta y_o = \frac{\Delta a.(wd - 0.5.r + z_n)}{wd} \qquad \textit{Equation 7.21}$$

where Δa is the difference in the measured L.E.D. heights at the image plane. In the case of finding the coordinates of the first L.E.D., Δa would simply be equal to a.

The central radius of curvature is found from equation 7.20 and Δa is found by $\Delta b/m$ (where m is the system magnification and Δb the adjacent mire separation). Δy represents the vertical elevation from the nth point on the corneal surface to the n+1th point. However, observation of figure 7.04 shows that the values required are Δy_o and Δz_o in order to calculate the point of reflection. The following steps illustrate how these values can be calculated.

Applying the Sine rule to triangle $R_o R_n P_1$

$$\frac{P_1 R_o}{Sin(U_n)} = \frac{\Delta y}{Sin(90 - U_n - \alpha_{n+1})}$$

and thus,

$$P_1R_o = \frac{\Delta y.Sin(U_n)}{Cos(U_n + \alpha_{n+1})} \qquad \textit{Equation 7.22}$$

From P_1R_o, Δz_o and Δy_o can be found from triangle $P_1P_2R_o$.

Thus, $$\Delta z_o = P_1R_o.Cos(\alpha_{n+1}) \qquad \textit{Equation 7.23}$$

and $$\Delta y_o = \Delta y + P_1R_o.Sin(\alpha_{n+1}) \qquad \textit{Equation 7.24}$$

The coordinates of the point R_o (the approximate position of the point of reflection initially for the first L.E.D.) may therefore be written as:

$$(z_o, y_o) = (z_n + \Delta z_o, y_o + \Delta y_o) \qquad \textit{Equation 7.25}$$

D. Refining the coordinates to find the exact value of (z_{n+1}, y_{n+1})

The coordinates of the L.E.D. (M_{n+1}) may be written as

$$(-BM_{n+1}.Cos(F_{n+1}) + 0.5.r, BM_{n+1}.Sin(F_{n+1})) \qquad \textit{Equation 7.26}$$

where F_{n+1} (derived from the reference surface) is known from equation 7.13. Using the equation of a straight line, the equation of line $M_{n+1}R_o$ is determined.

Thus, $$y = \frac{(y_M - y_o)}{(z_M - z_o)}.(z - z_o) + y_o \qquad \textit{Equation 7.27}$$

and the intercept at the z axis, A_o (which is dependent on the surface to analysed), is then calculated from

$$A_o = z_o - y_o.\frac{(z_M - z_o)}{(y_M - y_o)} \qquad \textit{Equation 7.28}$$

The sine rule is then applied to triangle $M_{n+1}BA_o$. in order to calculate ΔF_o.

Thus, $$\Delta F_o = Tan^{-1}\left(\frac{BA_oSin(F_{n+1})}{BM_{n+1} - BA_oCos(F_{n+1})}\right) \qquad \textit{Equation 7.29}$$

Combination of equations 7.07 and 7.13 gives

$$U_o = \frac{(F_{n+1} + \Delta F_o - \alpha)}{2} \qquad \textit{Equation 7.30}$$

The values of z_o, y_o, U_o have are now calculated, these parameters characterise the position of R_o. The estimated value of U_o is then replaced with the mean of U_n and the new value of U_o. The new value of U_o is re-substituted into equation 7.22 and the

whole procedure repeated until successive values of U change by less than 0.01% (according to Andersen et al (1993b)). A complete listing of the program is available in appendix 4. The program prints out raw data values i.e. the values of z and y for each reflection point of the unknown surface.

The present method of calculation makes two **initial** assumptions. Firstly, that when calculating the values of angle F, for the reference sphere, the image is assumed to lie at the focus of the sphere (i.e. half of the central radius of curvature of the reference sphere). Using the standard vergence formula it was shown that the actual distance of the image was only slightly different from the assumed distance, hence this assumption was valid. The second initial assumption, that the angle U remains constant when moving from a known point to an unknown point was also valid as by process of iteration the error in successive estimates of U was reduced to less than 0.01%. Thus, contrary to other methods (Mandell et al 1971; Doss et al, 1981; Klyce, 1984) the algorithms derived by Andersen et al (1993b) and modified in the present study make no assumptions regarding the pre-existing shape of the unknown surface.

E. Conic section curve fitting to semi-meridian coordinates

Numerous studies have fitted conic sections to the topographic coordinates of the entire corneal profile (Bibby, 1976; Edmund et al, 1985; Guillon et al, 1986; Edmund, 1986). However, it is well known that the cornea is asymmetric (Koch et al, 1993) and therefore using conic sections to model the entire corneal profile is appropriate. Quantitative analysis using the present videokeratoscope was performed using quadratic regression analysis to fit a conic section to the data points (derived from the topography calculation program) within a semi-meridian. Considering Baker's equation for a conic section:

$$y^2 = 2r_o x - px^2$$

it is obvious that the equation does not have a constant. Furthermore, Baker's equation in its present form it is not a true quadratic equation. In order to fit a quadratic equation and thus find the p-value, the value of y^2 must be replaced by Y.

Quadratic regression was performed using the statistical package SPSS (release 6.0, SPSS Inc.). SPSS allowed the user to choose whether a constant was required or not in the regression analysis. The values derived from the topography program were therefore input into the SPSS data sheet in order to derive the p-value and central radius of curvature (r_o). The p-value provides a unique quantitative description of every surface measured (see section 1.6.1 for a detailed mathematical description).

F. Calibration

Calibration was performed by capturing an image of the 7.8mm reference sphere and using either the manual or semi-automated digitisation method to measure the L.E.D. distances (see section 6.3). The procedure was performed three times and the mean distances were recorded. The distances were then inserted into the appropriate section of the topography calculation program (see appendix 4).

7.5 Statistics

The accuracy of any measurement device refers to its ability to determine the true value of the parameter being measured. Conversely, repeatability or precision is the ability to consistently reproduce the same result. Instrument accuracy and repeatability were assessed using the statistical technique advocated by Bland et al (1986). The method of statistical analysis was described earlier in chapter 5, however, a description is relevant to the present section. The accuracy of the present videokeratoscope was evaluated by taking measurements of 12 aspheric surfaces and then calculating apical radius and p-value. The accuracy of was determined by observation of the variance of the differences between the calculated and actual values. Bland et al (1986) also suggest that a plot of the differences against the actual values should be made (see figure 7.05). On the graph, three reference lines are drawn: the bias line and the 95% confidence limits. The bias simply shows the mean of the differences. The 95% confidence limits represent the range over which 95% of the difference would lie.

Another widely used method of assessing accuracy is to observe the cumulative frequency distribution (Hannush et al, 1990) of the difference between calculated and actual radius.

Repeatability was assessed by observation of the variance in measurements of p-value and apical central radius of curvature of five repeated reading on the same surface($p=0.8$, $r_o=7.8mm$).

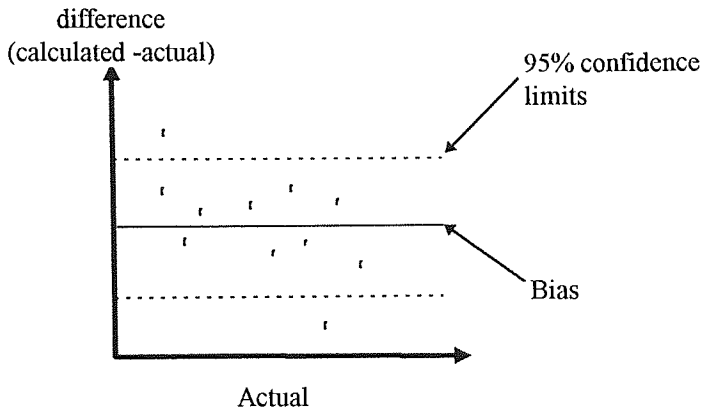

Figure 7.05: shows the plot suggested by Bland et al (1986). The bias represents the mean of the difference, the 95% confidence limits show the differences likely to be encountered in 95% of cases.

7.6 Results

As discussed in the method, not only was the accuracy and repeatability of videokeratoscope under investigation, but a further aim was to compare computerised automated digitisation with manual digitisation . Therefore, the results of accuracy and repeatability are presented in two sections - for the manual and automated digitisation techniques, respectively. The complete results are shown in appendix 5 and 6.

7.6.1 Accuracy of p-value using manual digitisation

The results obtained from quantitative analysis of the raw aspheric surface coordinates provided the p-value and apical radius of each semi-meridian for all twelve surfaces. Table 7.02 shows the means and standard deviations obtained for the calculated p-

values determined in eight semi-meridians for those surfaces with a p-value of 0.5, 0.8 and 1.

Table 7.02: Accuracy of determining individual p-values during manual digitisation.

p-value	Mean	Standard Deviation
0.5	0.47	±0.07
0.8	0.79	±0.05
1.0	1.01	±0.04

On average, each p-value was determined to a high degree of accuracy from analysis of a total of 32 semi-meridians (4 surfaces x 8 semi-meridians). The standard deviation was least for the spherical surface and small increases were seen as the surfaces became flatter in the periphery.

Figure 7.06: The correlation between calculated and actual p-value for twelve aspheric surfaces.

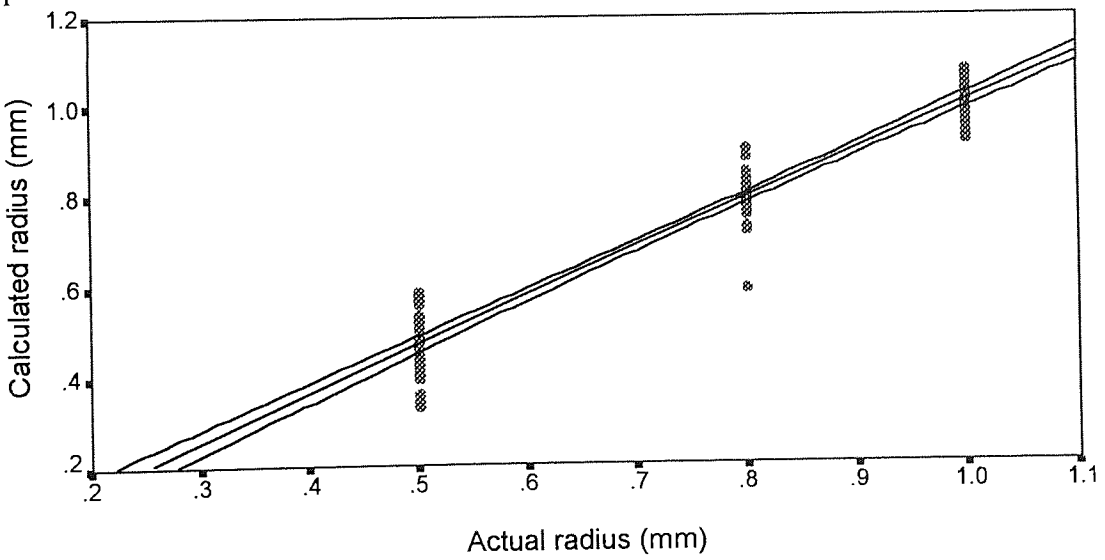

Figure 7.06 shows that there was a linear relationship between the actual and the measured p-values (r = 0.9695). Furthermore, as the 95% confidence intervals (the limits over which 95% of the points would be expected to lie from the regression line) were close to the regression line the best fit line (method of least squares) accurately modelled the scattered data. Bland et al suggested that the graph shown in figure 7.06 only shows a association and is not an accurate method of assessing accuracy.

The central line in figure 7.07 shows the bias (-0.009) and the two other lines show the 95% limits of agreement (from +0.105 to -0.123). Figure 7.07 represents the differences in p-values obtained for all the meridians of all twelve surfaces. The bias, standard deviation and 95% limits of agreement therefore represent overall values. The limits of agreement show the range over which the mean difference is found in 95% of cases.

Figure 7.07: Disparity between calculated and actual p-value for convex aspheric surfaces.

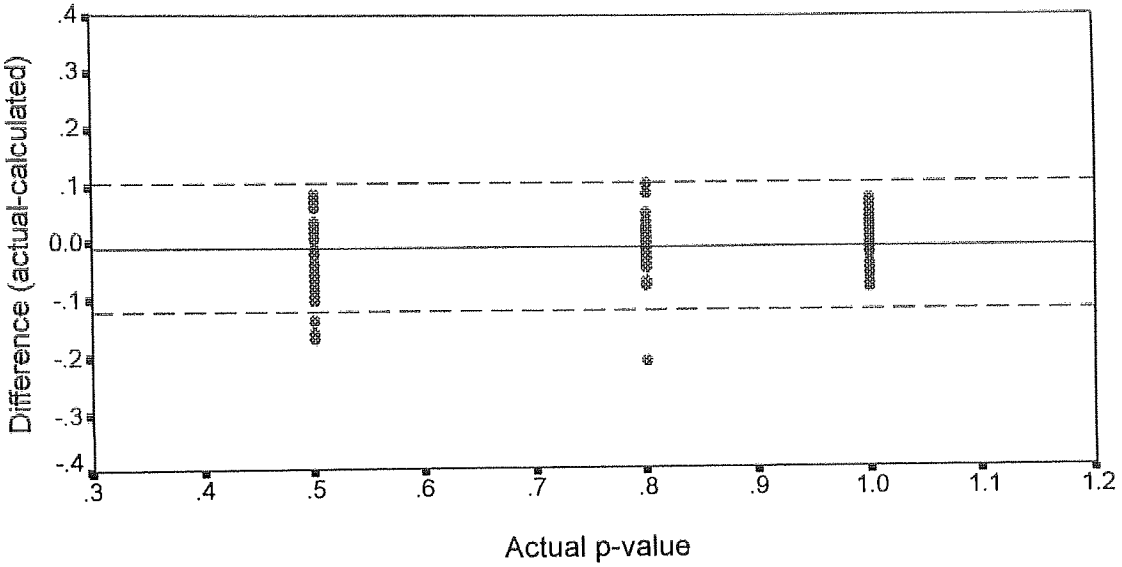

Table 7.03: The bias, standard deviation and 95% limits of agreement for overall p-value accuracy.

Bias	Standard deviation	95% limits of agreement
-0.009	±0.0581	+0.105 to -0.123

Another method used to confirm this result was by consideration of the cumulative frequency distribution of the difference in calculated and actual p-values. Table 7.04 shows that 90% of the results were obtained to within 0.1 of the true p-value. For errors in calculated and actual p-value, both methods showed similar levels of error; of the order 0.1.

Table 7.04: Cumulative frequency distribution of difference in calculated and actual p-value.

Error (difference)	Cumulative frequency (%)
<0.05	62%
<0.10	90%
<0.15	93%
<0.21	100%

7.6.2 Accuracy of central radius using manual digitisation

The calculated central radius of curvature of the aspheric surfaces were first compared in terms of the four radius groups. Table 7.05 shows the mean and standard deviations for all four radii. The mean shows that on average, central radius of curvature was determined correctly. However, the standard deviations show that greatest variation in central radius of curvature was obtained for the 7.00mm surfaces. The image of the 7.00mm surface was relatively small and therefore inaccurate localisation of the centre of L.E.D.s could have induced the variability in measurement.

Table 7.05: Accuracy of central radius of curvature for the videokeratoscope.

Radius (mm)	Mean (mm)	Standard deviation (mm)
7.00	7.02	±0.075
7.40	7.45	±0.047
7.80	7.82	±0.066
8.20	8.21	±0.067

The correlation coefficient shows a high degree of association between calculated and actual radius (r=0.989). The 95% confidence lines alongside the central correlation line show that the best fit line accurately fits the scattered data.

Figure 7.08: The correlation between calculated and actual radius for twelve aspheric surfaces.

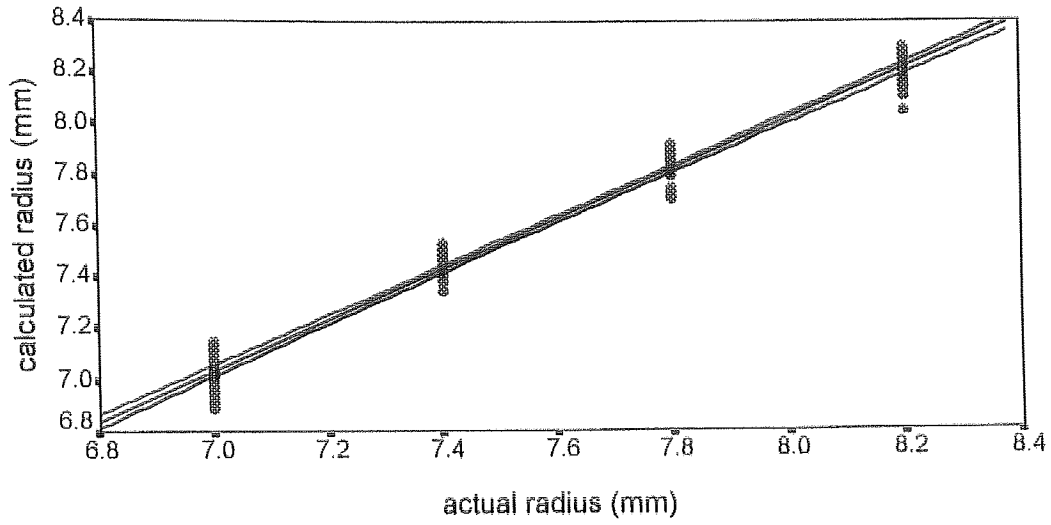

Comparison of actual and calculated radius using correlation coefficients was not an appropriate statistical procedure as it is only showed that a relationship existed between the calculated and actual radius. Therefore, the difference between calculated and actual radius was plotted against the actual radius (see figure 7.09 and table 7.06). The bias was low showing that, on average, the central radius was only 0.027mm flatter than the actual radius.

Table 7.06: summarises the results computed from figure 7.09. The results of the central radii were pooled in this table.

Bias (mm)	Standard deviation (mm)	95% limits of agreement (mm)
+0.027	± 0.066	+0.156 to -0.102

The 95% limits of agreement show that the variation of the videokeratoscope was not within the accuracy suggested by Stone (1962) (see section 2.1), however, the upper 95% confidence limit suggests that greatest difference between calculated and actual radius in 95% of cases would be 0.156mm or 0.78D.

Figure 7.09: Disparity between calculated and actual radius for twelve aspheric surfaces.

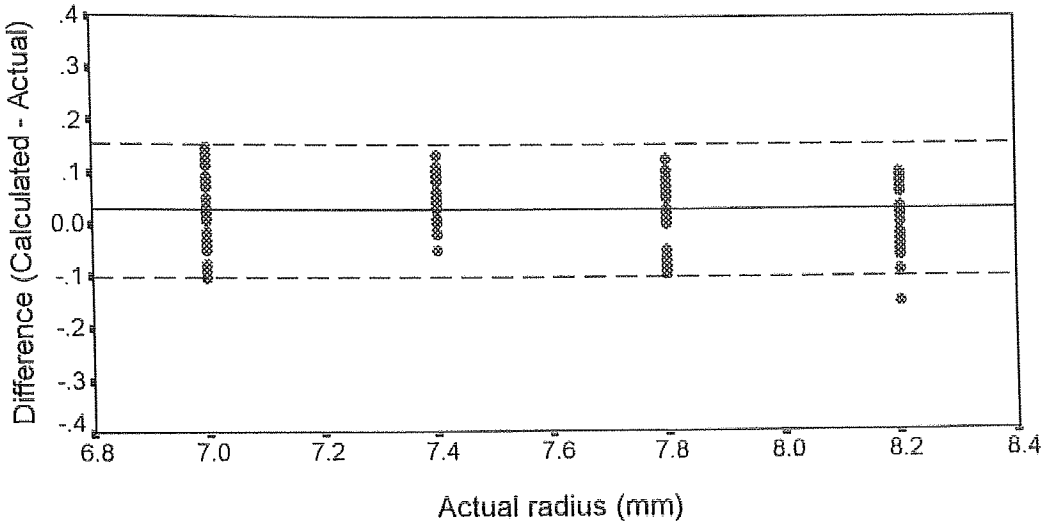

Table 7.07 shows that 83.3% of readings were obtained are within 0.1mm or 0.5D. These results are similar to those obtained from the limits of agreement and variance analysis.

Table 7.07: Cumulative frequency distribution of the differences (actual-calculated).

Error (difference)	Cumulative frequency (%)
<0.25D	45.8%
<0.50D	83.3%
<0.80D	100%

7.6.3 Repeatability of the videokeratoscope for manual digitisation

In order to evaluate repeatability or the precision of the Aston University videokeratoscope, five repeat readings were taken on a convex aspheric surface (r_o=7.8mm, p-value=0.8). Analysis of the standard deviation effectively showed the precision of the manual digitisation process. However, errors could also have occurred due to inaccurate focusing and therefore a further four images were captured. Each image was then digitised five times and the mean distance of each L.E.D. computed.

Table 7.08: Means and standard deviations of the computed p-value and central radius of curvature of 5 repeated readings for 5 different images after refocusing and recentring the videokeratoscope. The surface analysed was the p=0.8, r_o=7.8mm along the 180° meridian.

	Mean	Standard deviation
p-value	0.782	±0.0486
central radius	7.807	±0.067

Table 7.09: Means and standard deviations of the computed p-value and central radius of curvature of 5 repeated readings for the same image, along the 180° meridian.

	Mean	Standard deviation
p-value	0.732	±0.0322
central radius	7.846	±0.0453

The results showed that the standard deviation was greater for the radii than for p-value on both occasions. The effect of refocusing and recentring had little influence on p-value and central radius measurements. This was shown by the fact that little difference in standard deviation was observed between one single image and five images. The precision of the videokeratoscope was primarily effected by manual digitisation. The instrument was highly repeatable for p-values, however, central radius showed reduced repeatability. However, calculating the mean of both the p-values and central radius of multiple images improved the accuracy of the system.

7.6.4 Accuracy of p-value for semi-automated digitisation

The semi-automated digitisation system was developed in order reduce computation time and reduce subjective variability in determining L.E.D. positions from the manual digitisation program. A similar analysis was therefore performed to evaluate the accuracy of the automated system for the aspheric surfaces.

Manual digitisation assessed the accuracy of p-value and central radius of curvature of 96 semi-meridians, for the semi-digitisation procedure 74 semi-meridians. The reason

for this was that some of the meridians were not included for analysis as some detail was lost during the thresholding procedure. The surface r_o=7.00mm, p-value=0.5 was also not included in the comparison for semi-automated digitisation as almost all the L.E.D.'s merged during threshold digitisation. Furthermore, the images used for analysis of semi-automated digitisation were the same images used during the analysis of manual digitisation.

Table 7.10: calculated p-value with semi-automated digitisation.

Bias	Standard deviation	Limits of agreement
+0.001	± 0.043	+0.086 to -0.083

Table 7.10 shows that the use of semi-automated digitisation improved the accuracy of the p-value. The bias was very close to zero, indicating that on average little or no difference was observed between calculated and actual p-value. Furthermore, the 95% limits of agreement were smaller compared to those obtained with manual digitisation (see table 7.03). As stated earlier, another advantage of the automated technique was that subjective error from manual digitisation was eliminated, hence repeatability or precision was only influenced by instrument characteristics (see chapter 6).

Figure 7.10: Disparity between calculated and actual p-value for convex aspheric surfaces.

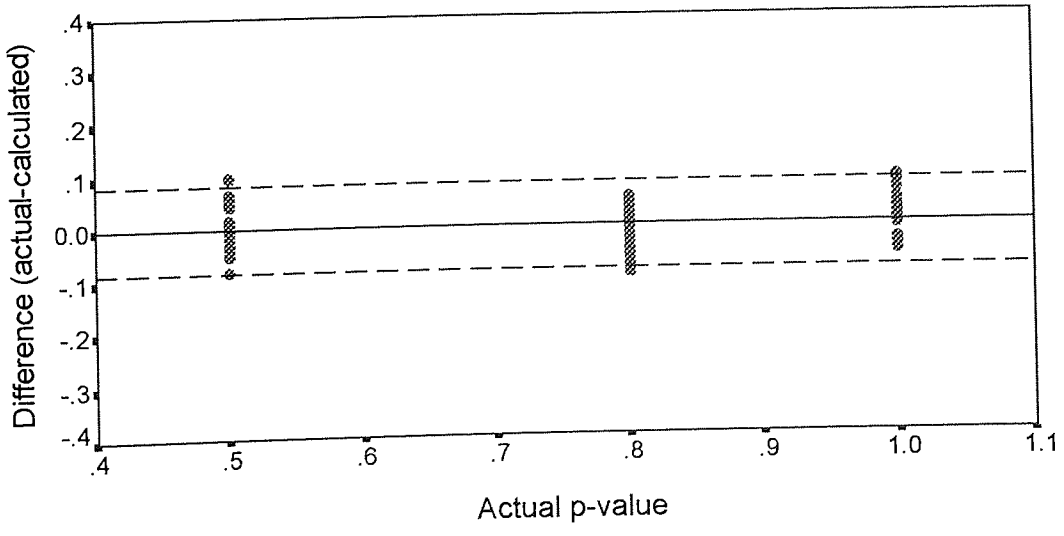

Comparing the cumulative frequency distribution for the semi-automated method showed that 98.6% of measurements were performed with less than 0.1 difference between calculated and actual p-value (see table 7.11).

Table 7.11: The cumulative frequency distribution of the differences between calculated and actual p-value.

Error (difference)	Cumulative frequency (%)
<0.05	74%
<0.10	98.6%
<0.11	100%

Analysis of the variance of calculated p-value for each asphericity showed greatest variation for flatter surfaces (see table 7.12). Greatest accuracy was obtained for spherical surfaces. The same trend was also observed with manual digitisation (table 7.02).

Table 7.12: Accuracy in determining individual p-values during semi-automated digitisation.

p-value	Mean	Standard Deviation
0.5	0.509	±0.05
0.8	0.784	±0.042
1.0	1.012	±0.035

However, comparison with table 7.02 reveals that the mean p-value is closer to the actual p-value with semi-automated digitisation. Also, the standard deviation is smaller for semi-automated digitisation - indicating that the spread of results was less with the semi-automated method.

7.6.5 Accuracy of central radius for semi-automated digitisation

Evaluating the accuracy of central radius of curvature for aspheric showed that little variation was found for those surfaces with central radii of 7.00, 7.40 and 7.80mm. However, greatest variation was found with the 8.20mm central radius surfaces (see table 7.13).

Analysis of the differences of calculated and actual radii, showed that the use of semi-automated digitisation improved the accuracy of central radius of curvature measurements (table 7.14). The narrow confidence intervals show that a maximum error of only approximately ±0.56D occurs in 95% of cases.

Table 7.13: the means and standard deviations for surfaces grouped in terms of central radius of curvature.

Central radius (mm)	Mean (mm)	Standard deviation (mm)
7.00	6.970	±0.059
7.40	7.396	±0.053
7.80	7.798	±0.041
8.20	8.203	±0.070

Table 7.14: calculated radius for semi-automated digitisation.

Bias (mm)	Standard deviation (mm)	Limits of agreement (mm)
-0.009	±0.057	+0.103 to -0.121

The graph shown in figure 7.12 displays the dispersion of the differences between calculated and actual radius for 11 aspheric surfaces. Furthermore, the cumulative frequency distribution showed that 95.9% of the differences between calculated and actual radius were obtained within 0.5D with semi-automated digitisation (see table 7.15). As with the p-value comparison, the 7.00mm apical radius surface with p-value=0.5 was omitted from calculations because digitisation could not be performed due to poor image quality

Table 7.15: Cumulative frequency distribution of the differences between calculated and actual radius with semi-automated digitisation.

Error (differences)	Cumulative frequency (%)
<0.25D	47.3
<0.50D	95.9
<0.60D	100

Figure 7.11: Disparity between calculated and actual radius for convex surfaces.

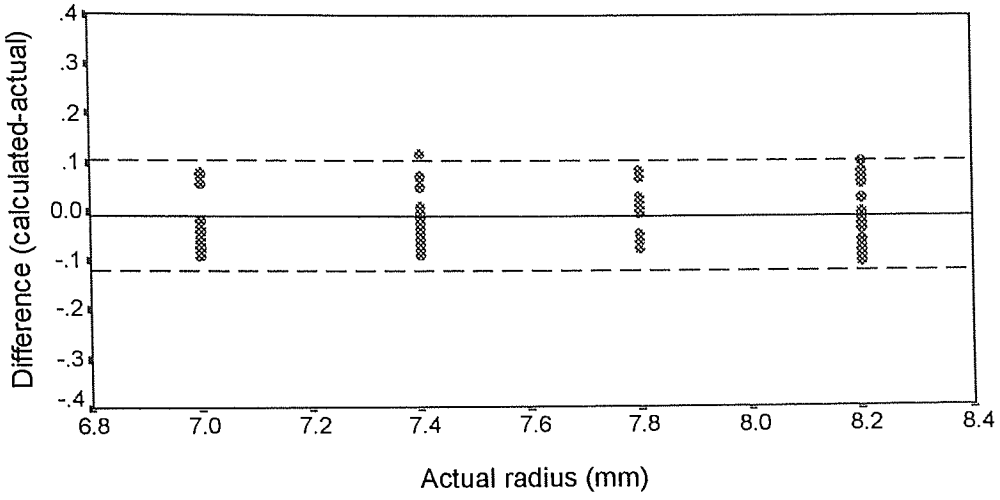

7.7 Discussion

The principal purpose of the current study was to analyse the accuracy and repeatability of the videokeratoscope. Previous investigators have analysed the accuracy of corneal topography devices by evaluating measurements performed on spherical surfaces (Hannush et al, 1989; Koch et al, 1989; McCarey et al, 1992; Legeais et al, 1993; Andersen et al, 1993b). Analysis of instrument accuracy using spherical surfaces is not appropriate as some methods of topography calculations perform better for spherical surfaces than for non-spherical surfaces (Mandell et al, 1969). In addition, the normal cornea is not spherical, its shape conforms more accurately to the family of ellipses (Howland et al, 1992). Wang et al (1989) evaluated the accuracy of their algorithms using a single convex aspheric surface (r_o=7.73mm, e=0.5) and compared the calculated sagittal radius to the actual radius of the surface. Wang et al (1989) found a maximum error with their algorithm of less than 2%. Using the modified multiple arc technique devised by Klyce (1984), Wang et al (1989) used the same surface to compute the saggital radius and a maximum error of 8% was found. Further, the multiple arc technique was found to be biased towards spherical surfaces.

The algorithms used in the present study were originally proposed by Andersen et al (1993b). No evaluation of the performance of the algorithms for convex aspheric

surfaces has been published to date. The present study showed a maximum error of only 1.15% (at the vertex normal) which reduced to only 0.876% at 4.52mm from the vertex normal along the 135 degree semi-meridian of a convex aspheric surface using manual digitisation (r_o=7.4mm, p=0.8). Using automated digitisation a maximum error of only 0.41% was found at the vertex normal. A minimum error of 0.06% was found at 4.19mm along the same semi-meridian. Furthermore, the current study evaluated the accuracy of the algorithms for 12 aspheric surfaces and showed a high level of association between calculated and actual p-value (r=0.9695 - manual digitisation). With respect to individual asphericities, lower asphericites showed higher variation for both manual and semi-automated digitisation procedures. However, the standard deviations were small and the mean asphericity was accurately determined (table 7.02 and table 7.12). A decrease in the accuracy for progressively flatter surfaces could be accounted for when considering the central resolution of the central L.E.D.s (see chapter 6). The central resolution of the videokeratoscope was not sufficient to provide information regarding the central cornea. Thus, for a progressively flattening surface, the central L.E.D.s would be reflected off a peripheral point whose radius has already begun to flatten (see figure 7.12). Therefore, an error occurred due to the incorrect assumption that the central L.E.D.s were reflected off a point on the surface that was close to the vertex normal. This error was confirmed by the greater error observed when individual p-values were compared (table 7.02 and table 7.12). Principally, the error was due to a design fault which could easily be remedied by reducing the spatial separation of the central L.E.D.s such that reflection would occur off a more central point.

The analysis of the differences between actual and calculated p-value for all the meridians of the twelve surfaces using manual digitisation showed that the bias was close to zero, thus indicating that on average there was little difference between calculated and actual p-value. The small standard deviation and narrow confidence intervals showed that p-value measurements were accurate using the present algorithms - this was also confirmed by tables 7.04 and 7.11 (for manual and semi

automated digitisation, respectively) which showed that more than 90% of measurements of p-values were calculated to within 0.1.

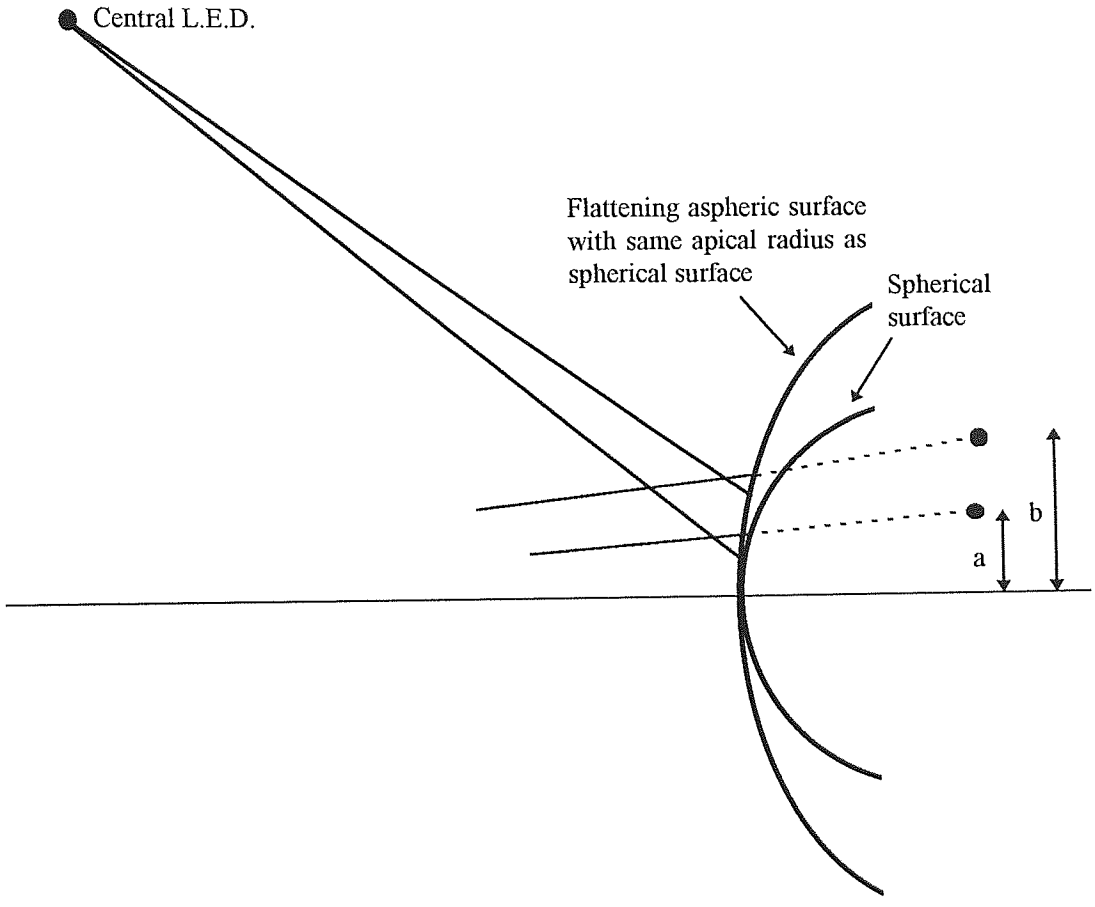

Figure 7.12: shows the differences in reflected central L.E.D. heights obtained by reflection from two surfaces with different asphericities. As central resolution is not sufficient, the central L.E.D.s are reflected from a peripheral point on the aspheric surface. The L.E.D. distance is not the same as the spherical surface and an error is introduced.

However, before drawing any absolute conclusions as to whether the videokeratoscope was capable of accurately calculating p-values, the effect of the error in p-value on peripheral sagittal radius must be established. To evaluate this, a small program was written in QUICKBASIC to print out the sagittal radius from a specified conic section at a point on a semi-meridian 1, 2, 3 and 4mm from the vertex normal. The error introduced in p-value calculation may be described by 1.96 x the standard deviation of the differences between actual and calculated p-values (i.e. 0.11). Using a theoretical p-value of 0.8 and apical radius of 7.8mm, the error in p-value in 95% of cases (using the data derived from the manual digitisation program) would be 0.91. Therefore,

computing these p-values with an apical radius of 7.8mm would result in the following errors in sagittal radius.

Table 7.16: Comparison between calculated and actual peripheral sagittal radius for an aspheric surface of p-value=0.8, r=7.8mm.

Distance from centre (mm)	**Actual sagittal radius (p-value=0.8, r=7.8mm)**	**Calculated sagittal radius (p-value=0.91 (1.96xS.D) r=7.80mm)**
1mm	7.81	7.81
2mm	7.85	7.82
3mm	7.91	7.85
4mm	8.00	7.89

Table 7.16 shows that the error in sagittal radius at 4mm from the centre would be 0.11mm. The error introduced corresponds to approximately 0.5D. For clinical purposes such an error would be acceptable. Thus the errors introduced by the videokeratoscope in the calculation of p-value were small and therefore acceptable for use in clinical practice. The automated digitisation further improved the accuracy of p-value measurement..

In chapter 5, the accuracy and repeatability of the EyeSys CAS was evaluated. The 95% confidence limits when determining the accuracy of peripheral radius of the all twelve aspheric surfaces in 4 semi-meridians were +0.105mm to -0.061. Thus, the maximum error in 95% of cases was also found to be approximately 0.5D (after transposing the upper confidence limit into a dioptric value).

Mean central radius of curvature was determined accurately (table 7.05), furthermore, the correlation coefficient between calculated and actual central radius was high (r=0.989) for manual digitisation. Little change in variance was observed in determining the 7.00, 7.40 and the 7.80mm radii using semi-automated digitisation, however, a greater variation is observed for those surfaces with 8.20mm central radii. This error was again due to insufficient central resolution as larger surfaces (such as the 8.20mm radii surfaces) caused the central L.E.D.s to be reflected from a peripheral point on the surface where the radius had already begun to change. Manual

digitisation showed a tendency for larger errors in determining the central radius for the 7.00mm radii (table 7.05), the smaller image size of these surfaces required the user to be more precise in locating the L.E.D.s, this was thought to be the most probable cause of the reduced accuracy (note that the corresponding standard deviation for semi-automated digitisation was not as high for the 7.00mm surface, table 7.13).

For the analysis of central radius of curvature of all the surface pooled together, the 95% confidence limits were wide - ranging from +0.156mm to -0.102mm (table 7.06) with manual digitisation. The use of semi-automated digitisation improved the accuracy however, the confidence limits (ranging from +0.103mm to -0.121mm) were still too wide for routine use in contact lens fitting (Stone, 1962). The cumulative frequency distribution showed that 83.3% and 95.9% of results obtained were within 0.50D for manual and semi-automated digitisation methods, respectively. The maximum error introduced in 95% of cases was ± 0.65D (for manual digitisation) and ± 0.56D (for semi-automated digitisation). In comparison, evaluation of the EyeSys CAS in calculating the central radius of curvature (chapter 5) for the same twelve surfaces in four meridians showed narrower confidence limits (+0.121mm to -0.037mm), however, the maximum error in 95% of cases was the same as the present videokeratoscope.

In order to compare the results of the present study with other studies, similar samples must be compared. The sample used in the present study clearly differed to that used by other investigators (Hannush et al, 1989; Koch et al, 1989; McCarey et al, 1992; Legeais et al, 1993; Andersen et al, 1993b) as measurements were performed using aspheric surfaces. If the results of central radius measurements of the aspheric surfaces were excluded so that only the central radii of spheres were analysed the results obtained compared even more favourably with those obtained from other studies (see table 7.17). The videokeratoscope in the present study was found to exhibit greater accuracy than the CorneaScope for central radius of curvature measurements in spherical surfaces. However, the Corneal Modelling System (Computed Anatomy, Inc.) and the photokeratoscope devised by Andersen et al (1993b) showed greater

accuracy. The values for the videokeratoscope in table 7.17 represent the means and standard deviations of the deviations between calculated and actual radius over an all 8 semi-meridians for spherical surfaces. In the study performed by Hannush et al (1989), measurements were taken at selected points on the surface in order to compare their results with the keratometer. Also, their measurements comprised of only assessing two points 90 degrees apart and then calculating the mean. The analysis for the present videokeratoscope was more comprehensive as it not only assessed the disparity along the entire semi-meridian, but also evaluated the disparity for each meridian (eight semi-meridians as opposed to only two in the Hannush et al (1989) study). Rowsey et al (1989) assessed the mean and standard deviations of the differences along the entire profile of an 8.00mm sphere using the CorneaScope. A mean and standard deviation of +0.004 and ±0.021mm, was found, respectively.

The principal reason for the greater accuracy of the Andersen et al (1993b) photokeratoscope was attributed to the high level of central resolution provided at vertex normal (1.92mm for the present videokeratoscope versus 0.2mm for the Andersen et al (1993b) photokeratoscope). However, as in the study by Hannush et al (1989), Andersen et al (1993b) also calculated the mean and standard deviation of the differences between calculated and actual radius at specific locations using spherical test surfaces. In the same paper, they assessed the deviation scores (the difference between calculated and actual radius) along the entire profile of an 8.00mm sphere (the reference sphere used for their photokeratoscope). They found a mean deviation of +0.003mm and a standard deviation of ±0.01mm. Further evaluation of the deviations of calculated and actual radius for spherical surfaces would have enabled better comparison with the results obtained with the present videokeratoscope.

Table 7.17: shows the averaged means and standard deviations of the difference between calculated and actual central radius of curvature for spheres. The values of mean and standard deviation for the Hannush et al (1989) study have been converted into millimeters so that they may be compared with the other results (conversion assumes 0.25D change is equivalent to 0.05mm change in radius of curvature).

	Instrument	**Sphere**	**Bias**	**Standard deviation**
Present study	(manual digitisation)	7.00 7.40 7.80 8.20	+0.019	±0.054
Present study	(semi-automated digitisation)	7.00 7.40 7.80 8.20	-0.014	±0.047
Hannush et al (1989)	CorneaScope	7.85 7.94 6.73 8.73	-0.056	±0.078
Hannush et al (1989)	Corneal Modelling System	7.85 7.94 6.73 8.73	+0.020	±0.014
Andersen et al (1993b)	Own design	7.00 8.00	+0.009	±0.010

In order to evaluate any relationship between the accuracy of measurements and the point on the surface from where measurements were performed, the results of the peripheral sagittal radius for all 4 spherical surfaces at each L.E.D. reflection point along all 8 semi-meridians were calculated. L.E.D. image distances were calculated using the semi-automated digitisation program. Figure 7.13 and equation 7.31 below, show how the sagittal radius was determined.

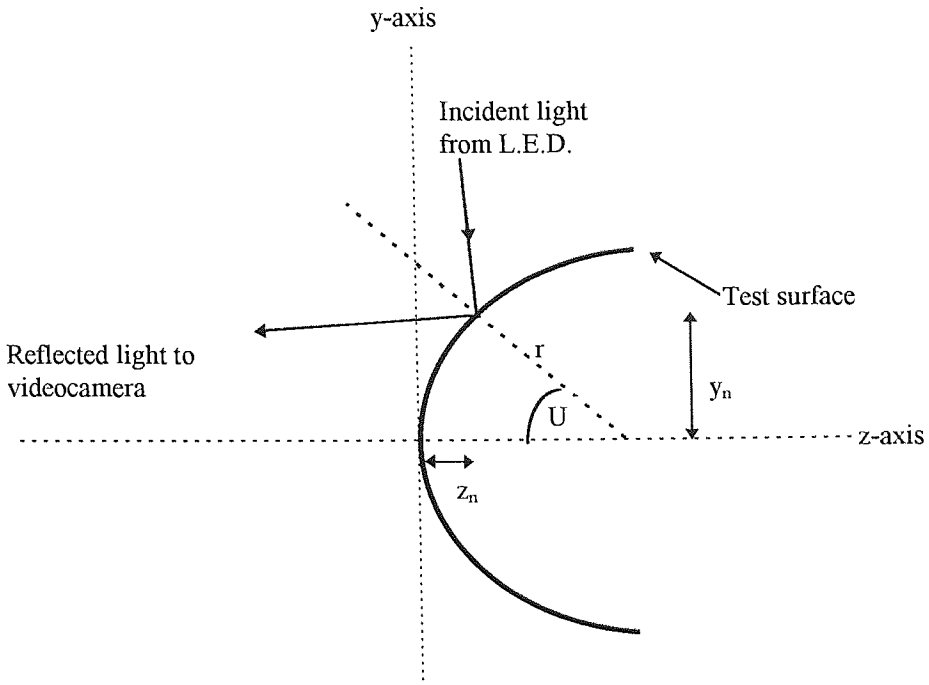

Figure 7.13: shows how the sagittal radius, r, was determined from the angular subtense of the normal at the z-axis, U, and the Cartesian coordinates, y_n and z_n.

From basic geometry, the sagittal radius, r, of a peripheral point on the surface may be calculated as follows:

$$r = \frac{y_n}{Sin(U)} \qquad \textit{Equation 7.31}$$

These results were then compared to the actual sagittal radius which, for a sphere, would be constant. The means and standard deviations of the absolute differences of calculated and actual sagittal radius were computed for all 4 spherical surfaces relative to each L.E.D. point of reflection. Table 7.18 shows the results obtained. Greatest variation was observed at the central L.E.D.s and the accuracy was seen to improve at the periphery. The primary cause of the larger error for the central L.E.D.s was due to the high level of accuracy required when determining the position of the central L.E.D.s. compared to the most peripheral L.E.D.s. Nevertheless, the accuracy of central and peripheral radius measurements across the profile showed an acceptable level of accuracy for spherical surfaces.

Table 7.18: shows the mean and standard deviation of the absolute differences between calculated and actual radius for all four spherical surfaces (with radii of 7.00mm, 7.40mm. 7.80mm, 8.20mm) in terms of each L.E.D. point of reflection.

L.E.D number	Mean absolute difference	Standard deviation
1 (innermost)	+0.025	±0.014
2	+0.024	±0.013
3	+0.022	±0.013
4	+0.021	±0.012
5	+0.019	±0.011
6	+0.017	±0.011
7	+0.014	±0.011
8 (most peripheral)	+0.011	±0.012

For videokeratoscopy, a fundamental requirement for the analysis of corneal topography is the ability to accurately locate the reflected L.E.D. or ring images. Analysis of the literature shows that numerous methods have been employed to improve the accuracy of measurements of the reflected L.E.D.. For example, the early studies by Ludlam et al (1966) used a microscope to measure reflected mires. With the development of computer systems manual measurements have been performed using computers (Klyce, 1984). More recently, sophisticated image processing applications have been used to analyse detailed images (Gormley et al, 1988). For the present system, the use of a versatile image processing application (*NIH Image 1.52*) enabled accurate detection of the reflected L.E.D.s. The macro program for semi-automated L.E.D. detection was described in Chapter 6. Basically, the program effectively removed the irregularities in background illumination from the iris to pupil (of complex 8-bit images) and then calculated the geometric centre of each L.E.D.. Accuracy of both radius and p-value measurements was improved using semi-automated digitisation. The improved accuracy was primarily attributed to the sub-pixel accuracy in locating the geometric centre and also because 8-bit images were used (which contained more detail than the 1-bit images used in the manual digitisation program). In addition to these factors, the influence of subjective variability was eliminated.

For a single image the videokeratoscope was found to be repeatable for both central radius of curvature and p-value (standard deviation of ±0.0322mm and ±0.0453,

respectively). Therefore, variation due to manual digitisation (as it was the only variable introduced is in the digitisation procedure) was the factor responsible for the variability. With respect to multiple images, the mean p-value and central radius were found to be calculated with greater accuracy (see tables 7.08 and 7.09). However, the repeatability was found to be slightly reduced (standard deviation ± 0.0486 for p-value and ± 0.067 for central radius of curvature), this was thought to be due to the increased variance introduced by taking multiple images. The use of semi-automated digitisation improved repeatability and any variability introduced was attributed to the instrument characteristics (such as alignment errors) which were shown to introduce only small errors (see chapter 6).

Koch et al (1989) performed an experiment where three spherical surfaces were measured four times along the horizontal meridian for the EyeSys topography system. Analysis of the variance showed that poorest repeatability was found at the central rings. However, the EyeSys topography system was in experimental development.

7.7 Summary

The classical method of calculating corneal topography has been to compare the radial distances of reflected mires from an unknown surface to the radial distances of reflected mires from spherical surfaces (Knoll, 1961; Townsley, 1967). This method had the greatest potential for inducing error. The main reason for this was because it was assumed that the instantaneous centre of curvature of each peripheral point on the cornea would lie on the optic axis of the instrument, although would this apply to a spherical surface, it would not apply to an aspheric cornea where the instantaneous radius of curvatures lie on an evolute (Bennett, 1968).

Later, Doss et al (1981) developed the multiple arc technique where constant curvature was assumed between each reflected ring or L.E.D.. Furthermore, Doss et al (1981) assumed a constant central radius of curvature of 7.80mm. Klyce (1984) refined the technique proposed by Doss et al (1981) by developing an algorithm to

calculate central radius of curvature. However, even with this modification, the technique assumed that the height of the reflected image corresponded to the point of reflection at the corneal surface. Wang et al (1989) showed that even with the modification by Klyce (1984), measurements on a single aspheric surface were biased towards sphericity. Subsequently, Wang et al (1989) avoided the error introduced by latter assumption by the use of the angular subtense of the reflected image in their algorithms. Other methods of calculating corneal topographic coordinates have also been developed such as comparing the radial profile of the cornea with geometric shapes (Edmund et al, 1985; Edmund, 1986).

The primary aim of the present study was to evaluate the accuracy of a new algorithm initially devised by Andersen et al (1993b) using convex aspheric surfaces. In order to achieve this, a videokeratoscope was constructed whose exact parameters were known. Unlike previous algorithms (Knoll, 1961; Townsley, 1967; Doss et al, 1981; Klyce, 1984; Edmund et al, 1985; Edmund, 1986), the algorithms modified in the present study make no assumptions regarding the pre-existing shape of the surface under test. The 7.80mm reference surface was used only to locate the angular subtense of the target mire with respect to the focal plane. The only initial assumptions involved in the analysis were that for the reference sphere, the image plane was situated at halve the centre of curvature of the reference sphere (it was proven that in reality the actual distance was very close to the assumed distance). Another initial assumption was that the value of angle U for an known point on the surface was equal to its preceding value. By the use of a iterative procedure the error induced by this assumption was reduced as the value of U was recalculated until successive values of U differed by less than 0.01%.

The results show greater accuracy than achieved by Wang et al (1989) for a similar aspheric surface (a maximum error of less than 2% and 0.41% for the Wang et al (1989) and present study, respectively). In fact, for all twelve aspheric surfaces only a small error in the determination of asphericity was found (S.D. of ± 0.0581 and ± 0.043 for manual and semi-automated digitisation, respectively). Therefore, the new

algorithms used in the present study had little or no effect in biasing the shape of aspheric surfaces. With respect to central corneal radius measurement, the accuracy (maximum error of ± 0.65D for manual digitisation and ± 0.56D semi-automated digitisation) was not sufficient for the instrument to be used for applications such as contact lens fitting (Stone, 1962). The insufficient level of central resolution was considered to be the cause for this error. However, it was not the purpose of the study to devise a state of the art corneal topography system but rather to devise a system to evaluate the new algorithms. Nevertheless, increasing central resolution would have increased the accuracy.

Repeatability was found to be acceptable for p-value but not for radius of curvature measurements. The principal reason was due to the manual digitisation procedure. The use of semi-automated digitisation would eliminate the variation induced by the manual digitisation procedure. For repeat readings the variation increases only slightly, confirming that errors due misalignment were small (as stated in chapter 6).

With the small modification of increasing central resolution, the present videokeratoscope would be a very accurate and useful tool to assess corneal topography. The algorithms were capable of successfully calculating the asphericity of unknown surfaces.

Chapter Eight

Conclusions

8.1 Introduction

The principal aims of this study have been to investigate the accuracy and repeatability of some of the commercially available videokeratoscopes and also to assess the accuracy of new algorithms in measuring the shape of aspheric surfaces. In order to achieve the latter, a videokeratoscope had to be constructed. The specific aims relating to each individual study have been described at the beginning of each chapter, the conclusions drawn from each of these aims is discussed below with respect to the preceding statistical analysis.

8.2 Investigations of the SUN SK-2000 and the EyeSys CAS

Although two different subject samples were used, the results were much the same for investigations of the SUN SK-2000 and the EyeSys CAS. For example, in the comparison of videokeratoscopy with keratometry, both the SUN SK-2000 and the EyeSys CAS showed a lack of agreement with the keratometer. In contrast to other studies (Tsilimbaris, 1991; Antalis et al, 1993), where an agreement between videokeratoscopy and keratometry was found, the results from the investigations in this thesis suggest that measurements performed using keratometers and videokeratoscopes should not be used interchangeably.

Using the SUN SK-2000 device, a decrease in the repeatability in the superior regions of the corneal surface was observed. It was suggested that this decrease may have been due to the influence of the ocular adnexa. However, as the SUN SK-2000 extrapolated the corneal profile, it was possible that the error in repeatability was also due to the extrapolating procedure itself. The EyeSys CAS on the other hand, produced a raw data table of points that were actually analysed on the cornea. The

results confirmed the hypothesis that measurements in the superior cornea were less repeatable than those in other meridians as a result of the interference of the ocular adnexa. Furthermore, the repeatability of measurements also decreased in the periphery of the cornea such that for the superior meridians results should be considered carefully after 1mm from the vertex normal; 2mm for the inferior meridian; 2mm for the nasal meridian, and 3mm for the temporal meridian.

The EyeSys CAS was also used to evaluate the accuracy in determining twelve convex aspheric surfaces. As the cornea cannot be measured mechanically, convex aspheric surfaces were used to assess the accuracy of measurements derived by the EyeSys videokeratoscope. In this way, the accuracy of the algorithms employed to reconstruct the surface profile were assessed. With respect to central radius of curvature measurements, the EyeSys algorithms exhibited greater error in measuring flatter surfaces. The most probable cause was the central resolution of the innermost Placido ring. For flatter surfaces, the central ring was therefore reflected off a point away from the vertex normal. The accuracy of peripheral measurements also showed a characteristic trend with respect to the shape of the surface being measured. Again, the measurement of flatter surfaces resulted in greater error in the periphery of the profile. The algorithms within the EyeSys CAS were accurate up to 4mm from the vertex normal for convex aspheric surfaces (Figure 5.16). Although a small bias was observed for spherical surfaces, the accuracy of the algorithms was sufficient for measurement of the peripheral corneal surface. As expected, no variation in the repeatability of measurements in terms of the meridian was detected for the aspheric surfaces.

8.3 Evaluation of a New Videokeratoscope

The accuracy of a videokeratoscope is dependent on two factors: the instrument design and the algorithms used to derive the surface coordinates. In order to assess the latter, a videokeratoscope was constructed. Basically, the only error in the construction was in the spatial separation of the central L.E.D.s. As their separation was too large, the

central resolution of the videokeratoscope was limited, however, the insertion of another ring of L.E.D.s would resolve this problem. The instrument characteristics showed that typically for 1mm defocus, an error of only 0.039mm or 0.195D would be found. Only a small error was induced due to the relatively large working distance used and the shallow depth of focus.

Having described the characteristics of the new videokeratoscope in chapter 6, chapter 7 evaluated the accuracy and repeatability of the videokeratoscope for twelve aspheric surfaces. Unlike previously proposed algorithms (Knoll, 1961; Townsley, 1967; Doss et al, 1981; Klyce, 1984; Edmund et al, 1985; Edmund, 1986), the algorithms modified in the present study made no assumptions regarding the pre-existing shape of the surface under test. As a result, the algorithms accurately calculated the asphericity of all twelve surfaces. This method of deriving the topographic coordinates of aspheric surfaces was shown to be highly effective, more so than the most recently proposed algorithms (Wang et al, 1989). The repeatability of the videokeratoscope was shown to be acceptable, the main reason for this was due to the accuracy of the instrument focusing characteristics and the digitisation programs.

8.4 Future Study

The present thesis did not examine every factor involved in the reconstruction of the corneal profile. Moreover, it showed that the accuracy of videokeratoscopy is limited by the variance induced be the cornea itself. Furthermore, the accuracy of a new modified algorithm proposed in this thesis shows that the error in peripheral measurements is less than the most recently proposed algorithm (Wang et al, 1989). Future studies should concentrate on the development of newer methods of quantitative analysis and their ability to clearly distinguish between pathological and non-pathological corneas. In addition, there are still some examples where computer hardware and software may be improved. For example, with pathological corneas, the reflected target image may be difficult to digitise, the development of software that

would accurately detect the reflected image would greatly benefit the evaluation of keratoconic corneas and those corneas suffering from pathologies.

References

Andersen, J. Koch-Jensen, P., and ϕsterby, O. (1993a). Corneal topography: photokeratoscopy including the central region. *Acta Ophthal.*, **71**, 145-150.

Andersen, J. Koch-Jensen, P., and ϕsterby, O. (1993b). Corneal topography: image processing and numerical analysis of keratoscopy. *Acta Ophthal.*, **71**, 151-159.

Antalis, J. J., Lembach, R. G. and Carney, L. G. (1993). A comparison of the TMS-1 and the Corneal Analysis System for the evaluation of abnormal corneas. *The CLAO Journal*, 19, 58-63.

Applegate, R. A. (1993). Optical and clinical issues in the measurement of corneal topography. *Ophthal. Visual Opt. Tech. Dig.* **3**, 19-23, x.

Arffa, R. C., Warnicki, J. W. and Rehkopf, P. G. (1989). Corneal topography using rasterstereography. *Refract. Corneal Surg.* **5**, 414-417.

Baker, T. Y. Ray tracing through non-spherical surfaces. (1943). *Proc. Phys. Soc.* **55**, 361-364.

Belin, M. W., Litoff, D., Strods, S. J., Winn, S. S. and Smith, R. S. (1992). The PAR technology corneal topography system. *Refract. Corneal Surg.* **8**, 88-96.

Belin, M. W. and Zloty, P. (1993). Accuracy of the PAR corneal topography system with spatial alignment. *The CLAO Journal,* **19**, 64-68.

Bennett, A. G. (1968). Part I Aspherical contact lens surfaces. *The Opthalmic Optician,* 5 October, 1037-1040.

Bennett, A. G. and Rabbetts, R. B. (1991). What radius does the conventional keratometer measure? *Ophthal. Physiol. Optics.* **11**, 239-247.

Bennett, A. G. and Rabbetts, R. B. (1989). *Clinical Visual Optics.* 2nd. edition, Butterworth, London, 106-106.

Bibby, M. M . (1976). Computer assisted photokeratoscopy and contact lens design. *Optician*, **171**(4423), 37, 39, 41, 43-44; **171**(4424), 11, 14-15, 17.

Bland, J. M. and Altman, D. G. (1986). Statistical methods for assessing agreement between two methods of clinical measurement. *The Lancet*, **1** (8746), 307-310.

Bland, M. (1993). An introduction to medical statistics. Oxford medical publications. p172.

Bogan, S. J., Waring, III G. O., Ibrahim, O., Drews, C. and Curtis, L. (1990). Classification of normal corneal topography based on computer-assisted videokeratography. *Arch. Ophthalmol.* **108**, 945-949.

Bonnet, R. and Cochet, D. (1962). New method of topographical ophthalmometry-its theoretical and clinical applications. *Am. J. Optom.* **39**, 227.

Clark, B. A. J. (1973a). Variations in corneal topography. *Aust. J. Optom.* **56**, 399-413.

Clark, B. A. J. (1973b). Keratometry: a review. *Aust. J. Optom.* **56**, 94-100.

Clark, B. A. J. (1973c). Systems for describing corneal topography. *Aust. J. Optom.*, **56**, 48, 48-55.

Clark, B. (1974). Validation testing of the autocollimating photokeratoscope. *Aust. J Optom.*, **57**, 22.

Cogan, D. G., and Kinsey, V. E. (1942). The Cornea. V: Physiological aspects. *Archs Ophthal.*, **28**, 661-669.

Cohen, K. L., Tripoli, N. K., Pellom, A. C., Kupper, L. L. and Fryczkowski, A. W. (1984). A new photogrammetric method for quantifying corneal topography. *Invest. Ophthalmol. & Vis. Sci.*, **25**, 323-330.

Dingledein, S. A., Klyce, S. D. and Wilson, S, E. (1989). Quantitative descriptors of corneal shape derived from computer-assisted analysis of photokeratographs. *Refract. Corneal Surg.* **5**, 372-378

Doss, J. D., Hutson, R. L., Rowsley, J. J. and Brown, D. R. (1981). Method for calculation of corneal profile and power distribution. *Arch. Ophthalmol.* **99**, 1261-1265

Dunne, M. C. M., Royston, J. M., and Barnes, D. A. (1992). Normal variations of the posterior corneal surface. *Acta Ophthalmol.* **70**, 255-261.

Edmund, C. and Sjϕntoft, E. (1985). The central-peripheral radius of the normal corneal curvature. A photokeratoscopic study. *Acta Ophtha.*, **63**, 670-677.

Edmund, C. (1986). The significance of using different methods for analysing photokeratoscopic data. *Acta Ophthal.*, **64**, 97-100.

Edmund, C. (1987). Location of the corneal apex and its influence in the stability of the central corneal curvature. A photokeratoscopy study. *Am J Optom & Physiol Opt.*, **64**, 846-852.

El Hage, S. G. (1969). Recherche de l'equation mathematique de la cornee a partir d'une methode photokeratoscopique. Opticien Lunetier, 192, 16.

El Hage, S. G. (1971). Suggested new methods for photokeratoscopy a comparison for their validities. Part I. *Am. J. Optom. Physiol. Opt.*, **48**, 897-912.

El Hage, S. G. (1972). Differential equation for the use of the diffused ring keratoscope. *Am. J. Optom. Physiol. Opt.*, **49**, 422-436.

Enoch, J. M. (1958). Summated response of the retina to light entering different parts of the pupil. *J Optical Soc Am.*, **48**, 392-406.

Fincham, E. F. (1953). New photokeratoscope utilizing a hemispherical object surface. *Medical and Biological Illustration*, **3**, 87.

Gipson, I. K., Spurr-Michaud, S. J., and Tisdale, A. S. (1987). Anchoring fibrils form a complex network in human and rabbit corneas. *Invest. Ophthal. Vis. Sci.*, **28**, 212-220.

Gormley, D. J., Gersten, M., Koplin, R. S. and Lubkin, V. (1988). Corneal Modelling. *Cornea* 7, 30-35.

Goss D., and Eskridge. J. B. (1991). Keratometry. In Clinical Procedures in Optometry, by Eskridge, J. B., Amos, J. F. and Bartlett, J. D.. Lippincott, Philadelphia, USA, pp. 135-154.

Guillon, M., Lyndon, D. P. and Wilson, C. (1986). Corneal topography: a clinical model. *Ophthal. Physiol. Opt.* **6**, 47-56.

Gullstrand, A. (1896). Photographisch-ophthalometrische und klinische Untersuchungen uber die Hornautretraktion. Part I. Kung. Sv. Vet. Akad. Handl., 28, (Photographic-ophthalmometric and clinical investigations of corneal refraction), Part I translated by S. M. Ludlum, (1966). *Am. J. Optom.*, **43**, 143.

Hannush, S. B., Crawford, S. L., Waring, G. O., Gemmill, M. C., Lynn, M. J. and Nizam, A. (1989). Accuracy and precision of keratometry, photokeratoscopy, and corneal modeling on calibrated steel balls. *Arch. Ophthalmol.* **107**, 1235-1239.

Hannush, N. B., Crawford, S. L., Waring, G. O. Gemmill, M. C., Lynn, M. J. and Nizam, A. (1990). Reproducibility of normal corneal power measurements with a keratometer, photokeratoscope and video imaging system. *Arch. Ophthalmol.* **108**, 539-544.

Hodd, N. F.B., and Ruston, D. M. (1993). The EyeSys corneal analysis system its value in contact lens practice. *Optometry Today,* September 20th.

Howland, H. C., Glasser, A. and Applegate, R. (1992). Polynomial approximations of corneal surfaces and corneal curvature topography. *Ophthal. Visual Opt. Tech. Dig.* **3**, 34-36.

Hubbe, R. E. (1994). The effect of poor fixation on computer-assisted topographic corneal analysis. *Ophthalmol.*, **101**, 1745-1748.

Knoll, H. A., Stimson, R. and Weeks, C. L. (1957). New photokeratoscope utilizing a hemispherical object surface. *J. Opt. Soc. Am.*, **47**, 221.

Knoll, H. A. (1961). Corneal contours in the general population as revealed by the photokeratoscope. *Am. J. Optom. and Arch. Am. Acad. Optom.*., **38** (7), 389-397.

Klein, S. A. (1993). Improvements for video-keratography. *Ophthal. Visual Opt. Tech. Dig.*

Klyce, S. D. (1984). Computer-assisted corneal topography. *Invest. Ophthalmol. Visual Sci.* **25**,1426-1435.

Koch, D. D., Foulks, G. N., Moran, C. T., and Wakil, J. S. (1989). The corneal EyeSys system: accuracy analysis and reproducibility of first-generation prototype. *Refract. Corneal Surg.* **5**, 424-429.

Koch, D. D., Wakil, J. S., Samuelson, S. W., and Haft, E. A. (1992). Comparison of the accuracy and reproducibility of the keratometer and the EyeSys Corneal Analysis System Model I. *J. Cataract Refract. Surg.* **18**, 342-347.

Koch, D. D. and Haft, E. A. (1993). Introduction to Corneal Topography. In Saunders D. R. and Koch, D. D.: *An Atlas of Corneal Topography*. Thorofare, N. J, Slack, **1**, pp 1-30.

Koepfler, J. W. (1983). Moire topography in medicine. *J. Biol. Photogr.* **51**.

Legeais, J. M., Ren, Q., Simon, G., and Parel, J. M. (1993). Computer-assisted corneal topography: accuracy and reproducibility of the topographic modelling system. *Refract. & Corneal Surg.*, **9**, September/ October.

Littman, H. (1951). *V Graefe's Arch Ophthal.*, **151**, 249.

Ludlum, W. M., Wittenburg, S., Rosenthale, J. and Harris, G. (1967). Photographic analysis of the ocular dioptric components. *Am. J. Optom. Arch. Am. Acad. Optom.*, **44**, 276-296.

Maguire, L. J., Singer, D. E., and Klyce, S. D. (1987a). Graphic presentations of computer-analyzed keratoscope photographs. *Arch. Ophthalmol.* **105**, 223-230.

Maguire, L. J., Klyce, S. D., Singer, D. E., McDonald, M. B. and Kaufman, H. E. (1987b). Corneal topography in myopic patients undergoing epikeratophakia. *Am. J. Ophthalmol.* **103**, 404-416.

Maguire, L. J. and Bourne, W. M. (1989). Corneal topography of early keratoconus. *Am. J. Ophthalmol.* **108**, 107-112.

Maguire, L. J. and Lowry, J. C. (1991). Identifying progression of subclinical keratoconus by serial topography analysis. *Am. J. Ophthalmol.* **112**, 41-45.

Mandell, R. B. (1965a). Corneal topography. Chapter 3 in *Contact Lens Practice, Basic and Advanced.* Thomas, Springfield. IL. USA. p.35-47.

Mandell, R. B. and St. Helen, R. (1965b). Position and curvature of the corneal apex. *Am J Optom.*, **46**, 25-29.

Mandell, R. B. (1967). Corneal contour of the human infant. Arch. Ophthal., 77, 345.

Mandell, R. B., and St. Helen, R. (1968). Stability of the corneal contour. *Am. J. Optom. and Arch. Am. Acad. Optom.*, **45**, 12, 797-806.

Mandell, R. B. and York, M. (1969). A new calibration system for photokeratoscopy. *Am. J. Optom. and Arch. Am. Acad. Optom.* 410-417.

Mandell, R. B. and St. Helen, R. (1971). Mathematical model of the corneal contour. *Br. J. Physiol. Opt.* **26**, 183-187.

Mandell, R. B. (1992). The enigma of the corneal contour. *The CLAO Journal*, **18**, 267-273.

Mandell, R. B. and Horner, D. . (1993). Alignment of videokeratoscopes. In Saunders D. R. and Koch, D. D.: *An Atlas of Corneal Topography*. Thorofare, N. J, Slack.

Matilla T., and Douthwaite, W. A. (1994). Accuracy of the TMS videokeratoscope on calilbrated ellipsoidal convex surfaces. *Suppl. Optom. & Vis. Sci.*, vol. 71, No. 12s, 91.

Maurice, D. M. (1957). The structure and transparency of the cornea. *J. Physiol.*, **136**, 263-286.

Maurice, D. M. (1988). Mechanics of the cornea. In Cavanagh, H. D. The cornea: transactions of the world congress on the cornea III. New York, Raven Press, 187-194.

McCarey, B. E., Zurawski, C. A. and O'Shea, D. S. (1992). Practical aspects of a corneal topography system. *The CLAO Journal.* **18**, 248-254.

McCarey, B. E., Amos, C. F. and Taub, L. R. (1993). Surface topography of soft contact lenses for neutralizing astigmatism. *The CLAO Journal.* **19**, 114.

McDonnell, P. J., McClusky, D. J. and Garbus, J. J. (1989). Corneal topography and fluctuating visual acuity after radial keratotomy. *Ophthalmology*, **96**, 665-670.

Miller, D. and Carter, J. (1980). A proposed new division of corneal functions. In Cavanagh, H. D., editor: *The Cornea*, Transactions of the World Congress on the Cornea III, New York, Raven Press, 155-158.

Mosher, D. F. (1984). Physiology of fibronectin. *Annu. Rev. Med.*. **35**, 561-575.

Nieves, J. E. and Applegate, R. A. (1992). Alignment errors and working distance directly influence the accuracy of corneal topography measurements. *ARVO Abstract*, May 3-8.

Rodrigues, M. M., Rowden, G., Hackett, J., and Bakos, I. (1981). Langerhans' cells in the normal conjunctiva and peripheral cornea of selected species. *Invest. Ophthalmol. Vis. Sci.*, **21**, 759-765.

Rodrigues, M. M.,Waring, G. O., Hacket, J., Donohoo, P. Cornea. (1982). In Tasman, W., Jaeger, E. A., editors: Duane's biomedical foundations of ophthalmology. Vol. 1, Philadelphia, J. B. Lippincott Co., 1-13.

Rowsey, J. J. and Isaac, M. S. (1983). Corneoscopy in keratorefractive surgery. *Cornea*, **2**, 133-141.

Rowsey, J. J., Monlux, R., Balyeat, H. D. *et al.* (1989). Accuracy and reproducibility of KeraScanner analysis in PERK corneal topography. *Current Eye Research*, **8**, 661-674.

Ruben, M. (1975). Introduction to kerato-topography and keratometry. Chapter 6 in *Contact Lens Practice, Visual, Therapeutic and Prosthesis,* Baillie're-Tyndall, London, UK.

Ruskell, G. L. (1989). Anatomy and physiology of the cornea and related structures. In: Contact Lenses. Edited by Phillips, A. J., Stone, J. 3rd edition, Butterworths, 34-71.

Stone, J. (1962). The validity of some existing methods of measuring corneal contour compared with suggested new methods. *Br. J. Phy. Opt.* **19**, 205-230.

Sturrock, G. D., Sherrard, E. S., and Rice, N. S. C. (1978). Specular microscopy of the corneal endothelium. *Br. J. Ophthalmol.*, **62**, 809-814.

Tate, G. W., Safir, A., Mills, C. Z., Bowling, J. E., McDonald, J. L., and Craig. M. R. (1987). Accuracy and Reproducibility of Keratometry Readings. CLAO J, 13, 1, 50-58.

Thoft, R. A., and Friend, J. (Editors) (1979). The ocular surface. Boston, Little, Brown and Co. Inc.

Townsley, M. (1967). New equipment and methods for determining the contour of the human cornea. *Contacto*, **11**, 72.

Townsley, M. (1970). New knowledge of the corneal contour. *Contacto*, **14**, 38-44.

Townsley, M. (1974). The graphic presentation of corneal contours. *Contacto*, **18**, 24-32.

Tsilimbaris, M. K., Vlachonikolis, I. G., Siganos, D., Makridakas, G. and Pallikaris, I. G. (1991). Comparison of keratometric readings as obtained by Javal ophthalmometer and corneal analysis system (EyeSys). *Refract. Corneal Surg.* 7, 368-373.

Wang, J., Rice, D. A. and Klyce, S. D. (1989). A new reconstruction algorithm for improvement of corneal topographical corneal analysis. *Refract. & Corneal Surg.* **5**, 379-387.

Waring, G. O. (1982). Posterior collagenous layer of the cornea: ultrastructural classification of abnormal collagenous tissue posterior to Descemet's membrane in 30 cases. *Arch. Opthalmol.*, **100**, 122-134.

Waring, G. O. (1984). Corneal structure and pathophysiology. In Leiowiitz H. M., editor: Corneal disorders. Clinical diagnosis and management, Philadelphia, W. B. Saunders Co., 3-28.

Waring, G. O. (1989). Making sense of keratospeak. II. Proposed conventional terminology for corneal topography. *Refract & Corneal Surg.*, **5**, 362-367.

Waring, G. O. (1992). Refractive Keratotomy for myopia and astigmatism. Mosby-Year Book, 17-35.

Warnicki, J. W., Rehkopf, P. G., Curtin, D. Y., Burns, S. A., Arffa, R.C., and Stuart, J. C. (1988). Corneal topography using computer analyzed rasterstereographic images. *Applied Optics*, **Vol 27**, No. 6, 1135-1140.

Wilson, S. E. and Klyce, S D. (1991a). Quantitative descriptors of corneal topography. *Arch. Ophthalmol.* **109**, 349-353.

Wilson, S. E., Lin, D. T. C. and Klyce, S. D. (1991b). Corneal topography of keratoconus. *Cornea* **10**, 2-8.

Wittenburg, S. (1966). Appendix notes to translation of Gullstrand (1896). Am. J. Optom., 43, 198.

Zadnik, K., Mutti, D. O., and Adams, A. J. (1992). The repeatability of measurement of the ocular components. *Invest. Ophthalmol. Visual Sci.*, **33**, 7, 2325-2333.

Appendices

Appendix 1

Comparison of EyeSys CAS central resolution for convex surfaces

Appendix 2

Listing and documentation of the manual digitisation program

Appendix 3

Listing and documentation of the semi-automated digitisation program

Appendix 4

Listing of the topography calculation program

Appendix 5

Accuracy of measurements of p-value and central radius of curvature of a new videokeratoscope for twelve convex aspheric surfaces

Appendix 6

Repeatability of measurements of p-value and central radius of curvature of a new videokeratoscope for twelve convex aspheric surfaces

Appendix 7

List of publications and presentations

Appendix 1: Comparison of EyeSys CAS central resolution for convex surfaces

r_o=7.80mm, p=0.5

Flattest Axis (at 0 degrees)

NAS quad	Distance	Radius(mm)	Diopters	TMP quad	Distance	Radius(mm)	Diopters
# 01	0.48	7.93	42.56	# 01	0.47	7.93	42.56
# 02	0.75	7.93	42.56	# 02	0.75	7.93	42.56
# 03	0.99	7.94	42.51	# 03	0.99	7.94	42.51
# 04	1.29	7.95	42.45	# 04	1.29	7.95	42.45
# 05	1.54	7.97	42.35	# 05	1.53	7.96	42.40
# 06	1.84	7.99	42.24	# 06	1.84	7.98	42.29
# 07	2.09	8.03	42.03	# 07	2.07	8.01	42.13
# 08	2.43	8.07	41.82	# 08	2.39	8.04	41.98
# 09	2.70	8.11	41.62	# 09	2.65	8.09	41.72
# 10	3.03	8.16	41.36	# 10	2.98	8.14	41.46
# 11	3.32	8.22	41.06	# 11	3.27	8.20	41.16
# 12	3.68	8.27	40.81	# 12	3.62	8.26	40.86
# 13	4.00	8.33	40.52	# 13	3.92	8.32	40.56
# 14	4.37	8.38	40.27	# 14	4.29	8.37	40.32
# 15	4.72	8.42	40.08	# 15	4.63	8.41	40.13
# 16	5.13	8.45	39.94	# 16	4.98	8.44	39.99

Steepest Axis (at 90 degrees)

SUP quad	Distance	Radius(mm)	Diopters	INF quad	Distance	Radius(mm)	Diopters
# 01	0.47	7.88	42.83	# 01	0.47	7.87	42.88
# 02	0.73	7.89	42.78	# 02	0.73	7.88	42.83
# 03	0.97	7.91	42.67	# 03	0.97	7.89	42.78
# 04	1.26	7.93	42.56	# 04	1.25	7.92	42.61
# 05	1.51	7.95	42.45	# 05	1.49	7.95	42.45
# 06	1.81	7.98	42.29	# 06	1.80	7.98	42.29
# 07	2.06	8.02	42.08	# 07	2.04	8.02	42.08
# 08	2.37	8.05	41.93	# 08	2.35	8.06	41.87
# 09	2.63	8.10	41.67	# 09	2.61	8.10	41.67
# 10	2.96	8.15	41.41	# 10	2.92	8.15	41.41
# 11	3.26	8.21	41.11	# 11	3.20	8.20	41.16
# 12	3.60	8.27	40.81	# 12	3.51	8.26	40.86
# 13	3.93	8.33	40.52	# 13	3.82	8.32	40.56
# 14	4.30	8.39	40.23	# 14	4.17	8.37	40.32
# 15	4.63	8.43	40.04	# 15	4.50	8.40	40.18
# 16	5.03	8.46	39.89	# 16	4.73	8.43	40.04

r_o=7.80mm, p=1

Flattest Axis (at 0 degrees)

NAS quad	Distance	Radius(mm)	Diopters	TMP quad	Distance	Radius(mm)	Diopters
# 01	0.46	7.83	43.10	# 01	0.47	7.83	43.10
# 02	0.75	7.82	43.16	# 02	0.75	7.82	43.16
# 03	0.99	7.82	43.16	# 03	0.98	7.82	43.16
# 04	1.28	7.82	43.16	# 04	1.27	7.82	43.16
# 05	1.51	7.82	43.16	# 05	1.51	7.81	43.21
# 06	1.80	7.82	43.16	# 06	1.80	7.81	43.21
# 07	2.04	7.81	43.21	# 07	2.04	7.81	43.21
# 08	2.35	7.81	43.21	# 08	2.33	7.81	43.21
# 09	2.59	7.81	43.21	# 09	2.57	7.81	43.21
# 10	2.89	7.80	43.27	# 10	2.87	7.81	43.21
# 11	3.14	7.80	43.27	# 11	3.13	7.81	43.21
# 12	3.45	7.80	43.27	# 12	3.42	7.82	43.16
# 13	3.73	7.80	43.27	# 13	3.68	7.82	43.16
# 14	4.01	7.80	43.27	# 14	3.99	7.82	43.16
# 15	4.31	7.80	43.27	# 15	4.27	7.82	43.16
# 16	4.58	7.80	43.27	# 16	4.55	7.82	43.16

Steepest Axis (at 90 degrees)

SUP quad	Distance	Radius(mm)	Diopters	INF quad	Distance	Radius(mm)	Diopters
# 01	0.46	7.83	43.10	# 01	0.47	7.83	43.10
# 02	0.72	7.82	43.16	# 02	0.73	7.83	43.10
# 03	0.96	7.82	43.16	# 03	0.96	7.83	43.10
# 04	1.25	7.81	43.21	# 04	1.26	7.83	43.10
# 05	1.47	7.81	43.21	# 05	1.49	7.83	43.10
# 06	1.78	7.81	43.21	# 06	1.76	7.82	43.16
# 07	2.00	7.81	43.21	# 07	2.00	7.82	43.16
# 08	2.30	7.81	43.21	# 08	2.27	7.82	43.16
# 09	2.55	7.81	43.21	# 09	2.52	7.82	43.16
# 10	2.85	7.81	43.21	# 10	2.81	7.82	43.16
# 11	3.10	7.81	43.21	# 11	3.05	7.82	43.16
# 12	3.40	7.81	43.21	# 12	3.33	7.82	43.16
# 13	3.67	7.81	43.21	# 13	3.59	7.82	43.16
# 14	3.97	7.81	43.21	# 14	3.86	7.82	43.16
# 15	4.25	7.81	43.21	# 15	4.14	7.82	43.16
# 16	4.53	7.81	43.21	# 16	4.43	7.82	43.16

r_o=8.20mm, p=1

				Flattest Axis (at 0 degrees)			
NAS quad	Distance	Radius(mm)	Diopters	TMP quad	Distance	Radius(mm)	Diopters
# 01	0.49	8.18	41.26	# 01	0.50	8.18	41.26
# 02	0.78	8.18	41.26	# 02	0.77	8.19	41.21
# 03	1.03	8.18	41.26	# 03	1.03	8.20	41.16
# 04	1.34	8.18	41.26	# 04	1.34	8.20	41.16
# 05	1.58	8.18	41.26	# 05	1.58	8.20	41.16
# 06	1.89	8.18	41.26	# 06	1.89	8.20	41.16
# 07	2.15	8.18	41.26	# 07	2.13	8.20	41.16
# 08	2.46	8.18	41.26	# 08	2.45	8.20	41.16
# 09	2.72	8.18	41.26	# 09	2.71	8.20	41.16
# 10	3.05	8.18	41.26	# 10	3.01	8.20	41.16
# 11	3.31	8.18	41.26	# 11	3.29	8.21	41.11
# 12	3.63	8.17	41.31	# 12	3.60	8.21	41.11
# 13	3.91	8.17	41.31	# 13	3.88	8.21	41.11
# 14	4.23	8.16	41.36	# 14	4.19	8.20	41.16
# 15	4.52	8.16	41.36	# 15	4.48	8.20	41.16
# 16	4.84	8.16	41.36	# 16	4.78	8.20	41.16
				Steepest Axis (at 90 degrees)			
SUP quad	Distance	Radius(mm)	Diopters	INF quad	Distance	Radius(mm)	Diopters
# 01	0.49	8.23	41.01	# 01	0.48	8.22	41.06
# 02	0.77	8.23	41.01	# 02	0.77	8.21	41.11
# 03	1.01	8.22	41.06	# 03	1.02	8.21	41.11
# 04	1.32	8.21	41.11	# 04	1.29	8.20	41.16
# 05	1.56	8.21	41.11	# 05	1.56	8.20	41.16
# 06	1.86	8.20	41.16	# 06	1.85	8.20	41.16
# 07	2.11	8.20	41.16	# 07	2.09	8.20	41.16
# 08	2.42	8.19	41.21	# 08	2.39	8.20	41.16
# 09	2.68	8.19	41.21	# 09	2.65	8.20	41.16
# 10	2.99	8.19	41.21	# 10	2.94	8.20	41.16
# 11	3.25	8.19	41.21	# 11	3.20	8.20	41.16
# 12	3.58	8.19	41.21	# 12	3.49	8.20	41.16
# 13	3.86	8.19	41.21	# 13	3.77	8.20	41.16
# 14	4.17	8.18	41.26	# 14	4.06	8.20	41.16
# 15	4.46	8.18	41.26	# 15	4.36	8.20	41.16
# 16	4.77	8.18	41.26	# 16	4.65	8.21	41.11

Appendix 2: A listing and documentation of the manual digitisation program.

PROGRAM	DOCUMENTATION
REM set diam dimension array DIM diam(64)	*The* DIM *command told the computer that variable* DIAM *contained 64 numbers labelled as* DIAM(1), DIAM(2) *etc..*
REM more resolution for central reading (mag=x3.75) OPEN "clip:picture" FOR INPUT AS #1 Image$=INPUT$(LOF(1),1) CLOSE#1 PICTURE (-900,-600)-(1404,1128) , image$	*Once the image was captured and copied into computer memory, the* OPEN *command created a window within QUICKBASIC and displayed the image over a span of 2304 pixels by 1728 pixels. In this way, the image was magnified by a factor of x3.75. This resulted in only the central L.E.D.s being displayed - thus allowing greater resolution.*
REM change mouse cursor CHANGECURSOR 2	*The mouse cursor was changed from an arrow to a cross wire so that accurate location of each L.E.D. was possible.*
1 REM Calculates Geom. Centre FOR I=1 TO 2 LOCATE 1,1 PRINT "Geom. Centre ";I;" " GOSUB SUBR LET diam (I)= DIST CALL PENMODE (10) CALL MOVETO (X1,Y1) CALL LINETO (X2,Y2)	*Before measurements of the central L.E.D.s was commenced, a reference point from which measurements were taken was established (see figure 6.05). This point was the geometric centre of the central L.E.D.s. It is found by drawing two lines ninety degrees apart extending from opposing L.E.D.s. The point of intersection of the two lines represented the measurement reference point.*

```
NEXT I

REM measure central LED
FOR a=1 TO 2
LOCATE 1,10
PRINT " 1st ring ";a;"  "
GOSUB SUBR
LET di(a)= DIST
LET di(a)=(di(a)/3.75)
NEXT a
```

The FOR/NEXT *loop made the user measure the magnified central L.E.D.s twice. A sub-program, known as a subroutine in programming jargon, sent the computer to another section of the program* (SUBR:'***) *which calculated the pixel distance from one L.E.D. to the reference point. Once this distance was calculated, the computer returned to the next program line from where it was originally diverted. A numerical variable* DI(A) *was defined that was equal to the magnified L.E.D. distance* (DIST). *In order to account for the magnification,* DI(A) *was divided by the magnification factor (x3.75).*

```
REM choose your resolution
OPEN "clip:picture" FOR
INPUT AS #1
image$=INPUT$(LOF(1),1)
CLOSE#1
LOCATE 1,1
PICTURE (0,0)-(614.4,460.8),
image$
PRINT "More mag. (y/n)";
INPUT z$
IF z$="n" THEN GOTO 10
5 OPEN "clip:picture" FOR
INPUT AS #1
image$=INPUT$(LOF(1),1)
CLOSE#1
```

The original image was again pasted in another window within QUICKBASIC. The magnification factor was now reduced so that the entire image could be viewed. A choice of two magnifications were given to the user.

```
PICTURE (-250,-190)-
(902,674) ,image$

10 REM Calculates Geom.
Centre
FOR I=1 TO 2
LOCATE 1,1
PRINT "Geom. Centre ";I;" "
GOSUB SUBR
LET diam (I)= DIST
CALL PENMODE (10)
CALL MOVETO (X1,Y1)
CALL LINETO (X2,Y2)
NEXT I

REM meridians
LET a=7
20 FOR a=a-6 TO a
LOCATE 1,1
PRINT "meridian  point
";a;" "
GOSUB SUBR
LET diam(a)= DIST
IF z$= "y" THEN
diam(a)=(diam(a)/1.5)*.8
NEXT a
LOCATE 1,20
PRINT"another meridian
(yes/no)";
INPUT v$
IF v$="no" THEN GOTO 30
```

Before measurements on the location peripheral L.E.D.s was commenced, a reference point was established once again.

A FOR/NEXT *loop was set so that measurements of peripheral points could be made. Measurement was governed by the subroutine called* SUBR. *The measured value was assigned to the variable* DIAM(A).

Depending on which magnification was used, a simple division/multiplication was performed to rescale the value. The user was also given the choice as to whether another meridian needed to be analysed. If the user chooses 'yes' then the computer recommenced the measurement again with the value of the

```
LET a=a+7
IF v$="yes" THEN GOTO 20

REM output data
30 CLS
FOR b = 1 TO a
LOCATE  b,1
PRINT b;"point =";diam(b)
NEXT b
PRINT a+1;"central dist =
";di(1)
PRINT a+2;"central dist =
";di(2)
LET di(3)=(di(1)+di(2))/2
LET di(1)=(di(1)+di(2))/2
PRINT di(3)

REM copies output window to
clipboard
OPEN "clip:" FOR OUTPUT
AS #1
WRITE #1, di(1)
FOR b = 1 TO 7
WRITE #1, diam(b)
NEXT b
CLOSE #1
END

SUBR: '*******measurement
subroutine *******
```

variable 'A' adjusted. If the 'no' option is chosen then the program continued to the next section.

Once the measurements were completed, the values were displayed on the computer screen. A simple FOR/NEXT *loop was set-up to display the values of* DIAM. *Then, both of the central L.E.D. values were shown with the calculated mean.*

The L.E.D. positions were eventually to be input into the topography calculation program. The output values of the L.E.D. positions were therefore copied into computer memory.

END *terminated the program.*

The measurement subroutine was defined.

```
WHILE MOUSE (0) = 0:
WEND
'stops program to wait for
mouse click'
X1 = MOUSE (3)
Y1 = MOUSE (4)
LOCATE 1,45
PRINT  "x1="; X1
LOCATE 2,45
PRINT "y1="; Y1
```

The program was halted until the user depressed the mouse button (the cross hair cursor was by this time placed at the measurement reference point). Two numerical variables X1 *and* Y1 *were assigned the horizontal and vertical locations of the mouse, respectively. These values are displayed on the monitor.*

```
WHILE MOUSE (0)= -1:
WEND
'stops program to wait for
mouse click'
IF MOUSE (0) = 0 THEN X2 =
MOUSE (1)
IF MOUSE (0) = 0 THEN Y2 =
MOUSE (2)
LOCATE 3,45
PRINT "x2="; X2
LOCATE 4,45
PRINT "y2="; Y2
DIST=SQR((X2-X1)^2+(Y2-
Y1)^2)
LOCATE 5,45
PRINT "Distance =";
PRINT USING "####.# ";
DIST;
PRINT "  "
RETURN
```

Until the user had correctly aligned the mouse cursor on the L.E.D., the mouse button was depressed. The WHILE *and* WEND *commands told the computer to stop continuing the program whilst the mouse button was depressed. The* IF *and* THEN *commands set the condition that if the mouse button was released then the numerical variables* X2 *and* Y2 *must be assigned the new horizontal and vertical positions of the mouse. Once again the position of the mouse, the new mouse position, was displayed on the monitor. The distance between the old and new mouse positions was calculated and the value displayed. The command* RETURN *signified the end of the subroutine and the computer returned back to the next line after the* GOSUB *command.*

Appendix 3: A listing and documentation of the semi-automated digitisation program.

PROGRAM	DOCUMENTATION
{*** Find Centroids 4 ***	
{Program to segment the input image into a set of blobs, and list their centroids (x,y) in the Results arrays}	
{Run the first 3 macros in that order, & follow instructions at each stage}	*General information regarding the primary functions of the program for the user.*
{1: the user finds the image centre by eye, and notes coords from values window}	
{2: Then image is processed & blobs found}	
{3: Finally x,y coordinates are re-expressed rel. to centre, and grouped by meridian}	
{Distance from centre is given as Length }	
VAR	*Sets up variables to be used in the program calculations*
nBlobs,i,j,k,x0,y0,x1,y1 : Integer;	
Macro 'Instructions..';	*Reminds the user to make sure that the 'Invert y-coordinates' box in the preferences is not selected. The computer locates points on the screen*
Begin	

```
PutMessage('NB: "Invert Y-coordinates" must NOT be selected in Preferences. Image origin (0,0) is top LH corner; Y is +ve downwards.');
PutMessage('Open test image; move cursor to centre & note x,y coords. Then select ROI & run Process K-scope...');

End;

MACRO 'Process K-scope image';
VAR
left,top,width,ht, nBlobs, i,j : Integer;

BEGIN
nBlobs:=80;
SetBackground(0);
SetOptions('X-Y Center;Angle;Length;User1;User2');
;
SetCOUNTER(0);
SetCOUNTER(nBlobs);
For i:=1 to nBlobs do Begin
  rUser1[i]:=0; rUser2[i]:=0; End;
PutMessage('Region of Interest set already ?');
GetRoi(left,top,width,ht);
rUser1[1]:=left; rUser2[1]:=top;
```

according to pixel distances from a point of origin at the top left-hand corner of the monitor. Inverting y-coordinates would alter the position of the origin and hence effect calculations of L.E.D. distances. The other 'PutMessage' commands display inform the user to open the test image and then centre cursor so that it is at the geometric centre of the innermost L.E.D.s, the x,y value of this point must be noted by the user. The region of interest on the image must be selected and then the user must select the process k-scope command situated in the special menu.

Commences digitisation of the L.E.D.S. First the user must select the region of interest in the picture and then select the 'Process K-scope image' macro in the SPECIAL menu.

Produces two windows with only the selected portion of the image. The windows are labelled 'test0' and 'test1'.

```
SetPicName('Test0');
Duplicate('Test0');
SetPicName('Test1');

SelectWindow('Test0');
SelectWindow('Test1');
Invert;
```

The image within the 'test1' window is inverted - i.e. a negative is produced. Invert is another command part of Image. Inverting the image improved the detection of the L.E.D.s.

```
SubtractBackground('2D Remove Streaks',15);
SetDensitySlice(57,254);
PutMessage('Set best slice level, then Analyze Particles');
END;
```

A predetermined level of intensity is subtracted from the whole image so that a uniform background is present to enable accurate digitisation. The user is then asked to select the Analyse particles command which counts and locates the co-ordinates of any high intensity area in the region of interest.

The scanning procedure employed by the computer is such that particles are analysed from top to bottom of the image. Hence, L.E.D. co-ordinates are not in order. Another macro program was therefore devised that re-orders the data into a radial format.

```
MACRO 'Re-order data by radii';
VAR
nBlobs, meridian, orient,i,j,k : Integer;
x,y,r,x1,y1,x0,y0,crit,range,c,s,pi : Real;

BEGIN
{Assume particles analyzed; rX, rY contain the uncorrected blob locations}
{& rUser1[1] rUser2[1] contain coords of ROI, from 'Process K-scope...' }
```

```
nBlobs:=rCount; {the no. of blobs found}
pi:=3.1415927;
range:=15; {blob must lie within +/- range deg of the meridian to be accepted}
crit:=cos(range*pi/180);
x0:=GetNumber('Xcentre=',100);
y0:=GetNumber('Ycentre=',100);
{First express blob locations re Centre, compensating for effect of ROI offset }
For i:=1 to nBlobs do Begin
rX[i]:=rX[i]+rUser1[1]-x0 ;
rY[i]:=rY[i]+rUser2[1]-y0 ;
End;
SetOptions('X-Y Center;Angle;Length;User1;User2') ;

SetCOUNTER(nBlobs);
{NB Horiz merid is 0, RobI=45, Vert=90, LobI=135}

Begin
orient:=45*meridian; {degrees}
c:=cos(orient*pi/180);
s:=sin(orient*pi/180);
For i:=1 to nBlobs do
```

Four meridians are analysed - horizontal, vertical, 45 degrees and 135 degrees. Before analysis is commenced, the user is asked to type in the co-ordinates of the geometric centre of the central L.E.D. s (this is found by centring the cross-hair cursor on the test image and noting the x and y values). This macro is therefore merely an organisation sub-program that sequentially selects those particles with co-ordinates that lie on a linear line through each of the four meridians. Only those particles within +/- 15 degrees of each meridian are accepted.

```
Begin
x:=rX[i];
y:=rY[i];
r:=sqrt(x*x+y*y);
x1:=x*c+y*s;
{if angle betw meridian & dirn of
point is less than criterion....}
{then the pt belongs to that
meridian}
if abs(x1/r)>crit then begin
j:=j+1; rUser1[j]:=x; rUser2[j]:=y;
rLength[j]:=r;  rAngle[j]:=orient;
end;
End;
End;

SetUser1Label('X-x0');
SetUser2Label('Y-y0');
ShowResults;
{SetExport('Measurements');}
{Export(resultsfile);}
END;  {end of macro}
{****************************************
}
```

The newly formatted data is then 'exported' into a results table that shows the x, y co-ordinates, the distance of the particle from the defined geometric centre the orientation of the meridian and also the new x, y co-ordinates assuming the origin is at the geometric centre of the L.E.D.'s. This information is all that is required to located the position and length of each L.E.D. along each semi-meridian.

Appendix 4: Listing of the topography calculation program (written in Quickbasic programming language for any IBM compatible personal computer).

```
REM INPUT b and calc a
CLS
DIM b(1 TO 8)
DIM a(1 TO 8)
DIM vr(0 TO 8)
DIM ur(0 TO 8)
FOR p = 1 TO 8
READ b(p)
LET a(p) = b(p) / 33.045832#
NEXT p
DATA 31.3956, 60.81118, 76.38062, 91.93476, 106.1037, 122.3806, 136.5613,
151.3803

REM TARGET L DATA
DIM l(1 TO 8)
FOR p = 1 TO 8
READ l(p)
NEXT p
DATA 27.875, 58.25, 73.5, 87.5, 100, 110, 118.5, 123.75

REM TARGET Z DATA
DIM m(1 TO 8)
FOR c = 1 TO 8
READ m(c)
NEXT c
DATA 124.2281, 117.5225, 108.3531, 97.1263, 80.5592, 68.9069, 53.0319, 36.6108

REM D
LET d = 128

REM 7.8mm reference sphere
LET c = 0
DIM ba(1 TO 8)
DIM BM(1 TO 8)
DIM fo(1 TO 8)
DIM f(1 TO 8)
DIM CHF(1 TO 8)
FOR e = 1 TO 8
LET vr(e) = ATN(a(e) / d)
LET ur(e) = (d + 3.9) * SIN(vr(e)) / 7.8
LET ur(e) = (ATN(ur(e) / SQR(-ur(e) * ur(e) + 1)))
LET ur(e) = ur(e) - vr(e)
LET fo(e) = (2 * ur(e)) + vr(e)
```

```
LET ba(e) = 7.8 * (COS(ur(e)) - .5 - (SIN(ur(e)) / TAN(fo(e))))
LET BM(e) = SQR(l(e) ^ 2 + m(e) ^ 2)
LET j = ba(e) * (SIN(fo(e)) / BM(e))
LET CHF(e) = ATN(j / SQR(-j * j + 1))
LET f(e) = fo(e) - CHF(e)
NEXT e

REM origin location
DIM v(0 TO 8)
DIM u(0 TO 8, 0 TO 1500)
CLS
DIM led(0 TO 8)
PRINT " TYPE IN LED HEIGHTS  ";
FOR p = 1 TO 8
INPUT led(p)
LET led(p) = led(p) / 33.045832#
LET v(p) = ATN(led(p) / d)
LET u(p, 0) = (f(p) - v(p)) / 2
NEXT p
LET r1 = led(1)

REM CENTRAL RADIUS
LET r1 = r1 * d / (d * SIN(u(1, 0)) + (r1 * (COS(u(1, 0)) - .5)))
DIM x(0 TO 10000)
DIM y(0 TO 10000)
LET x(0) = 0
LET y(0) = 0
LET u(0, 0) = 0

REM 1st point
LET k = 1
LET x(0) = 0
LET u(0, 0) = 0
LET y(0) = 0
LET led(0) = 0
c = ((led(1) - led(0)) * (d - (.5 * r1) + x(0))) / d
LET PRO = c * SIN(u(0, 0)) / COS(u(0, 0) + v(1))
LET w = PRO * COS(v(1))
LET t = c + (PRO * SIN(v(1)))

REM EST COORDINATE
LET x(1) = w + x(0)
LET y(1) = t + y(0)

REM CALC A(E) - THE INTERSEPT
LET sept = y(1) * (((-BM(1) * COS(f(1))) + (.5 * r1)) - x(1))
LET sept = sept / ((BM(1) * SIN(f(1))) - y(1))
LET sept = x(1) - sept
```

```
LET ba(1) = (.5 * r1) - sept
LET CHF(1) = ATN(ba(1) * SIN(f(1)) / (BM(1) - (ba(1) * COS(f(1)))))
LET u(1, 1) = (f(1) + CHF(1) - v(1)) / 2
LET u(1, 0) = u(1, 1)
LET u(1, 1) = (u(1, 1) + u(0, 0)) / 2
h = 1
DO
h = h + 1
GOSUB REFINE
10 LET Z = 100 * (ABS(u(1, h) - u(1, 0))) / u(1, h)
LET u(1, 0) = u(1, h)
LET u(1, h) = (u(1, h) + u(0, 0)) / 2
LOOP UNTIL Z < .01#

REM 2nd point
LET k = 2
c = ((led(k) - led(k - 1)) * (d - (.5 * r1) + x(k - 1))) / d
LET PRO = c * SIN(u(1, 0)) / COS(u(1, 0) + v(2))
LET w = PRO * COS(v(2))
LET t = c + (PRO * SIN(v(2)))

REM EST COORDINATE
LET x(2) = w + x(1)
LET y(2) = t + y(1)

REM CALC A(E) - THE INTERSEPT
LET sept = y(2) * (((-BM(2) * COS(f(2))) + (.5 * r1)) - x(2))
LET sept = sept / ((BM(2) * SIN(f(2))) - y(2))
LET sept = x(2) - sept
LET ba(2) = (.5 * r1) - sept
LET CHF(2) = ATN(ba(2) * SIN(f(2)) / (BM(2) - (ba(2) * COS(f(2)))))
LET u(2, 1) = (f(2) + CHF(2) - v(2)) / 2
LET u(2, 0) = u(2, 1)
LET u(2, 1) = (u(2, 1) + u(1, 0)) / 2
h = 1
DO
h = h + 1
GOSUB REFINE
20 LET Z = (100 * (ABS(u(2, h) - u(2, 0)))) / u(2, h)
LET u(2, 0) = u(2, h)
LET u(2, h) = (u(2, h) + u(1, 0)) / 2
LOOP UNTIL Z < .01#

REM 3rd point
LET k = 3
c = ((led(k) - led(k - 1)) * (d - (.5 * r1) + x(k - 1))) / d
LET PRO = c * SIN(u(2, 0)) / COS(u(2, 0) + v(3))
LET w = PRO * COS(v(3))
```

```
LET t = c + (PRO * SIN(v(3)))

REM EST COORDINATE
LET x(3) = w + x(2)
LET y(3) = t + y(2)

REM CALC A(E) - THE INTERSEPT
LET sept = y(3) * (((-BM(3) * COS(f(3))) + (.5 * r1)) - x(3))
LET sept = sept / ((BM(3) * SIN(f(3))) - y(3))
LET sept = x(3) - sept
LET ba(3) = (.5 * r1) - sept
LET CHF(3) = ATN(ba(3) * SIN(f(3)) / (BM(3) - (ba(3) * COS(f(3)))))
LET u(3, 1) = (f(3) + CHF(3) - v(3)) / 2
LET u(3, 0) = u(3, 1)
LET u(3, 1) = (u(3, 1) + u(2, 0)) / 2
h = 1
DO
h = h + 1
GOSUB REFINE
30 LET Z = 100 * ABS(u(3, h) - u(3, 0)) / u(3, h)
LET u(3, 0) = u(3, h)
LET u(3, h) = (u(3, h) + u(2, 0)) / 2
LOOP UNTIL Z < .01#

REM 4th point
LET k = 4
c = ((led(k) - led(k - 1)) * (d - (.5 * r1) + x(k - 1))) / d
LET PRO = c * SIN(u(3, 0)) / COS(u(3, 0) + v(4))
LET w = PRO * COS(v(4))
LET t = c + (PRO * SIN(v(4)))

REM EST COORDINATE
LET x(4) = w + x(3)
LET y(4) = t + y(3)

REM CALC A(E) - THE INTERSEPT
LET sept = y(4) * (((-BM(4) * COS(f(4))) + (.5 * r1)) - x(4))
LET sept = sept / ((BM(4) * SIN(f(4))) - y(4))
LET sept = x(4) - sept
LET ba(4) = (.5 * r1) - sept
LET CHF(4) = ATN(ba(4) * SIN(f(4)) / (BM(4) - (ba(4) * COS(f(4)))))
LET u(4, 1) = (f(4) + CHF(4) - v(4)) / 2
LET u(4, 0) = u(4, 1)
LET u(4, 1) = (u(4, 1) + u(3, 0)) / 2
h = 1
DO
h = h + 1
GOSUB REFINE
```

```
40 LET Z = 100 * ABS(u(4, h) - u(4, 0)) / u(4, h)
LET u(4, 0) = u(4, h)
LET u(4, h) = (u(4, h) + u(3, 0)) / 2
LOOP UNTIL Z < .01

REM 5th point
LET k = 5
c = ((led(k) - led(k - 1)) * (d - (.5 * r1) + x(k - 1))) / d
LET PRO = c * SIN(u(4, 0)) / COS(u(4, 0) + v(5))
LET w = PRO * COS(v(5))
LET t = c + (PRO * SIN(v(5)))
REM EST COORDINATE
LET x(5) = w + x(4)
LET y(5) = t + y(4)

REM CALC A(E) - THE INTERSEPT
LET sept = y(5) * (((-BM(5) * COS(f(5))) + (.5 * r1)) - x(5))
LET sept = sept / ((BM(5) * SIN(f(5))) - y(5))
LET sept = x(5) - sept
LET ba(5) = (.5 * r1) - sept
LET CHF(5) = ATN(ba(5) * SIN(f(5)) / (BM(5) - (ba(5) * COS(f(5)))))
LET u(5, 1) = (f(5) + CHF(5) - v(5)) / 2
LET u(5, 0) = u(5, 1)
LET u(5, 1) = (u(5, 1) + u(4, 0)) / 2
h = 1
DO
h = h + 1
GOSUB REFINE
50 LET Z = 100 * ABS(u(5, h) - u(5, 0)) / u(5, h)
LET u(5, 0) = u(5, h)
LET u(5, h) = (u(5, h) + u(4, 0)) / 2
LOOP UNTIL Z < .01#

REM 6th point
LET k = 6
c = ((led(k) - led(k - 1)) * (d - (.5 * r1) + x(k - 1))) / d
LET PRO = c * SIN(u(5, 0)) / COS(u(5, 0) + v(6))
LET w = PRO * COS(v(6))
LET t = c + (PRO * SIN(v(6)))

REM EST COORDINATE
LET x(6) = w + x(5)
LET y(6) = t + y(5)

REM CALC A(E) - THE INTERSEPT
LET sept = y(6) * (((-BM(6) * COS(f(6))) + (.5 * r1)) - x(6))
LET sept = sept / ((BM(6) * SIN(f(6))) - y(6))
LET sept = x(6) - sept
```

```
LET ba(6) = (.5 * r1) - sept
LET CHF(6) = ATN(ba(6) * SIN(f(6)) / (BM(6) - (ba(6) * COS(f(6)))))
LET u(6, 1) = (f(6) + CHF(6) - v(6)) / 2
LET u(6, 0) = u(6, 1)
LET u(6, 1) = (u(6, 1) + u(5, 0)) / 2
h = 1
DO
h = h + 1
GOSUB REFINE
60 LET Z = 100 * ABS(u(6, h) - u(6, 0)) / u(6, h)
LET u(6, 0) = u(6, h)
LET u(6, h) = (u(6, h) + u(5, 0)) / 2
LOOP UNTIL Z < .01#

REM 7th point
LET k = 7
c = ((led(k) - led(k - 1)) * (d - (.5 * r1) + x(k - 1))) / d
LET PRO = c * SIN(u(6, 0)) / COS(u(6, 0) + v(7))
LET w = PRO * COS(v(7))
LET t = c + (PRO * SIN(v(7)))

REM EST COORDINATE
LET x(7) = w + x(6)
LET y(7) = t + y(6)

REM CALC A(E) - THE INTERSEPT
LET sept = y(7) * (((-BM(7) * COS(f(7))) + (.5 * r1)) - x(7))
LET sept = sept / ((BM(7) * SIN(f(7))) - y(7))
LET sept = x(7) - sept
LET ba(7) = (.5 * r1) - sept
LET CHF(7) = ATN(ba(7) * SIN(f(7)) / (BM(7) - (ba(7) * COS(f(7)))))
LET u(7, 1) = (f(7) + CHF(7) - v(7)) / 2
LET u(7, 0) = u(7, 1)
LET u(7, 1) = (u(7, 1) + u(6, 0)) / 2
h = 1
DO
h = h + 1
GOSUB REFINE
70 LET Z = 100 * ABS(u(7, h) - u(7, 0)) / u(7, h)
LET u(7, 0) = u(7, h)
LET u(7, h) = (u(7, h) + u(6, 0)) / 2
LOOP UNTIL Z < .01#

REM 8th point
LET k = 8
c = ((led(8) - led(7)) * (d - (.5 * r1) + x(7))) / d
LET PRO = c * SIN(u(7, 0)) / COS(u(7, 0) + v(8))
LET w = PRO * COS(v(8))
```

```
LET t = c + (PRO * SIN(v(8)))

REM EST COORDINATE
LET x(8) = w + x(7)
LET y(8) = t + y(7)

REM CALC A(E) - THE INTERSEPT
LET sept = y(8) * (((-BM(8) * COS(f(8))) + (.5 * r1)) - x(8))
LET sept = sept / ((BM(8) * SIN(f(8))) - y(8))
LET sept = x(8) - sept
LET ba(8) = (.5 * r1) - sept
LET CHF(8) = ATN(ba(8) * SIN(f(8)) / (BM(8) - (ba(8) * COS(f(8)))))
LET u(8, 1) = (f(8) + CHF(8) - v(8)) / 2
LET u(8, 0) = u(8, 1)
LET u(8, 1) = (u(8, 1) + u(7, 0)) / 2
h = 1
DO
h = h + 1
GOSUB REFINE
80 LET Z = 100 * ABS(u(8, h) - u(8, 0)) / u(8, h)
LET u(8, 0) = u(8, h)
LET u(8, h) = (u(8, h) + u(7, 0)) / 2
LOOP UNTIL Z < .01
FOR s = 0 TO 8
PRINT x(s)
NEXT s
FOR s = 0 TO 8
PRINT y(s)
NEXT s
END

REFINE:
LET PRO = c * SIN(u(k, h - 1)) / COS(u(k, h - 1) + v(k))
LET w = PRO * COS(v(k))
LET t = c + (PRO * SIN(v(k)))
REM EST COORDINATE
LET x(k) = w + x(k - 1)
LET y(k) = t + y(k - 1)

REM CALC A(h) - THE INTERSEPT
LET sept = y(k) * ((-BM(k) * COS(f(k)) + (.5 * r1)) - x(k))
LET sept = sept / ((BM(k) * SIN(f(k))) - y(k))
LET sept = x(k) - sept
LET ba(k) = (.5 * r1) - sept
LET CHF(k) = ATN((ba(k) * SIN(f(k))) / (BM(k) - (ba(k) * COS(f(k)))))
LET u(k, h) = (f(k) + CHF(k) - v(k)) / 2
RETURN
```

Appendix 5

Results of calculated p-value and central radius of curvature for manual digitisation.

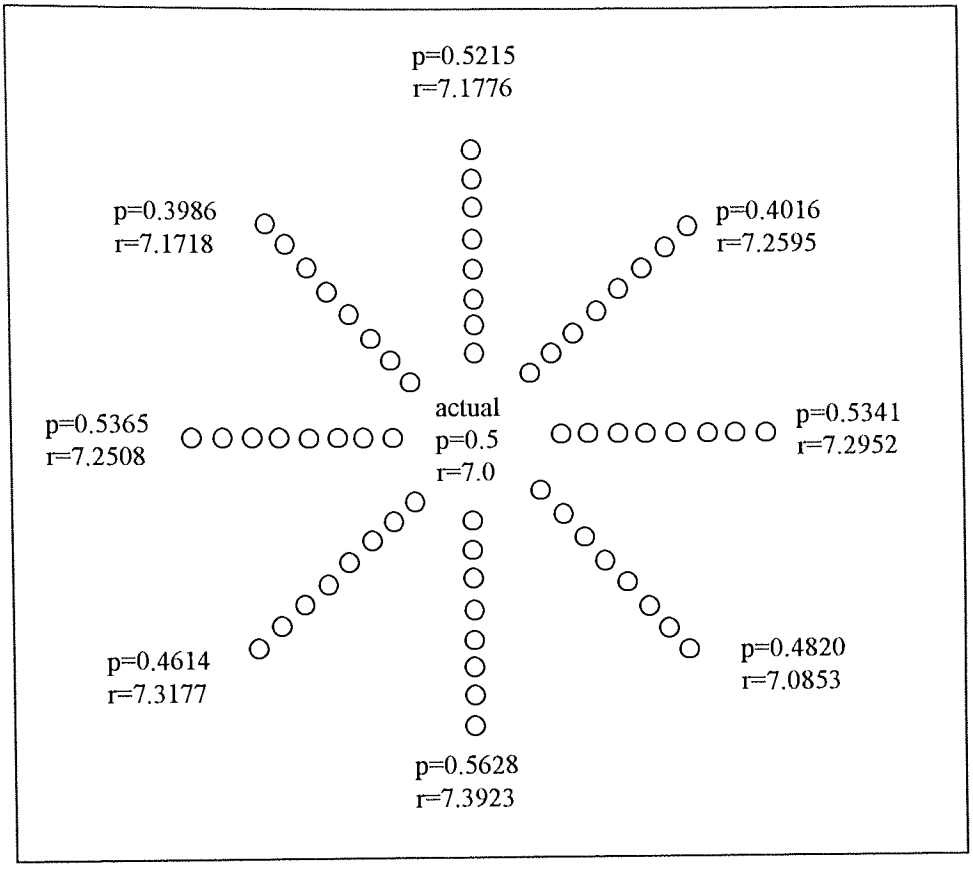

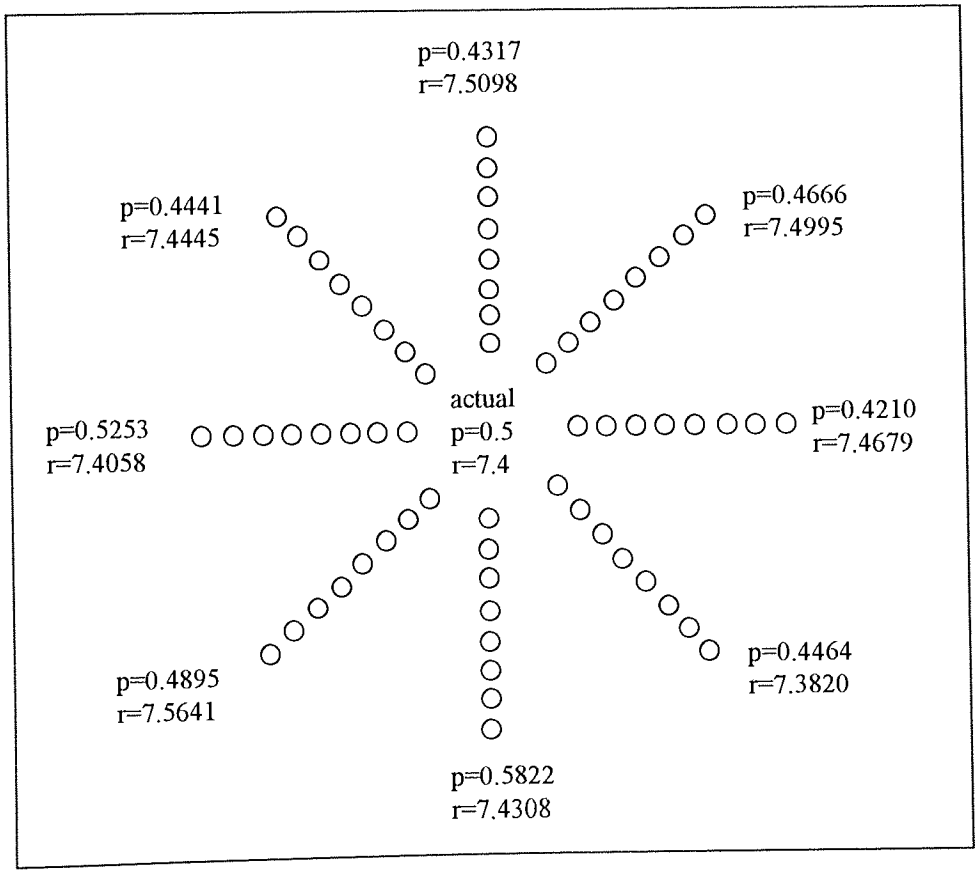

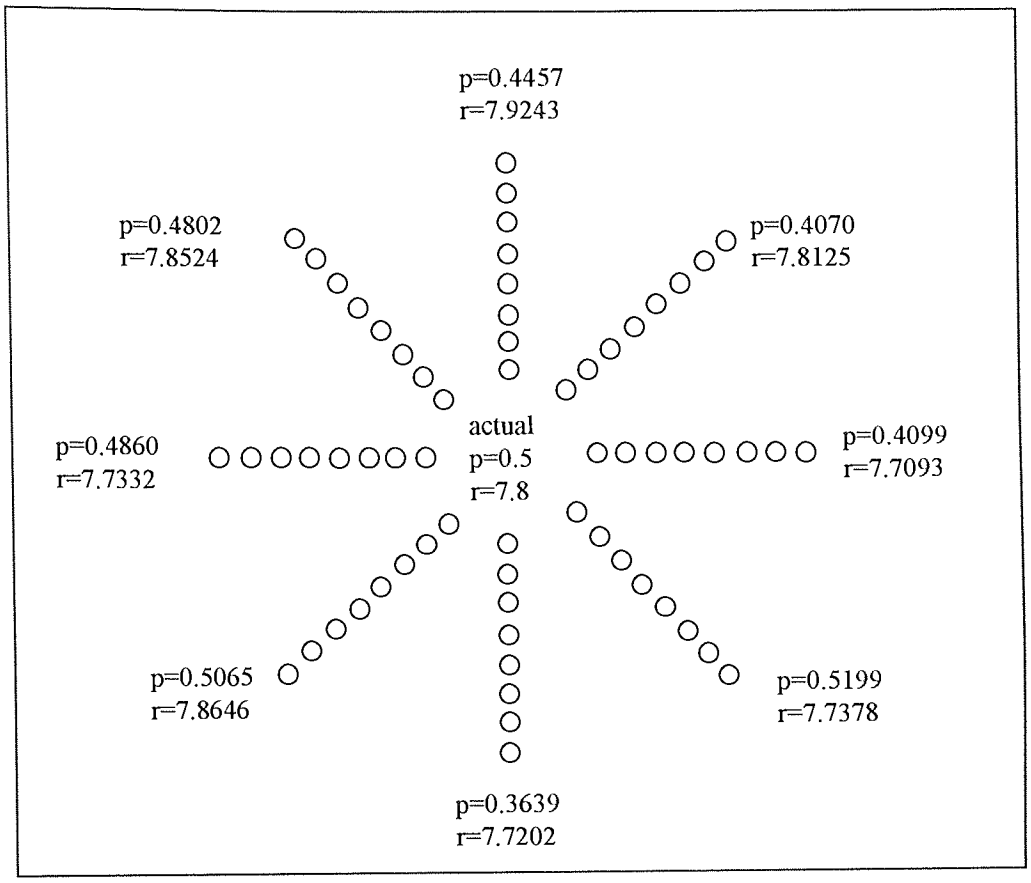
p=0.4457
r=7.9243
p=0.4802
r=7.8524
p=0.4070
r=7.8125
p=0.4860
r=7.7332
actual
p=0.5
r=7.8
p=0.4099
r=7.7093
p=0.5065
r=7.8646
p=0.5199
r=7.7378
p=0.3639
r=7.7202

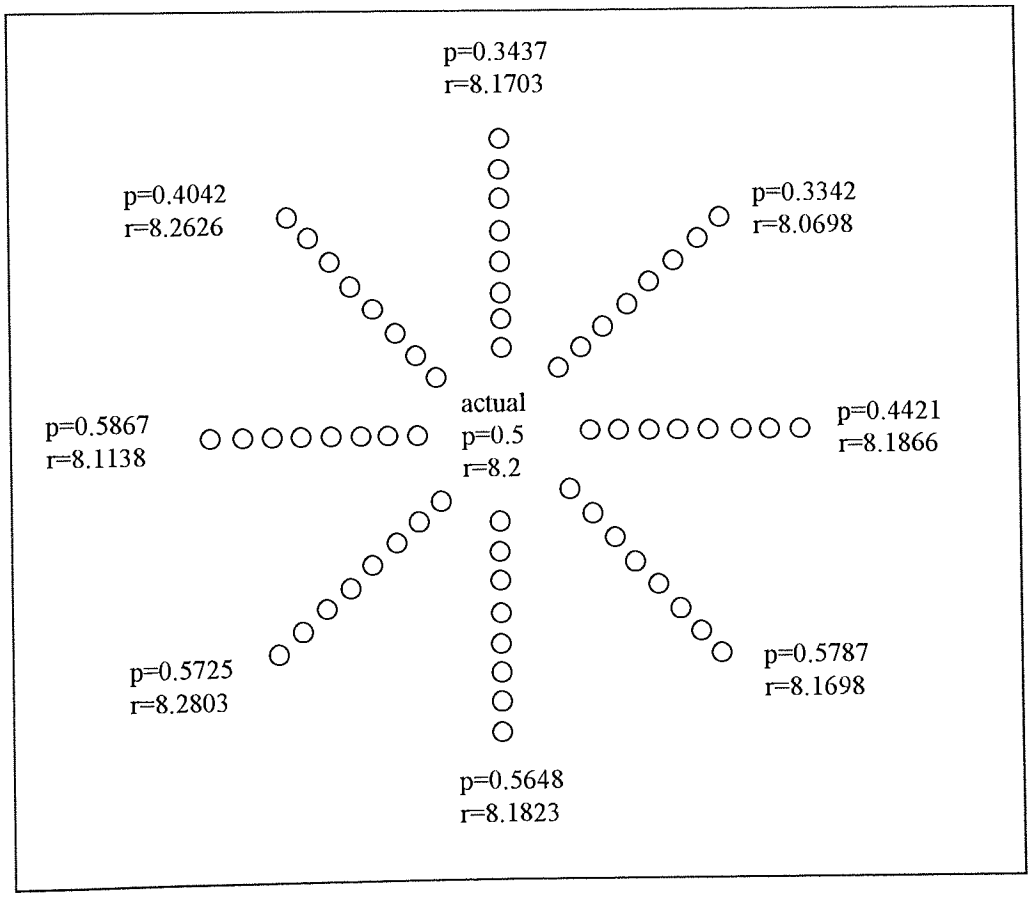
p=0.3437
r=8.1703
p=0.4042
r=8.2626
p=0.3342
r=8.0698
p=0.5867
r=8.1138
actual
p=0.5
r=8.2
p=0.4421
r=8.1866
p=0.5725
r=8.2803
p=0.5787
r=8.1698
p=0.5648
r=8.1823

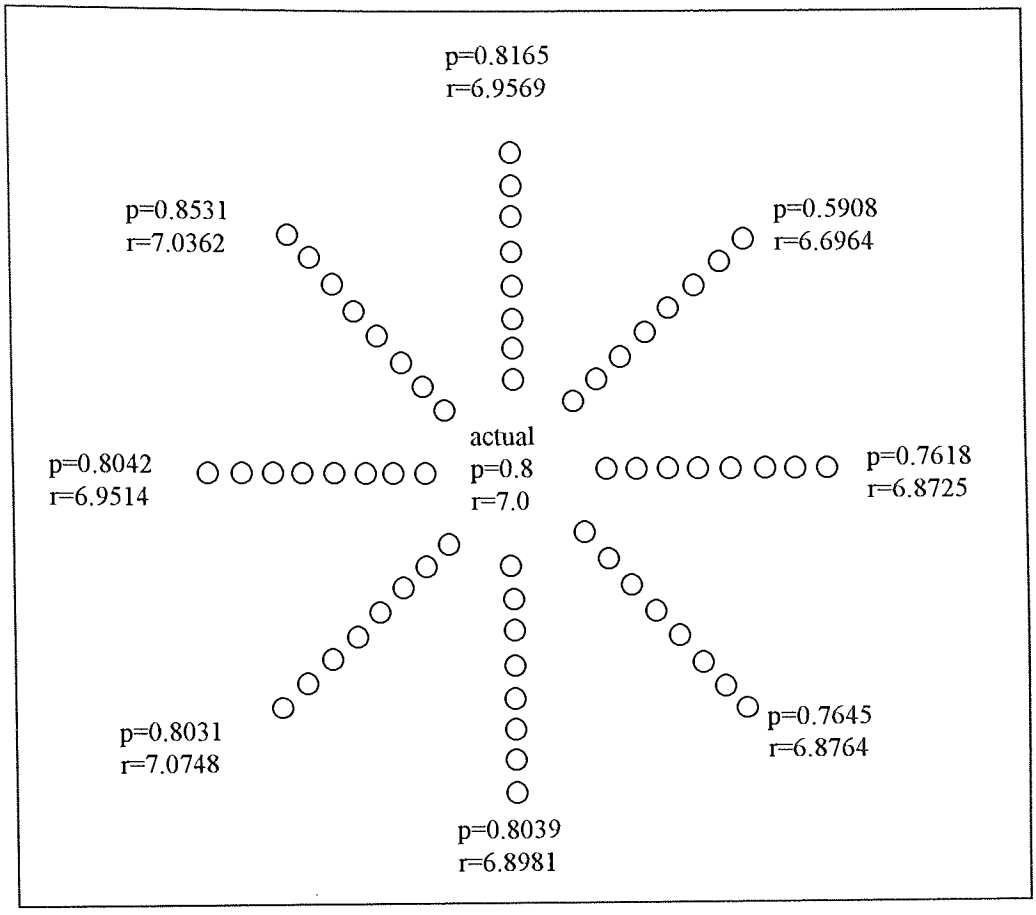
p=0.8165
r=6.9569
p=0.8531
r=7.0362
p=0.5908
r=6.6964
p=0.8042
r=6.9514
actual
p=0.8
r=7.0
p=0.7618
r=6.8725
p=0.8031
r=7.0748
p=0.7645
r=6.8764
p=0.8039
r=6.8981

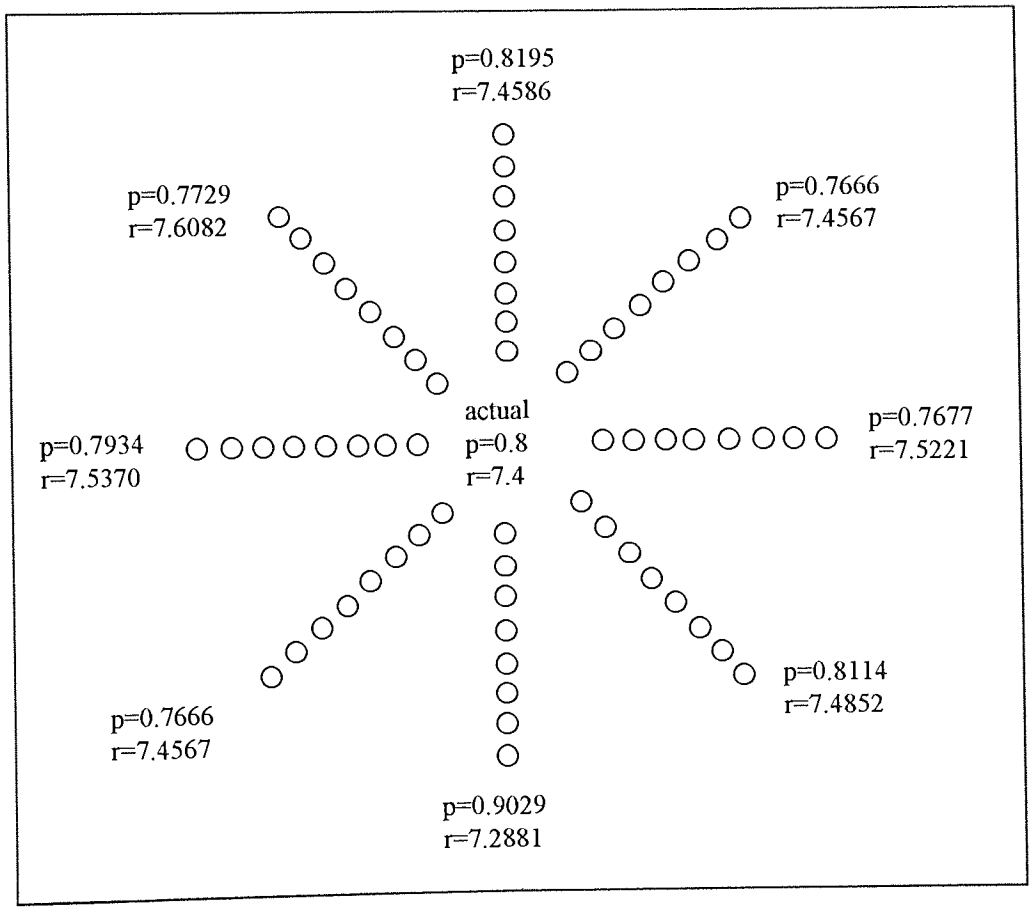
p=0.8195
r=7.4586
p=0.7729
r=7.6082
p=0.7666
r=7.4567
p=0.7934
r=7.5370
actual
p=0.8
r=7.4
p=0.7677
r=7.5221
p=0.7666
r=7.4567
p=0.8114
r=7.4852
p=0.9029
r=7.2881

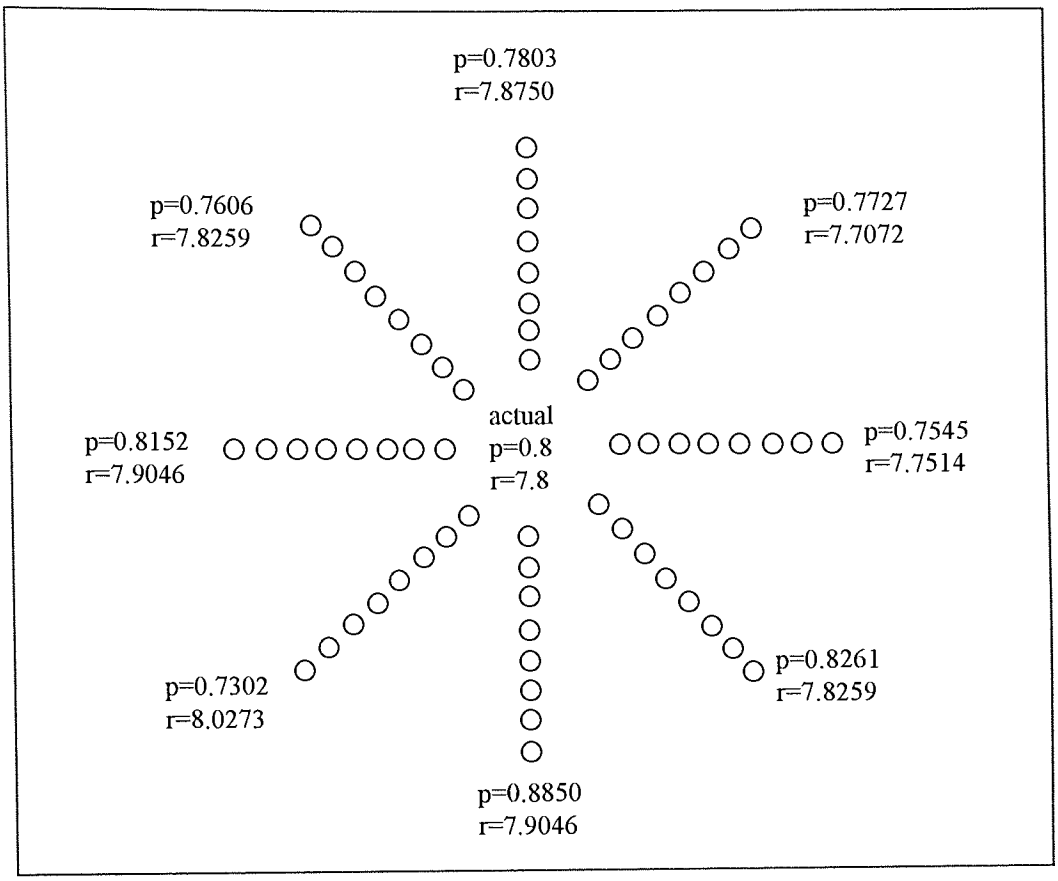
p=0.7803
r=7.8750
p=0.7606
r=7.8259
p=0.7727
r=7.7072
p=0.8152
r=7.9046
actual
p=0.8
r=7.8
p=0.7545
r=7.7514
p=0.7302
r=8.0273
p=0.8261
r=7.8259
p=0.8850
r=7.9046

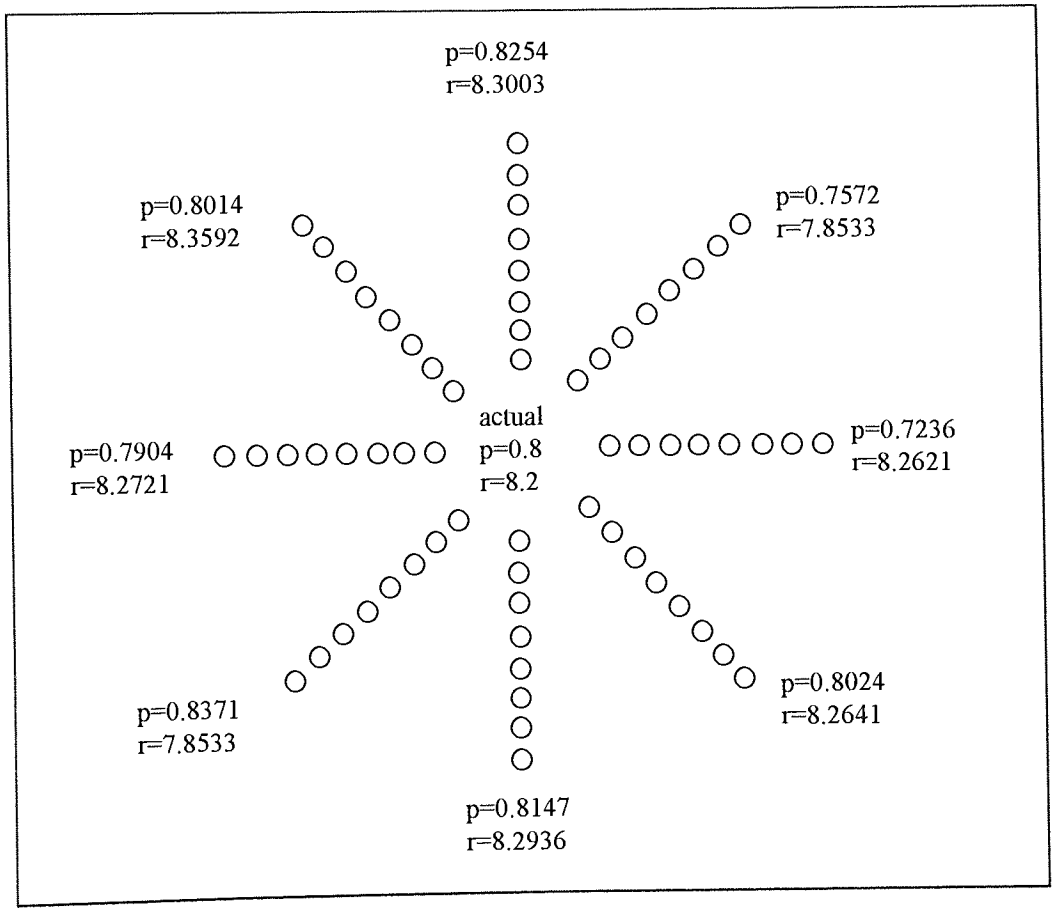
p=0.8254
r=8.3003
p=0.8014
r=8.3592
p=0.7572
r=7.8533
p=0.7904
r=8.2721
actual
p=0.8
r=8.2
p=0.7236
r=8.2621
p=0.8371
r=7.8533
p=0.8024
r=8.2641
p=0.8147
r=8.2936

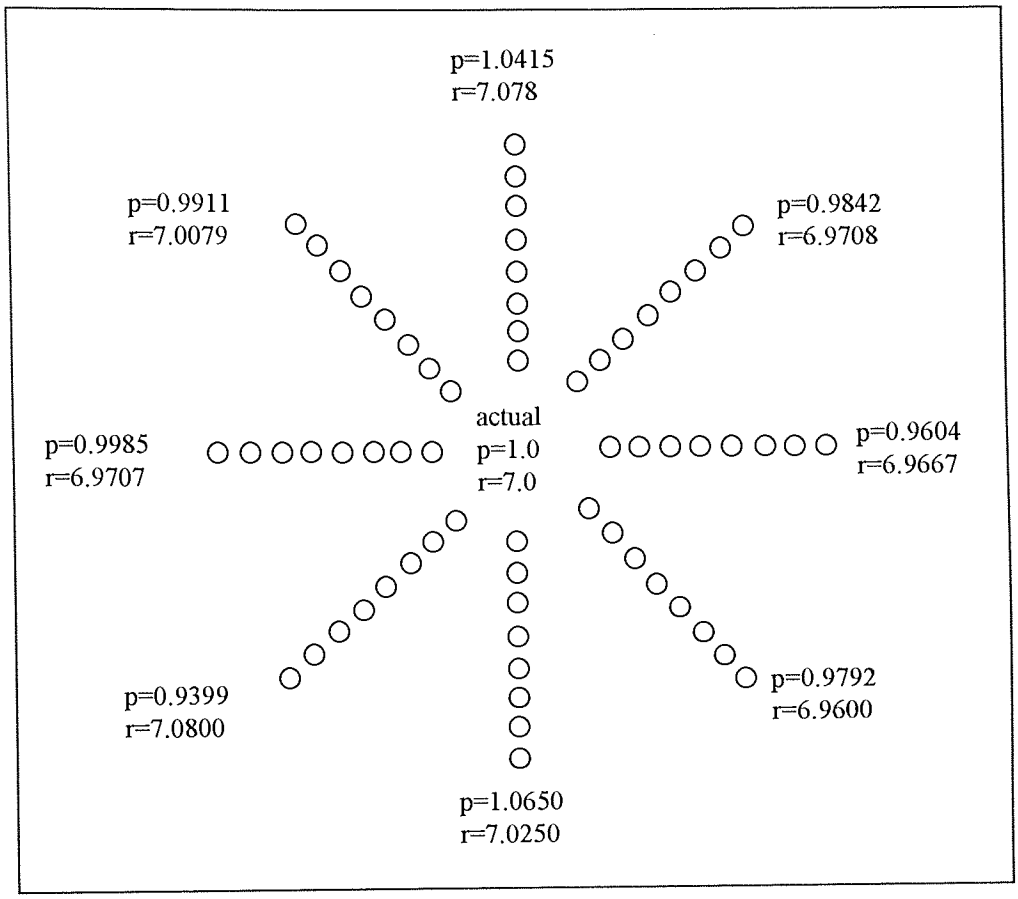
p=1.0415
r=7.078
p=0.9911
r=7.0079
p=0.9842
r=6.9708
p=0.9985
r=6.9707
actual
p=1.0
r=7.0
p=0.9604
r=6.9667
p=0.9399
r=7.0800
p=0.9792
r=6.9600
p=1.0650
r=7.0250

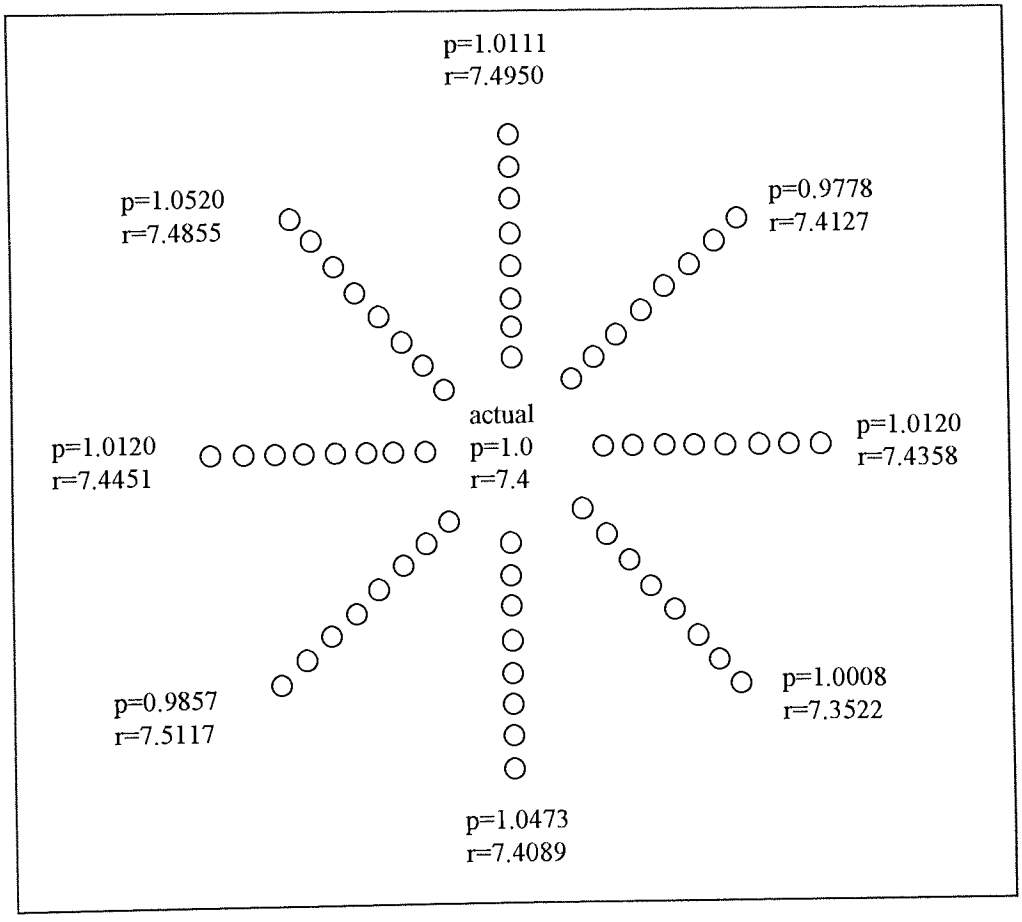
p=1.0111
r=7.4950
p=1.0520
r=7.4855
p=0.9778
r=7.4127
p=1.0120
r=7.4451
actual
p=1.0
r=7.4
p=1.0120
r=7.4358
p=0.9857
r=7.5117
p=1.0008
r=7.3522
p=1.0473
r=7.4089

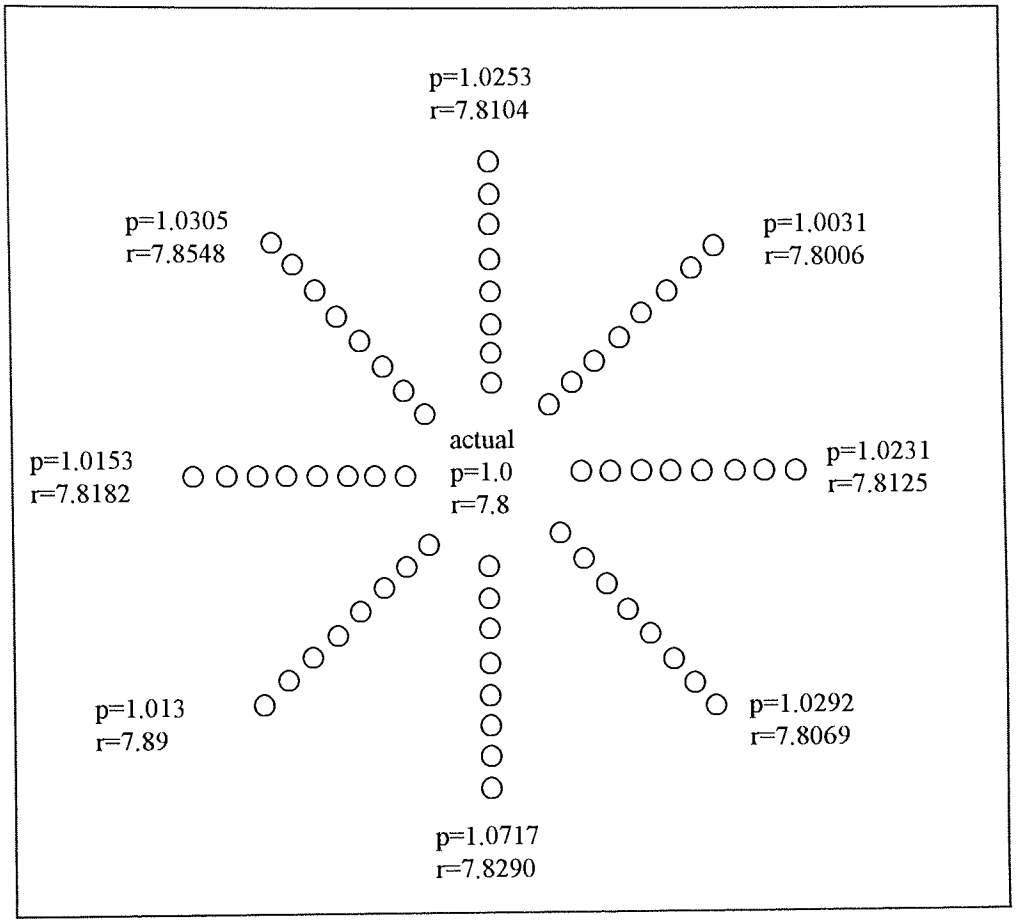
p=1.0253
r=7.8104
p=1.0305
r=7.8548
p=1.0031
r=7.8006
p=1.0153
r=7.8182
actual
p=1.0
r=7.8
p=1.0231
r=7.8125
p=1.013
r=7.89
p=1.0292
r=7.8069
p=1.0717
r=7.8290

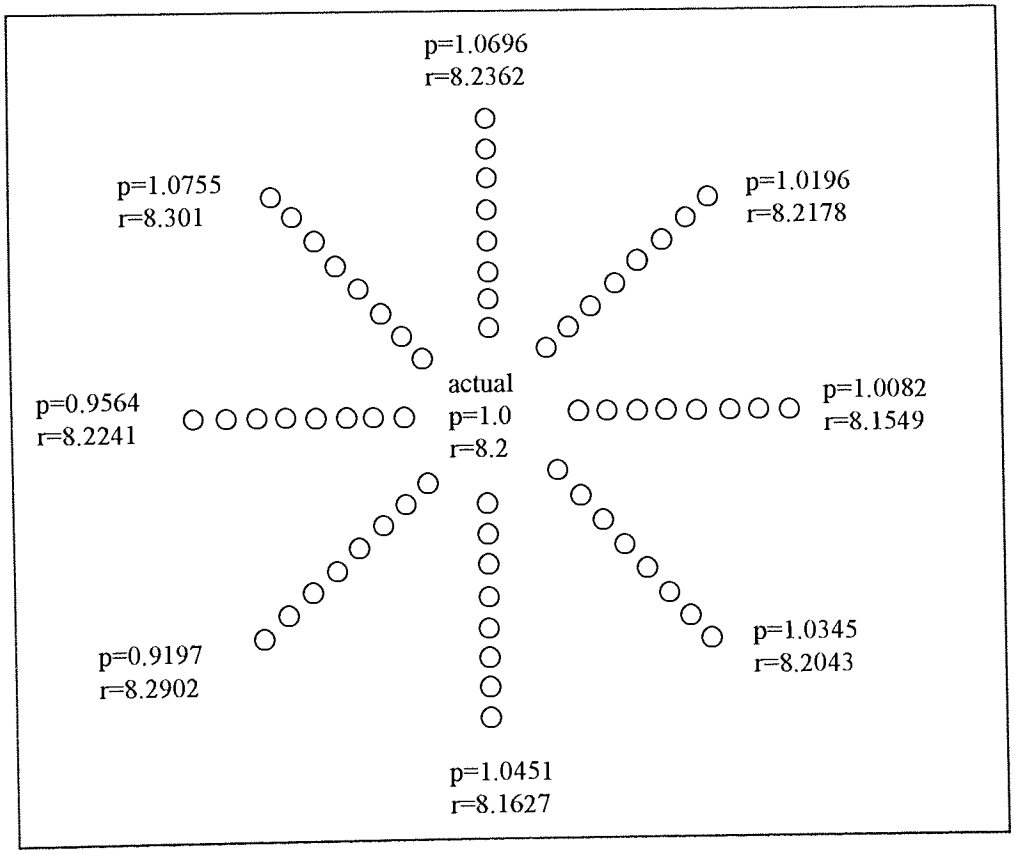
p=1.0696
r=8.2362
p=1.0755
r=8.301
p=1.0196
r=8.2178
p=0.9564
r=8.2241
actual
p=1.0
r=8.2
p=1.0082
r=8.1549
p=0.9197
r=8.2902
p=1.0345
r=8.2043
p=1.0451
r=8.1627

Results of calculated p-value and central radius of curvature for semi-automated digitisation.

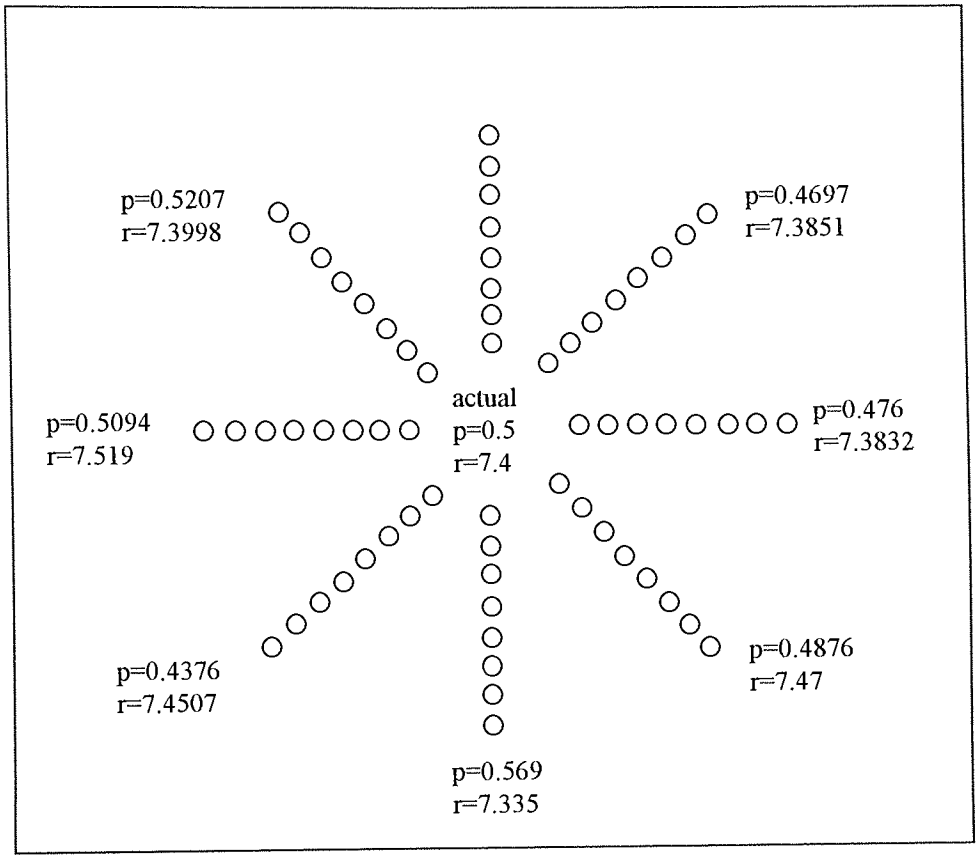

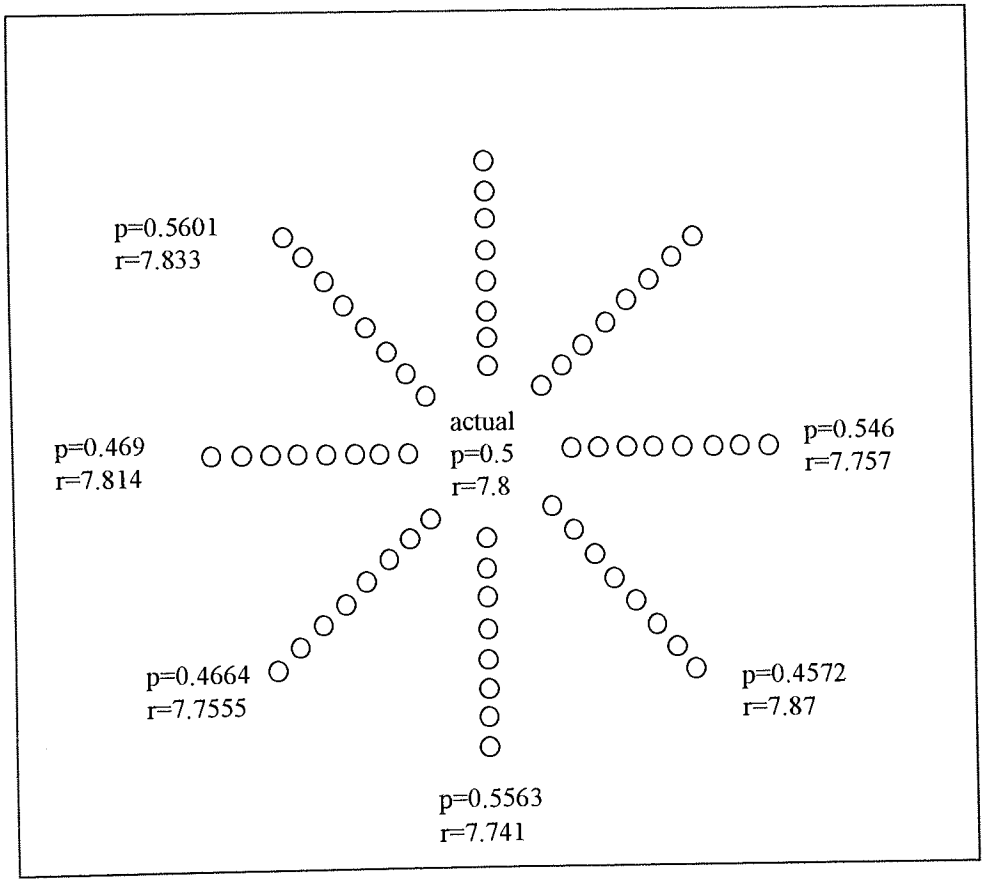

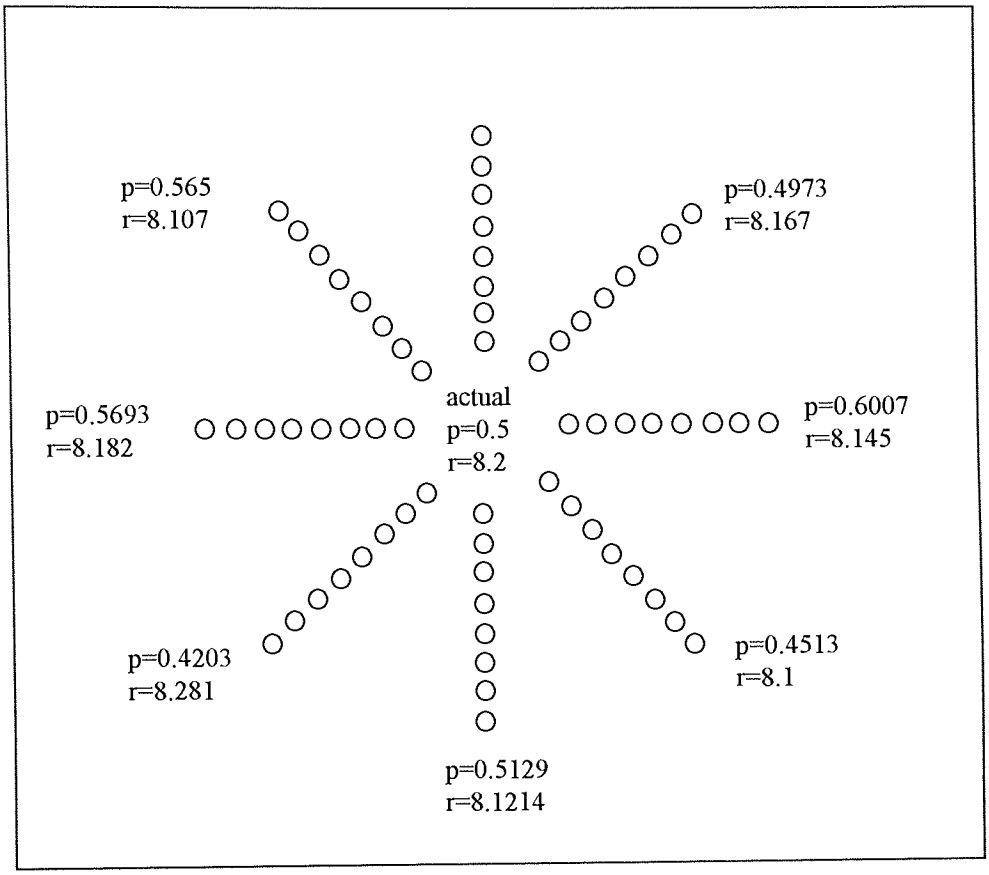
p=0.565
r=8.107
p=0.4973
r=8.167
p=0.5693
r=8.182
actual
p=0.5
r=8.2
p=0.6007
r=8.145
p=0.4203
r=8.281
p=0.4513
r=8.1
p=0.5129
r=8.1214

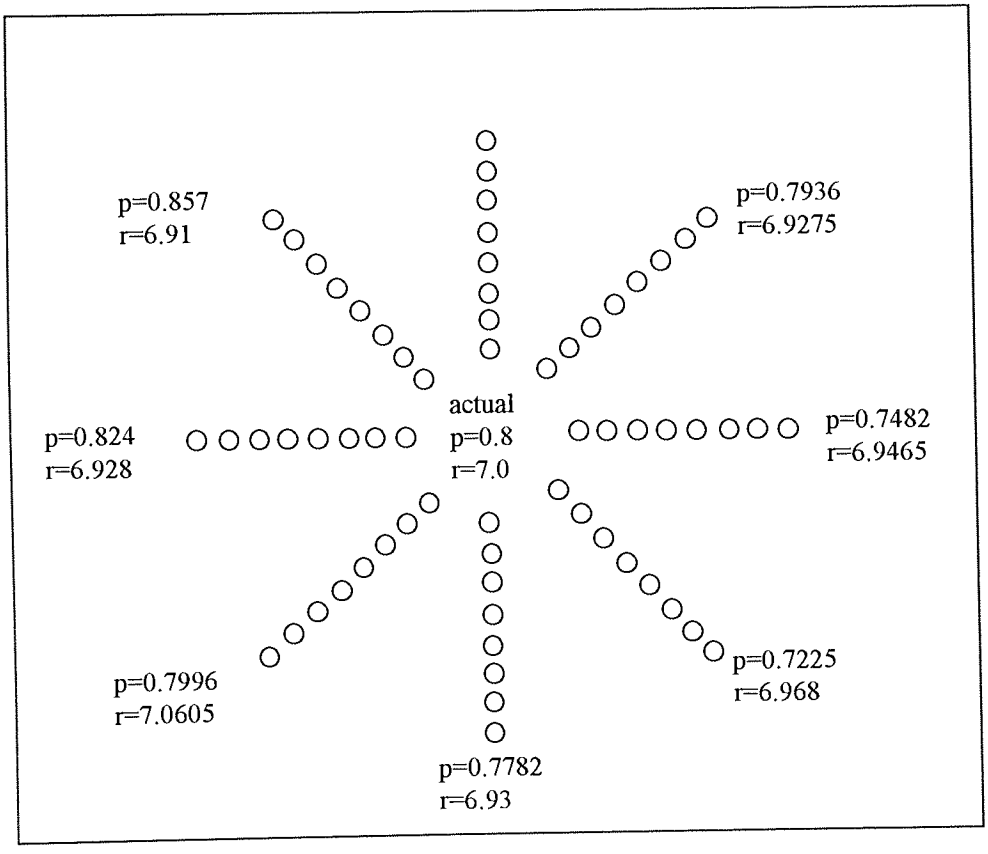
p=0.857
r=6.91
p=0.7936
r=6.9275
p=0.824
r=6.928
actual
p=0.8
r=7.0
p=0.7482
r=6.9465
p=0.7996
r=7.0605
p=0.7225
r=6.968
p=0.7782
r=6.93

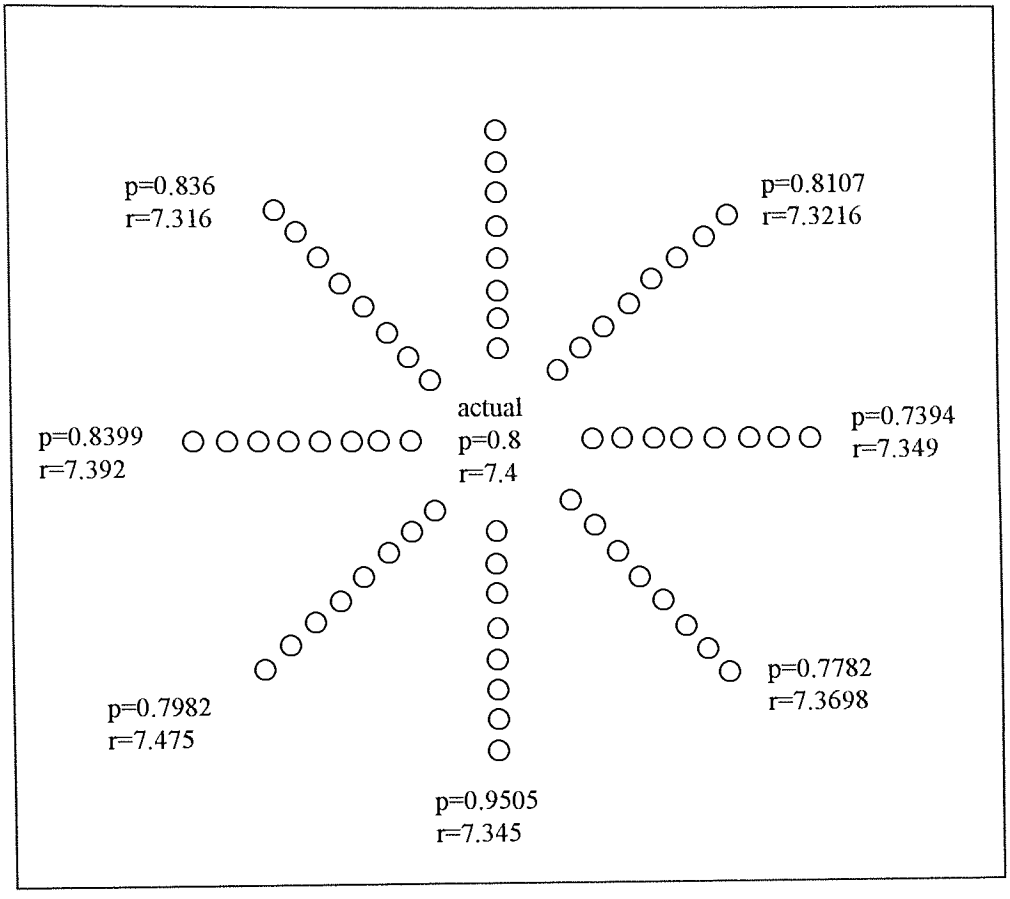
p=0.836
r=7.316
p=0.8107
r=7.3216
p=0.8399
r=7.392
actual
p=0.8
r=7.4
p=0.7394
r=7.349
p=0.7982
r=7.475
p=0.7782
r=7.3698
p=0.9505
r=7.345

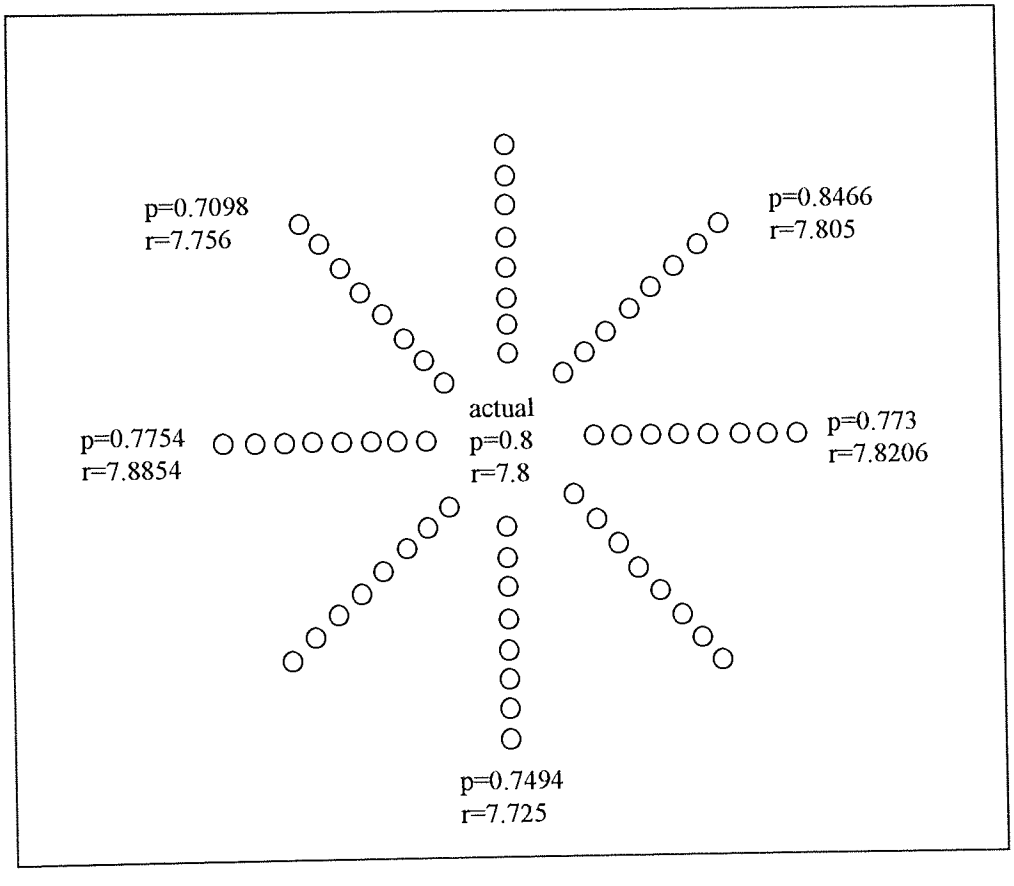
p=0.7098
r=7.756
p=0.8466
r=7.805
p=0.7754
r=7.8854
actual
p=0.8
r=7.8
p=0.773
r=7.8206
p=0.7494
r=7.725

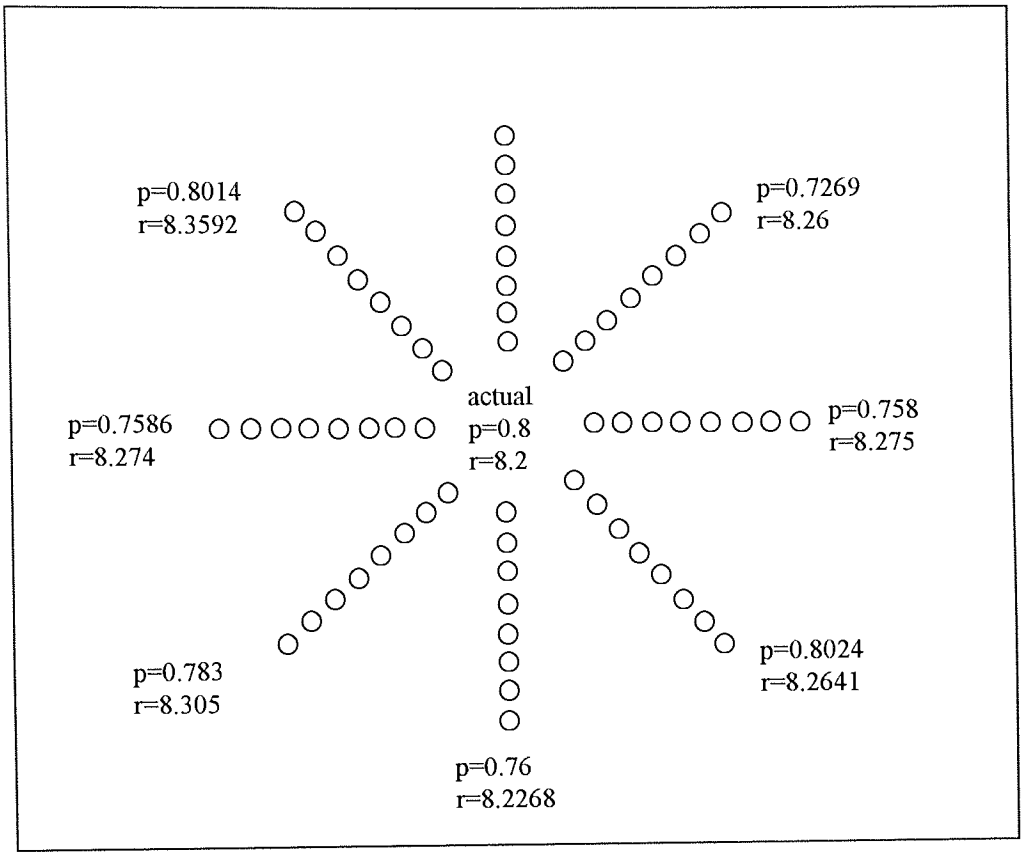
p=0.8014
r=8.3592
p=0.7269
r=8.26
p=0.7586
r=8.274
actual
p=0.8
r=8.2
p=0.758
r=8.275
p=0.783
r=8.305
p=0.8024
r=8.2641
p=0.76
r=8.2268

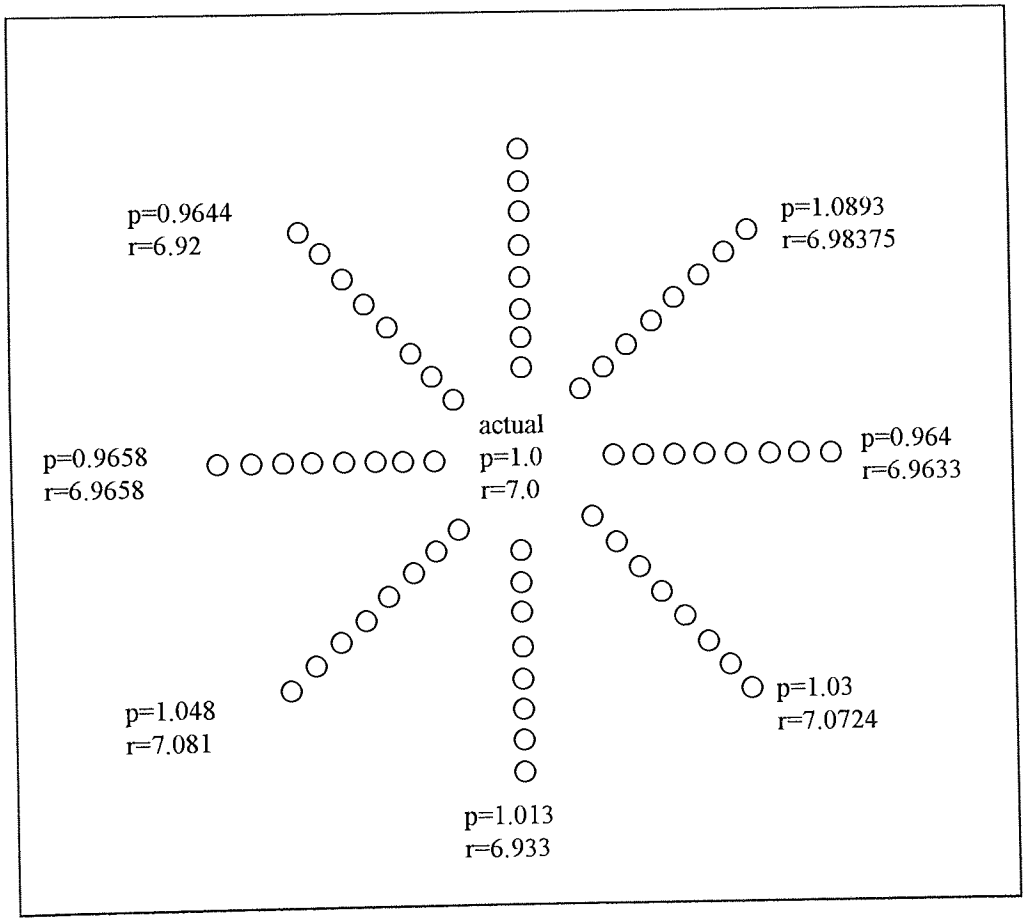
p=0.9644
r=6.92
p=1.0893
r=6.98375
p=0.9658
r=6.9658
actual
p=1.0
r=7.0
p=0.964
r=6.9633
p=1.048
r=7.081
p=1.03
r=7.0724
p=1.013
r=6.933

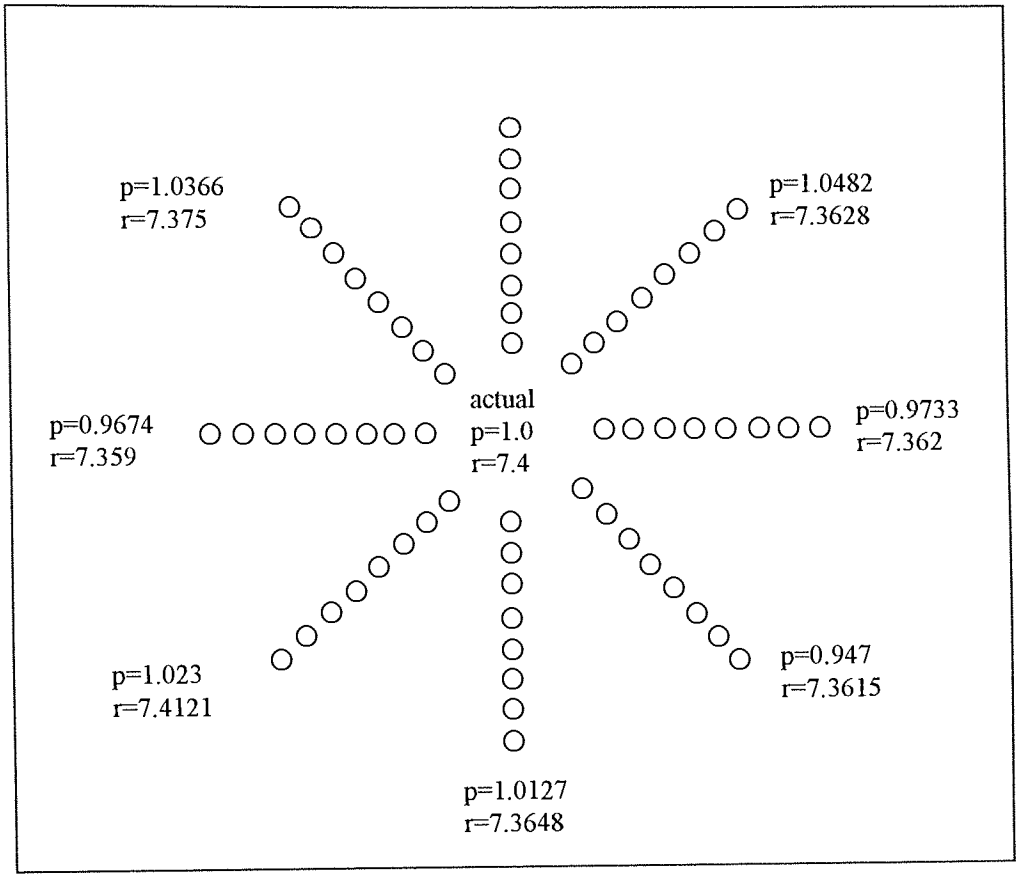
p=1.0366
r=7.375
p=1.0482
r=7.3628
actual
p=1.0
r=7.4
p=0.9674
r=7.359
p=0.9733
r=7.362
p=1.023
r=7.4121
p=0.947
r=7.3615
p=1.0127
r=7.3648

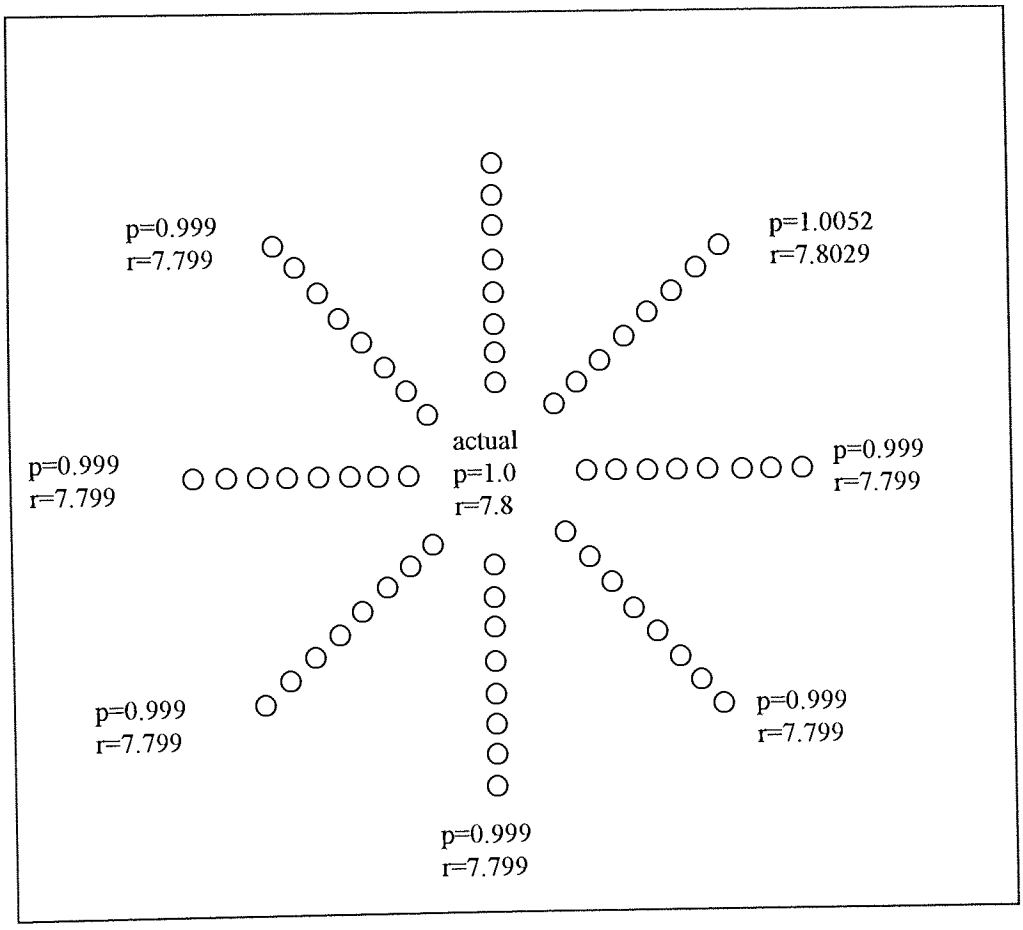
p=0.999
r=7.799
p=1.0052
r=7.8029
actual
p=1.0
r=7.8
p=0.999
r=7.799
p=0.999
r=7.799
p=0.999
r=7.799
p=0.999
r=7.799
p=0.999
r=7.799

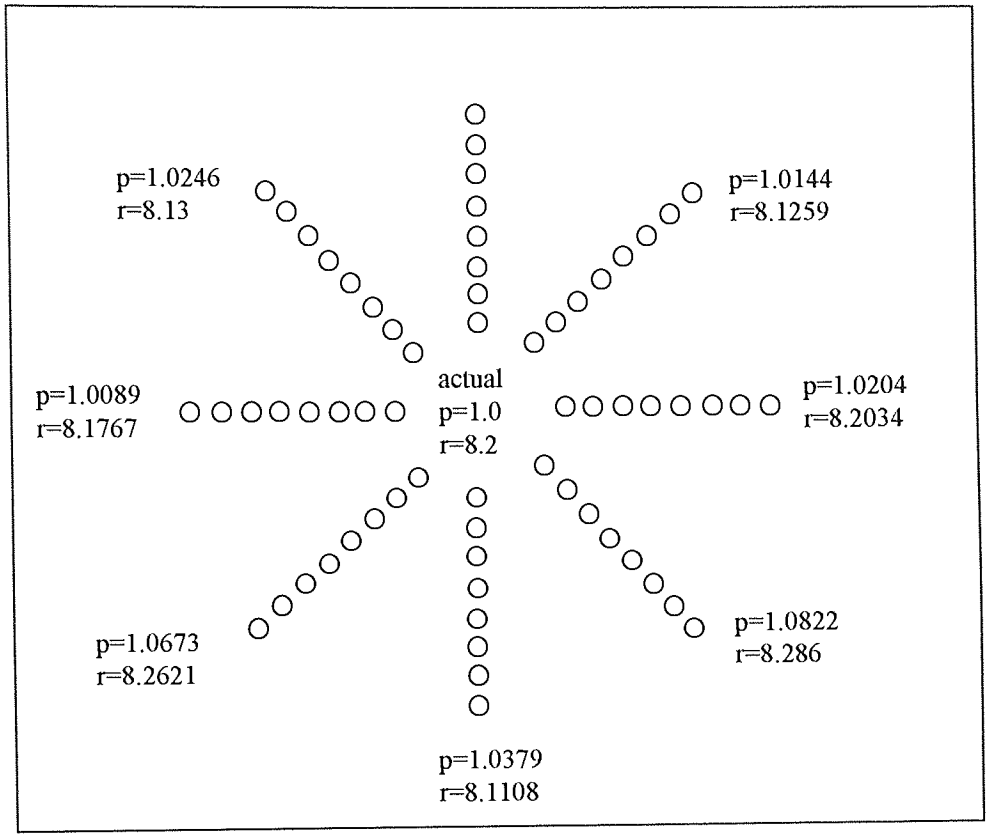
p=1.0246
r=8.13
p=1.0144
r=8.1259
p=1.0089
r=8.1767
actual
p=1.0
r=8.2
p=1.0204
r=8.2034
p=1.0673
r=8.2621
p=1.0822
r=8.286
p=1.0379
r=8.1108

Appendix 6: Repeatability data. Numerical data shows the L.E.D. pixel distances using the manual digitisation method for A. five repeated images measured once and B. a single image digitised five times. Only the horizontal meridian was measured for the surface p=0.8, r=7.80mm.

A 180 right meridian, five images.

L.E.D. dist. (1st)	L.E.D. dist. (2nd)	L.E.D. dist. (3rd)	L.E.D. dist. (4th)	L.E.D. dist. (5th)
29.873	29.606	29.205	29.074	29.20576
60.008	59.0085	60	59.0085	59.03309
74.007	74.00676	76	74.0068	75.0067
93	92.005	93.0215	91.0055	91
111.0045	110.0045	111.018	110.0045	109.004
127.0354	124.0363	126.0635	123.034	124.0363
144.0313	143.0315	145.0552	141.032	142.031
157.0796	158.0791	159.1132	155.0806	157.0509
r=7.88 p=0.816	r=7.79 p=0.803	r=7.88 p=0.7882	r=7.78 p=0.874	r=7.779 p=0.8242

A 180 left meridian, five images.

L.E.D. dist. (1st)	L.E.D. dist. (2nd)	L.E.D. dist. (3rd)	L.E.D. dist. (4th)	L.E.D. dist. (5th)
29.541	29.67281	29.20487	29.00628	29.20487
58.0775	60.07495	59.03389	58.0345	59.03389
76.0263	76.02631	76.00658	74.027	75.02667
92.00538	93.00538	92.00543	90.0056	91
109.0183	109.0183	108.0046	106.0047	107.0047
124	126	125	122	124.004
141	143	142.0035	139.0036	140.0036
156	158	157.0032	154.013	156.0032
r=7.805 p=0.7437	r=7.90 p=0.753	r=7.81 p=0.708	r=7.67 p=0.747	r=7.78 p=0.762

B 180 right meridian, one image.

L.E.D. dist. (1st)	L.E.D. dist. (2nd)	L.E.D. dist. (3rd)	L.E.D. dist. (4th)	L.E.D. dist. (5th)
29.606	29.209	29.0146	29.0114	29.017
61	61	60	60.00847	60.00833
74	74	74.00676	74.00685	74.00676
92.00543	91.00549	91.00549	90.00555	91.00549
110.0182	111.018	109.0183	109.0183	109.0046
125.064	125.036	123.0366	124.0363	124.0363
142.0563	143.0539	142.0563	141.0567	142.0563
155.1161	156.0801	155.1161	155.1161	155.0806
r=7.91	r=7.855	r=7.79	r=7.776	r=7.788
p=0.8121	p=0.7179	p=0.7369	p=0.732	p=0.7147

B 180 left meridian, one image.

L.E.D. dist. (1st)	L.E.D. dist. (2nd)	L.E.D. dist. (3rd)	L.E.D. dist. (4th)	L.E.D. dist. (5th)
29.341	29.2412	29.1415	29.0114	29.0047
59.03389	59.03333	59.03389	59.03333	59.03333
77.00649	77.00649	77.00649	77.00649	77.00649
94	94	94	94.00526	94.00526
110.0045	110.0045	110.0045	110.0045	110.0045
128.0039	128.0039	128	128	128
144.0035	145.0034	145.0034	145.0034	145.0034
161.0031	161.0031	161.0031	161.0031	161.0031
r=7.88	r=7.874	r=7.868	r=7.86	r=7.862
p=0.7577	p=0.7273	p=0.7153	p=0.7061	p=0.7056

Appendix 7: List of Publications

Fowler, C. W., and T. N. Dave. (1994). Review of the past and present techniques of measuring corneal topography. *Ophthal. & Physiol. Opt.*, **14**, 49-58.

Dave, T. N., C. W. Fowler, M. E. A. Elawad and Dunne, M. C. M. (1995). A clinical trial of the SUN SK-2000 computer assisted videokeratoscope. *Ophthal. & Physiol. Opt.*, **15**, 105-116.

Papers in preparation

The accuracy repeatability of the EyeSys CAS in a normal patient sample.

The accuracy and repeatability of the EyeSys CAS for twelve convex aspheric surfaces.

A description of a new videokeratoscope.

Evaluation of the performance of a new topographic reconstruction algorithm for twelve convex aspheric surfaces.

Conference Presentations

T. N. Dave, and Fowler, C. W. (1993). A clinical trial of the SUN SK-2000 computer assisted videokeratoscope - its level of agreement with the keratometer and its repeatability. The American Academy of Optometry, Boston, USA.